Synthesis and Reactivity of Low-Valent Group 14-15 Compounds

by

Nick Giffin

A Thesis Submitted to the Saint Mary's University, Halifax, Nova Scotia
in Partial Fulfillment of the Requirements for the
Degree of Master of Science in Applied Science

SAINT MARY'S UNIVERSITY SINCE 1802

One University. One World. Yours.

July 2012, Halifax, Nova Scotia

Approved:	Dr. Jason Masuda Supervisor Department of Chemistry
Approved:	Dr. Glen Briand External Examiner Department of Chemistry and Biochemistry Mount Allison University
Approved:	Dr. Jason Clyburne Supervisory Committee Member Deparment of Chemistry
Approved:	Dr. Colleen Barber Supervisory Committee Member Department of Biology
Date:	July 23, 2012

Library and Archives Canada

Published Heritage Branch

395 Wellington Street
Ottawa ON K1A 0N4
Canada

Bibliothèque et Archives Canada

Direction du Patrimoine de l'édition

395, rue Wellington
Ottawa ON K1A 0N4
Canada

Your file Votre référence
ISBN: 978-0-494-88937-4

Our file Notre référence
ISBN: 978-0-494-88937-4

Abstract

Synthesis and Reactivity of Low-Valent Group 14-15 Compounds

by Nick Giffin

The synthesis, characterization and preliminary reactivity of a new diphosphine is discussed. Calculations indicated a favorable dissociation of the central P-P bond, corresponding to roughly 100kJ/mol relaxation energy for the full system.

Reactions of $(Dipp_2C_2H_4N_2P)_2$ with elemental phosphorus (P_4), sulfur (S_8), oxygen (O_2), selenium (Se^0) and tellurium (Te^0) yielded the *trans,trans*-tetraphosphabicyclobutane (LP-P_4-PL), persulfide/sulfide (LP-S-S-PL/LP-S-PL), ethereal oxidative products (LP(O)-O-(O)PL, LP(Se)-Se-PL) as well as bridging selenide (LP-Se-PL) and telluride (LP-Te-PL) species. Reactions with boranes (BR_3, R = H or C_6F_5) supported an FLP-type reactivity profile (LP→BR_3) and subsequent hydrogen abstraction forming LPH→BR_3. Activation of heteroallenes including CS_2, Ph-NCO, and Ph-NCS was achieved, forming the corresponding insertion products (LP-C(=R)-X-PL).

The nucleophilic ring-opening of S_4N_4 with carbenes was investigated. IMes formed IMes=N-S_3N_3 while more electrophilic carbenes formed zwitterionic R-S-N-S_4N_3 (R = SIPr, CAAC) structures. Introduction of nucleophilic solvents induced degradation of the S_3N_3 rings to R=NSNSS (R = IMes, SIPr) structures.

July 23, 2012

Acknowledgements

I thank my supervisor Dr. Jason Masuda for turning me into a scientist.

I would also like to thank: Dr. Mike Lumsden at NMR^3 for assistance with NMR and for simulating complex ^{31}P NMR spectra, Drs. Tracey L. Roemmele and René T. Boeré at the University of Lethbridge for their EPR expertise as well as Patricia Granados, Darlene Goucher, Elizabeth McLeod and Andrea Corrigan at Saint Mary's University for their assistance and technical support.

A special thank you is due to Art Hendsbee at Saint Mary's University for his endless contributions in crystallography. Likewise, thank you to the other Masuda group members: Tom Rogers, Sarah MacDonald, Lauren Keyes and Amber Blair for their assistance and support.

I would like to acknowledge NSERC, SMU FGSR and Dean of Science offices for financial support.

Finally, I would like to thank my remaining committee members Dr. Jason Clyburne, Dr. Colleen Barber for their time and effort throughout this process.

Table of Contents

List of Figures

List of Schemes

List of Tables

Table A.6 Energy of $PEtAm_2Ph_2$ forms (kJ/mol) relative to C_2 structure.

Table A.7 Energy of bis-$PEtAm_2Ph_2$ forms (kJ/mol) relative to C_2 #2structure. The C_2 #2 form is relative to 2 $PEtAm_2$ Ph_2 C_2 units (i.e. the bond dissociation energy D_e).

Table A.8 Energy of bis-$PEtAm_2Ph_2{}^iPr_4$ forms (kJ/mol) relative to C_2 #2 structure. The C_2 form is relative to 2 $PEtAm_2$ $Ph_2{}^iPr_4$ C_2 units (i.e. the bond dissociation energy D_e).

Table A.9 Total energies of all structures. Underlined energies correspond to a local minimum energy structure.

List of Abbreviations

$a(^{x}R)$	Hyperfine coupling to element R, isotope x
Å	Angstrom
Ar	Aryl
B3LYP	Becke, three-parameter, Lee-Yang-Parr
br	Broad
Cp	Cyclopentadiene
Cp*	Pentamethylcyclopentadiene
COD	Cyclooctadiene
CAAC	Cyclic(Alkyl)(Amino) Carbene
*c*Hex	Cyclohexyl
°	Degrees
°C	Degrees celsius
δ	Chemical shift
DFT	Density Functional Theory
Dipp	2,6-diisopropylphenyl
DMF	Dimethylformamide
DMP	2,6-dimethylphenyl
d	Doublet
dd	Doublet of doublets
D	Deuterium
E	Energy
ERO	Electron Rich Olefin
Et	Ethyl
Et_2O	Diethyl ether
eV	Electron volt
EPR	Electron Paramagnetic Resonance
FLP	Frustrated Lewis Pair
FT	Fourier Transform
G	Gauss
GED	Gas-phase Electron Diffraction
GHz	Gigahertz
g	Landé *g*-factor
g	Gram
HF	Hartree-Fock
HOMO	Highest Occupied Molecular Orbital
Hz	Hertz
hr	Hour
IMes	1,3-bis(2,4,6-trimethylphenyl)imidazol-2-ylidene
^{i}Pr	*iso*-propyl
IPr	1,3-bis(2,6-diisopropylphenyl)imidazol-2-ylidene
J	Coupling constant
K	Kelvin
kJ	Kilojoules
L	Ligand = $Dipp_2C_2H_4N_2$

LDA	Lithium diisopropylamide
LUMO	Lowest Unoccupied Molecular Orbital
MHz	Mega Hertz
Mes	2,4,6-trimethylphenyl
Mes*	2,4,6-tri-*tert*-butylphenyl
Me	Methyl
mg	milligram
mL	milliliters
mmol	millimole
min	Minute
mT	milli-Tesla
mol	Mole
M	mol L^{-1}
m	Multiplet
NHC	N-Heterocyclic Carbene
NHP	N-Heterocyclic Phosphenium
nm	Nanometer
NMM	N-methylmorpholine
NMR	Nuclear Magnetic Resonance
Np	Neopentyl
o	*ortho*
ORTEP	Oakridge Thermal Ellipsoid Plot
p	*para*
PP	Pharmacopeia Point
ppm	Parts per million
Ph	Phenyl
R.T.	Room Temperature
s	Singlet
S	Electron spin
SIPr	1,3-bis(2,6-diisopropylphenyl)imidazolidin-2-ylidene
SOMO	Singly Occupied Molecular Orbital
STO	Slater-Type Orbital
^{t}Bu	*tert*-butyl
T	Tesla
TDE	Tetrakis(dimethylamino)ethane
TEMPO	2,2,6,6-tertramethylpiperidine N-oxyl
TGA–ms	Thermo Gravimetric Analysis – Mass Spectrometry
THF	Tetrahydrofuran
TMS	Trimethylsilyl
t	Triplet
$t_{1/2}$	Half-life
Tripp	2,4,6-triisopropylphenyl
UV	Ultra-violet
VT	Variable Temperature
V	Volt

New Compounds Prepared

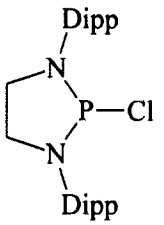

1

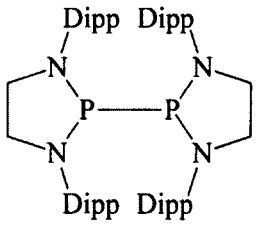

2

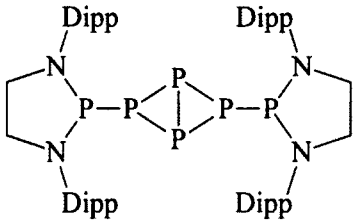

3

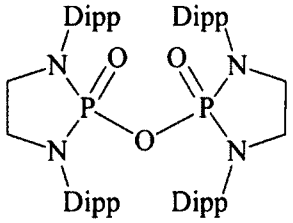

4

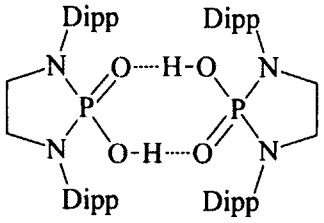

5

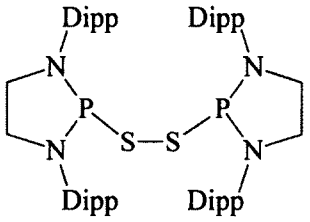

6

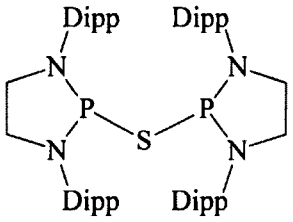

7

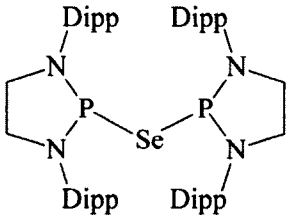

8

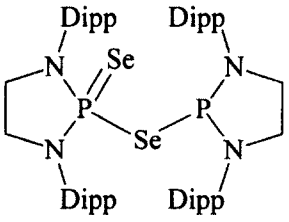

9

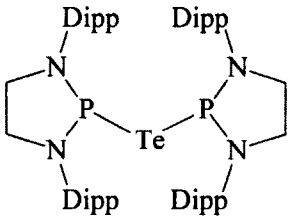

10

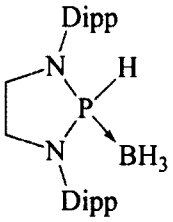

11

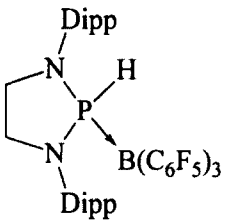

12

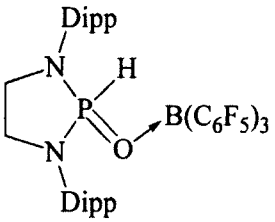

13

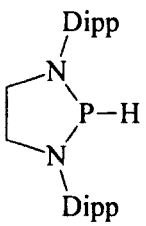

14-15

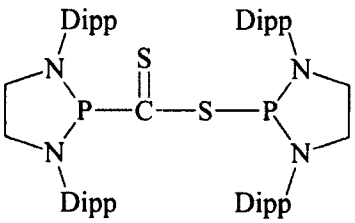

16

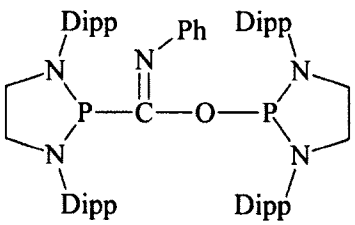

17

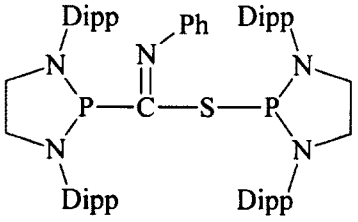

18

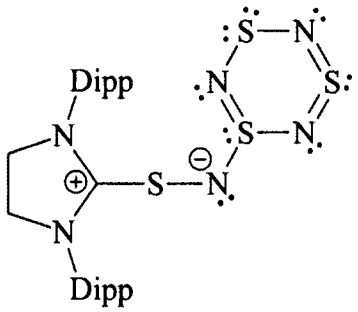
Dipp
N
S
N
S
N
S
N
Dipp

19

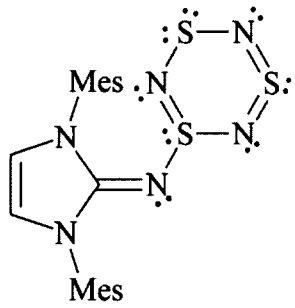
Mes
N
S
N
S
N
S
N
Mes

20

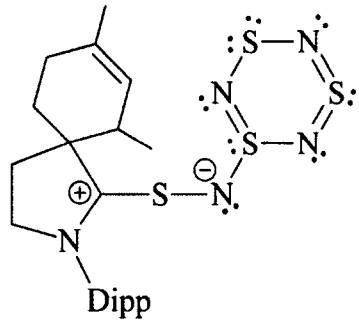
S
N
S
N
S
N
N
Dipp

21

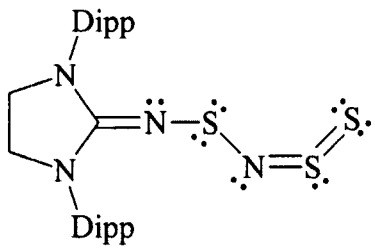
Dipp
N
N
S
S
N
S
N
Dipp

22

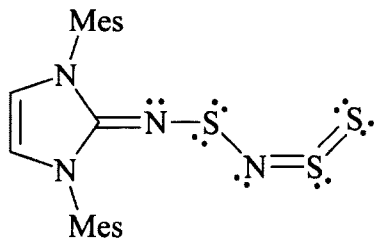
Mes
N
N
S
S
N
S
N
Mes

23

Chapter 1 – Phosphorus Radicals

Section 1.1 – Brief Overview

- Section 1.1.1 – Introduction to Phosphorus Radicals

First-row main group free radicals have been evident in the literature since the mid-19th century, spurred by the discovery of the triphenylmethyl or Gomberg radical first speculated upon in 1900.[1] Isolating heavier main group centered radicals has proven to be a more difficult task. Preliminary forays toward the characterization of radical containing main group species were based upon reaction products that could be explained using radical mechanisms.[2,3] Early radicals could be generated photolytically in the presence of electron-rich olefins (ERO) and were characterized using electron paramagnetic resonance (EPR) spectroscopy, which allowed for the elucidation of radical character in solution.[4-7] Two principals are generally employed to stabilize inherently reactive radical centers: (1) increasing steric bulk, providing kinetic and thermodynamic stabilization which can prevent unwanted reactivity or dimerization of the radical containing species, (2) electronic stabilization of the singly occupied molecular orbital (SOMO) through delocalization either by placing radical centers adjacent to electronegative atoms or a conjugated π-system.

Phosphorus centered radicals emerged in the literature in the mid-1960's with the monomeric radical of bis(*p*-dimethylamino-phenyl)phosphine (g = 2.003).[3] Although phosphorus radicals were suspected intermediates in organic coupling reactions, definitive spectroscopic evidence was not published until 1969. The reaction of a trialkyl-phosphorus with *tert*-butoxyl radical yielded the first unequivocal evidence of a

phosphorus centered compound containing an unpaired electron facilitating carbon-carbon bond formation.[4] Notable advances in structurally characterized persistent phosphorus centered radicals include recent resonance supported tungsten and vanadium structures[8,9] as well as an air-tolerant diphosphacyclobuten-4-yl radical.[10,11] Recent isolation of carbene-stabilized phosphoniumyl,[12,13] imididazolidin-2-iminato[14] and vanadium-iminatophosphorus[14] centered radicals will all be discussed further in the proceeding review, illustrating the myriad of techniques available to synthetic chemists to potentially isolate inherently reactive compounds containing a phosphorus radical.

- Section 1.1.2 – Classification of Radicals

In 1976 Griller and Ingold aimed to clarify the nomenclature which is applied to radical containing molecules in the literature. Beginning with a quote from *Through the looking glass* the authors contended "When I use a word it means just what I choose it to mean – neither more nor less".[15] Using discussion of relevant manuscripts on the kinetics of radical decay and/or coupling reactions they chose to define a radical as: (1) *stable* when it is so unreactive to air and water it can be stored indefinitely without concern for the integrity of the bulk sample, (2) *persistent* when its stability depends on the conditions under which it is kept, and (3) *transient* when having fleeting stability under most conditions leading to decay or coupling reactions on relatively short timescales. The significance of this lies in the authors' attempt to dissolve the ambiguity regarding the classification of radical species in the literature. The use of these terms will be reflected upon in the following discussion of relevant literature regarding phosphorus centered radicals.[16]

Since the introduction of phosphorus centered radicals in the literature, several types of persistent or stable radicals have been characterized. The sub-classes of phosphorus centered radicals include: phosphinyl ($\cdot PR_2$),[17] phosphonyl ($\cdot POR_2$),[18,19] phosphoniumyl $[\cdot PR_3]^+$,[20] and phosphidyl radical ions $[\cdot PR_3]^-$,[20] as well as phosphoranyl ($\cdot PR_4$) species.[21-24] The isolation and reactivity of these radicals have been the topic of several recent reviews, exemplifying a sustained interest in phosphorus radicals by those in the chemical sciences.[25-30]

- Section 1.1.3 – Historical Synopsis

Moses Gomberg published the first reported observation of a low-valent main group element in 1900, describing the synthesis and characterization of the triphenylmethyl radical ($Ph_3C\cdot$).[1] Having been unsuccessful in synthesizing tetraphenylmethane, a molecule of interest because of the considerable steric bulk surrounding the central carbon atom, Gomberg chose hexaphenylethane as a suitable substitute to pursue. Gomberg's goal was to reduce chlorotriphenylmethane in benzene with available reducing agents (zinc, silver, mercury) to yield the phenyl-substituted ethane. The result of the author's analysis was the formation of two products in equilibrium based on a crude elemental analysis in a bayonet tube (Scheme 1.1).[1]

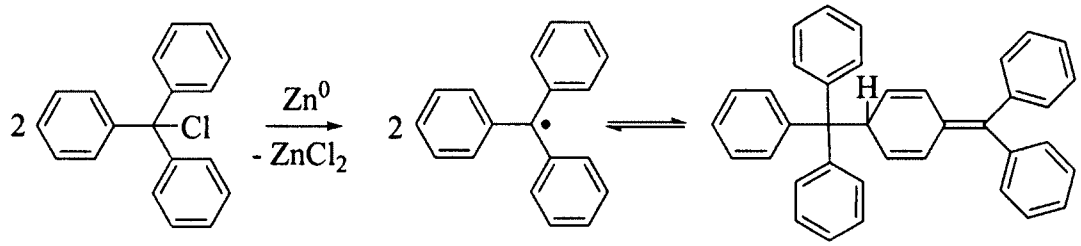

1(a) 1(b)

Scheme 1.1 Characterization of the first "low-valent" main group compound, the Gomberg radical.[1]

The significance of this discovery is embedded in the trivalent carbon species (Scheme 1.1a), the first characterized example of a low- or sub-valent main-group atom. This molecule has stimulated a new field of chemistry and altered the perceived limits of synthetically available molecules.

Candidly, the first direct observation of phosphorus centered radicals resonates from the isolation of elemental phosphorus in 1669 by Hennig Brandt, who was in search of the philosopher's stone. The reaction of freshly distilled white phosphorus (P_4) with small quantities of O_2 proceeds through a radical intermediate [$O + PO \rightarrow PO_2^*$] which emits light.[31,32] Due to its chemiluminescent properties, phosphorus was named after an ancient Greek word for the planet Venus, the morning star or bringer of light.[33]

The chronological origin of radical organophosphorus compounds emanates from proposed biological reactions in which free radical intermediates yield new carbon-carbon bonds.[34] Direct spectroscopic evidence of these phosphorus centered radicals was not observed until the late 1960s. Using a relatively new technique to synthetic chemists, electron paramagnetic resonance spectroscopy (EPR), Kochi *et al.* were able to describe the homoloysis pathway for organophosphorus compounds to act as free radical mechanism propagators. Through a series of experiments with known alkoxy- and thiyl-radicals the authors were able to identify the phosphoranyl [$\cdot\{(CH_3)_2CH\}PO(CH_3)_2$, g = 2.4, $a(^{13}C)$ = 23.2 mT (septet), $a(^{31}P)$ = 35.6 mT (doublet)] species responsible for observed homolytic displacement reactions in the EPR spectrum as a doublet of septets (Scheme 1.2).[4] This represents the cardinal description of a phosphorus-centered radical involved in carbon-carbon bond formation with substantiated mechanistic proposals.

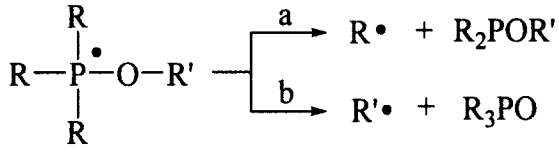

Scheme 1.2 The phosphoranyl species responsible for forming akyl-radical intermediates.[4]

Moving toward more recent synthetic approaches, Gynane *et al.* prepared the parent chlorides of the arsenic- and phosphorus-centered compounds $[(Me_3Si)_2CH]MCl$ (M = P or As).[7] The authors were successful in photolytically reducing the halo-pnictogens to the corresponding radical species in the presence of an electron rich olefin (Scheme 1.3). The products $[(Me_3Si)_2CH]M\cdot$ (M = P or As) were characterized using EPR in toluene at room temperature (g = 2.009, $a(^{31}P)$ = 9.63 mT, $a(^{1}H)$ = 0.640 mT). The authors contended that the steric bulk surrounding the phosphorus center hinders dimerization of the radical species in solution adding to their relative stability (>1 month) under inert conditions. Their findings lead the authors to define the phosphorus radical as the first "stable" phosphinyl ($\cdot PR_2$) in the literature.

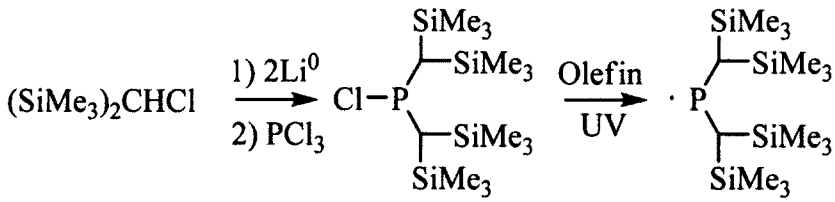

Scheme 1.3 Synthesis of the disilyl-phosphinyl radical.[7]

Later, Cowley *et al.* prepared the aforementioned $\cdot P[CH(SiMe_3)_2]_2$ radical (Scheme 1.3) using an alternate pathway and identified the reduction by-products.[35] The parent chlorophosphine $[CH(SiMe_3)_2]PCl$ was reduced to the corresponding diphosphine $\{P[CH(SiMe_3)_2]_2\}_2$, as well as the previously uncharacterized phosphine $[CH(SiMe_3)_2]_2PH$ and phosphaalkene $(Me_3Si)_2C{=}PC(H)(SiMe_3)_2$. These products were

synthesized independently and compared to unassigned peaks in the original $^{31}P\{^{1}H\}$ NMR spectrum. Furthermore, *via* reduction of the phosphinyl with sodium metal the phosphide $[P\{CH(SiMe_3)_2\}_2][Na]$ was able to be characterized (Scheme 1.4). The presence of phosphide suggested that the original synthesis from the chlorophosphine to the neutral diphosphine occurs though a mechanism based on the anionic derivative.[7]

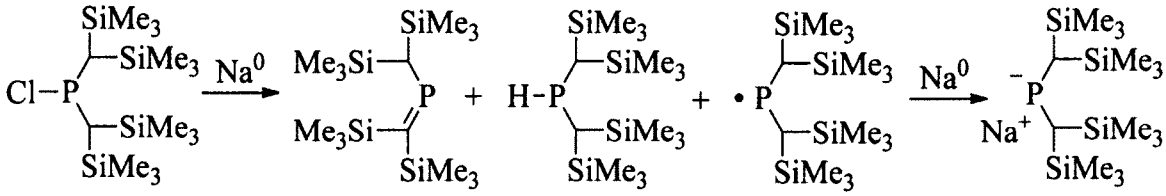

Scheme 1.4 Synthesis of $\cdot P[CH(SiMe_3)_2]_2$, $[CH(SiMe_3)_2]_2PH$, $(Me_3Si)_2C{=}PC(H)(SiMe_3)_2$ and $[P\{CH(SiMe_3)_2\}_2][Na]$ through reduction of $[CH(SiMe_3)_2]PCl$ with sodium metal.[35]

At this point it would be of value to interject with a brief overview of the principles and practical outcomes of electron paramagnetic resonance spectroscopy and its utility in describing compounds with unpaired electrons.

Section 1.2 – Introduction to EPR

The following outlines the basic theory of electron paramagnetic resonance (EPR) spectroscopy. The objective of this review will be to provide a rudimentary understanding of the theoretical beginnings of EPR such that discussion of experimental findings and comparison to relevant literature may be conducted with confidence. The *g*-value, a measure of relative energy of an unpaired electron to that of a free electron, as well as hyperfine coupling, the interaction of the unpaired electron with the magnetic field generated by adjacent nuclei, will be discussed.

- Section 1.2.1 – Fundamental Principles of EPR Spectroscopy

Electrons are identified by an intrinsic mechanical angular momentum (m_s) referred to simply as spin (*S*). They behave analogously to a spinning top and are defined by a vector of angular momentum based on this rotation. Spin can be identified by two degenerate states, $\alpha = + ½$ or $\beta = - ½$, which is the vector property of rotation in the Cartesian *z*-plane. Because a range of *x* and *y* components exist simultaneously for an electron and cannot be determined in a given sample, the *z*-coordinate is given as the base definition. The magnetic moment (μ_e) of an electron is proportional to the electron spin angular momentum (*S*) which can be defined by the equation $\mu_e = g\mu_B S$ in which: *g* is the Landé factor, an energetical definition of a particle in a magnetic field (free electron $g = 2.002319$) having both spin angular momentum (*S*) and orbital angular momentum; μ_B is the atomic unit of the magnetic moment also referred to as the Bohr magneton ($\mu_B = -|e|h/4\pi m_e = -9.27410^{-24}\,JT^{-1}$ where m_e = mass of electron, *e* = electron charge *h*, = Planck constant = $6.626 \times 10^{-34}\,m^2kgs^{-1}$); *S* is the spin angular momentum of an electron ($\alpha = + ½$ or $\beta = - ½$). This is the functional equation that permits analysis of electrons in a magnetic field using EPR spectroscopy. By measuring the energetical absorption (microwave radiation) in an external magnetic field, experimental *g*-values for unpaired electrons can be established and used toward identification and characterization of radical containing species.

For a bulk sample the sum of the magnetic moments of the electron spins is defined as a vector (M). The rotation of this vector in the *x,y*-planes is called the *Larmor precession*. Simply put, EPR spectroscopy aims to manipulate the bulk electron spin

vector of a sample using microwave radiation in a magnetic field monitoring the absorption and emission of energy. The effective magnetic field applied to the sample must overcome the *Larmor frequency* such that the spin vector (M) is converted to a parallel orientation with the applied magnetic field (B_1) and perpendicular to the *z*-plane. During this process the degenerate energy levels of the electron split based on spin (*S*), a phenomenon referred to as the *Zeeman effect*. The interaction of an external magnetic field with an electron is called the electron *Zeeman interaction*. For an electron to transition from a β-spin (lower energy) to an α-spin (higher energy) state, the β-state can absorb a quantum of electromagnetic (microwave) energy and be excited to the α-state defined by the equation $h\nu = E_\alpha - E_\beta = g|\mu_B|B_0$ (3.5T is a standard magnetic field). To absorb the energetical quanta the oscillating magnetic field should be perpendicular to the static B_0 (*Zeeman field*, if $B_0 \neq 0$ then α and β are not degenerate). The energy associated with this transition is $E = -\mu_e \cdot B = g|\mu_B|S \cdot B$. Along the *z*-axis $E = g|\mu_B|S_z B_0$ and because *S* = (α = + ½ or β = – ½), the energy of an unpaired electron can be defined as $E = \mp(1/2)g|\mu_B|B_0$. In short, EPR spectroscopy defines unpaired electrons by energetical absorption in a magnetic field.

Several experimental concerns emerge while considering the nature of identifying unpaired electrons based on orbital geometry and the orientation of the sample. Since spin-orbital interactions are anisotropic, orbital character is important to define the *g*-value of the electron. Based on phase considerations single crystal EPR spectroscopy can provide static *g*-values, a function of anisotropy in the crystalline state, while solution EPR spectroscopy can only provide average *g*-values due to molecular tumbling which

quenches the orbital angular momentum of an electron by effectively averaging out all orientations simultaneously. In this process, electron angular momentum, in the absence of spin-orbital coupling, is only due to spin. Because $\Delta g = g - g_e$ for an organic molecule and spin-orbital coupling are atom dependent, the g-values in organic molecules do not deviate far from the value of a free electron.[36]

- Section 1.2.2 – Hyperfine Coupling

As would be found in traditional nuclear magnetic resonance (NMR) spectroscopy, coupling can be observed with adjacent atomic nuclei. Electrons are affected by the nuclear spin of adjacent nuclei which are also defined by a spin angular momentum and directional magnetic fields (*nuclear Zeeman effect*). Because a nucleus has a spin angular momentum, an electron can interact with the magnetic moment of that nucleus, in turn affecting the resonance conditions of the electron, a phenomenon referred to as the hyperfine interaction.

The magnitude of hyperfine coupling for a given sample is dependent on two factors: (1) the aforementioned *nuclear Zeeman effect* which is based on the magnetic moment of the nucleus and (2) the hyperfine field (dipole) experienced by an electron. When only considering nuclei with only one isotopic spin state, the *nuclear Zeeman effect* is canceled and we may only consider the hyperfine interaction. Hyperfine coupling considers the dipole-dipole interaction between the electron spin magnetic dipole and the magnetic dipole moment of a nucleus. Nuclear movement generates a magnetic field which is "felt" by the electron. Because the dipolar interaction is anisotropic the hyperfine separation in the EPR spectrum depends on the orientation of the molecule in

the magnetic field (B). In a solution sample the orientations are assimilated and the dipolar interaction is defined as an average value. Practically, the coupling of unpaired electrons with spinning nuclei follows the $2n + 1$ rule of coupling where I is the isotope's spin. Complex splitting patterns can be present if the unpaired electron is distributed throughout a molecule, interacting with several nuclei. The rules for splitting patterns in EPR spectroscopy are analogous to those found in NMR spectroscopy. The magnitude of the coupling constant defined as $E_{hf} = aS \cdot I$ where a is the hyperfine coupling constant, S is electron spin quantum number and I is the nuclear spin number.[36]

- Section 1.2.3 – Basic Instrument Set-Up

There are two requirements to invoke a response by unpaired electrons in an EPR sample: (1) a sufficient microwave source and magnetic field to drive the EPR transition, and (2) to convert the response to a discernable signal. EPR spectroscopy is completed in the X-band (8-12 GHz) of microwave radiation. A sample is introduced into a magnetic field and is exposed to a microwave source travelling through a resonator. The sample absorption is monitored by a detector and converted to a digital readout.

The source is most commonly a 9.5 GHz medium frequency continuous wave (CW) microwave region (klystron) passing through a resonator (1-100 GHz). The resonator is simply a resonant cavity that allows microwaves to pass through an iris, maximizing the applied magnetic field at the sample site. The applied magnetic field is generated by an oscillator in a tunable cavity and is monitored with a Hall-effect detector, a transducer that changes its output voltage depending on the external magnetic field. A detector monitors the emission of energy derived from the spin vector relaxation of the

sample to the *Larmor* precession. This is generally a solid-state diode that is sensitive to microwave radiation. The absorption of microwave frequency is plotted against the magnetic field intensity and the derivative of the absorption curve is then generated for analysis.[37]

Section 1.3 – Review of Relevant Literature

The synthesis and characterization of the disilyl-diphosphine, $\{P[CH(SiMe_3)_2]_2\}_2$, informally re-oriented the research of phosphorus centered radicals toward modern synthetic approaches and spectroscopic techniques. The following review will cover transition metal complexes, aryl-substituted and carbene- radical ions, diphosphenyl radical systems, as well as neutral phosphinyl species since the $\{P[CH(SiMe_3)_2]_2\}_2$ diphosphine was reported in the literature, highlighting recent advances in the field of phosphorus centered radicals.

- Section 1.3.1 – Transition-Metal Coordination Chemistry

The first method of stabilizing phosphorus centered radicals that will be examined is coordination complexes with transition metals. The addition of the radical electron into an empty metal-centered *d*-orbital can serve as a useful trapping mechanism of potentially unstable radical species. Based on the ligands surrounding the metal center, delocalization of the unpaired electron as well as steric protection by the ligands in the coordination complex can aid in stabilizing the reactive species.

Stemming from the success of the disilyl-phosphorus radical,[6,7,35,38,39] Cowley *et al.* set out to use phosphinyl radicals ($\cdot PR_2$) as ligands in coordination chemistry as a synthetic intermediate between phosphenium cations $^{+}[PR_2]$ and phosphide anions $^{-}$

$[PR_2]$.[38] The focus was to make metal-carbonyl complexes with a phosphinyl radical ligand, thereby yielding synthetically and catalytically interesting organometallic complexes. The first target metal complex was $Fe_2(CO)_9$ which upon reaction with the phosphinyl radical $[(Me_3Si)_2CH]_2P\cdot$ yielded an organometallic radical $[\{(Me_3Si)_2CH\}_2PFe(CO)_4]\cdot$ and $Fe(CO)_5$, which was removed *in vacuo* (Scheme 1.5a, g = 2.004). NMR, Mössbauer and EPR spectroscopy were used to characterize the product which indicated that the unpaired electron was centered on iron with no observed hyperfine coupling to phosphorus or hydrogen. The phosphorus radical was also reacted with $Co_2(CO)_8$ forming a three membered hetero-metallocycle with an unpaired electron shared through resonance between the two cobalt atoms (Scheme 1.5b, g = 2.001, $a(^{59}Co)$ = 3.4 mT). This indicates that phosphinyl radicals acting as ligands in conjunction with metal complexes can act as three electron donors to the metal complex. The phosphorus lone pair forms the dative interaction while the radical electron is transferred into the lowest unoccupied molecular orbital (LUMO) of the metal forming the singly occupied molecular orbital (SOMO).

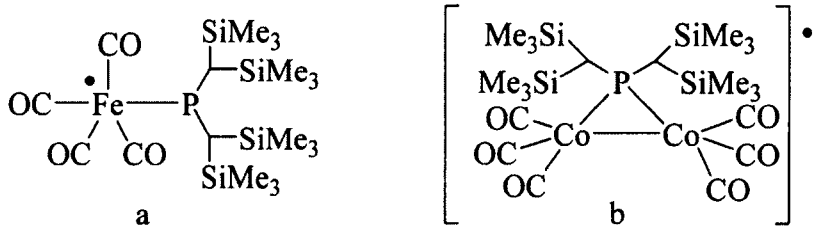

Scheme 1.5 Complexes formed by the reaction with metal carbonyls and a bulky phosphinyl radical.[38]

Ndiaye *et al.* also synthesized paramagnetic metal carbonyl complexes.[9] Addition of diphenylphosphinyl radical to metal hexacarbonyls $M(CO)_6$ yields the corresponding phosphinyl metal carbonyl complexes $[M(CO)_5P(C_6H_5)_2$, M = Cr, Mo, W]. Single crystal

X-ray crystallographic analysis, Density Functional Theory (DFT) calculations and single crystal EPR measurements were used to characterize the products. Evidence in the increase in anisotropy (g = 2.0050→2.0211) indicated significant delocalization of spin density from the phosphorus center 3*p* orbital to the *d*-orbital of the molybdenum and tungsten pentacarbonyl complexes.

Interested in studying the manner in which a Li/Cl-phosphinidenoid complexes with a metal center, Schön *et al.* prepared a *P*-chlorophosphane complex of tungsten pentacarbonyl.[40] The resulting species was shown to undergo a one-electron oxidation using a trityl borate $[Ph_3C][BF_4]$ at low temperatures and subsequent elimination of the triphenylmethyl radical (Gomberg radical).[1] The transient phosphanyl intermediate was characterized using EPR spectroscopy which indicated coupling of an unpaired electron to a phosphorus nuclei [g = 2.002(2)]. Radical coupling reactions with the eliminated Gomberg radical were observed yielding a rearrangement product, the first phosphaquinomethane complex described in the literature (Scheme 1.6).

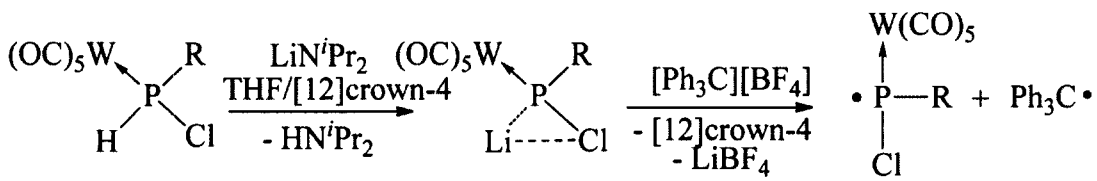

Scheme 1.6 Synthesis of a transient chlorophosphanyl-tungsten complex.[40]

Based on the chemical similarities between phosphorus and carbon, Scheer *et* al. set out to synthesize the phosphorus analogue of an allyl radical.[41] The triphosphaallyl radical (Scheme 1.7) is a three membered phosphorus functional group containing a delocalized radical electron. Photolytic cleavage of pentamethylcyclopentadienyl radical and addition of *Mes-diphosphene affords the triphosphaallyl species coordinated to a

tungsten carbonyl complex. The EPR spectrum indicated a doublet of triplets (g = 2.0176) derived from hyperfine coupling with the apical phosphorus atom ($a(^{31}P)$ = 2.11 mT) as well as the terminal phosphorus atoms ($a(^{31}P)$ = 8.91 mT) in the triphosphaallyl structure.

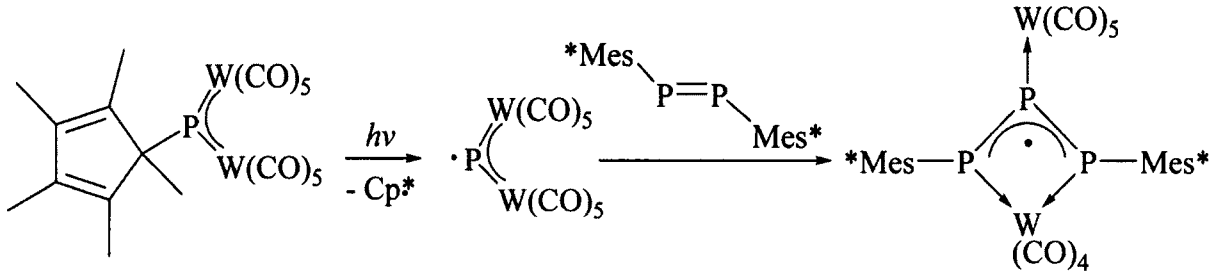

Scheme 1.7 Synthesis of a triphosphaallyl radical and its tungsten complex.[41]

Reactions of phosphorus centered radicals with metal centers outline their utility as one- or three-electron donors. The formation of various metal complexes with significant spin density transfer to the metal centers indicates a promising synthetic route toward radical metal species with potential applications in catalysis or as spin trapping agents.[42,43]

- Section 1.3.2 – Diphosphenyl Radicals

A second method for stabilizing phosphorus radicals is to provide an adjacent electronegative atom.[10,11,44] Delocalization of the radical electron among the multiple atoms can electronically stabilize the unpaired electron while the ligands about the diphosphenyl core provide steric hindrance against dimerization or intermolecular degradation.[43,45,46] Under these pretences, Loss *et al.* attempted the synthesis of phosphorus based free-radicals as potentially effective spin labeling molecules.[47] Their choice was based on the nuclear spin of ^{31}P, the only isotope of phosphorus, which has

spin ½ and 100% abundance making it an ideal spin trap agent to induce large anisotropic hyperfine coupling in EPR spectra. As a model molecule to display the potential of phosphorus centered radicals, the authors set out to synthesize the diphosphanyl [Mes*(Me)P–PMes*]· radical which has both steric bulk and delocalization potential (Scheme 1.8). The synthetic route chosen was to reduce the parent phosphonium triflate [Mes*(Me)P=PMes*][O_3SCF_3] electrochemically ($E_{1/2}$ = -0.37V) in the presence of tetrakis(dimethylamino)ethylene (TDE) yielding the diphosphanyl radical [Mes*(Me)P–PMes*]· (g = 2.008, spin density P_1 = 62%, P_2 = 15%, $a(^{31}P_1)$ = 250 MHz, $a(^{31}P)$ = 390 MHz). The stability (>7days) of the diphosphanyl species is much longer than previously thought to be isolable and were well positioned to study fast molecular movements based on the observed anisotropy.

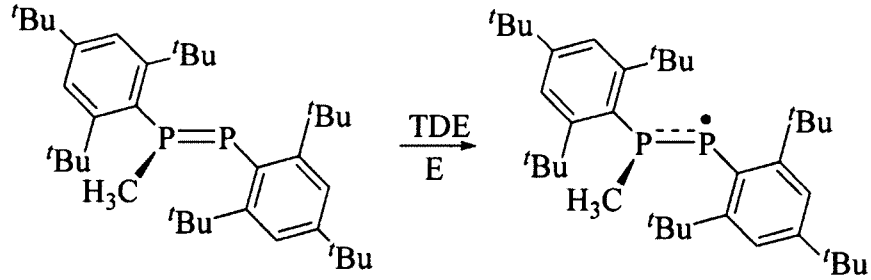

Scheme 1.8 Electrochemical synthesis of a persistent diphosphanyl radical.[47]

Later, Geier *et al.* questioned whether "naked" dianionic phosphorus species in the $[R_4P_4]^{2-}$ scaffold could be made synthetically through reduction of $[Na_2(P_4Ph_4)(THF)_4$tetramethylurea] in a mixture of tetramethylethylenediamine (tmeda) and dimethoxyethane (dme) using a sodium/potassium complexing [2.2.2]cryptand reducing agent.[48] Fractional crystallization yielded an EPR active species (g = 2.0089) with hyperfine coupling indicative of two identical phosphorus atoms ($a(^{31}P)$ = 115 MHz). The spectrum was assigned to the free diphenyldiphosphenyl radical anion

$[P_2Ph_2]^{\cdot -}$. It was suggested that the radical was generated by the homolytic cleavage of the $[P_4Ph_4]^{2-}$ dianion formed in the initial reduction. This process was found to be reversible as introduction of sodium triflate yields the parent structure. The authors interject that the relative instability of the "naked" $[P_4R_4]^{2-}$ chain is based on Columbic repulsion between adjacent negative charges, therefore undergoing an elimination reaction yielding the radical anion.

- Section 1.3.3 – Aryl-Substituted Phosphorus-Centered Radical Ions

Another useful tool in isolating radical phosphorus species is to synthesize molecules with the ability to delocalize electron density through the charge distribution of an ionic or zwitterionic framework.[44,49-54] These principles can generally be extended to include highly conjugated or cage structures.[55-59] Although the following species can be defined through alternative Lewis structure arguments their classification will be based on spin density distribution data when available.

The first poignant example of a phosphorus centered radical ion comes from Sasaki *et al.* who set out to synthesize quinoid analogues of heavier main group elements. The challenge is embedded in the relative instability of double bonds between carbon and heavier elements such as phosphorus.[60] The authors' approach was to surround the phosphorus-carbon double bond with steric bulk forming a kinetically stabilized P=C bond. The structure of the 3,5-di-*tert*-butyl-4-oxocyclohexa-2,5-dien-1-ylidene phosphaalkene was characterized using X-ray crystallography which indicated a P=C bond distance of 1.705(2) Å, typical for P=C double bonds. Reduction of the phosphaalkene with sodium metal in THF yielded the corresponding radical anion

(Scheme 1.9). Conjugation in the system allowed for resonance stabilization of the product *p*-phosphaquinone characterized as a doublet in the EPR spectrum. Analysis indicated that 64% of the electron density of the unpaired electron is centered on the phosphorus (3*p*) atom (g = 2.0069, $a(^{31}P)$ = 9.3 mT).

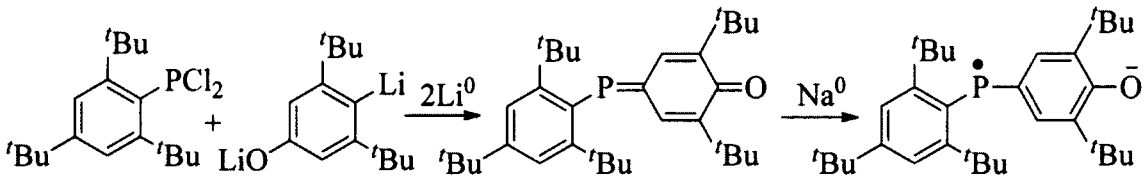

Scheme 1.9 Synthesis of the first stable *p*-phosphaquinone.[60]

Sasaki *et al.* then probed the electronic properties of sterically encumbered triaryl-pnictogens. Their interest in tris(2,4,6-triisopropylphenyl)pnictogens was based upon the steric protection surrounding the pnictogen center.[61] Theoretically, this provides a site in which a potentially reactive species could be isolated. The authors employed an organo-copper reducing agent to generate the triply substituted pnictogen (Scheme 1.10). X-ray crystallography indicated that the aryl-substituents were arranged in a propeller-like sequence about the pnictogen center. The phosphorus radical cation [(2,4,6-triisopropylphenyl)$_3$P]$^{+\cdot}$ was synthesized through oxidation with silver perchlorate (g = 2.007, $a(^{31}P)$ = 23.7 mT).

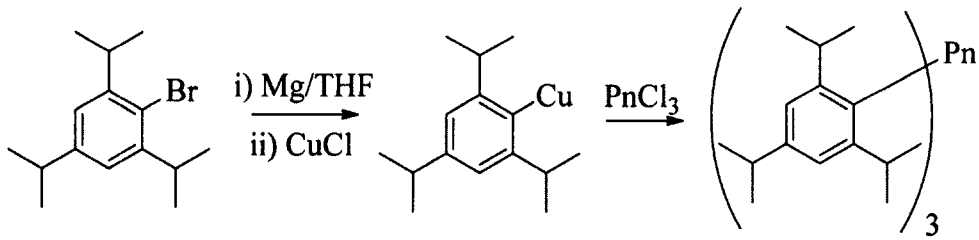

Scheme 1.10 Synthesis of sterically bulky triaryl-pnictogens.[61]

Sutoh *et al.* also synthesized sterically bulky triarylphosphines featuring one, two or three 2,6-diisopropylphenyl groups substituted by a para-ferrocenyl group.[62] Electrochemical oxidation of the triarylphosphines suggested a reversible process in one to four steps from the neutral P(4-ferrocenyl-2,6-diisopropylphenyl)$_3$ to the subsequent oxidation products [P(4-ferrocenyl-2,6-diisopropylphenyl)$_3$]$^{+\cdot}$ (0.16V), [P(4-ferrocenyl-2,6-diisopropylphenyl)$_3$]$^{2+\cdot}$ (0.23V), [P(4-ferrocenyl-2,6-diisopropylphenyl)$_3$]$^{3+\cdot}$ (0.23V) and [P(4-ferrocenyl-2,6-diisopropylphenyl)$_3$]$^{4+\cdot}$ (0.57V). Silver perchlorate in dichloromethane was used as a reducing agent to yield the radical cation derivatives. The samples were cooled to cryogenic temperatures (5 K) to record EPR spectra which displayed hyperfine coupling to phosphorus (g = 2.005, $a(^{31}P)$ = 38.6 mT) in the frozen solution. Based on the electrochemical and EPR analysis, the sterically crowded triarylphosphines were shown to have considerable stabilization effects toward hosting radical cations.

Furthering these observations, Yasui *et al.* set out to identify the degradation pathway of triarylphosphines (PAr_3) to the corresponding phosphine-oxides ($O{=}PAr_3$), anticipating it proceeds through a radical mechanism.[63] The electrochemical one-electron oxidation of sterically encumbered triarylphosphines was shown to lead to the radical cation $[PAr_3]_3^{+\bullet}$ which while undergoing photolytic reactions with oxygen was suspected to go through a peroxy radical cation intermediate [Ar_3P^+-O-O$^\bullet$]. The suggested intermediate was observed in the case of $Mes_3P^{+\bullet}$ and its transition to Mes_3P^+-O-O$^\bullet$ as an intermediate to $Mes_3P{=}O$. Varying the bulk of the ligands surrounding the phosphorus

center affected the quantum yields and provided insight into the oxidation mechanism of tertiary phosphines to the corresponding phosphine-oxides.

Recently, Boeré *et al.* looked extensively at tris(2,6-diisopropylphenyl)phosphine ($Dipp_3P$).[64] $Dipp_3P$ was synthesized starting from the arylbromide by converting it to the aryl-copper reagent and adding PCl_3. Fluoresence, solution and solid state NMR, dynamic NMR, quantum mechanical calculations [HF/6-31G(d) and B3LYP/6-31G(d)], electrochemical analysis, Fourier transform voltammetry, EPR and X-ray crystallography were all used to characterize the tertiary phosphine ($Dipp_3P$) and its radial cation $[Dipp_3P]^{+\bullet}$ generated through bulk electrolysis ($E_{1/2}$ = 0.09V vs $F_c^{+/0}$). Based on the electrochemical analysis, the authors were able to chemically generate the radical cation using several one-electron oxidizing agents ($AgClO_4$, $AgPF_6$ and $AgSbF_6$). The radical cation was shown to be persistent (weeks or months) in solution and was characterized using EPR spectroscopy (77 K). Hyperfine coupling was observed between the unpaired electron and the phosphorus nucleus (g = 2.008, $a(^{31}P)$ = 23.9 mT) generating a large doublet featuring small coupling owing to interactions with unidentified hydrogen nuclei.

- Section 1.3.4 – Carbene-Stabilized Phosphorus Radical Ions

Betrand and coworkers have recently been successful using carbenes to stabilize phosphorus radicals. Carbenes are compounds with a divalent carbon atom featuring a lone pair of electrons. Bertrand *et al.* used the electron donating ability of N-Heterocyclic Carbenes (NHC) and Cyclic(Alkyl)(Amino) Carbenes (CAAC) to isolate P_2-radical cations and P_2-dications.[12] Specifically, the reaction of a CAAC with white phosphorus yielded a P_2 bridged, 2,3-diphosphabutadiene species which through resonance

arguments can be viewed as an electron rich P_2 *bis*-phosphinidene fragment capped by two carbenes, or as a zwitterionic structure (Scheme 1.11). Electrochemical analysis indicated a one-electron oxidation at $E_{1/2}$ = -0.536 V (vs. Fc^+/Fc) which the authors exploited synthetically using a trityl borate $[Ph_3C][B(C_6F_5)_4]$ under an inert atmosphere to yield a crystalline radical cation. EPR spectroscopy of the radical diplayed a triplet of quintets (g = 2.009, $a(^{31}P)$ = 42 G, $a(^{14}N)$ = 3 G), a result of coupling of the radical electron with the two equivalent phosphorus atoms and two nitrogen atoms. A similar synthesis was carried out with an NHC yielding an analogous radical cation to that of the CAAC.

Cyclic(Akyl)(Amino) Carbene (CAAC) N-Heterocyclic Carbene (NHC)

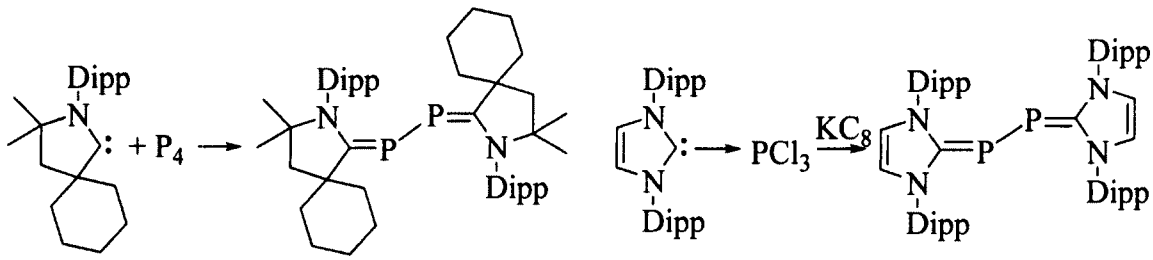

Scheme 1.11 Synthesis of the precursors to carbene stabilized phosphorus centered radical cations.[12]

Later, Bertrand *et al.* set out to isolate the $[PN]^{\cdot+}$ radical cation.[65] This species was of particular interest as a component of the interstellar media surrounding Jupiter and Saturn. This species had only been observed previously as a monomer in coordination with metal atoms at 10 K, a finding which was debated in the literature. A synthetic route employing both an NHC and CAAC was proposed, installing the PN fragment sandwiched between the two carbene ligands (Scheme 1.12). After identifying the one-electron reduction potential ($E_{1/2}$ = -0.51V) electrochemically, a trityl borate $[Ph_3C][B(C_6F_5)_4]$ was employed to synthesize the radical cation $[(NHC)[PN](CAAC)]^{\cdot+}$

of the PN-bridged, carbene-capped parent structure. EPR spectroscopy displayed a large doublet (g = 2.0048; $a(^{31}P)$ = 44 G) based on coupling to phosphorus. This species has since been examined as a possible phosphorus mononitride (PN) transfer reagent based on the leaving group ability of carbenes.[66]

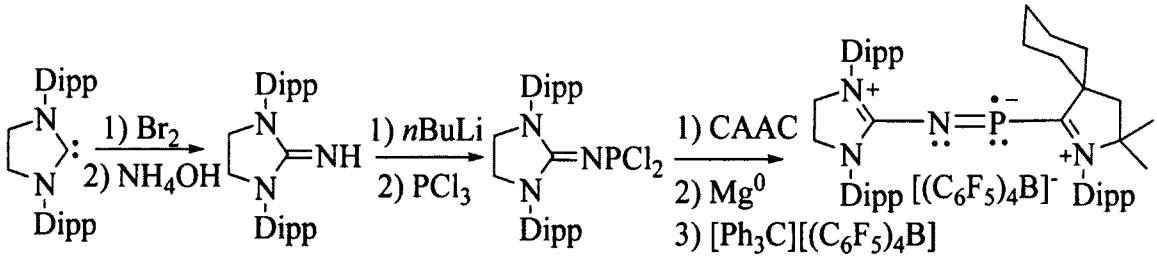

Scheme 1.12 Synthesis of the precursor to the carbene stabilized $[PN]^{\cdot+}$ radical cation.[65]

Back *et al.* then set out to isolate a crystalline, monomeric phosphinyl radical cation.[13] Starting with a commercially available dichlorophosphine, addition of a Cyclic(Alkyl)(Amino) carbene and reduction with magnesium yielded an amine substituted phosphaalkene.

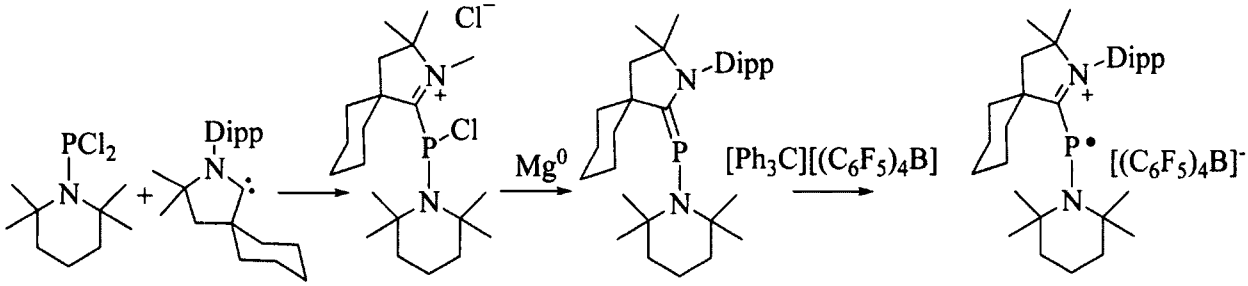

Scheme 1.13 Synthetic route to a persistent phosphinyl radical cation.[13]

One-electron oxidation with a trityl borate $[Ph_3C][B(C_6F_5)_4]$ provided a synthetic route to a relatively stable phosphinyl radical cation (Scheme 1.13). Admittedly, there are two resonance structures which could contribute to the molecule: (1) a phosphinyl radical adjacent to a cationic carbene ligand or (2) a carbene stabilized phospheniumyl radical. EPR spectroscopy of the radical cation displayed a doublet of multiplets owing to large

hyperfine coupling to phosphorus (g = 2.007, $a(^{31}P)$ = 99 G) and small coupling to either one or two nitrogen atoms [$a(^{14}N)$ = 4 G].

- Section 1.3.5 – Phosphinyl Radicals

The following section will evaluate compounds under the heading of phosphinyl radicals ($\cdot PR_2$). This section will focus on ligand design as a method for preventing reactivity or irreversible dimerization of phosphorus radicals starting with a reinvestigation of a model phosphinyl radical in the literature, the aforementioned "jack-in-the-box" radical.

The nature of the diphosphine $[P\{CH(SiMe_3)_2\}_2]_2$ and its dissociated monomeric radical $\cdot P[CH(SiMe_3)_2]_2$ was re-evaluated with modern techniques by Hinchley *et al.* to ascertain the mechanism of radical formation.[67] The authors described this species as a "molecular jack-in-the-box", a moniker attributed to the diphosphine due to the strained rotation of the bulky trimethylsilyl ligand groups. Observed in the solid state using single crystal X-ray diffraction, the parent diphosphine serves as an energy storage unit in which energy is cached in the central P-P bond. While undergoing solvation the diphosphine springs apart forming two equivalents of the monomeric phosphinyl radical. Gas-phase *ab initio* calculations at the UB3LYP/DZP level suggested an exothermic dissociation process overall, supporting the observed qualitative relationship between the solid phase dimer and solvated monomer. Hinchley *et al.* then attempted to elucidate the role of bulky ligands in the kinetic stabilization of coordinatively unsaturated molecules.[17] The $\cdot P[CH(SiMe_3)_2]_2$ and $\cdot As[CH(SiMe_3)_2]_2$ "jack-in-the-box" radicals were discussed in the context of kinetic as well as thermodynamic stabilization. The authors described the

competing nature of the homolytic dissociation process yielding the monomeric radical, which is based on the steric strain on the central bond as a result of the bulky ligands surrounding it. In an attempt to minimize steric interactions the central P-P bond dissociates, destabilizing the parent dipnictogen. Simultaneously, the steric bulk of the ligand infers kinetic stabilization to the monomeric, dissociated radical by physically shielding the coordinately unsaturated pnictogen center and hindering undesired dimerization.[68]

Recently, Cowley *et al.* revisited the "jack-in-the-box" diphosphine (Scheme 1.3) investigating its reactivity profile with the heavier chalcogens (Scheme 1.14).[69] The result was the formation of the chalcogen-bridged, ethereal products of the diphosphine (S_8, Se^0, Te^0). The reported yields with sulfur (one crystal, <1%), selenium (72%) and tellurium (31%) are low. Characterization of the products was admittedly incomplete by the authors leading to questions regarding the purity of the bulk samples which were characterized by X-ray diffraction, $^{31}P\{^1H\}$ NMR and mass spectrometry.

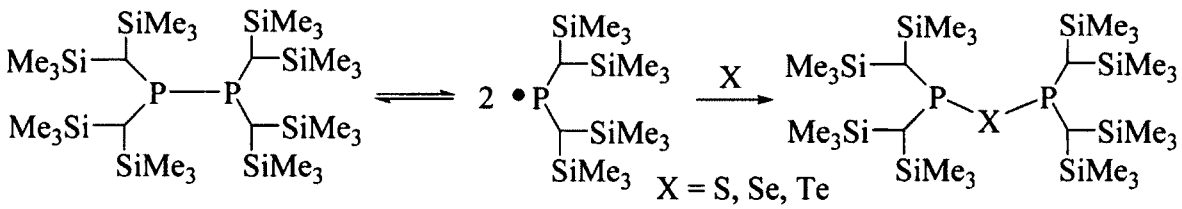

Scheme 1.14 Reactivity of the "jack-in-the-box" diphosphine with elemental chalcogens.[69]

Several other sterically encumbered diphosphines have been reported in the literature, including those by Gynane *et al.* who prepared a series of related phosphorus and arsenic radicals.[6] Their study aimed to identify trends based on: (i) the link to the trimethylsilyl ligands, (ii) the ligands themselves, (iii) and the symmetry about the

pnictogen center (M = P or As). Rather than the methyne ($M[CH(SiMe_3)_2]_2$) link in the "jack-in-the-box" diphosphine (Scheme 1.3),[67] the new species contained amine links $M[N(SiMe_3)_2]_2$, as well as mixed ligand species including $M(N^iPr_2)[N(SiMe_3)_2]$, $M(N^iPr_2)[N(SiMe_3)(CMe_3)]$ and $M(CMe_3)[N(SiMe_3)_2]$. These ligands infer alternative steric and electronic properties to the phosphorus- and arsenic-centered radicals. A correlation was attempted to be drawn between the relative stability of the radical species and their structural components. The results indicated a modest trend toward symmetry incurring stability and longevity on the radicals over non-symmetrical species. The conclusions of the paper suggested that a large proportion of the unpaired spin density was found on the pnictogen centers with hyperfine coupling from the heteroatom substituents (Table 1.1).

Table 1.1 EPR spectroscopy data for asymmetric phosphinyl radicals.[6]

Radical	a(M)/mT	$a(^1H)$/mT	$a(^{14}N)$/mT	g	$t_{1/2}$
$\cdot P[CH(SiMe_3)_2)_2]$	9.63	0.64		2.009	> 1 year
$\cdot P[N(SiMe_3)_2)_2]$	9.18			2.008	10 days
$\cdot P[CH(SiMe_3)_2][N(SiMe_3)_2]$	9.3	0.81		2.008	10 days
$\cdot P[CH(SiMe_3)_2][N^iPr_2]$	6.3		0.37	2.005	1 day
$\cdot P[N(SiMe_3)_2][N^iPr_2]$	7.72		0.52	2.007	1 day
$\cdot P[N(CMe_3)SiMe_3]_2$	10.15			2.007	5 days
$\cdot P[N(CMe_3)(SiMe_3)(N^iPr_2)]$	7.4		0.51	2.007	3 days
$\cdot P[CH(SiMe_3)_2](NMe_2)$	6.5			2.008	
$\cdot P(2,4,6\text{-}C_6H_2Me_3)[N(SiMe_3)_2]$	9.67			2.008	

Later, Bezombes *et al.* successfully reduced the parent chlorophosphine $PCl[N(SiMe_3)_2](N^iPr_2)$ yielding a colourless crystalline solid identified as the asymmetric diphosphine $\{P[N(SiMe_3)_2](N^iPr_2)\}_2$.[70] Sublimation induced dissociation of the elongated central P-P bond (2.259(2) Å) and permitted the isolation of the yellow monomeric

radical (g = 2.0046, $a(^{31}P)$ = 75.9 G, $a(^{14}N)$ = 5.95 G). Upon cooling to ambient temperatures, the P-P dimer was reformed (Scheme 1.15). The dissociation enthalpy of the system was determined to be 54 $kJmol^{-1}$ based on the GED and X-ray solid state structures, supporting the author's conclusion that the sterically crowded diphosphine is primed for homolytic cleavage.

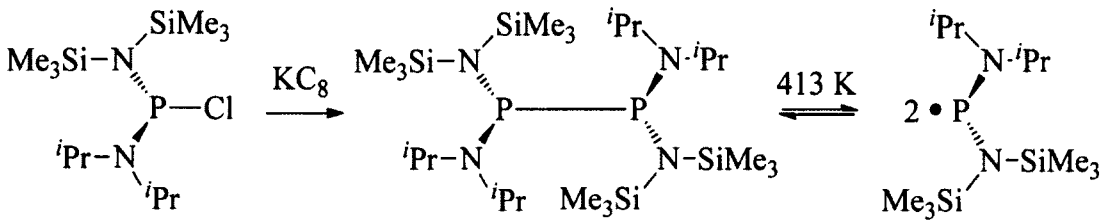

Scheme 1.15 Synthesis and temperature induced dissociation of the asymmetric $\{P[N(SiMe_3)_2](N^iPr_2)\}_2$ diphosphine.[70]

Bezombes *et al.* also employed their asymmetric, sterically bulky diphosphine to activate white phosphorus (P_4).[71] The dissociation of the diphosphine and activation of P_4 was only possible in refluxing benzene, yielding the *trans,trans*-tetraphosphabicyclobutane insertion product referred to in the literature as a "butterfly" structure. The central P-P bond retains partial double bond character (2.165(5) Å) compared to those of the remaining P-P bonds. The mechanism of activation is presumably based on a radical initiated ring opening reaction of one bond in the P_4 tetrahedron and subsequent radical coupling with a second phosphinyl moiety, as suggested in a recent review on the main group reactivity of white phosphorus.[72] Also included in this paper are the reactions of the asymmetric diphosphine with: (i) chromium hexacarbonyl yielding a phosphinyl-capped, chromium tricarbonyl bridging species and (ii): $Co(NO)(CO)_3$ forming a terminal complex of one phosphinyl moiety and cobalt tricarbonyl featuring the elimination of nitric oxide (NO).

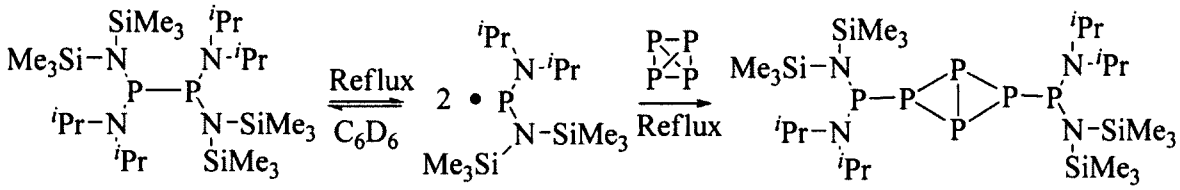

Scheme 1.16 Dissociation of a sterically bulky diphosphine and subsequent activation of P_4 at reflux temperatures in toluene.[71]

Dumistrescu *et al.* recently attempted to synthesize a series of phosphinyl radicals featuring the bulky 2,6-bis(trifluoromethyl)phenyl substituent.[73] The bis(trifluoromethyl)phenyl group acts as a steric wall and can prevent intramolecular C-H activation of other bulky aryl substituents (Dipp, Mes). Electronically these ligands are stabilizing and act as σ-withdrawing substituents. Reduction of the parent chlorophosphines (Scheme 1.17) to the corresponding phosphinyl radicals was achieved using UV irradiation (λ = 254 nm) in the presence of tetrakis(dimethylamino)ethene (TDE). The EPR spectra displayed coupling with phosphorus (^{31}P), nitrogen (^{14}N), six fluorine (^{19}F) and two hydrogen nuclei (^{1}H). Furthermore, the EPR signal was present for time periods greater than one week indicating persistent nature of these phosphinyl radicals.

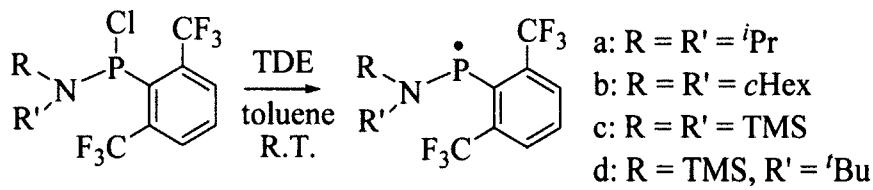

Scheme 1.17 Synthesis of persistent phosphinyl radicals featuring 2,6-bis(trifluoromethyl)phenyl and bulky amino substituents.[73]

Agarwal *et al.* then set out to isolate a neutral phosphinyl radical which could be characterized in the solid state as a monomer, something which had not been done to date.[8] The authors contended that two criteria must be met: (1) steric protection such that

the monomer cannot undergo coupling reactions and (2) delocalization of the SOMO such that the radical is not so high in energy to be unstable in its dissociated, monomeric form. The authors employed a substituted vanadium(IV/V) redox couple by substituting the vanadium centers with bulky alkyl-amino groups. The flanking ligands provided steric protection while electronically, the vanadium centers can undergo redox resonance, stabilizing the radical electron. Room temperature EPR spectroscopies indicated delocalization of the unpaired electron across the V-NPN-V core of the molecule confirming the theoretical electronic stabilization (g = 1.984, $a(^{31}P)$ = 42.5 G, $a(^{51}V)$ = 23.8 G). Unsurprisingly considering literature parallels,[9,38,40,41,71] calculations indicated significant contributions by vanadium in hosting the unpaired electron spin density (39.49 % $3d_{xy}$ and 8.33 % $d_{x^2-y^2}$) along with phosphorus (31.30 % $3p_y$).

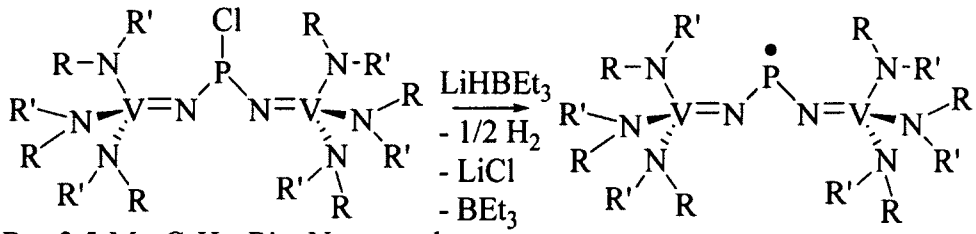

R = 3,5-$Me_2C_6H_3$, R' = Neopentyl

Scheme 1.18 Reduction with lithium triethylborohydride yielding a vanadium resonance-stabilized phosphinyl radical.[8]

Recently, Edge *et al.* synthesized sterically hindered N-heterocyclic P-P dimers which undergo dissociation to persistent 7π radicals at increased temperatures.[74] Bulky diamino-diphosphines are of interest to main-group radical chemists as they satisfy both the electronic and kinetic requirements for achieving stability. By employing π-delocalization and steric protection, the authors were able to synthesize three diphosphines of varying steric constraint from their parent chlorophosphines through

reduction with magnesium. The result was structurally characterized diphosphines with elongated central P-P bonds ranging from 2.2439(8) Å (R = ^{t}Bu), 2.324(2) Å (R = Mes) and 2.21 Å (R = Dipp). EPR spectra of the dissociated radicals were observed at elevated temperatures (353K R = ^{t}Bu, g = 2.00088, $a(^{31}P)$ = 41 G, $a(^{14}N)$ = 5.8 G; 315K R = Mes, g = 2.01775, $a(^{31}P)$ = 40 G, $a(^{14}N)$ = 5.2 G; 298K in R = Dipp, g = 2.0248, $a(^{31}P)$ = 41 G, $a(^{14}N)$ = 5.8 G) displaying an expected trend between increasing steric bulk and decreasing dissociation temperatures.

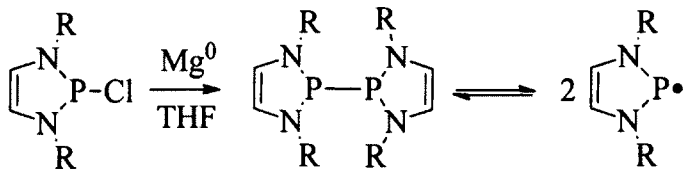

R = ^{t}Bu, 2,4,6-trimethylphenyl, 2,6-diisopropylphenyl

Scheme 1.19 Synthesis of sterically bulky 7π-phosphinyl radicals.[74]

Stemming from earlier success isolating phosphorus radical cations,[12,13] Back *et al.* synthesized two phosphinyl radicals to compare their relative stability based on the ligands around them.[14] The authors contended that using N-heterocyclic carbenes as ligands could hinder dimerization of the phosphorus radical through electrostatic repulsion as well as steric interactions of the flanking aryl-groups. Vanadium centers can act as a redox couple adjacent to radical centers, providing resonance stabilization of the unpaired electron (Scheme 1.16).[8] The EPR spectrum of the resulting imidazolidin-2-iminato species (Scheme 1.20, bottom) indicated a large doublet (g = 2.005) from coupling to phosphorus ($a(^{31}P)$ = 78 G). The vanadium-iminato species displayed an EPR splitting pattern of eight lines (g = 1.981), owing to hyperfine coupling with the vanadium atom ($a(^{51}V)$ = 58 G). From the X-ray diffraction, computational and EPR

studies of the two phosphinyl radicals it was concluded the imidazolidin-2-iminato system is best described as a phosphorus centered radical while the vanadium-iminato system is a vanadium(IV)-imidazolidin-2-iminatophosphinimide, although both contain large spin densities on phosphorus.

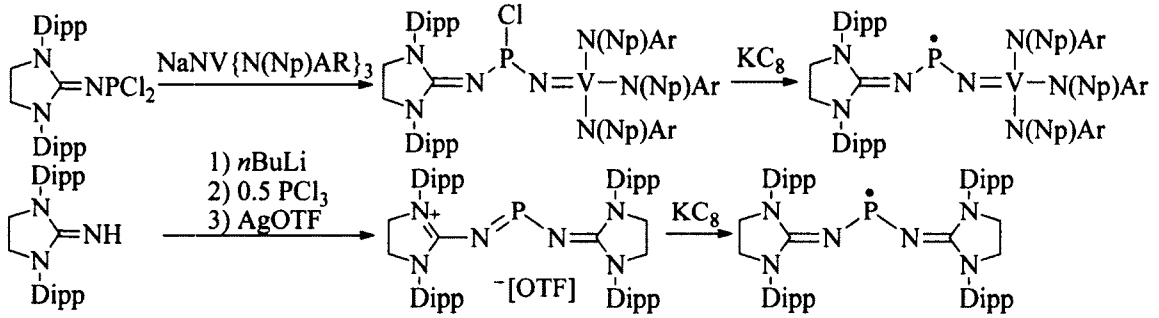

Ar = 3,5-$Me_2C_6H_3$, Np = Neopentyl, Dipp = 2,6-diisopropylphenyl

Scheme 1.20 Synthetic routes to carbene stabilized phosphinyl radicals capped by vanadium-iminato (above) and imidazolidin-2-iminato (below) ligands.[14]

To this point in the literature, solid state monomeric phosphinyl radicals have had at least one nitrogen substituent adjacent to phosphorus. Based on previous success stabilizing low-valent group 14 species using a dialkyl ligand system, Ishida *et al.* set out to synthesize a group-15 analogue. Reduction of the parent chlorophosphine with potassium on graphite (KC_8) yielded a yellow material which was found to be moderately stable in solution and in the solid state as the monomeric radical (Scheme 1.21). The room temperature EPR spectrum of the dialkylphosphinyl radical displayed a doublet (g = 2.0086) owing to coupling with the ^{31}P nucleus ($a(^{31}P)$ = 9.07 mT). Spin densities were found to have significant contributions by phosphorus [70% $3p$(P) and 2% $3s$(P)].

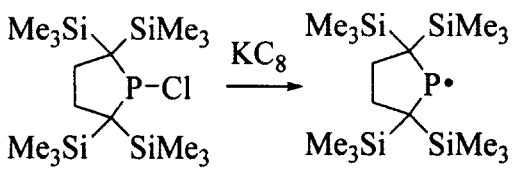

Scheme 1.21 Synthesis of a persistent dialkylphosphinyl radical.[75]

Section 1.4 – Objectives

The preceding review covered several techniques by which synthetic chemists can stabilize phosphorus centered radicals. Transition metal complexes (radical donation), aryl-substituted (steric protection) and carbene-stabilized radical ions (delocalization, steric protection), diphosphenyl radical systems (π-delocalization) as well as neutral phosphinyl species were discussed in an attempt encapsulate the current state of the field. Two general principals have been shown to be effective in stabilizing inherently reactive radical centers: (1) steric bulk, providing kinetic and thermodynamic stabilization, preventing reactivity and dimerization at the radical center, (2) electronic stabilization of SOMO using adjacent electronegative atoms or conjugation. Direct characterization of phosphorus centered radicals emerged in the literature in the mid-1960's with the monomeric radical of bis(*p*-dimethylamino-phenyl)phosphine and proposed radical mechanism intermediates.[3,4] The emergence of EPR spectroscopy and modern computation techniques has enabled chemists to characterize these radicals in detail. The reactivity of phosphorus centered radicals has been outlined in the formation of metal complexes with significant spin density transfer to the metal centers. Although this represents a promising synthetic route toward paramagnetic metal species with potential applications in catalysis and/or spin-trapping experiments, their interaction with small molecules on an exploratory level is largely unmapped.[69,71] Phosphinyl radicals ($\cdot PR_2$) have the potential to act as one-electron acceptors, as well as one-, two- and three-electron donors. The amphiphilic and inherently reactive nature of these molecules provides synthetic chemists with a powerful tool toward identifying novel molecular

architectures and reaction pathways. The goal of the following chapter is to outline the synthesis and reactivity of a new, persistent N-heterocyclic phosphinyl radical and investigate its reactivity profile toward main group elements and other small molecules.

Section 1.5 – Discussion

- Section 1.5.1 Synthesis of a New Phosphinyl Radical

The literature synthesis of 2-chloro-1,3-bis(2,6-diisopropylphenyl)-1,3,2-diazaphospholidine (**1**)[76] yielded a single phosphorus containing product by $^{31}P\{^{1}H\}$ NMR spectroscopy and was confirmed to be the desired chlorophosphine using single crystal X-ray diffraction. Structural characterization of this product indicated an elongated phosphorus-chlorine bond of 2.2108(8) Å and a distorted trigonal pyramidal geometry about the phosphorus center. The sum of angles at phosphorus were found to be approximately 299°, in part due to the restricted N(2)-P(1)-N(1) bond angle of 91.57(7)°. The length of the P(1)-Cl(1) bond is similar to other N-heterocyclic-chlorophosphines.

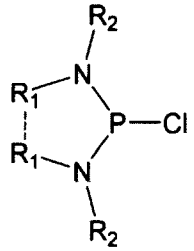

Figure 1.1 Parent structure for various N-heterocyclic chlorophosphines.

Table 1.2 Literature bond lengths for N-heterocyclic chlorophoshines.

Compound	P-Cl length (Å)	Reference
R_1 = CH, R_2 = Dipp	2.243(1)	77
R_1 = C-Me, R_2 = Dipp	2.325(1)	77
R_1 = CH, R_2 = DMP	2.362(1)	77
R_1 = C-Me, R_2 = Mes	2.354(1)	77
R_1 = CH_2, R_2 = 3-methoxyphenyl	2.1993(6)	76
R_1 = CH_2, R_2 = Dipp	2.2108(8)	This work

It is evident that conjugation in the backbone of the N-heterocyclic chlorophosphine and the steric bulk surrounding the phosphorus center both play a significant role in the length of the P-Cl bond. The saturated backbone of the system as well as the orientation of the 2,6-diisopropylphenyl groups result in a P-Cl distance of 2.2108(8) Å for **1**, less than any of the sterically bulky literature examples from Burck *et al.* which contain essentially planar geometry at phosphorus, likely a function of conjugation in the system.[77]

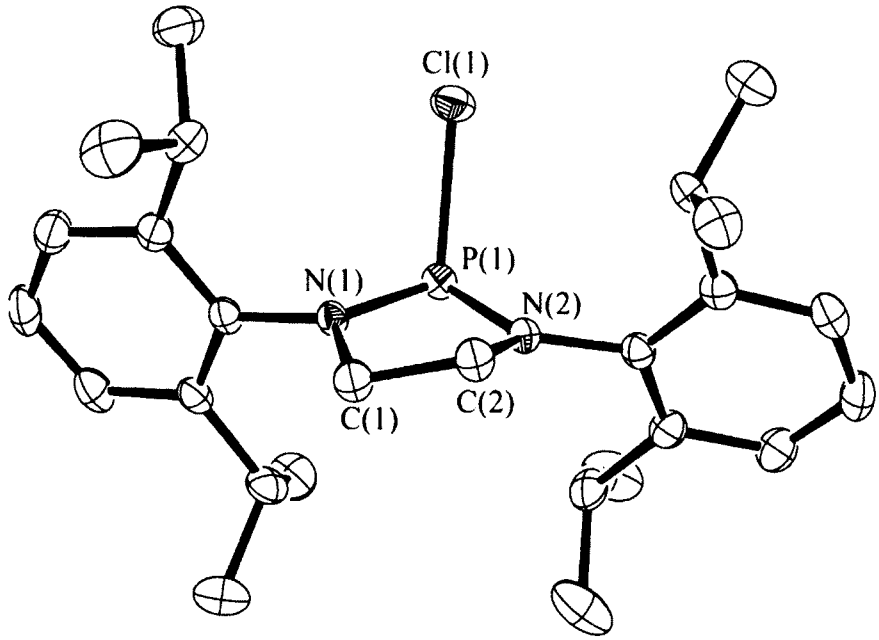

Figure 1.2 ORTEP of **1**, 50% ellipsoids are shown. Hydrogen atoms are omitted for clarity. Distances (Å) angles (°): P(1)-Cl(1) 2.2108(8), P(1)-N(2) 1.6556(14), P(1)-N(1) 1.6569(15), N(1)-C(1) 1.469(2), N(2)-C(2) 1.472(2), C(1)-C(2) 1.507(2), N(2)-P(1)-N(1) 91.57(7), N(2)-P(1)-Cl(1) 103.49(6), N(1)-P(1)-Cl(1) 103.75(6), C(1)-N(1)-P(1) 115.99(11), C(2)-N(2)-P(1) 114.06(11), N(1)-C(1)-C(2) 105.15(13), N(2)-C(2)-C(1) 105.43(13).

Several attempts were made to reduce the chlorophosphine to the corresponding diphosphine $(Dipp_2C_2H_4N_2P)_2$. Several alkali and alkaline metals including Na^0, Li^0, K^0, Zn^0 and Mg^0 were unsuccessful in reducing any meaningful quantity of the chlorophosphine to the diphosphine or the monomeric phosphinyl (Scheme 1.22).

Attributing the synthetic challenges to the reliance on surface reaction and/or reduction potential, it was concluded that either a more soluble or stronger reducing agent was required. Sodium naphthalenide was made *in situ* and employed to reduce the chlorophosphine (**1**) to the corresponding diphosphine (**2**) in good yields (~80%).

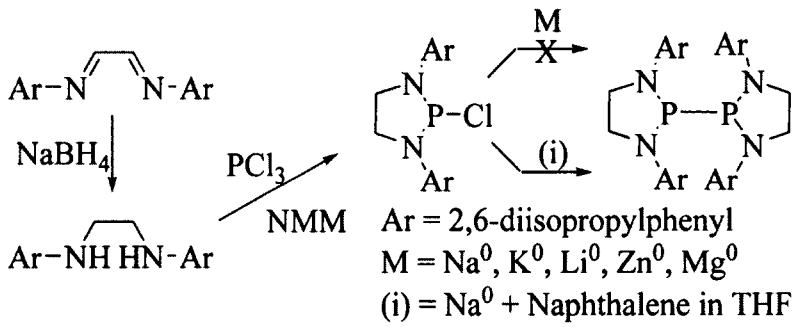

Scheme 1.22 Synthetic route to $(Dipp_2C_2H_4N_2P)_2$ (**2**).

This synthesis was found to be repeatable in multi-gram quantities and was spectroscopically free of impurities by $^{31}P\{^1H\}$ NMR. Single crystals of **2** can be grown from concentrated solutions of pentanes quickly (overnight) or toluene (several days) at -35 °C (Figure 1.3). The structure of **2** (Figure 1.3) illustrates the considerable steric strain present in the molecule as the Dipp groups orient themselves to minimize their interactions. This steric influence, as well as the increased electron density donation to the phosphorus centers from the adjacent amino-substituents leads to elongation of the phosphorus-phosphorus distance (2.3207(9) Å). The central P-P bond is similar to other strained diphosphines in the literature such as those recently characterized by Edge *et al.* (Table 1.3) while being significantly longer than tetraphenyldiphosphine (2.260(1) Å).[74] The similarity in the P-P bond distances is interesting given the much larger difference between the saturated (**1**) and unsaturated Dipp-chlorophosphines discussed previously

(Table 1.2),[77] indicating sterics rather than electronics may dictate the length of the P-P bonds.

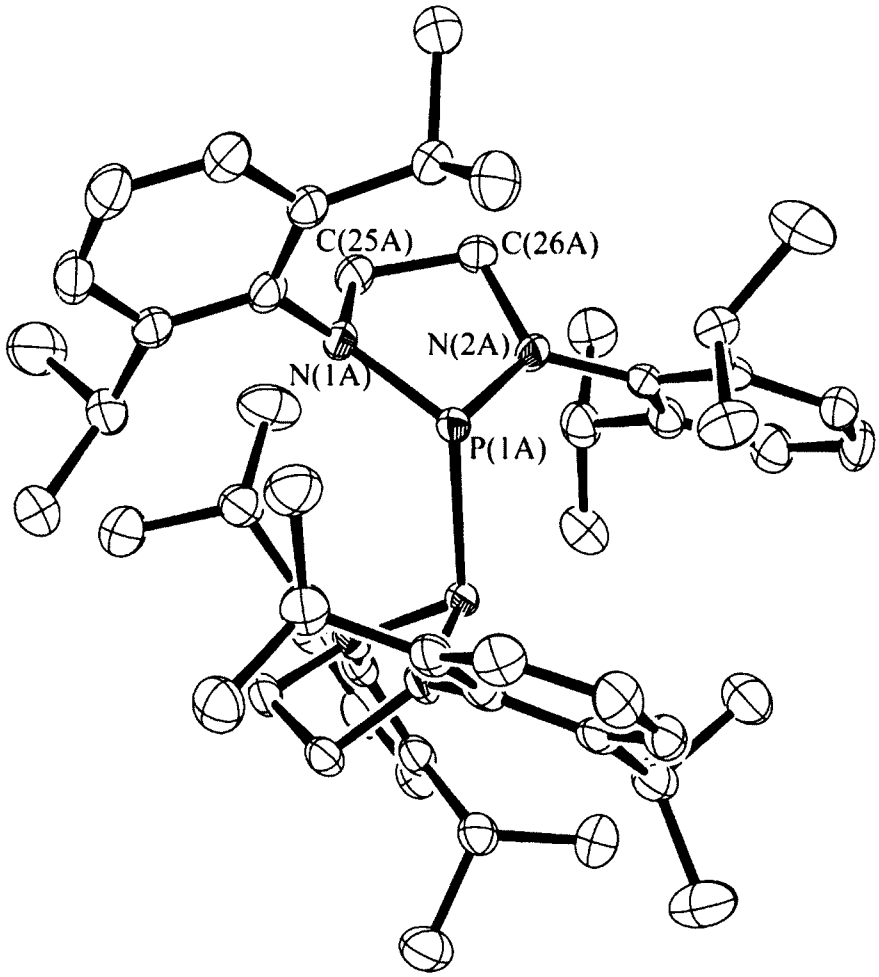

Figure 1.3 ORTEP of **2**, 50% ellipsoids are shown. Hydrogen atoms are omitted for clarity. Distances (Å) angles (°): P(1A)-P(1A') 2.3207(9), P(1A)-N(1A) 1.7007(17), P(1A)-N(2A) 1.7271(17), N(1A)-C(1A) 1.475(2), N(2A)-C(2A) 1.469(2), C(1A)-C(2A) 1.526(3), N(1A)-P(1A)-N(2A) 91.80(8), N(1A)-P(1A)-P(1A') 118.54(6), N(2A)-P(1A)-P(1A') 96.09(7), C(1A)-N(1A)-P(1A) 112.26(12), C(2A)-N(2A)-P(1A) 113.90(13), N(1A)-C(1A)-C(2A) 106.70(14).

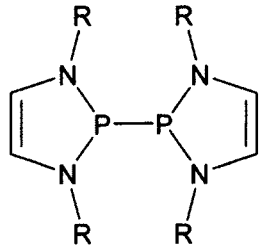

Figure 1.4 Parent structure for various N-heterocyclic diphosphines found in Table 1.3.

Table 1.3 Literature bond lengths for structurally characterized diphosphines.

Compound	P-P length (Å)	Reference
$R_2 = {}^tBu$	2.2439(8)	74
R_2 = Dipp	2.33	74
R_2 = Mes	2.324(2)	74
$(C_6H_5)_2P\text{-}P(C_6H_5)_2$	2.260(1)	78
$(Dipp_2C_2H_4N_2P)_2$ - (**2**)	2.3207(9)	This work

- Section 1.5.2 VT EPR, NMR, Raman and X-ray Spectroscopies

A single peak was observed in the $^{31}P\{^1H\}$ NMR at 143.46 ppm, corresponding to the two magnetically and chemically equivalent phosphorus atoms. Dissolution of **2** in hexanes yielded a pale yellow solution that produced strong EPR signals at ambient temperatures (Figure 1.5). Upon cooling to 280K, the EPR signal becomes weak, and is completely gone by 263 K. The presence of radical character reappears near ambient temperatures suggesting a reversible dissociation process (Figure 1.7).

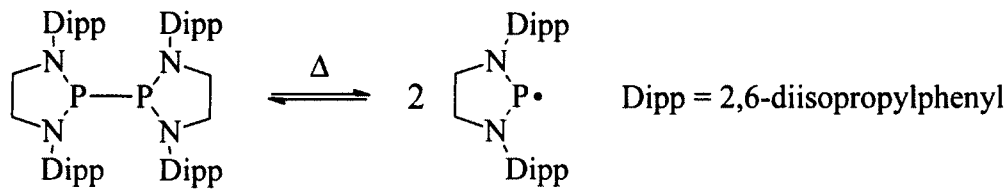

2 **2•**

Scheme 1.23 Reversible dissociation of $(Dipp_2C_2H_4N_2P)_2$ to the monomeric phosphinyl radical, $Dipp_2C_2H_4N_2P^{\bullet}$.

This result confirms the predicted dissociation of the P-P dimer **2** into two equivalents of the monomeric radical **2•** at elevated temperatures. The resulting

phosphinyl is stabilized kinetically by the bulky Dipp groups and electronically by delocalization of the unpaired electron over the two nitrogen and four hydrogen atoms in the heterocyclic ring. Similar stabilization of neutral P(III) radicals has been reported previously.[29,74] At 295 K, the EPR spectrum consists of a doublet which is split into nonets (g = 2.0031), consistent with hyperfine coupling to one phosphorus atom ($a(^{31}P)$ = 6.09 mT), two equivalent nitrogen atoms ($a(^{14}N_{1-2})$ = 0.37 mT), and four equivalent hydrogen ($a(^{1}H_{1-4})$ = 0.29 mT) nuclei on the ethyl-backbone. The equivalence of the hydrogen nuclei is congruent with dynamic averaging of the four atoms for which *ab initio* calculations (B3LYP/6-31G*) predict hyperfine splitting of 0.39 mT (2 H) and 0.09 mT (2 H) with an average value of 0.24 mT, in good agreement with experimental results. In contrast, the recently published EPR spectrum of the unsaturated analogue $(Dipp_2C_2H_2N_2P)_2$ is a doublet of quintets with no indication of coupling to the hydrogen atoms in the heterocyclic core.[29,74]

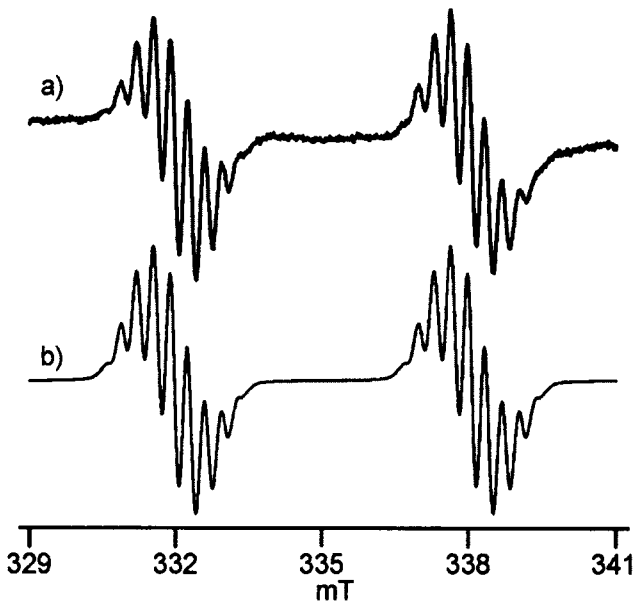

Figure 1.5 a) Experimental EPR spectrum of 1.1 mM **2** in hexanes at 295 K, SW = 12.0 mT, mod. amp = 0.3 mT; and b) simulated spectrum, a_P = 6.09 mT; $a_{N1,2}$ = 0.37 mT; a_{H1-4} = 0.29 mT; LW = 0.175 mT; g = 2.0031.

This difference can be explained by the nature of the SOMO. The literature example $(Dipp_2C_2H_2N_2P)_2$ (Figure 1.4) has more π-orbital character such that the hydrogen atoms from the $(CH)_2$ backbone are only expected to make a minor contribution to the EPR spectrum.[74] In contrast, the SOMO for **2•** shows less planarity in the heterocyclic core, leading to a larger contribution by the four hydrogen atoms in the carbon backbone (Figure 1.6). The value of the phosphorus hyperfine coupling constant suggests that the unpaired electron is located in a phosphorus orbital of predominantly 3*p* character. However, the value is slightly smaller than that seen for other similar P(III) radicals, likely due to the delocalization of the unpaired electron over the nitrogen and hydrogen centers (Figure 1.6).

Figure 1.6 Spin density isosurface for **2•** calculated at the B3LYP/6-31G* level.

Concentrated room temperature solutions of **2** in non-halogenated organic solvents are an intense orange colour. As the solution is cooled to sub-ambient temperatures, it transitions from orange to a bright yellow. Conversely, while heating past ambient temperatures, the intensity of the orange-red colour increases. This reversible observation is found not only in solution, but also in the crystalline state.

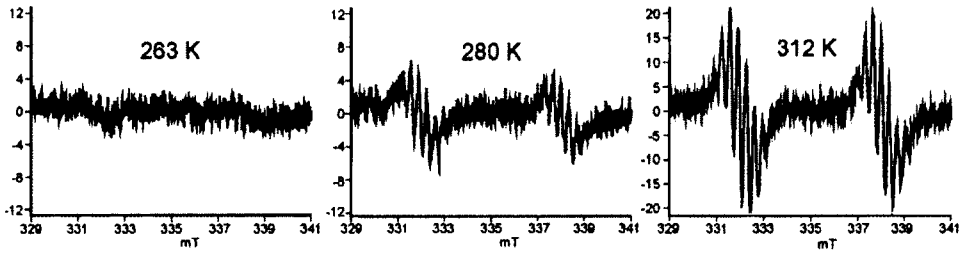

Figure 1.7 Experimental EPR spectra of **2** in hexanes at: a) 312 K (top), b) 280 K (middle), and c) 263 K (bottom).

Elongation of the central bond could lead to either polarization (P-P → P^+/P^-) or homolytic cleavage (P-P → 2 P·) of the central P-P bond which would affect the absorbance properties of the sample. Alternatively, changing the temperature of the solid sample could simply affect the Boltzmann distribution between the diphosphine/phosphinyl in the crystal. Variable temperature EPR indicated a reversible dissociation process in solution (Figure 1.7). Observationally, the same colour transitions are evident in the solid state. Two experiments were proposed to elucidate the nature of the P-P dissociation in the solid state: (1) variable temperature single crystal EPR spectroscopy, (2) variable temperature single crystal X-ray crystallography which would indicate elongation or contraction of the average central P-P bond depending on the temperature of the crystal. Because we did not have access to single crystal EPR, the second strategy was employed. The propensity for the central P-P bond to elongate in the solid state could lead to the presence of radical character.

A single crystal of $(Dipp_2C_2H_4N_2P)_2$ grown from toluene was mounted in a 0.5 mm capillary with Apiezon H© and flame sealed to prevent degradation due to air and moisture. Full structure runs were completed at 100 K and 323 K on the same crystal indicating little or no change in the geometric positions of the core atoms of **2** (Table

1.4). Heating **2** past 323 K induced irreversible degradation of the crystal, likely a function of toluene loss from the crystal lattice.

Table 1.4 Selected bond lengths and sum of angles for the diphosphine (**2**) at 100 K and 323 K.

Temperature (K)	100	323
	Bond Lengths (Å)	
P(1)-P(2)	2.3146(11)	2.3220(15)
P(1)-N(1)	1.730(3)	1.718(2)
P(1)-N(2)	1.706(2)	1.689(2)
P(2)-N(3)	1.723(3)	1.713(2)
P(2)-N(4)	1.702(2)	1.699(2)
	Sum of Angles (Σ°)	
P(1)	310.8	309.9
P(2)	308.3	309.0
N(1)	359.4	359.1
N(2)	353.8	354.8
N(3)	360.0	359.7
N(4)	356.1	356.5

The room temperature ^{1}H NMR spectrum displayed significant broadening of the signals, presumably due to the presence of the paramagnetic phosphinyl radical at ambient temperatures (Figure 1.8). The ^{1}H NMR spectrum of **2** was run at 298, 280 and 268K in toluene-d_8, improving the resolution of the peaks at sub-ambient temperatures. When approaching 268 K, the spectrum can be assigned with some confidence as only the fine splitting of the backbone (triplet) and *iso*-propyl (septets) protons are distorted.

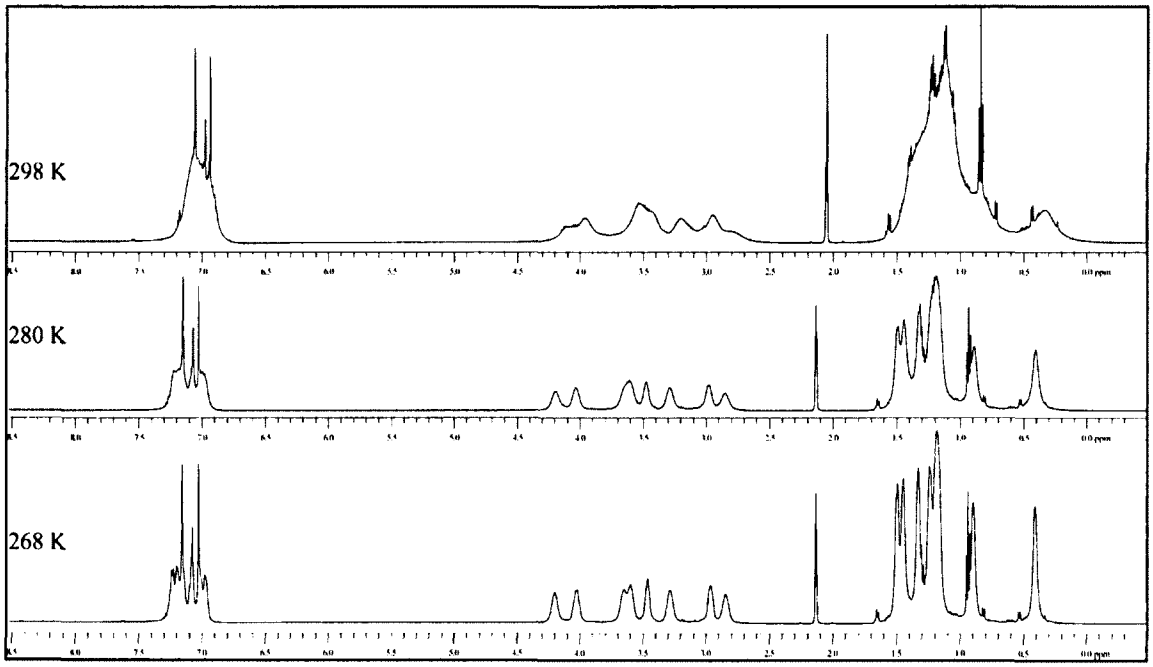

Figure 1.8 VT ^{1}H NMR of **2**. 500 MHz (toluene-d_8) at 268, 280, 298K.

Frequency calculations at the B3LYP/6-31G(d) level suggested that the central P-P bond is Raman active. Table 1.5 contains predicted values for the vibrational frequencies of the central P-P bond with and without a scaling factor (0.9613) applied. High resolution FT Raman spectroscopy was initially collected at room temperature on a Thermo Scientific DXR SmartRaman (Figure 1.9). In order to investigate the nature of the central P-P bond in **2**, Raman spectra were collected at three approximate temperature ranges. If the central P-P bond elongates as a function of temperature in the solid state, a shift would be expected in the vibrational mode associated with the P-P bond.

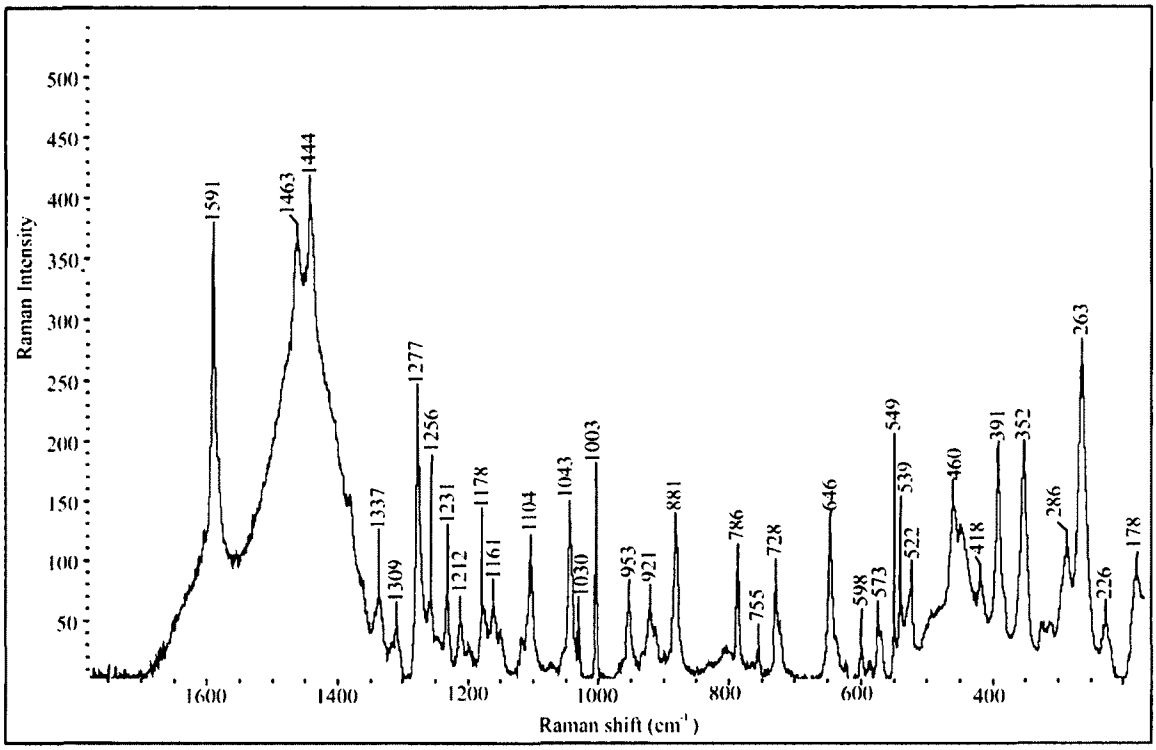

Figure 1.9 Raman spectrum of the diphosphine (**2**). Thirty samples of 1.0 seconds were collected. Resolution is ± 1 cm^{-1}.

Table 1.5 Predicted values for the stretching frequencies of the central P-P bond at the B3LYP/6-31G(d) level of theory. Scaling factor for B3LYP/6-31G(d) is 0.9613.

Experiment	Raman Frequencies
Predicted [B3LYP/6-31G(d)]	422.83, 445.41, 468.93
Predicted w. Scaling Factor	406.47, 428.17, 450.78
Observed Peaks	417.53, 448.48, 459.57

A sample of **2** was flame sealed in a capillary. As a qualitative experiment, Raman spectra were collected after the sample was exposed to: (1) liquid nitrogen (~77 K), (2) ambient temperatures (~298 K), (3) boiling H_2O (~373 K) and allowed to equilibrate thermally. There was no observable change in the region associated with the central P-P bond across the three approximate temperatures as can be seen in Figure 1.10. The lack of observable change in the Raman spectra suggests that the positions of atoms (in the solid state) do not change as a function of temperature. This implies that solvent effects

are likely a major factor in the dissociation of the diphosphine (**2**) to its monomeric radical. In order to investigate this process further, a systematic computational study was completed.

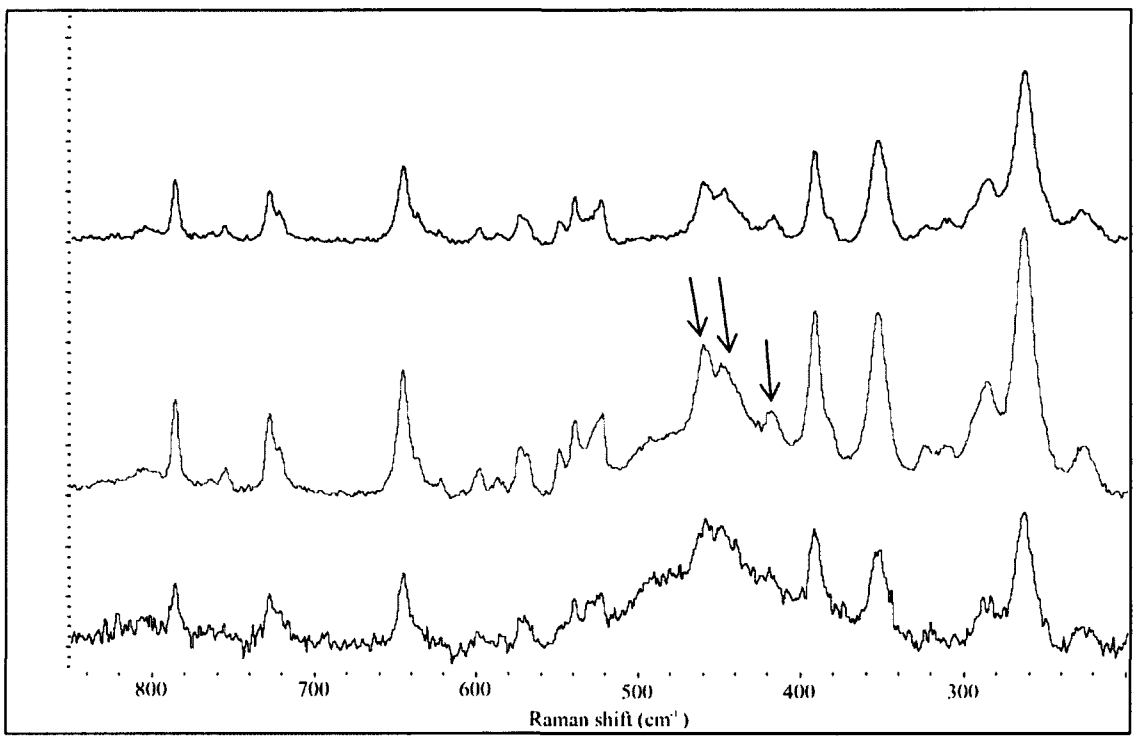

Figure 1.10 Variable temperature high resolution Raman spectroscopy of the diphosphine (**2**). Thirty samples of 1.0 seconds were collected for ambient temperatures (middle) while 5 samples of 1.0 seconds were collected for low temperature (bottom) as well as elevated temperature (top). Resolution is ± 1 cm^{-1}.

- Section 1.5.3 Computational Results

The computational preface and all calculations were completed by Dr. Cory Pye at Saint Mary's University using the Atlantic Computational Excellence Network (ACEnet) cluster. The computation results can be found as tables in Appendix A (Tables A1-9) along with representative structures (Figures A1-3). Discussion of the results was completed independently by the thesis author.

Preface

Calculations were performed using Gaussian 03, using a stepping-stone approach in which the geometries at the levels HF/STO-3G, HF/3-21G, HF/6-31G*, HF/6-31+G*, B3LYP/6-31G*, and B3LYP/6-31+G* were sequentially optimized using default specifications. After each level, a frequency calculation was performed to verify the nature of the stationary point. Z-matrix coordinates constrained to the appropriate symmetry were used for efficiency, as any problems would manifest themselves by an imaginary mode orthogonal to the spanned Z-matrix space. The Hessian was also evaluated at the starting STO-3G geometry to aid convergence.

Discussion of Computational Results

It is evident from the EPR and ^{1}H VT-NMR that there is a temperature-dependant relationship between the diphosphine and its dissociated radical in solution. The question remains, what gives rise to this dissociation? Conceptually, it could be reasoned that the bulky 2,6-diisopropylphenyl groups flanking the diphosphine core apply steric strain on the central P-P bond. These spatial interactions could raise the energy of the system such that the favorable electron pairing energy in the P-P bond can be overcome. In order to elucidate the details of this process in regards to the role of the bulky heteroatom substituents, a systematic computational study was performed by Dr. Corey Pye including the following dimer-monomer pairs: $[H_2P]_2$ & $H_2P\bullet$, $[(H_2N)_2P]_2$ & $(H_2N)_2P\bullet$, $[(\{H_2C\}NH)_2P]_2$ & $(\{H_2C\}NH)_2P\bullet$, $[(\{H_2C\}NPh)_2P]_2$ & $(\{H_2C\}NPh)_2P\bullet$ and $[(\{H_2C\}NDipp)_2P]_2$ & $(\{H_2C\}NDipp)_2P\bullet$ (Figure 1.11). All energies discussed in the

following will be the result of calculations run at the B3LYP/6-31+G* level unless otherwise stated.

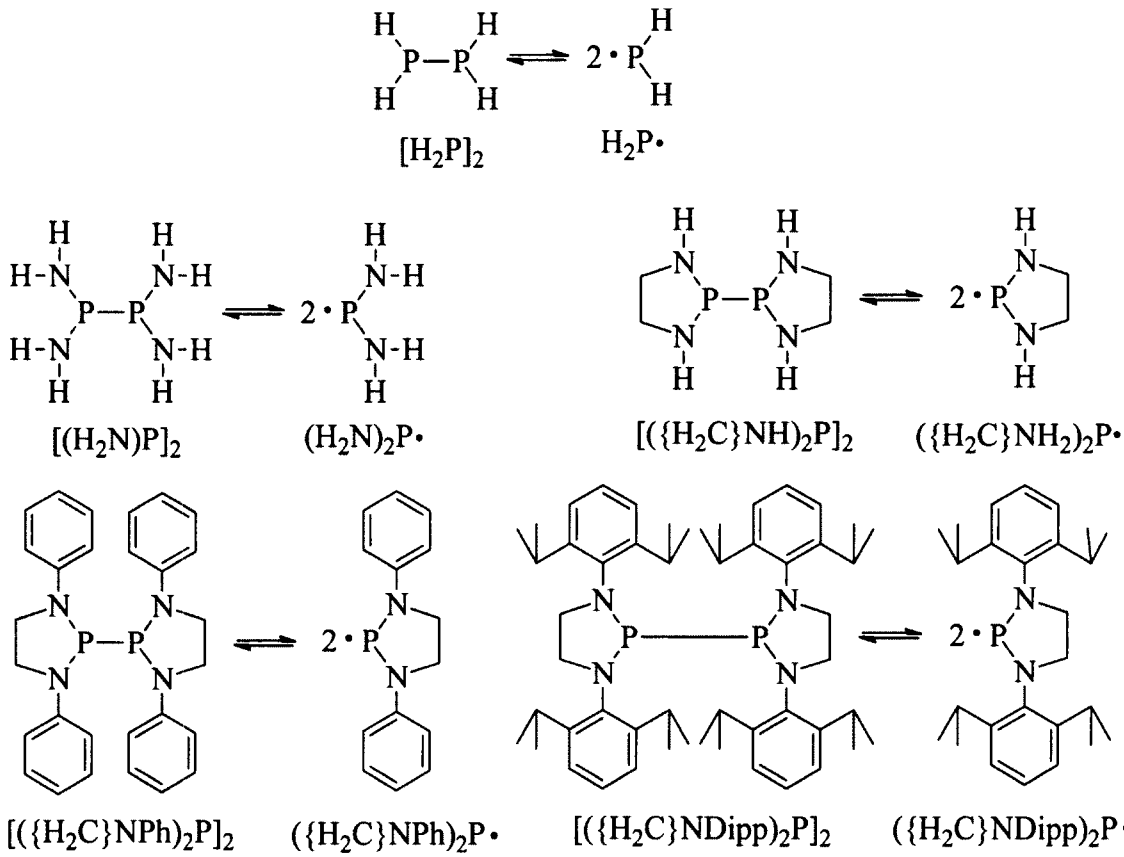

Figure 1.11 Structures in the systematic computational study of $[(\{H_2C\}NDipp)_2P]_2$.

Calculations were completed using several different point groups starting with the smallest parent structure $[H_2P]_2$ (Table A.1). The results indicated that the C_2 point group was favored followed by C_{2h} (+ 0.5 kJ/mol) and C_{2v} (+ 17.4 kJ/mol). Ascending to higher symmetry point groups (D_{2h}, D_{2d} and D_2) did not yield stationary points. The dissociated monomer ($H_2P\bullet$) was found to be 225 kJ/mol higher in energy than the parent diphosphine $[H_2P]_2$. This result is not unexpected given the minimal steric effects which could contribute to the dissociation process. This value is significantly higher than calculated for the homolytic dissociation of $Me_2P\text{-}PMe_2$ to 2 $Me_2P\bullet$ (102.6 kJ/mol).[17] The

P-P bond length was found to be 2.251 Å while the H-P-H angle increases from 91.74° in the phosphinyl (H_2P•) to 93.83° in the diphosphine $[H_2P]_2$.

The only stable conformation for the $(H_2N)_2P$• radical was optimized in C_2 symmetry. The diphosphine $[(H_2N)_2P]_2$ was found to have two stationary points associated with a C_2 point group, the lowest energy of which (C_2*#1*) was 8.0 kJ/mol higher in energy than the second C_2*#2* conformation. The P-P bond distance is the same as the parent diphosphine (2.251 Å) while the sum of angles around phosphorus increased from 289.3° in $[(H_2N)_2P]_2$ to 301.0° for $(H_2N)_2P$•. The N-P-N angle increases from 94.9° in the phosphinyl $(H_2N)_2P$• to 108.4° in the diphosphine $[(H_2N)_2P]_2$. The P-P bond dissociation energy was found to be 175.8 kJ/mol, approximately 50 kJ/mol lower than the parent $[H_2P]_2$.

Next is the $[(\{H_2C\}NH)_2P]_2$ and $(\{H_2C\}NH)_2P$• heterocyclic system in which the two amino substituents are connected through an ethane backbone. The N-P-N angle is distorted to accommodate the five-membered ring structure in each case. Two minima were identified for the $(\{H_2C\}NH)_2P$• monomer. The C_2 symmetry was found to be lower in energy than the structure with C_1 symmetry by 6.4 kJ/mol. The C_2 phosphinyl N-P-N angle of 89.81° reflects the aforementioned constraint applied by the heterocyclic structure. In the dimerization process of the C_2 phosphinyls, several combinations of monomers with different symmetries are possible. Only those that were the product of symmetrical dimerization were considered. The C_2*#4* structure is the lowest in energy however, C_i*#1* is approximately isoenergetic (+1.0 kJ/mol). The C_2*#4* and C_i*#1* structures are derived from the "C_{2h}" monomer indicating that steric interactions of the two ethylene

backbones increases the energy of the "C_2" coupling process which was favored in the non-heterocyclic structure. The P-P bond length was found to be slightly longer than the acyclic version at 2.264 Å. The diphosphine $[(\{H_2C\}NH)_2P]_2$ was calculated to be 141.1 kJ/mol lower in energy than the two-phosphinyl monomers $(\{H_2C\}NH)_2P\bullet$ and is roughly 40 kJ/mol lower than the dissociation energy (175.8 kJ/mol) of the noncyclic diamino-system $[(H_2N)_2P]_2$.

Phenyl groups were then added as substituents to the nitrogen atoms in place of amine-hydrogens generating $[(\{H_2C\}NPh)_2P]_2$ and $(\{H_2C\}NPh)_2P\bullet$, increasing the steric bulk about the central P-P bond. In the phosphinyl monomer, the C_2 geometry was found to be lowest in energy displaying an N-P-N angle of 90.28°. Transitioning to the diphosphine, two stationary points were identified in C_2 geometries which differed by 7.5 kJ/mol. The lower energy C_2 structure was found to be 100 kJ/mol lower in energy than two equivalents of the monomeric phosphinyl $(\{H_2C\}NPh)_2P\bullet$. This represents roughly a 40 kJ/mol reduction in the energetical gap for the dissociation of the parent heterocyclic diphosphine $[(\{H_2C\}NH)_2P]_2$ to the phenyl substituted $[(\{H_2C\}NPh)_2P]_2$ structure. The steric strain of the phenyl groups starts to affect the central P-P bond at this point, increasing to 2.345 Å.

When 2,6-diisopropyl groups were added to the phenyl substituents, it generates the full system $[(\{H_2C\}NDipp)_2P]_2$ and $(\{H_2C\}NDipp)_2P\bullet$. The diphosphine optimizes in C_2 geometry which roughly mimics the distorted nature of the structure seen in the single crystal X-ray structure of **2** (Figure 1.3). The calculations indicate significant elongation of the central P-P bond to 2.410 Å based on the distortion required to accommodate the

bulky Dipp groups. This is significantly longer than the X-ray structure suggested (2.3207(9) Å), although the gas-phase calculations neglect factors such as ambient temperature and packing effects during crystallization. The Dipp groups are less distorted in the calculated structure as can be seen in Figure 1.12. This can be attributed to the elongated P-P bond, permitting partial relaxation of the strained Dipp interactions. Transitioning from the diphosphine to the phosphinyl monomer, the flanking Dipp groups relax to a more energetically favorable geometry (Figure 1.12).

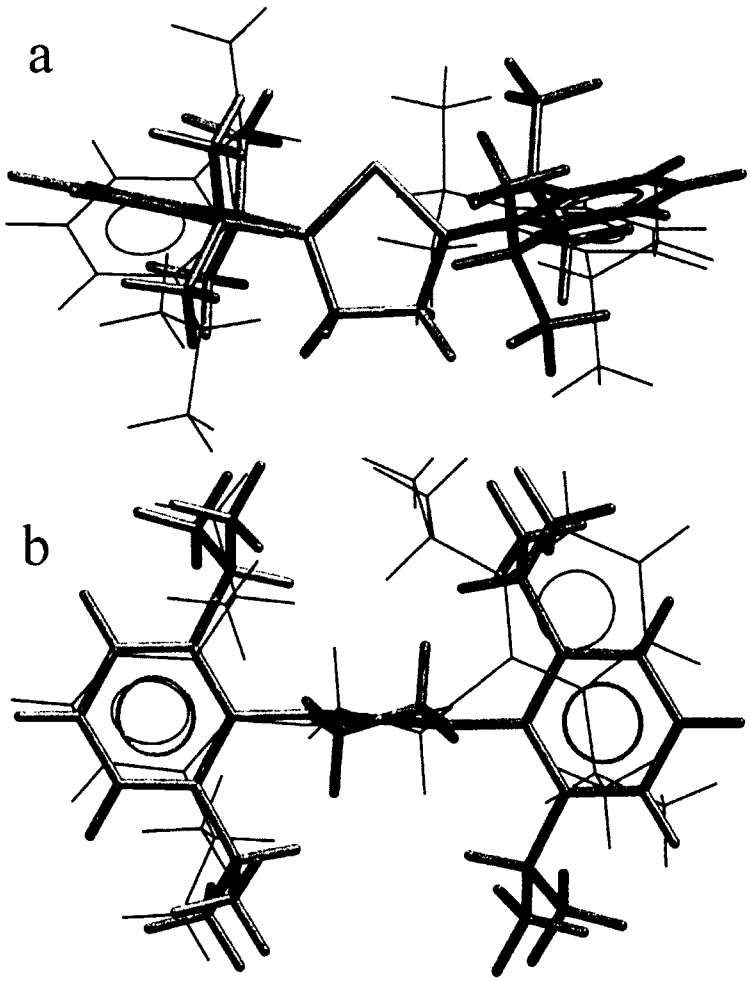

Figure 1.12 Top (a) and front (b) views of the optimized structure (B3LYP/6-31+G*) of the phosphinyl (grey) overlaid with one-half of the optimized diphosphine structure (black).

Several levels of theory were used to calculate the energy associated with the relaxation (Table 1.6) of the full system $[(\{H_2C\}NDipp)_2P]_2$ and its dissociation product $(\{H_2C\}NDipp)_2P\bullet$. The results indicate that between 50-80 kJ/mol is released upon relaxation of the fixed position monomer (from the parent diphosphine atom coordinates) to the relaxed, optimized monomer. The dissociation energy of the central P-P bond in the full system would then be approximately twice the energies found in Table 1.6. To investigate this relaxation process further, several scans were undertaken in which the central P-P bond was elongated intentionally and the system energies monitored. To allow for the singlet-triplet transition energy to be accounted for, the guess=mix parameter was included. A summary of the calculations in which the atom positions were fixed from the optimized diphosphine structure (distorted) or by keeping the P-P bond distance fixed and permitting the remaining atoms to coalesce (relaxed) can be found in Tables 1.6 and 1.7.

Table 1.6 Relaxation energies at different level of theories for the dissociation of the P-P bond.

Method	E_{relax} (kJ/mol)	$2*E_{relax} = E_{full}$ (kJ/mol)
HF/STO-3G	67.6	135.2
HF/3-21G	52.9	105.8
HF/6-31G*	77.7	155.4
HF/6-31+G*	79.1	158.2
B3LYP/6-31G*	49.0	98.0
B3LYP/6-31+G*	52.3	104.6

Unsurprisingly, the only descriptive relaxation process is a product of the steric bulk introduced by the 2,6-diisopropyl groups on the phenyl substituents. The full system could only be run at the HF/3-21G level because of the computational time constraints imposed by such a large system.

Table 1.7 P-P bond distances and energies calculated at the HF/3-21G level for the fixed (strained) and relaxed (optimized) full diphosphine system.

Relaxed scan	HF/3-21G	HF/3-21G
P-P Distance	relaxed guess = mixed	fixed guess = mixed
2.0	210.95	209.97
2.2	122.42	130.44
2.4	94.26	94.92
2.6	94.77	95.70
2.8	108.99	115.56
3.0	129.32	94.83
3.2	30.45	93.44
3.4	14.05	93.55
3.6	4.90	94.94
3.8	0.14	97.21
4.0	-2.05	100.07

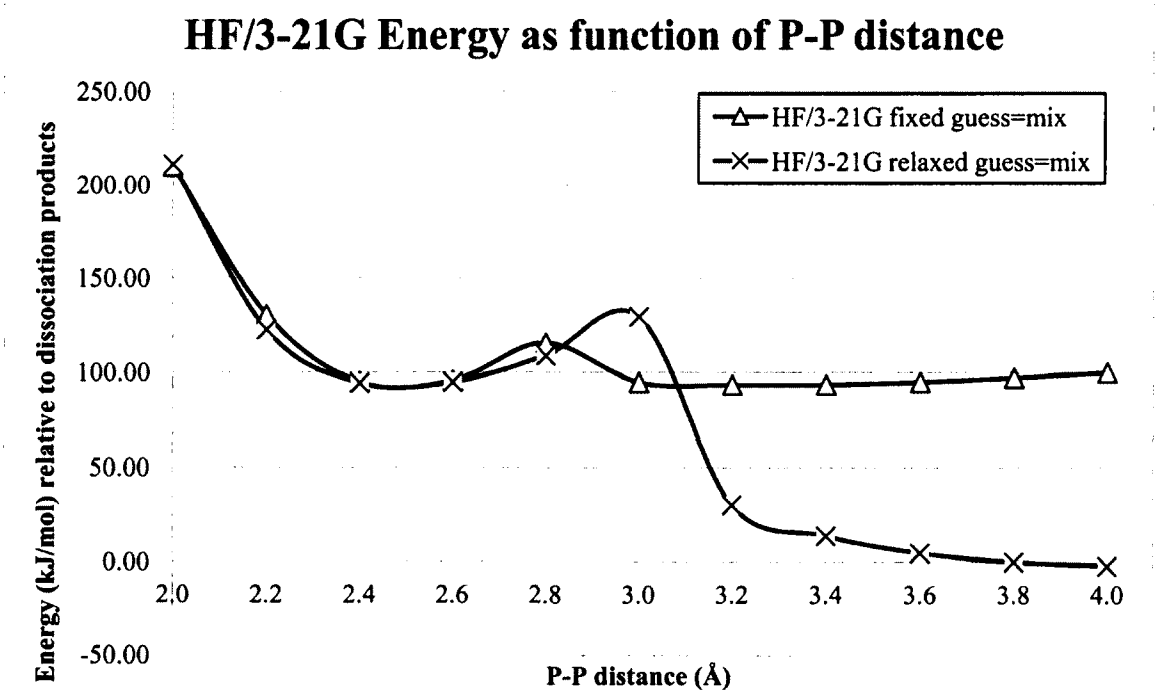

Figure 1.13 Scan calculations at the HF/3-21G level of theory plotting energy as function of P-P distance on the full $[(\{H_2C\}_2NDipp)_2P]_2$ and $(\{H_2C\}_2NDipp)_2P\bullet$ system.

In Figure 1.13, the energy of the system starts relatively high because of steric constraints of a short (< 2.4 Å) P-P central bond. The energy of the system goes through a local minimum approximately equal to the bond distance of the solid state structure (~2.4 Å) and levels out as the bond is pulled apart. The increase in energy at 2.8-3.0 Å for the relaxed system can be attributed to the singlet-triplet gap which must be overcome in order to from the two phosphinyl moieties. The energy gap between the fixed and relaxed structures from 3.2 and 4.0 Å corresponds roughly to a 100kJ/mol dissociation energy, transitioning from a fixed $[(\{H_2C\}NDipp)_2P]_2$ to two relaxed $(\{H_2C\}NDipp)_2P\bullet$ phosphinyl monomer equivalents. Admittedly, there is a discrepancy among the values for the relaxation energy of the fixed phosphinyl (Table 1.6, 105.8 kJ/mol) and the calculated difference in energy between the diphosphine and dissociated monomer phosphinyl equivalents (Table A8, +92.1 kJ/mol). The approximately 13.7 kJ/mol may be derived from the energy required to uncouple the electron pair, essentially the singlet-triplet gap for the system during P-P bond dissociation.

This computational study indicates that the bulky 2,6-diisopropylphenyl groups play a significant role in the experimentally observed dissociation process. The relaxation of the distorted diphosphine structure to the relaxed phosphinyl moieties is able to overcome the energy of the central P-P bond, resulting in homolytic cleavage of the diphosphine $[(\{H_2C\}NDipp)_2P]_2$ and thereby yielding two monomeric $(\{H_2C\}NDipp)_2P\bullet$ radical equivalents.

- Section 1.5.4 Reactivity with Main Group Elements

The persistence of the monomeric radical in solution at ambient temperatures is of interest to us specifically regarding its utility toward the activation of main group elements. In particular, room temperature activation of white phosphorus with main-group compounds has been an ongoing goal of our research group.

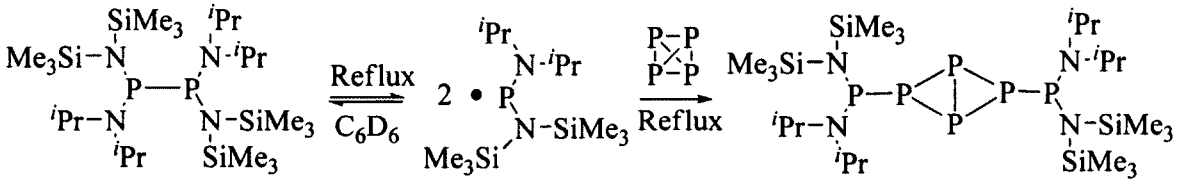

Scheme 1.24 Dissociation of a sterically bulky diphosphine and subsequent activation of P_4 at reflux temperatures in toluene forming the corresponding *trans,trans*-tetraphosphabicyclobutane insertion product.[70, 71]

Recently, Bezombes *et al.* employed an asymmetric sterically bulky diphosphine to activate white phosphorus. The dissociation of the diphosphine and activation of P_4 was only possible in refluxing benzene.[70,71] Assuming that the dissociation of the diphosphine at elevated temperatures facilitates the ring opening of the P_4 tetrahedron by a radical mechanism, **2** and its dissociation product **2•** is a candidate to activate P_4 at ambient temperatures based on room temperature EPR data. As can be seen in Figures 1.14 and 1.15, the *trans,trans*-tetraphosphabicyclobutane P_4 insertion product (**3**) of the dissociated diphosphine was isolated from the reaction of **2** with P_4, presumably following a radical mechanism outlined in a recent review on the main group chemistry of white phosphorus.[72]

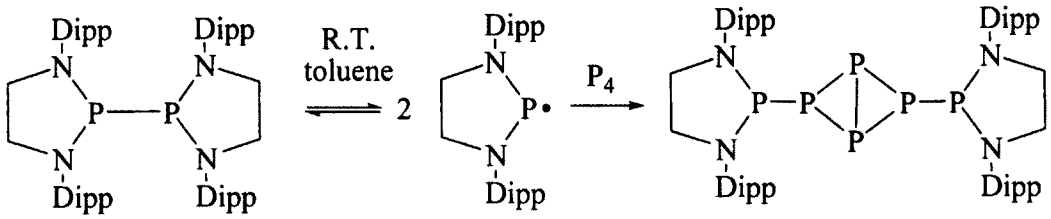

Scheme 1.25 Room temperature activation of white phosphorus by a phosphinyl radical.

As with other radical P_4 insertion products in the literature,[71] the central P(3)-P(3) bond retains partial double bond character (Figure 1.14), evident in the bond length of 2.1571(17) Å compared to the other typical phosphorus-phosphorus single bond lengths of 2.2894(12) and 2.2277(12) Å in **3**.

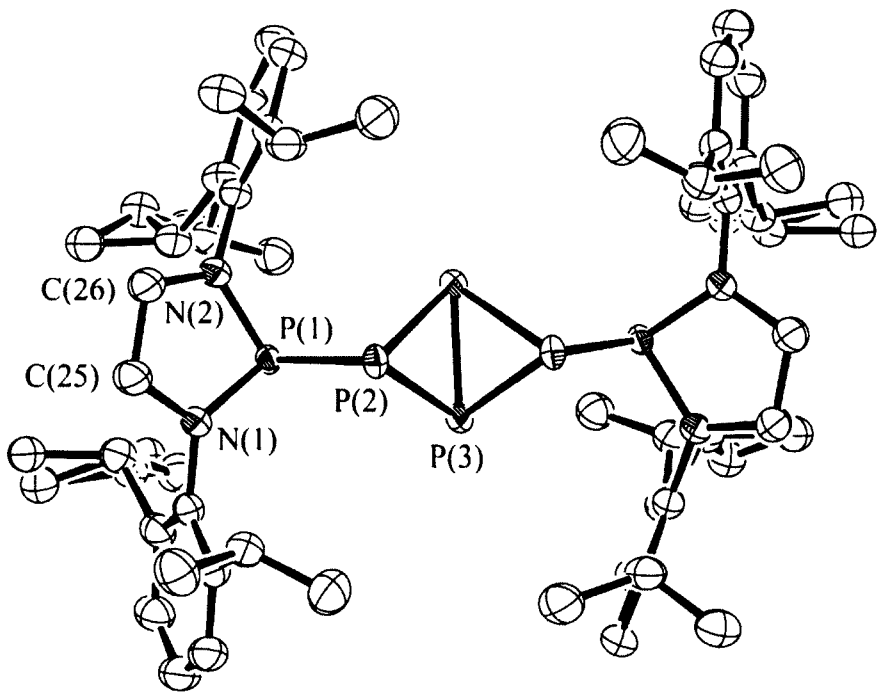

Figure 1.14 ORTEP of **3**, 50% ellipsoids are shown. Hydrogen atoms are omitted for clarity. Distances (Å) angles (°): P(1)-P(2) 2.2894(12), P(2)-P(3) 2.2277(12), P(3)-P(3) 2.1571(17), P(1)-N(1) 1.693(3), P(1)-N(2) 1.693(3), N(1)-C(25) 1.430(5), N(2)-C(26) 1.457(5), C(25)-C(26) 1.470(5), N(1)-P(1)-N(2) 90.60(14), N(1)-P(1)-P(2) 102.79(11), N(2)-P(1)-P(2) 103.04(11), P(3)-P(2)-P(3) 58.05(4), P(3)-P(2)-P(1) 92.84(4), P(3)-P(3)-P(2) 60.75(4), P(2)-P(3)-P(2) 80.27(5), C(25)-N(1)-P(1) 115.3(2), C(26)-N(2)-P(1) 115.1(2), N(1)-C(25)-C(26) 110.0(3), N(2)-C(26)-C(25) 107.7(3).

This is supported by Schoeller *et al.* whose calculations indicate partial double bond character for alkyl and amine substituted tetraphosphabicyclobutadienes.[79,80] The *trans,trans*-geometry about the P_4 core in **3** is similar to those other tetraphosphabicyclobutane insertion products found in the literature such as the super-silyl radical asymmetric diphosphines (Table 1.1).[71,81] This is in line with Schoeller's calculations which suggested that the *trans,trans* conformation is the lowest in energy.[80] The molecule was found to be symmetry equivalent down the P(3)-P(3) bond at the centre of the P_6 fragment along a C_2 rotation axis.

To simulate the complex $^{31}P\{^1H\}$ NMR spectrum of **3** (Figure 1.16), experimental data were obtained at three external magnetic field strengths (202.4, 101.2 and 24.3 MHz respective to ^{31}P). Using Pople notation to asssign letter designations to the ^{31}P NMR, the spin system was defined by calculating the ratio of the phosphorus chemical shift differences to the magnitude of the coupling constant. As a result of the simulation, the sample yielded chemical shift values of δ_A = 160.7 ppm, δ_M = -108.2 ppm, δ_X = -349.5 ppm which models well when defined as an AA'MM'X_2 spin system.

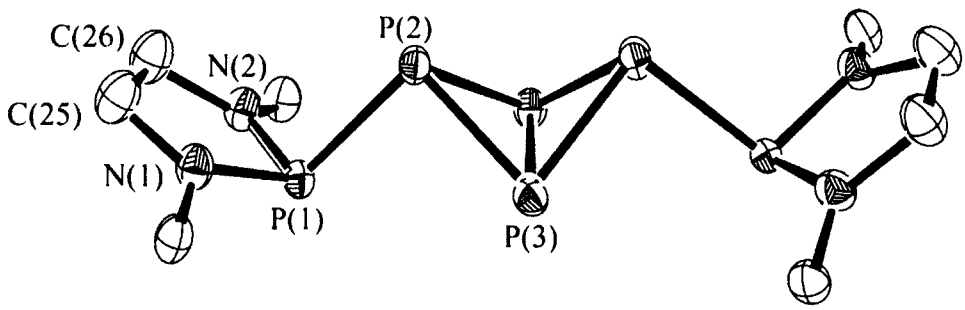

Figure 1.15 ORTEP of the core fragment of **3**, 50% ellipsoids are shown. Hydrogen atoms and 2,6-diisopropylphenyl groups are removed for clarity in observing both the spin labeling motif for the simulated ^{31}P NMR as well as the *trans,trans*-geometry about the P_6 core.

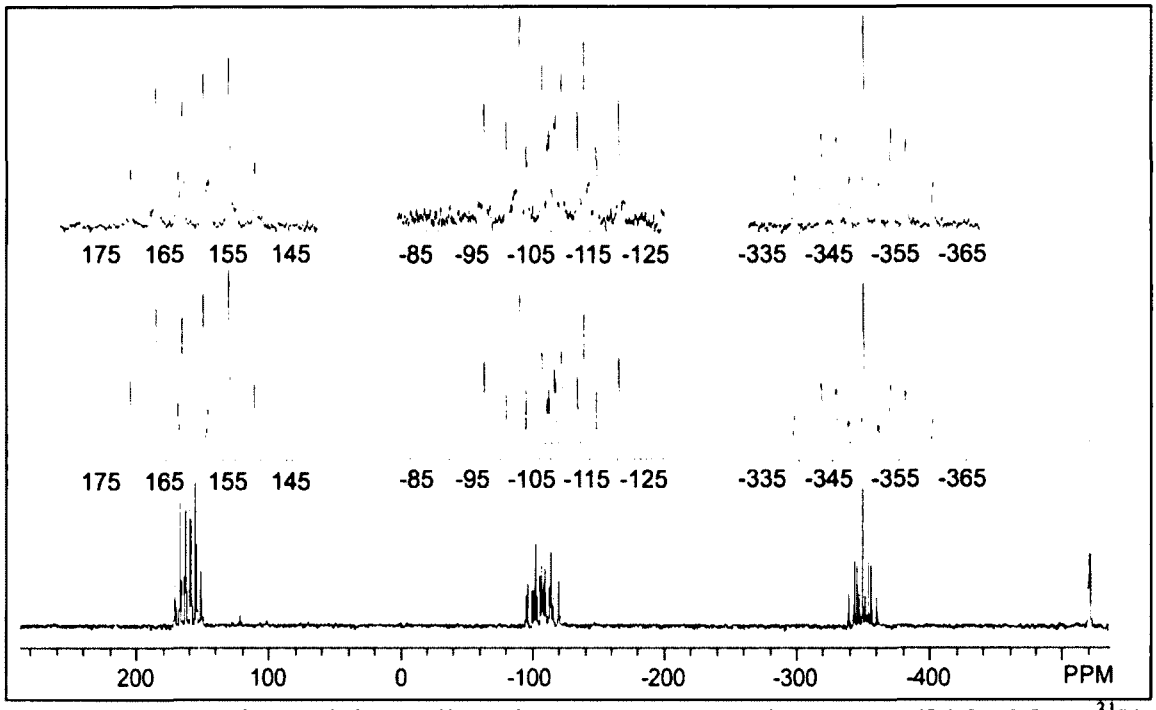

Figure 1.16 Experimental data collected on 60 MHz NMR instrument (24.3 MHz to ^{31}P). Expansion (above) is experimental coupling used to simulate (lower) coupling for the P_6 core. Modeling of the P_6 system core as $AA'MM'X_2$ yielded: $^{31}P\{^1H\}$: δ_A = 160.7 ppm, δ_M = -108.2 ppm, δ_X = -349.5 ppm, $J_{AM} = J_{A'M'}$ = -214.9 Hz, $J_{MX} = J_{M'X}$ = -152.8 Hz, $J_{AX} = J_{A'X}$ = +99.2 Hz, $J_{MM'}$ = +101.1 Hz, $J_{AM'} = J_{A'M}$ = -61.2 Hz. Residual singlet at -519.13 ppm in the full experimental spectrum (bottom) is excess white phosphorus.

After elemental phosphorus, the goal of the subsequent research was to allow the diphosphine to react with the elemental chalcogens. First, $(Dipp_2C_2H_4N_2P)_2$ was allowed to react with O_2 at ambient temperatures. Following several freeze-pump-thaw cycles to degas a solution of **2** in toluene, gaseous O_2 was introduced at approximately 1 atm in a J. Young NMR tube. Several products were possible from this reaction given the oxophilic nature of phosphorus and the potential for radical coupling to oxygen. Upon addition of oxygen and vigorous shaking of the NMR tube, the solution transitioned from bright orange to a pale-yellow.

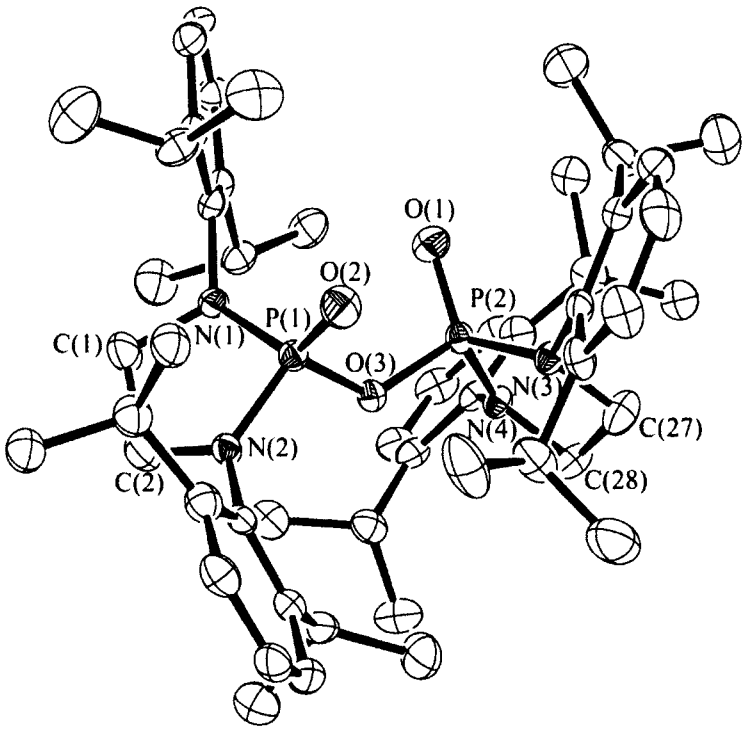

Figure 1.17 ORTEP of **4**, 50% ellipsoids are shown. Hydrogen atoms are omitted for clarity. Distances (Å) angles (°): P(1)-O(2) 1.444(2), P(1)-O(3) 1.6290(18), P(1)-N(2) 1.647(2), P(1)-N(1) 1.660(2), O(1)-P(2) 1.446(2), P(2)-O(3) 1.6270(18), P(2)-N(3) 1.641(2), P(2)-N(4) 1.661(2), C(1)-N(1) 1.464(3), C(1)-C(2) 1.507(4), N(1)-C(3) 1.448(3), C(2)-N(2) 1.462(3), N(3)-C(27) 1.467(3), N(4)-C(28) 1.470(3), C(27)-C(28) 1.506(4), O(2)-P(1)-O(3) 108.25(11), O(2)-P(1)-N(2) 118.31(12), O(3)-P(1)-N(2) 104.46(10), O(2)-P(1)-N(1) 122.09(12), O(3)-P(1)-N(1) 107.66(10), N(2)-P(1)-N(1) 94.20(11), N(1)-C(1)-C(2) 107.1(2), C(3)-N(1)-C(1) 116.4(2), C(3)-N(1)-P(1) 126.63(17), C(1)-N(1)-P(1) 112.52(17), O(1)-P(2)-O(3) 108.93(11), O(1)-P(2)-N(3) 118.42(11), O(3)-P(2)-N(3) 103.91(10), O(1)-P(2)-N(4) 121.37(11), O(3)-P(2)-N(4) 107.99(10), N(3)-P(2)-N(4) 94.27(11), N(2)-C(2)-C(1) 105.6(2), C(2)-N(2)-P(1) 113.49(17), C(27)-N(3)-P(2) 112.99(17), P(2)-O(3)-P(1) 125.08(11), C(28)-N(4)-P(2) 112.43(17), N(3)-C(27)-C(28) 105.4(2), N(4)-C(28)-C(27) 106.4(2).

The result of the reaction was the P(V) oxidation product with a bridging ethereal oxygen atom ($Dipp_2C_2H_4N_2PO$)-O-($Dipp_2C_2H_4N_2PO$) (**4**), a phosphinic anhydride(Scheme 1.26). Conversion to **4** was quantitative by $^{31}P\{^1H\}$ NMR (4.39 ppm) and can be crystallized through slow evaporation of a toluene solution at ambient temperatures yielding small colourless block-like crystals of **4**.

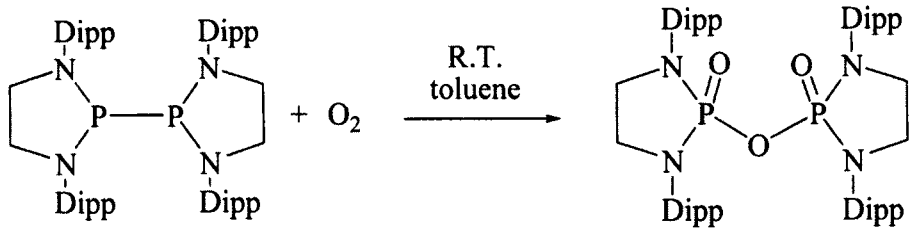

Scheme 1.26 Synthesis of $(Dipp_2C_2H_4N_2PO)$-O-$(Dipp_2C_2H_4N_2PO)$ (**4**) by addition of gaseous oxygen to a solution of $(Dipp_2C_2H_4N_2P)_2$ in toluene.

Significant twisting of the molecule about the central oxygen atom defined by a dihedral angle of O(1)-P(2)-P(1)-O(2) 82.5(2)° (Figure 1.17) which can be better visualized in the rendering of the core fragment of the molecule in which the Dipp groups have been removed (Figure 1.18). This is not simply a result of the steric constraints present in **4**. Analysis of phosphinic-anhydrides in the literature such as dimethylphosphinic acid ($Me_2P(O)$-O-$P(O)Me_2$), which lacks the steric constraints in **4** (Figure 1.17), displayed a similar dihedral angle of 84.91° (no s.u. given).[82]

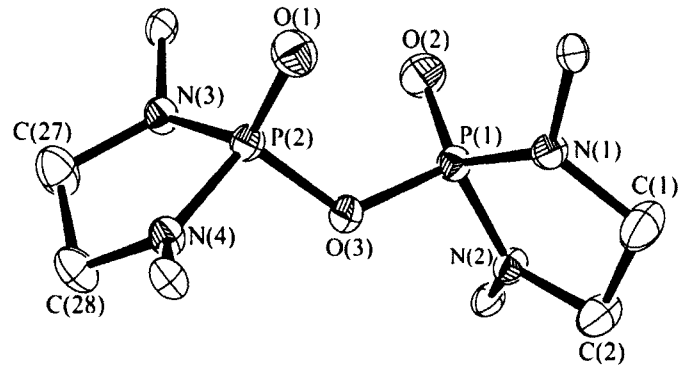

Figure 1.18 ORTEP of the core fragment of **4**, 50% ellipsoids are shown. Hydrogen atoms and Dipp groups are removed for clarity.

The P=O distances (1.444(2) Å, 1.446(2) Å) in **4** are shorter than those in $Me_2P(O)$-O-$P(O)Me_2$ (1.471(2) Å) while the ethereal P-O distances in **4** (1.627(2) Å and 1.629(2) Å) are essentially the same as in $Me_2P(O)$-O-$P(O)Me_2$ (1.6256(9) Å). Likewise, the central P-O-P angle (125.08(11)°) was found to be similar to that in $Me_2P(O)$-O-

$P(O)Me_2$ (124.6(1)°).[82] On multiple occasions, X-ray diffraction analyses on crystals obtained from reactions of the diphosphine were found to be a structure related to **4**. The formation of the phosphinic acid was observed in these cases, likely due to contamination of the reagents with oxygen atom sources such as O_2 and H_2O. As seen in Figure 1.18, the structure is a phosphorus analogue of a carboxylic acid dimer in the solid state. To investigate the formation of this product, reactions were proposed based on simple organic chemistry procedures (Scheme 1.27). Reactions of the diphosphine (**2**) with: (i) H_2O_2 (40% in H_2O) in THF, and (ii) O_2 in toluene forming the phosphinic anhydride **4** and subsequent treatment with H_2O in THF were both found to produce the phosphinic acid structure by $^{31}P\{^1H\}$ NMR (δ = 6.45 ppm) as well as in the solid state X-ray diffraction analyses.

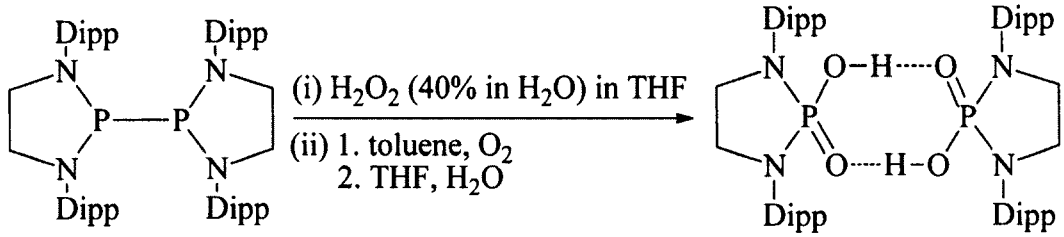

Scheme 1.27 Conversion of the diphosphine (**2**) to the phosphinic acid (**5**).

The crystal structure of the phosphinic acid (**5**) was found in two different space groups depending on the solvent used for crystallization. As seen in Figure 1.19, the structure is found in a dimeric hydrogen bonded conformation that would be expected in phosphinic acids. The P=O distance was found to be 1.501(2) Å, significantly longer than that in $Me_2P(O)$-O-$P(O)Me_2$ (1.471(2) Å),[82] and comparable to the $(CH_2PhCH)_2P(O)$-OH P=O bond (1.499 Å, no s.u. given). The P-OH phosphorus-oxygen bond was found to be 1.519(2) Å, shorter than that in $(CH_2PhCH)_2P(O)$-OH (1.543 Å, no s.u. given). The O(1)-

O(2) P=O•••(H)O hydrogen bond distance was found to be 2.508(3) Å which is not unexpected for a phosphinic acid dimer. In the case of $(CH_2PhCH)_2P(O)$-OH, a single hydrogen bond link (O•••O) was observed to be a similar 2.452 Å (no s.u. given).[83]

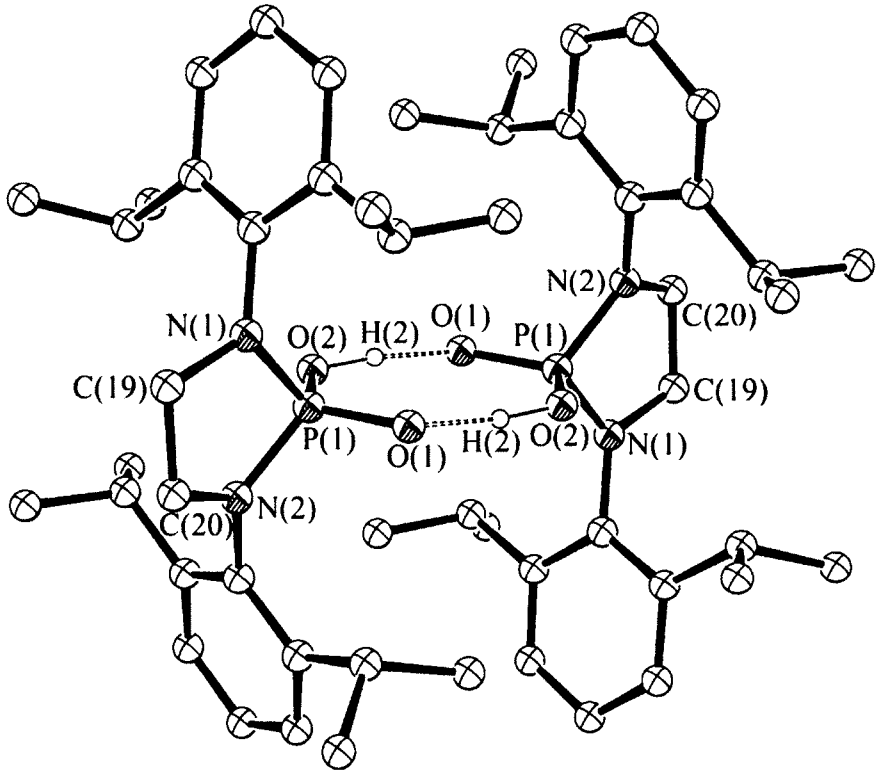

Figure 1.19 ORTEP of **5**, 50% ellipsoids are shown. Hydrogen atoms (other than H(2)) are removed for clarity. Distances (Å) angles (°): P(1)-O(2) 1.501(2), P(1)-O(1) 1.519(2), P(1)-N(2) 1.624(3), P(1)-N(1) 1.642(2), O(2)-H(2) 0.98(4), N(1)-C(19) 1.439(4), N(2)-C(20) 1.457(4), C(19)-C(20) 1.496(4). O(2)-P(1)-O(1) 112.19(12), O(2)-P(1)-N(2) 112.04(13), O(1)-P(1)-N(2) 113.28(12), O(2)-P(1)-N(1) 113.02(12), O(1)-P(1)-N(1) 110.85(12), N(2)-P(1)-N(1) 94.28(13), P(1)-O(2)-H(2) 114.9(17), C(19)-N(1)-P(1) 113.1(2), C(20)-N(2)-P(1) 112.7(2), N(2)-C(20)-C(19) 106.1(3), N(1)-C(19)-C(20) 108.7(3). O(2)•••HO(1) 2.508(3) Å.

Recently, Cowley and coworkers revisited the "jack-in-the-box" diphosphine featuring reactivity with the heavier chalcogens (Scheme 1.28). The result was the formation of the chalcogen bridged, ethereal product of the diphosphine isolated in poor yields.[69]

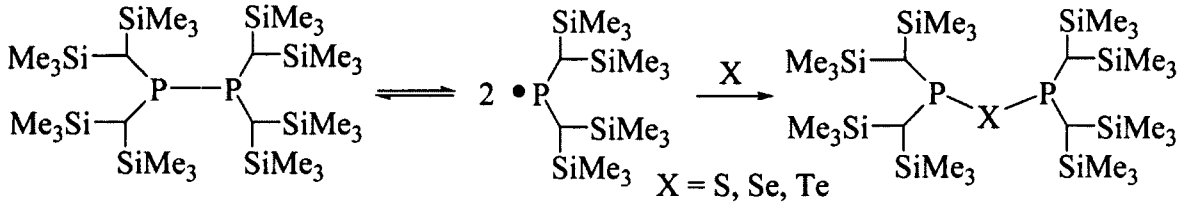

Scheme 1.28 Reactivity of the Cowley *et al.* diphosphine with elemental chalcogens.[69]

In our case, the product isolated from the reaction of $(Dipp_2C_2H_4N_2P)_2$ and elemental sulfur yielded both the persulfide and sulfide bridged insertion products, which co-crystallize in an approximately 87:13 ratio (and *vice versa*) as is depicted in Figures 1.20 and 1.21. Colourless crystals were grown by slowly evaporating a concentrated toluene solution of the reaction mixture, yielding large colourless block-like crystals of **6** and **7**.

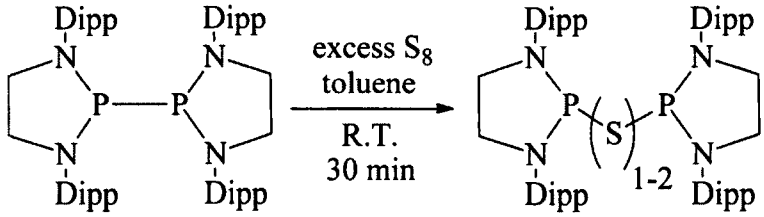

Scheme 1.29 Room temperature activation of elemental sulfur forming a phosphine-capped bridging persulfide/sulfide.

Triclinic and monoclinic space groups containing a roughly 87:13 ratio of the persulfide:bridging sulfide product were found in both cases as substitutional disorder in the crystal lattice. Limiting the reaction stoichiometry to one sulphur atom equivalent to one diphosphine does not force the reaction toward the sulfide insertion product completely. This finding corresponds well with the $^{31}P\{^1H\}$ NMR spectrum of the reaction mixture which only contains two peaks (154 and 136 ppm) in an approximate 9:1 ratio based on crude integration of the $^{31}P\{^1H\}$ signals. Several attempts at finding alternative products *via* X-ray crystallography from these two structures were

unsuccessful, supporting the $^{31}P\{^{1}H\}$ NMR evidence that **6-7** are the only significant products in the reaction. No reaction conditions were identified which resolved the stoichiometric discrepancies for the reaction of **2** with S_8.

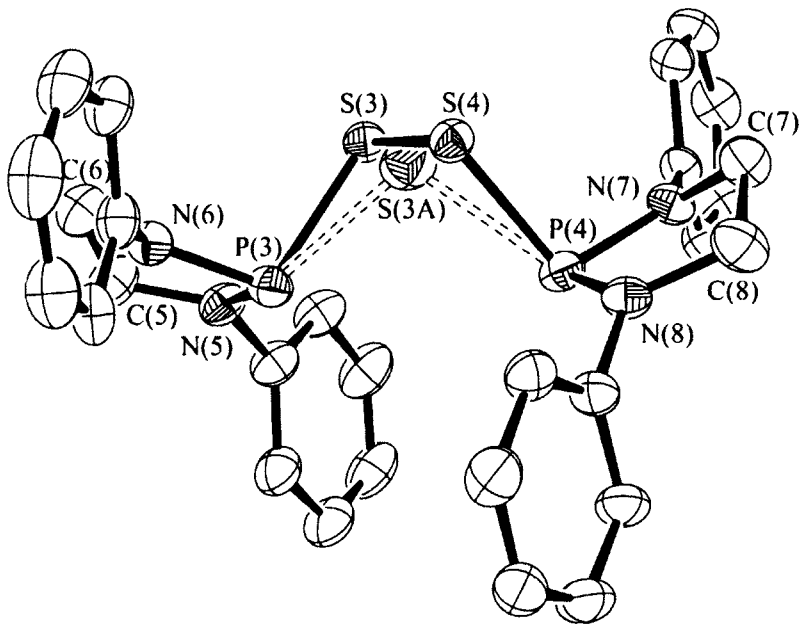

Figure 1.20 ORTEP of **6**, 50% ellipsoids are shown. Hydrogen atoms and ^{i}Pr groups are removed for clarity. One of two in the asymmetric unit. P(3)-S(3) 2.2006(18), P(3)-S(3A) 2.316(11), P(4)-S(3A) 2.322(10), P(4)-S(4) 2.1916(17), S(3)-S(4) 2.060(3), P(4)-N(7) 1.683(3), P(3)-N(5) 1.671(3), P(3)-N(6) 1.681(3), P(4)-N(8) 1.678(3), N(8)-C(8) 1.475(5), N(7)-C(7) 1.460(5), N(5)-C(5) 1.454(5), N(6)-C(6) 1.466(5), C(7)-C(8) 1.510(6), C(6)-C(5) 1.510(5). N(8)-P(4)-N(7) 90.78(16), N(8)-P(4)-S(3A) 122.3(3), N(8)-P(4)-S(4) 97.10(13), N(5)-P(3)-S(3) 106.83(14), N(6)-P(3)-S(3) 97.39(14), N(5)-P(3)-S(3A) 113.4(3), N(6)-P(3)-S(3A) 122.3(3), N(7)-P(4)-S(4) 104.94(13), N(7)-P(4)-S(3A) 111.6(3), N(5)-P(3)-N(6) 90.46(16), C(8)-N(8)-P(4) 115.9(3), C(7)-N(7)-P(4) 113.0(2), C(5)-N(5)-P(3) 114.0(2), C(6)-N(6)-P(3) 115.6(3), N(7)-C(7)-C(8) 106.2(3), N(6)-C(6)-C(5) 104.3(3), N(8)-C(8)-C(7) 105.1(3), N(5)-C(5)-C(6) 105.2(3).

The major product in Figure 1.20 is the persulfide (LP-S-S-PL) insertion product. In **6**, the P-S single bond distances were found to be 2.316(11) and 2.322(10) Å (Figure 1.20) which are slightly longer than those in Cowley's $[(Me_3Si)_2CH]_2P$-S-$P[(Me_3Si)_2CH]_2$ which has P-S bonds of 2.182(2) and 2.141(2) Å respectively.[69] The disulfide S-S bond (2.060(3) Å) is elongated, likely a result of the steric bulk around the

center of the molecule and electron donation throughout the NN'PSSPNN' core. When comparing the two structures it seems that substitutional disorder, when one product is in vast excess, promotes a significant change in the observed bond lengths for the minor product than might be expected.

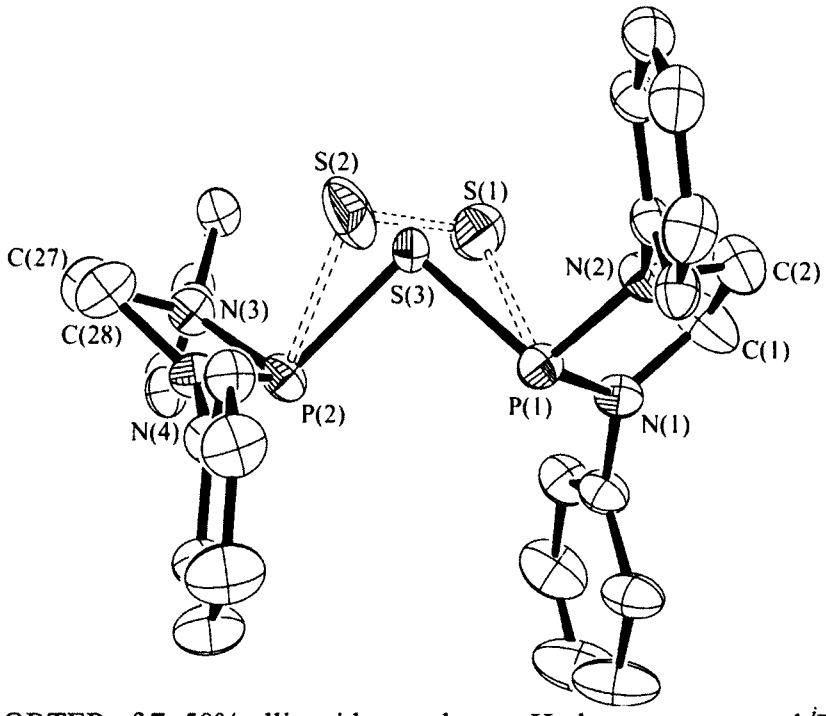

Figure 1.21 ORTEP of **7**, 50% ellipsoids are shown. Hydrogen atoms and ^{i}Pr groups are removed for clarity. Distances (Å) angles (°): P(1)-S(1) 2.237(4), P(1)-S(3) 2.1905(15), P(1)-N(1) 1.682(2), P(1)-N(2) 1.689(2), P(2)-S(2) 2.249(5), P(2)-S(3) 2.1912(14) P(2)-N(4) 1.691(3), P(2)-N(3) 1.695(2), N(1)-C(1) 1.421(4), N(2)-C(2) 1.455(4), N(4)-C(28) 1.457(4), N(3)-C(27) 1.452(4), C(2)-C(1) 1.479(4), S(2)-S(1) 1.952(16), C(27)-C(28) 1.495(4). N(1)-P(1)-N(2) 89.82(12), N(1)-P(1)-S(1) 83.8(2), N(2)-P(1)-S(1) 90.05(19), N(4)-P(2)-N(3) 89.90(11), N(4)-P(2)-S(2) 85.9(3), N(3)-P(2)-S(2) 90.8(2), N(1)-P(1)-S(3) 108.58(8), N(2)-P(1)-S(3) 102.96(9), N(4)-P(2)-S(3) 108.50(9), N(3)-P(2)-S(3) 102.79(9), C(1)-N(1)-P(1) 114.56(19), C(2)-N(2)-P(1) 115.74(17), C(28)-N(4)-P(2) 113.50(18), C(27)-N(3)-P(2) 115.52(17), N(2)-C(2)-C(1) 106.2(2), N(1)-C(1)-C(2) 108.1(3), N(3)-C(27)-C(28) 105.8(2), N(4)-C(28)-C(27) 105.4(2), S(1)-S(2)-P(2) 90.7(4), S(2)-S(1)-P(1) 88.2(3).

The structure of **7** contains the sulfide (LP-S-PL) as the major product (Figure 1.21). The P-S distances were found to be 2.1905(15) and 2.1912(14), corresponding well

with the phosphorus sulphide P-S single bonds of $[(Me_3Si)_2CH]_2P$-S-$P[CH(Me_3Si)_2]_2$ (2.182(2) and 2.141(2) Å),[69] and $Ph_2(S)P$–S–S–$P(S)Ph_2$ (2.193(1) Å).[84] In **7**, the central S(2)-S(1) bond was found to be 1.952(16) Å, marginally shorter than in **6** above (Figure 1.20).

The reactivity of **2** with the heavier chalcogens was also examined. One equivalent of gray selenium metal was allowed to stir overnight in THF with the diphosphine (**2**). The orange solution transitions to bright yellow over the reaction period. The THF was removed *in vacuo* and the resulting colourless solid was dissolved in toluene and filtered through a pad of diatomaceous earth. Slow evaporation of the pale yellow solution at ambient temperatures yielded X-ray quality colourless crystals of $(Dipp_2C_2H_4N_2P)_2Se$ (Scheme 1.30). The result of the reaction was the P(III) capped bridged selenide **8**.

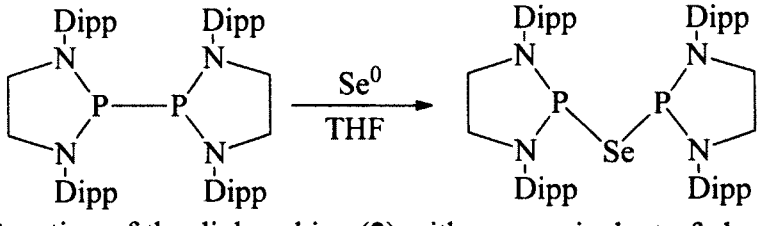

Scheme 1.30 Reaction of the diphosphine (**2**) with one equivalent of elemental selenium in THF yielding **8**.

A single peak was observed in the $^{31}P\{^1H\}$ NMR spectrum at 160.01 ppm with satellite coupling to ^{77}Se (7.63 % abundance, spin = ½, $^1J_{P\text{-}Se}$ = 141 Hz). The P(1)-Se(1) and P(2)-Se(1) single bond distances were found to be 2.346(2)and 2.351(2) Å respectively, which are longer than Cowley's $[(Me_3Si)_2CH]_2P$-Se-$[(Me_3Si)_2CH]_2$ which has a P-Se single bond lengths of 2.333(2) and 2.295(2) Å.[69] The bridging selenide insertion product is similar in appearance to that observed in the case of the sulfide

described earlier (**6** and **7**). The P-Se bond lengths of the four molecules in the asymmetric unit are consistent, ranging from 2.3440(18)-2.3712(19) Å.

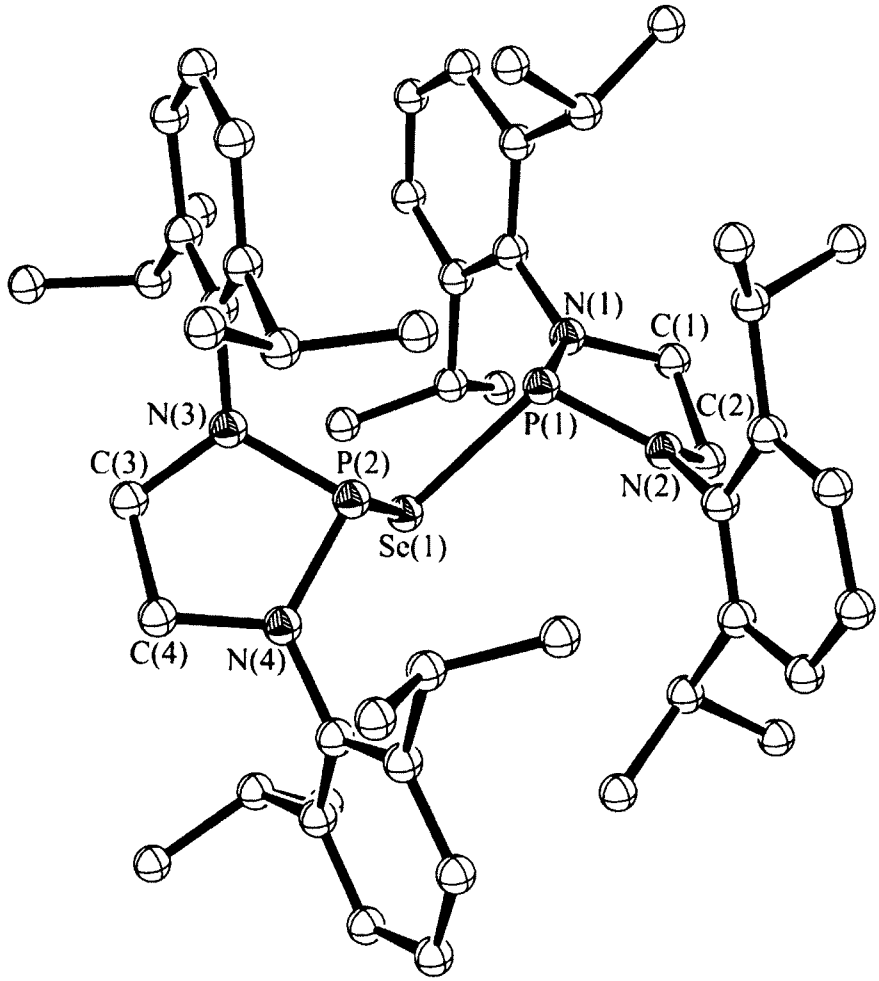

Figure 1.22 ORTEP of **8**, 50% ellipsoids are shown. Hydrogen atoms are removed for clarity. One of four in the asymmetric unit. Distances (Å) angles (°): Se(1)-P(1) 2.3466(19), Se(1)-P(2) 2.3514(18), P(2)-N(3) 1.681(5), P(2)-N(4) 1.689(6), P(1)-N(2) 1.684(5), P(1)-N(1) 1.706(5), N(2)-C(2) 1.475(8), N(3)-C(3) 1.461(9), N(4)-C(4) 1.477(8), N(1)-C(1) 1.465(8), C(1)-C(2) 1.507(9), C(4)-C(3) 1.521(9). P(1)-Se(1)-P(2) 85.57(7), N(3)-P(2)-N(4) 90.1(3), N(3)-P(2)-Se(1) 109.4(2), N(4)-P(2)-Se(1) 102.2(2), N(2)-P(1)-N(1) 90.2(3), N(2)-P(1)-Se(1) 109.2(2), N(1)-P(1)-Se(1) 102.4(2), C(2)-N(2)-P(1) 113.3(4), C(1)-N(1)-P(1) 114.7(4), C(3)-N(3)-P(2) 114.0(4), C(4)-N(4)-P(2) 115.7(4), N(1)-C(1)-C(2) 104.7(5), N(2)-C(2)-C(1) 104.3(5), N(4)-C(4)-C(3) 103.6(5), N(3)-C(3)-C(4) 104.6(5).

If an excess of gray selenium metal (5 equivalents Se^0) is allowed to stir for three days in THF with the diphosphine (**2**), the result is a mixed P(V)/P(III) ethereal oxidation

product (Scheme 1.31). The bright orange solution transitions to colourless over the reaction period. By slowly evaporating the THF solvent at ambient temperatures, X-ray quality colourless crystals of **9** were isolated (Figure 1.23).

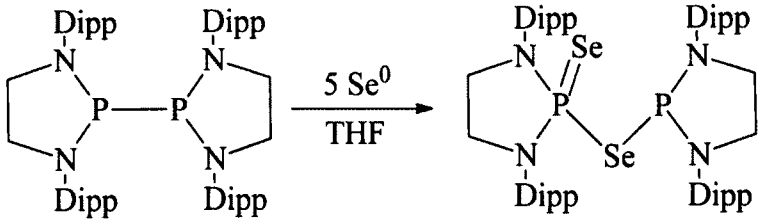

Scheme 1.31 Reaction of the diphosphine (**2**) with five equivalents of elemental selenium in THF to yield **9**.

Multiple peaks were observed in the $^{31}P\{^{1}H\}$ NMR at 160.01 (LP-Se-PL), 39.88, 35.10, 34.91 and 4.30 ppm for this reaction and are indicative of a P(III) and multiple P(V) phosphorus environments. Because the reaction stoichiometry is not selective and could not be controlled after the first equivalent is added (Figure 1.23), the reaction of diphosphine (**2**) with excess selenium was not pursued further. Disorder was present in the crystal structure in which one phosphorus atom is oxidized fully to P(V) forming a phosphorus-selenium double bond. For this particular crystal, the P(2) phosphorus atom was found to be oxidized to P(V) with a second equivalent of selenium [Se(2A)] approximately 60% of the time. P(1)-Se(1) and P(2)-Se(1) single bond distances were found to be 2.302(2) and 2.355(2) Å respectively, similar to the P-Se bonds in $[(Me_3Si)_2CH]_2P$-Se-$[(Me_3Si)_2CH]_2$ (2.333(2) and 2.295(2) Å).[69] The P(2)=Se(2) and P(1)=Se(2A) double bonds were found to be significantly different at 2.058(2) and 2.024(2) Å. These bond lengths are similar to P=Se double bonds reported in the literature such as in $[HN(SP^{i}Pr_2)(SePPh_2)]$ (2.0971(8) Å).[85] The molecular structure of **9**

is similar in appearance to that observed in the reaction of **2** with elemental oxygen but it only has one phosphorus atom oxidized to P(V).

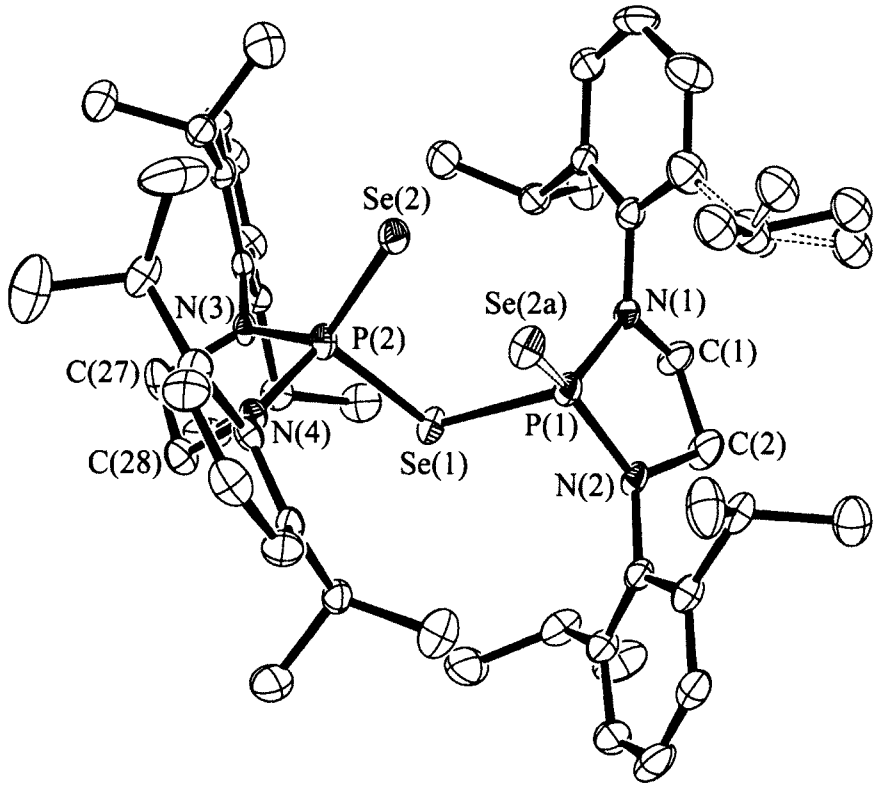

Figure 1.23 ORTEP of **9**, 50% ellipsoids are shown. Hydrogen atoms are removed for clarity. Distances (Å) angles (°): Se(1)-P(2) 2.3024(15), Se(1)-P(1) 2.3549(16), P(2)-Se(2) 2.0581(16), P(1)-Se(2A) 2.024(2), P(1)-N(1) 1.667(4), P(1)-N(2) 1.684(4), N(1)-C(1) 1.463(5), C(1)-C(2) 1.494(6), P(2)-N(4) 1.665(4), P(2)-N(3) 1.676(4), N(2)-C(2) 1.444(6), N(3)-C(27) 1.458(6), N(4)-C(28) 1.460(6), C(27)-C(28) 1.501(6). P(2)-Se(1)-P(1) 100.10(5), N(1)-P(1)-N(2) 90.7(2), N(1)-P(1)-Se(2A) 117.57(16), N(2)-P(1)-Se(2A) 132.29(17), N(1)-P(1)-Se(1) 108.73(15), N(2)-P(1)-Se(1) 99.50(15), Se(2A)-P(1)-Se(1) 105.53(8), C(1)-N(1)-P(1) 112.7(3), N(1)-C(1)-C(2) 104.8(4), N(4)-P(2)-N(3) 92.3(2), N(4)-P(2)-Se(2) 115.79(15), N(3)-P(2)-Se(2) 128.76(16), N(4)-P(2)-Se(1) 110.38(14), N(3)-P(2)-Se(1) 100.80(14), Se(2)-P(2)-Se(1) 107.16(7), C(2)-N(2)-P(1) 115.0(3), N(2)-C(2)-C(1) 105.4(4), C(27)-N(3)-P(2) 113.8(3), C(28)-N(4)-P(2) 111.5(3), N(3)-C(27)-C(28) 105.2(4), N(4)-C(28)-C(27) 105.3(4).

The atomic size of elemental selenium may be prohibitive for this reaction, as the second and third equivalents of selenium may not fit easily into the sterically crowded LP-Se-PL core, therefore not converging to a single product over the arbitrary reaction

period. Extended reaction times and/or heating may facilitate alternative reactivity of the diphosphine with elemental chalcogens. The focus of this project was not to explore harsh reaction conditions as we were probing the activation of main group elements at ambient temperatures so the reaction of **2** with excess Se^0 was not pursued further.

It appears that the allotropic conformation and atomic size of the chalcogen can greatly affect the reactivity with the diphosphine (**2**). The main group element cages (P_4, S_8) are capped by the diphosphine as one would expect of a halogen mimic while other elements (O_2, Se^0) are fragmented and feature oxidation of at least one phosphorus atom to P(V). Any further investigation into the activation of elemental selenium should include the reaction of the diphosphine (**2**) with red selenium (Se_8), a cage analogous to elemental sulfur, enabling direct comparsion of reactivity based on allotropic structure.

The final elemental chalcogen readily available was tellurium. An excess of tellurium metal (5 equivalents) was stirred with the diphosphine (**2**) over three days in THF at ambient temperatures. The solution transitions slowly from orange to bright yellow over the reaction period. The THF was removed and the resulting pale-yellow solid dissolved in toluene. Filtering off excess tellurium metal through a pad of diatomaceous earth and reducing the solvent *in vacuo* afforded a concentrated solution of **10** (Scheme 1.32) which upon cooling to -35 °C overnight afforded yellow crystals.

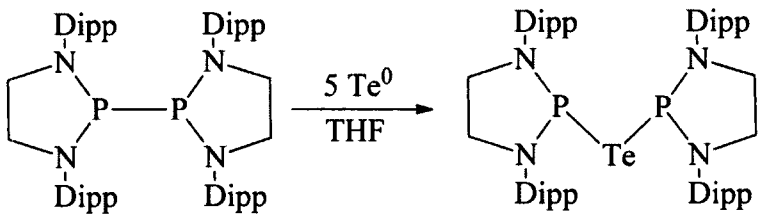

Scheme 1.32 Reaction of the diphosphine (**2**) with five equivalents of elemental tellurium in THF to yield **10**.

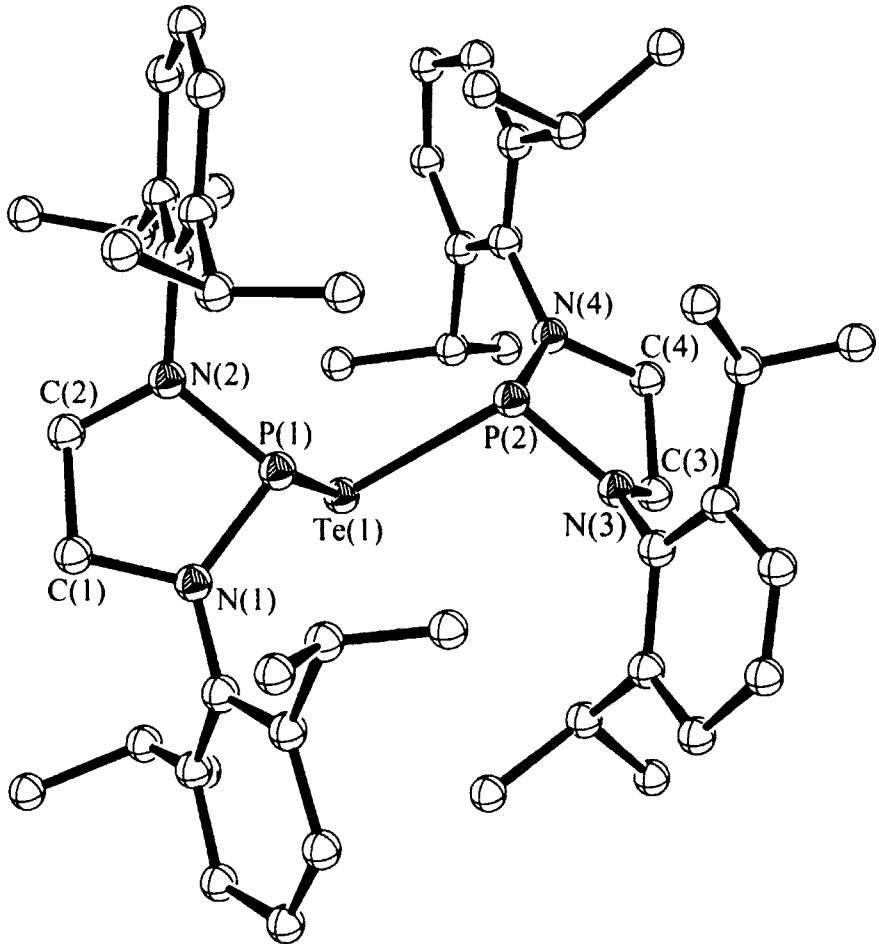

Figure 1.24 ORTEP of **10**, 50% ellipsoids are shown. Hydrogen atoms are removed for clarity. One of two in asymmetric unit. Distances (Å) angles (°): Te(1)-P(1) 2.587(8), Te(1)-P(2) 2.584(7), P(2)-N(4) 1.69(2), P(2)-N(3) 1.72(2), P(1)-N(1) 1.69(2), P(1)-N(2) 1.71(2), N(1)-C(1) 1.48(3), N(4)-C(4) 1.50(3), N(3)-C(3) 1.41(3), N(2)-C(2) 1.40(3), C(4)-C(3) 1.53(4), C(1)-C(2) 1.60(4). P(2)-Te(1)-P(1) 83.0(2), N(4)-P(2)-N(3) 90.9(12), N(4)-P(2)-Te(1) 103.1(8), N(3)-P(2)-Te(1) 109.0(9), N(1)-P(1)-N(2) 91.1(11), N(1)-P(1)-Te(1) 103.1(9), N(2)-P(1)-Te(1) 111.2(8), C(1)-N(1)-P(1) 114(2), C(3)-N(3)-P(2) 113.4(18), C(2)-N(2)-P(1) 113.4(18), N(4)-C(4)-C(3) 104(2), N(1)-C(1)-C(2) 103(2), N(2)-C(2)-C(1) 104(2), N(3)-C(3)-C(4) 105(2).

A single peak was observed in the $^{31}P\{^{1}H\}$ NMR spectrum at 177.07 ppm with satellite coupling to ^{125}Te (7.07 % abundance, spin = ½, $^{1}J_{P\text{-}Te}$ = 248 Hz). As can be seen in Figure 1.24, the P(1)-Te(1) and P(2)-Te(1) bond distances were found to be 2.587(8) and 2.584(7) Å respectively, similar to Cowley's $[(Me_3Si)_2CH]_2P\text{-}Te\text{-}[(Me_3Si)_2CH]_2$ which has P-Te single bond lengths of 2.505(2) and 2.552(2) Å.[69] The P-Te bond lengths

in the asymmetric unit are similar, ranging from 2.582(7)-2.587(8) Å. In spite of the vast excess of elemental tellurium, a single atom is inserted between the two phosphinyl moieties. The difference between this product and those observed for selenium (**8** and **9**) can be attributed to the increase in atomic size for tellurium. A space-filling model generated in Mercury (Figure 1.25) outlines the potential difficulty associated in adding a second equivalent of tellurium to the molecular center of **10**. The oxidation potential of the elemental chalcogens decreases as you descend down the group from oxygen to tellurium, providing a supporting electronic argument for the change in reactivity. This product suggests that the initial step in the formation of **9** is the LP-Se-PL P(III) species (**8**) which could then oxidize to the P(III)/P(V) product with another equivalent of selenium forming **9**. The analogous P(III)/P(V) species (PL(Te)-Te-PL) for tellurium may not be favored after the LP-Te-PL (**10**) insertion product is formed simply based on the atomic size of tellurium.

Figure 1.25 Space filling diagram of **10** generated in Mercury.

There are several molecular architectures which can be formed in reactions of the diphosphine (**2**) with group 16 elements. P(III) bridging (LP-X-PL, X = S, Se, Te) as well

as partial (LP(Se)-Se-PL) and full oxidation products (LP(O)-O-P(O)L) were formed in reactions with the elemental chalcogens. A general trend can be identified in the reactivity with an excess of elemental chalcogen as atomic size increases. From oxygen (LP(O)-O-(O)PL), to selenium (LP(Se)-Se-PL) and finally tellurium (LP-Te-PL) the increase in atomic radius appears to influence the stoichiometry of the reaction and potential for oxidation of a P(III) phosphorus atom to P(V) once initial chalcogen insertion has taken place. The exception to this trend is sulfur which was only identified to form the sulfide (LP-S-PL) or persulfide (PL-S-S-PL) insertion products. This may simply be a function of the allotropic conformation of sulfur which was employed (S_8). Future work in this area should include exploiting the versatile reactivity profile of the diphosphine (**2**) to explore the chemistry of other main group elements in varying stoichiometries, allotropes and reaction conditions looking for new functional groups.

- Section 1.5.5 Reactivity with Boranes

The reactivity of the diphosphine (**2**) was also investigated with Lewis acidic boranes. Numerous manuscripts have been recently published in which sterically bulky Lewis acid-base pairs have been employed to facilitate uncommon reactivity, specifically in reactions which traditionally depend on the presence of a transition metal. These Frustrated Lewis Pairs (FLPs) have been successful in activating industrially and environmentally relevant main group molecules such as hydrogen (H_2), carbon dioxide (CO_2) and carbon monoxide (CO).[86-88] Several of these reactions are based on the interaction of a sterically bulky phosphine (Lewis base) with a borane (Lewis acid). Phosphine-borane FLPs are predicated on the donation of the phosphine lone pair of

electrons into the empty *p*-orbital on boron. The steric strain at the bulky phosphorus and boron centers prevents the two centers from achieving their preferred proximity, generating a site in which molecules can react.

The phosphorus atom of the monomeric phosphinyl (**2**•) radical can act as a one- or two-electron donor to a borane (BR_3) *p*-orbital, thereby generating a scenario in which either: (1) a two-center, one-electron interaction takes place in which phosphorus retains its lone pair and the radical electron is shared between the two atoms (Scheme 1.33, middle), (2) the radical electron remains on phosphorus and its lone pair forms a traditional Lewis acid-base pair with the borane (Scheme 1.33, right), filling its empty *p*-orbital and generating an analogue of the phosphinyl which is relatively electron poor, potentially stabilizing a phosphinyl in its monomeric form.

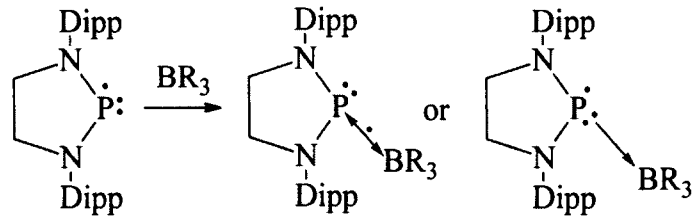

Scheme 1.33 Potential products of addition of the diphosphine (**2**) to a borane (BR_3).

The first reaction undertaken was the addition of the diphosphine (**2**) to one equivalent of the borane-dimethylsulfide complex (H_3B•SMe_2). Upon addition in THF, no $^{31}P\{^1H\}$ signal could be observed (including the parent diphosphine). This suggests that upon complexation to boron and displacement of SMe_2, a radical intermediate is formed supporting Scheme 1.33. After several minutes, a broad doublet can be observed at 82.0 ppm ($^1J_{P\text{-}B}$ = 73 Hz) in the $^{31}P\{^1H\}$ NMR, presumably from coupling to boron which expands to a doublet of doublets in the ^{31}P NMR spectrum ($^1J_{P\text{-}H}$ = 357, $^1J_{P\text{-}B}$ = 73 Hz). The $^1J_{P\text{-}B}$ coupling is not fully understood given that the NMR active nuclear spin of

^{11}B is 3/2 making the expected $^{1}J_{P\text{-}B}$ coupling a quartet. This system is almost certainly dynamic in solution (at ambient temperatures) and could simply be obscuring the true coupling through broadening. It is consistent with other phosphine-borane complexes in the literature which are reported as broad doublets in the $^{31}P\{^{1}H\}$ NMR with coupling constants of 50-100 Hz.[89] Interestingly, the ^{31}P NMR doublet of doublets ($^{1}J_{P\text{-}H}$ = 357 Hz) indicates that abstraction of a hydrogen atom from an unknown source has taken place forming the final LPH→BH_3 complex.

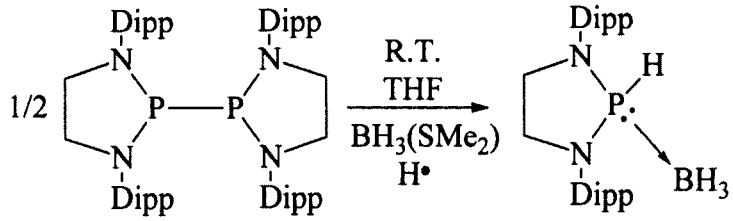

Scheme 1.34 Reaction of the diphosphine (**2**) with borane-dimethylsulfide complex in THF to yield **11**.

The NMR evidence is corroborated by the single crystal X-ray structure of **11** (Figure 1.26). The model features a Lewis acid-base pair in which the lone pair from phosphorus is coordinated to boron at a distance of 1.879(3) Å. This donor-acceptor distance is shorten than other phosphine→borane pairs in the literature such as $(H_3B)(Tripp)HP(CH_2)_3PH(Tripp)(BH_3)$ which has P-B distances of 1.916(4) and 1.918(4) Å.[90] This distance is far less than the sterically crowded FLP-type compounds such as $^{i}Pr_2P{=}N\text{-}P(^{c}Hex)_2{\rightarrow}B(C_6F_5)_3$ (2.135(5) Å). This is unsurprising given the relatively small size of BH_3.[91] Free refinement of the P-H bond in the single crystal X-ray structure indicated a bond length of 1.35(2) Å which would be slightly longer than those expected for literature phosphines (2220-2340 cm^{-1}).[92] Although X-ray analysis of a hydrogen atom position is an inexact method for determining bond length, the IR P-H stretching

frequency was found at 2236 cm^{-1} (KBr) which also suggests an elongated P-H bond compared to more traditional phosphines.[92] The IR spectrum of **11** was recorded as a KBr pellet of LPH-BD_3, made from the reaction of the phosphine $Dipp_2H_4C_2N_2P$-H (*vide infra*) and D_3B•THF, because the B-H absorbances were obscuring the P-H stretch in LPH-BH_3. The elongated P-H bond is not unexpected given the highly donating nature of the diamino-phosphine although the presence of the Lewis acidic borane should mitigate the electron donating ability at the phosphorus center. This finding makes the free phosphine ($Dipp_2H_4C_2N_2P$-H) an interesting synthetic target, a molecule which I will revisit shortly.

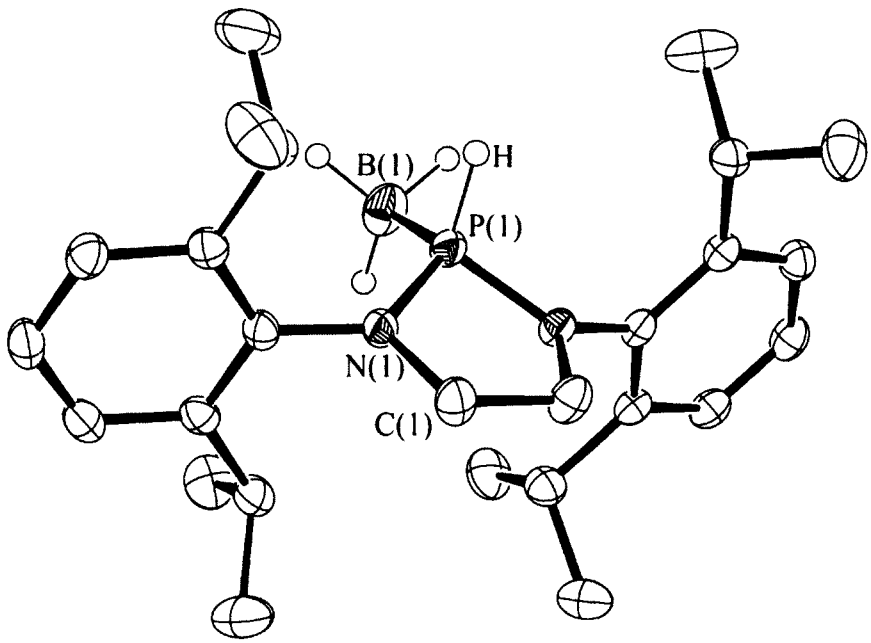

Figure 1.26 ORTEP of **11**, 50% ellipsoids are shown. Hydrogen atoms (other than on phosphorus and boron) are omitted for clarity. Distances (Å) angles (°): B(1)-P(1) 1.879(3), N(1)-C(1) 1.4689(19), N(1)-P(1) 1.6525(13), C(1)-C(1) 1.526(3). C(1)-N(1)-P(1) 112.87(10), N(1)-P(1)-N(1) 93.55(9), N(1)-P(1)-B(1) 120.46(8), N(1)-C(1)-C(1) 107.47(7).

The addition of the relatively small BH_3 allowed for the phosphorus radical to abstract a hydrogen atom from an unknown source. A bulky, more Lewis acidic borane

such as *tris*(pentafluorophenyl)borane may then be better positioned to stabilize a phosphinyl-borane intermediate. Addition of $B(C_6F_5)_3$ to the diphosphine (**2**) in toluene initiated a transition from the characteristic bright orange colour of **2** to pale yellow. The $^{31}P\{^1H\}$ NMR indicated a broad single peak at 66.8 ppm which expands to a doublet in the ^{31}P NMR ($^1J_{P-H}$ = 404 Hz). The P-H coupling once again indicates that hydrogen atom extraction is taking place (Scheme 1.35), forming an LPH→$B(C_6F_5)_3$ Lewis acid-base complex (**12**).

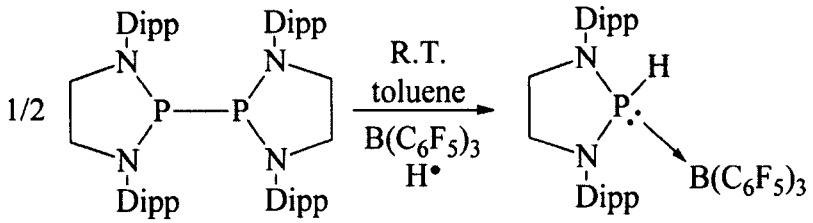

Scheme 1.35 Reaction of the diphosphine (**2**) with $B(C_6F_5)_3$ in toluene to yield **12**.

The presence of the P-H coupling in the NMR is again present in the single crystal structure (Figure 1.27). The steric bulk of tris(pentafluorophenyl)borane forms a strained Lewis acid-base pair in which the lone pair from phosphorus is coordinated to boron at a distance of 2.106(3) Å, significantly longer than in LPH→BH_3 (**11**, 1.879(3) Å). This B-P distance is similar to other sterically encumbered FLP-type, phosphine-borane interactions in the literature such as $^iPr_2P$=N-P(^{c}Hex)$_2$→$B(C_6F_5)_3$ (2.135(5) Å). The molecular center and can be better visualized as a reduced structure (Figure 1.28) based on the sterically encumbered nature of **12**.[91] Free refinement of the P-H bond in the single crystal X-ray structure indicated a bond length of 1.33(2) Å, slightly longer than those traditionally present in cyclic and acyclic diamino-phosphines.[92] The IR P-H stretching frequency was found at 2365 cm^{-1} (KBr), indicating a slightly weaker P-H bond than other diamino-phosphanes.[92] The elongated P-H bond may be expected given

the highly donating nature of **2**. As was the case with BH_3, the presence of the Lewis acidic borane should mitigate the electron donating ability at the phosphorus center. Since *tris*(pentafluorophenyl)borane is more Lewis acidic than borane (BH_3), the shift in the IR spectrum of **12** should be indicative of this increase in electrophilic character. This shift was identified in the IR spectra, transitioning from 2255 cm^{-1} in **11** to a broad absorbance at ~2365 cm^{-1} in **12**, a region which is more common for P-H absorbances.[93]

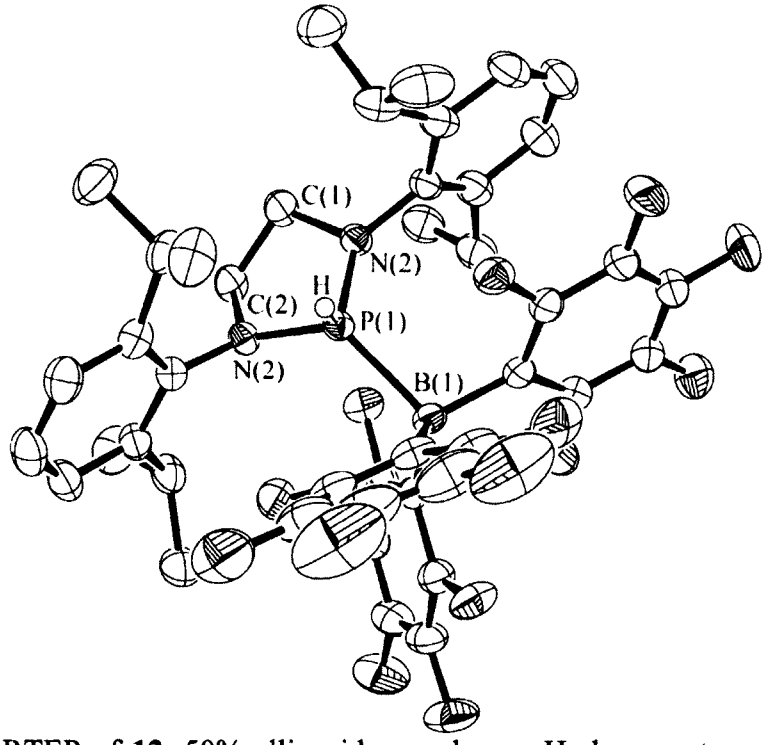

Figure 1.27 ORTEP of **12**, 50% ellipsoids are shown. Hydrogen atoms (other than on phosphorus) are omitted for clarity. Distances (Å) angles (°): P(1)-B(1) 2.106(3), N(1)-C(1) 1.482(3), N(1)-P(1) 1.671(2), N(2)-C(2) 1.475(3), N(2)-P(1) 1.677(2), P(1)-B(1) 2.106(3), C(1)-C(2) 1.508(4). C(1)-N(1)-P(1) 111.67(17), C(2)-N(2)-P(1) 111.62(16), N(1)-P(1)-N(2) 93.74(11), N(1)-P(1)-B(1) 121.16(12), N(2)-P(1)-B(1) 125.82(12), N(1)-C(1)-C(2) 104.6(2), N(2)-C(2)-C(1) 105.3(2).

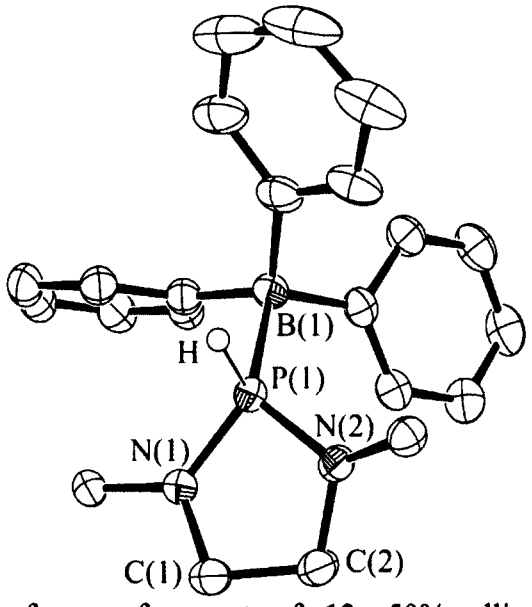

Figure 1.28 ORTEP of core fragment of **12**, 50% ellipsoids are shown. 2,6-diisopropylphenyl groups, fluorine and hydrogen atoms (other than on phosphorus) are omitted for clarity.

On several occasions while attempting to isolate **12**, a single crystal structure of another product was obtained. The same phosphine LP-H structure was observed, but included an oxygen atom link to the borane fragment (Scheme 1.36).

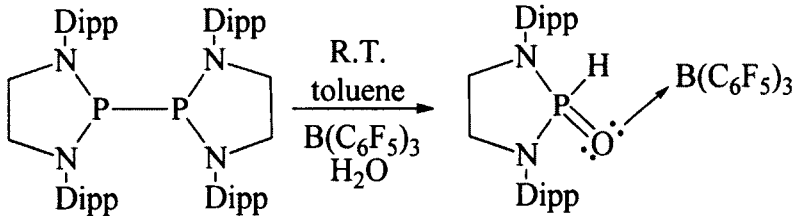

Scheme 1.36 Formation of an oxygen linked LPH phosphine-borane (**13**).

This product could be formed in a reaction with water coordinated *tris*(pentafluorophenyl)borane, not completely removed upon sublimation in the purification of the borane starting material. Initial hydrogen atom abstraction from the $(C_6F_5)_3B{\bullet}OH_2$ water molecule could form an equivalent of phosphine (LPH). Subsequent radical coupling to a second equivalent of phoshphinyl with $(C_6F_5)_3BHO{\bullet}$ followed by a final hydrogen atom transfer step to the phosphorus atom from the oxygen could yield **13**.

This compound was not pursued further as the chemistry of water coordinated *tris*(pentafluorophenyl)borane is not generally a focus of our research group. It was thought to be a useful structure to present as it conveys the highly sensitive nature of the reactivity profile of **2** toward any impurities.

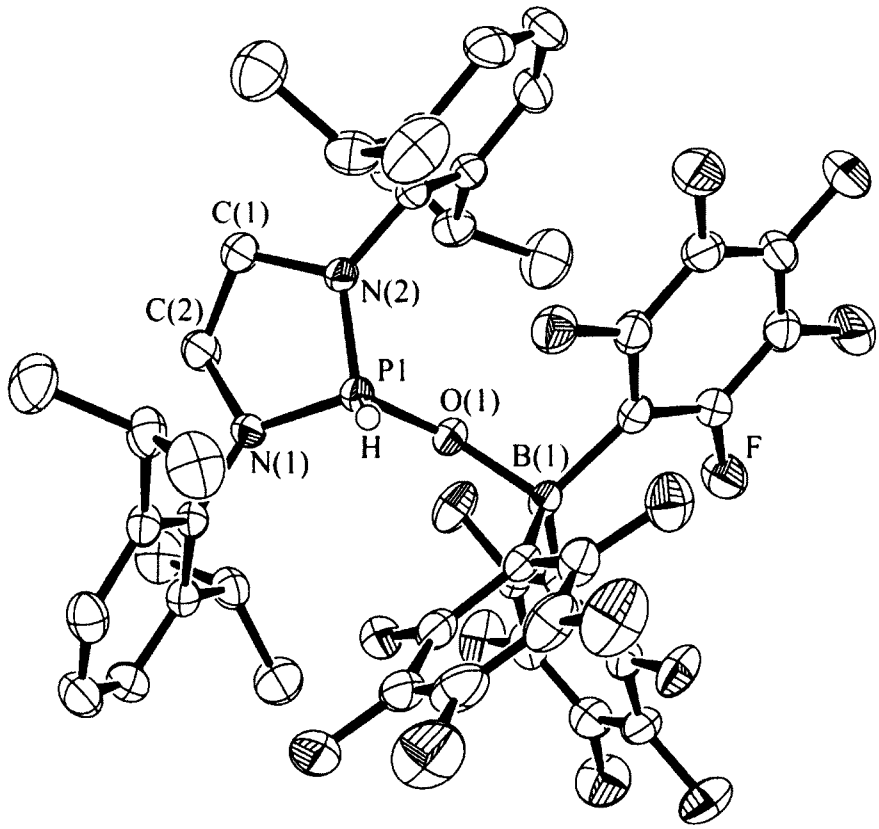

Figure 1.29 ORTEP of **13**, 50% ellipsoids are shown. Hydrogen atoms (other than on phosphorus) are omitted for clarity. Distances (Å) angles (°): C(1)-N(2) 1.471(3), C(1)-C(2) 1.488(4), C(2)-N(1) 1.474(3), P(1)-O(1) 1.5075(17), P(1)-N(2) 1.621(2), P(1)-N(1) 1.626(2), B(1)-O(1) 1.561(3). N(2)-C(1)-C(2) 105.5(2), N(1)-C(2)-C(1) 106.7(2), C(1)-N(2)-P(1) 112.97(16), P(1)-O(1)-B(1) 138.04(16), C(2)-N(1)-P(1) 111.38(16), O(1)-P(1)-N(2) 112.33(10), O(1)-P(1)-N(1) 119.78(10), N(2)-P(1)-N(1) 95.64(10).

Finally, the nature and origin of the P-H bond found in the phosphine-borane complexes was investigated. The IR spectra and X-ray crystal structures of **11** and **12** indicate that in spite of the presence of the Lewis acidic borane (BH_3 or $B(C_6F_5)_3$), the P-H bond is elongated compared to literature parallels. The question then arises, what

would be the fate of the P-H bond if the Lewis acidic borane was not present? The synthesis of the phosphine (LPH) was attempted independently from the chlorophosphine to investigate the LP-H functional group (Scheme 1.37).

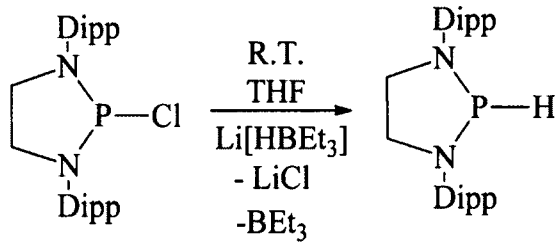

Scheme 1.37 Synthesis of the phosphine $Dipp_2H_4C_2N_2P$-H (**14**) from the parent chlorophosphine using super-hydride in THF.

Reduction of the chlorophosphine with superhydride ($Li[HBEt_3]$, 1.0 M in THF) was found to be the most reliable synthesis and could be repeated on multi-gram scales in good yields (~80%). Colourless crystals of **14** could be grown by slow evaporation of a concentrated pentane solution at ambient temperatures (Figure 1.30). The structure of **14** was found to be remarkably similar in conformation to the parent chlorophosphine (**1**) with the exception of the hydrogen for chlorine substitution. The single crystal structure of **14** indicated a P(1)-H(3) bond of 1.688(18) Å. This bond length would be far longer than a typical phosphorus-hydrogen interaction, even one which has a collection of highly donating atoms in the molecular scaffold such as the N-P-N core in **14**.

The P-H bond length is likely a function of the electronic structure coupled with a short contact interaction between H(3) and H(11B) present in the solid state structure, effectively pulling the P-H hydrogen atom toward an *iso*-propyl hydrogen atom in a second LPH molecule (Figure 1.30). The P(1)-C(11) distance is 4.238 Å while the H(3)-H(11B) distance was found to be approximately 2 Å. Similar proton-hydride interactions have been observed in the crystalline state, although generally involve a metal hydride.[94]

In order to investigate the P-H bond further, IR spectra were collected in a solid state KBr pellet as well as in a heptane solution. P-H stretching frequencies of 2025 and 2047 cm^{-1} were identified.

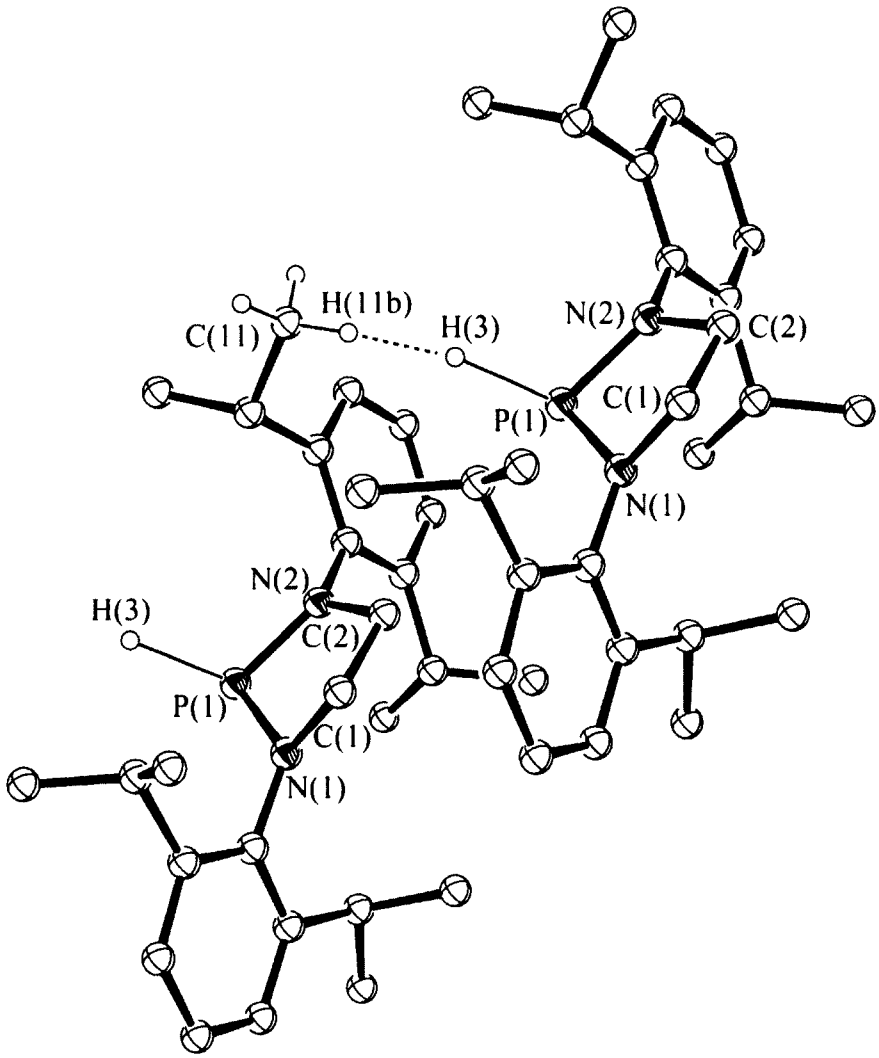

Figure 1.30 ORTEP of **14**, 50% ellipsoids are shown. Hydrogen atoms (other than on phosphorus) are omitted for clarity. Distances (Å) angles (°): P(1)-H(3) 1.688(18), P(1)-N(2) 1.683(2), P(1)-N(1) 1.698(2), N(1)-C(1) 1.480(4), N(2)-C(2) 1.485(4), C(1)-C(2) 1.511(4). N(2)-P(1)-N(1) 91.22(12), N(2)-P(1)-H(3) 111.5(6), N(1)-P(1)-H(3) 114.0(7), C(1)-N(1)-P(1) 110.06(18), C(2)-N(2)-P(1) 114.53(19), N(1)-C(1)-C(2) 105.2(2), N(2)-C(2)-C(1) 105.7(2). H(3)•••H(11B) 2.04 Å.

These IR stretches are at the extreme end of the traditional phosphine range and are indicative of an elongated bond, similar to those recently reported with phosphenium-hydride type character (Figure 1.31).[95] As can be seen in Table 1.8, there is a general trend in the ^{31}P NMR shifts, $^{1}J_{P-H}$ coupling constants and IR P-H stretching frequencies for molecules of this nature. As the P-H bond elongates, the ^{31}P NMR signal is more deshielded, the coupling constant is reduced from traditional P-H coupling (~300 Hz) to extreme cases in which it approaches 130 Hz and the IR stretching frequency is red shifted. According to the literature, the reduction in the magnitude of the coupling constant can be attributed to increased steric bulk around a phosphine (P-H).[93]

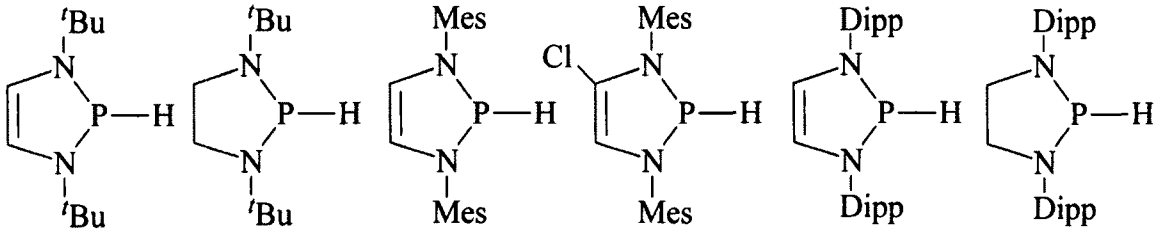

Figure 1.31 Molecules with polarized P-H bonds.

Table 1.8 Collection of spectroscopic data on polarized P-H bonds in Figure 1.7.

	^{31}P (ppm)	$^{1}J_{P-H}$ (Hz)	^{1}H (ppm)	υ P-H (cm^{-1})	P-H (Å)	Reference
A	57.1	181	6.07	2176 (gas)	-	96
B	57.9	156	5.67	2340	-	92
C	64.0	139	7.13	-	-	96
D	75.8	147	7.17	2120 (gas)	1.51(4)	95
E	71.6	132.6	7.39	-	1.48(1)	95
F	72.0	141	7.04	2025 (KBr) 2047 (heptane)	1.347(16)- 1.688(18)	This work

Steric strain affects the central bond angles at phosphorus, increasing the *s*-character in the P-H bond. Therefore, as steric bulk is added at the phosphorus atom the P-H becomes progressively more basic.[93] This implies that steric hindrance around a

phosphine is inversely proportional to the $^{1}J_{P\text{-}H}$ coupling-constant. Based on similar arguments, we would then expect the IR P-H stretch to become red shifted, transitioning to a lower wavenumber.

In **14** (F, Figure 1.31), the ^{31}P NMR shift (72.0 ppm), $^{1}J_{P\text{-}H}$ coupling constant (141 Hz), IR stretching frequency (2025 cm^{-1} in KBr, 2047 cm^{-1} in heptane) and the P-H bond distance in the single crystal structure 1.688(18) Å are indicative of an extreme case of a phosphorus-hydrogen bond. This molecule can be described as a highly polarized [LP][H] type interaction like those published recently by Burck *et al.*[95,96] In order to decouple the role of the short contact observed in Figure 1.30, crystals of the LPH were regrown from a slowly evaporating toluene solution, forming large colourless blocks of **15** (Figure 1.32). The new structural model lacks the short contact in Figure 1.30. The P(1)-H(1) bond distance was allowed to freely refine and was found to be 1.347(16) Å. This distance is still elongated compared to traditional phosphorus-hydrogen bonds although it is consistent with phosphenium-hydrides reported in the literature (Table 1.7).

The spectroscopic data collected of **14-15** supports the findings for the borane complexes, which in spite of the presence of a Lewis acidic borane contain elongated P-H bonds. Steric arguments as well as the X-ray and IR data collected suggest this may be among the most polarized P-H bonds that have been observed to date. As an organic molecule with the potential to act as a hydride source, this molecule should be investigated in the future to examine its reactivity profile.

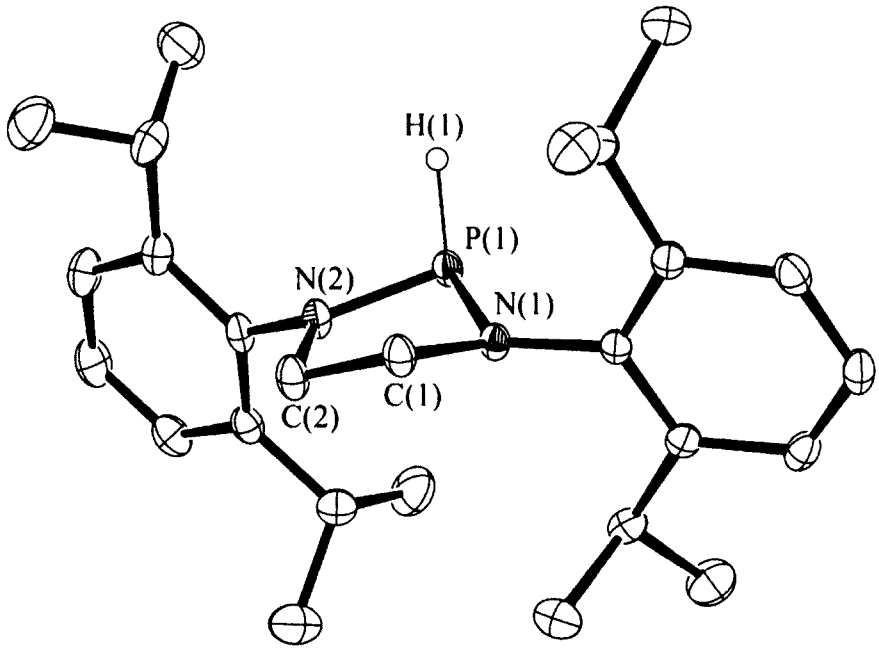

Figure 1.32 ORTEP of **15**, 50% ellipsoids are shown. Hydrogen atoms (other than on phosphorus) are omitted for clarity. Distances (Å) angles (°): P(1)-H(1) 1.347(16), P(1)-N(2) 1.6845(15), P(1)-N(1) 1.7000(14), N(1)-C(1) 1.474(2), N(2)-C(2) 1.468(2), C(1)-C(2) 1.518(2). N(2)-P(1)-N(1) 90.76(7), N(2)-P(1)-H(1) 100.5(8), N(1)-P(1)-H(1) 101.5(7), C(1)-N(1)-P(1) 110.41(11), C(2)-N(2)-P(1) 114.79(11), N(1)-C(1)-C(2) 104.83(14), N(2)-C(2)-C(1) 106.22(14).

The remaining question concerns the origin of the hydrogen atom in the phosphine-borane complexes described earlier (**11-12**). The ^{31}P NMR evidence and final structures suggest that a radical intermediate is formed initially, which then abstracts a hydrogen atom from an unknown source (Scheme 1.38).

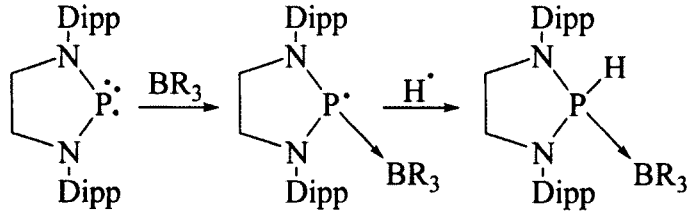

Scheme 1.38 The Lewis acid/base formation between the phosphinyl (**2**) and boranes featuring subsequent hydrogen atom abstraction.

There are several sources for the phosphine hydrogen atom including: (1) solvent, (2) reagents, BH_3 is only commercially available base coordinated (SMe_2, NMe_3) and

$B(C_6F_5)_3$ is prepared either as either an H_2O or Et_2O adduct before sublimation, (3) excess diphosphine and (4) other impurities.

A series of NMR experiments were proposed which should permit the identification of the $H^{\bullet}$ source through deduction (Scheme 1.39). The combination of solvent and reagents should yield either a singlet or triplet in the $^{31}P\{^1H\}$ NMR spectrum depending on the presence of a LPH (^1H spin = ½) or LPD (^2D spin = 1) phosphine.

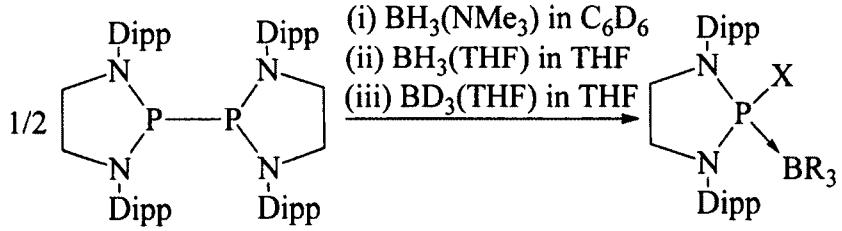

(i) R = H, X = H or D (ii) R = H, X = H (iii) R = D, X = H or D

Scheme 1.39 NMR experiments designed to indicate the origin of hydrogen atom abstraction forming LPH→BR_3 structures.

The NMR spectra collected in the reaction of diphosphine (**2**) with two equivalents of $BH_3(SMe_2)$ suggest that a hydrogen atom is abstracted forming **11**. The ^{31}P NMR was found to contain a doublet of doublets ($^1J_{P\text{-}H}$ = 357 Hz) resulting from coupling to boron as well as the hydrogen atom in the LPH→BH_3 structure. Under the assumption that the likely sources of the hydrogen atom include either a reagent (borane) or from solvent, three experiments were proposed between the diphosphine (**2**) and: (i) borane-trimethylamine complex in C_6D_6, (ii) borane-tetrahydrofuran complex in THF, or (iii) borane-d_3-tetrahydrofuran complex in THF. The first reaction undertaken was the diphosphine (**2**) with $Me_3N{\bullet}BH_3$ in C_6D_6. The $^{31}P\{^1H\}$ and ^{31}P NMR spectra of this reaction presented as a single peak corresponding to the diphosphine (143.46 ppm) indicating that no reaction had taken place. The ^{11}B was found to be a sharp quartet at -

7.55 ppm ($^{1}J_{B-H}$ = 98 Hz) which is the borane-trimethylamine starting material. In the second and third reactions, the $^{31}P\{^{1}H\}$ and ^{31}P NMR spectra included several broad peaks and were inconclusive regarding the nature of the hydrogen abstraction. The ^{11}B signals in both (ii) and (iii) were broad peaks and not conducive to the identification of a specific product or splitting pattern. The line broadening in the ^{11}B signal is representative of the dynamic nature of the phosphine-borane interaction as was the case in **11**. The reaction of **2** with $SMe_2 \cdot BH_3$ (Scheme 1.34) was found to be the only process which converges to a single product. Low temperature ^{31}P and ^{11}B experiments may be better suited to resolve the NMR spectra but unfortunately, is not currently available. An IR study was also completed comparing the spectra from the reaction of: (i) LPH (**14-15**) and $THF \cdot BD_3$ in THF forming $LPH \cdot BD_3$, (ii) diphosphine (**2**) and $SMe_2 \cdot BH_3$ in THF and (iii) diphosphine (**2**) and $THF \cdot BD_3$ in THF. Reaction (i) enabled the location of the borane coordinated P-H signal which was obscured by the borane B-H absorbances at 2265 cm^{-1}, a signal which could also be identified in reaction (ii). Reaction (iii) had no peak in the region associated with the P-H absorbance. If deuterium abstraction had taken place a weak P-D absorbance would expected at 1581 cm^{-1} (2265 cm^{-1} * $[\sqrt{2}]/2$ = ~1581 cm^{-1}). This region was obscured by several other signals including B-D absorbances and could not be identified. If a P-D absorbance was present it may suggest that excess borane reagent may be the source of the hydrogen atom in **11**. However, this would not be supported by the reaction of the diphosphine (**2**) with *tris*(pentafluorophenyl)borane (Scheme 1.35) forming **12**, which displays the same hydrogen atom abstraction but lacks an available hydrogen atom on boron. Likewise, the ^{31}P, $^{31}P\{^{1}H\}$ and ^{11}B NMR spectra

from the reaction of **2** with H_3B•THF indicated that it does not converge to a single product. Unfortunately, the data collected herein regarding the origin of the hydrogen atom abstraction in **11-12** was inconclusive any may suggest the phosphinyl→borane radical intermediate may be too reactive in the presence of a hydrogen atom source to be isolable.

- Section 1.5.6 Reactivity with Heteroallenes

The next series of reactions completed toward understanding the synthetic limits of the diphosphine (**2**) was to investigate its reactivity toward industrially and environmentally relevant main group compounds. The first molecules probed were carbon dioxide (CO_2) and carbon monoxide (CO). Neither was found to be reactive with **2**, even under refluxing conditions in toluene. Based on the relatively inert nature of CO and CO_2, it was reasoned that carbon centered molecules with different heteroatom substituents may be better suited to react with a halogen-mimic such as **2**. Three target heteroallenes were proposed including carbon disulfide (CS_2), phenyl isocyanate (Ph-NCO) and phenyl isothiocyanate (Ph-NCS).

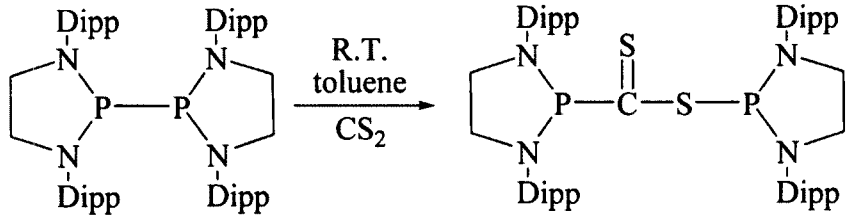

Scheme 1.40 Reaction of carbon disulfide with the diphosphine (**2**) forming LP-C(S)-S-PL to yield **16**.

Upon addition of CS_2 to a toluene solution of the diphosphine (**2**), the orange solution transitions to bright green instantaneously. Crystallization by slow evaporation of a concentrated toluene solution yielded pale green crystals of **16** (Scheme 1.40).

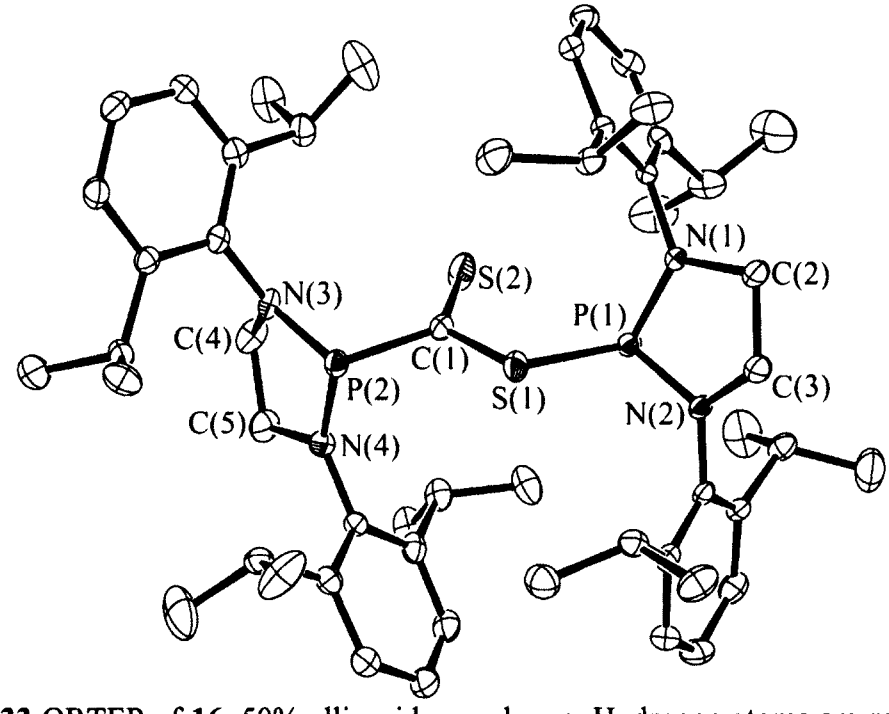

Figure 1.33 ORTEP of **16**, 50% ellipsoids are shown. Hydrogen atoms are removed for clarity. Distances (Å) angles (°): P(1)-N(2) 1.663(3), P(1)-N(1) 1.671(3), P(1)-S(1) 2.2774(17), P(2)-N(3) 1.683(3), P(2)-N(4) 1.709(3), P(2)-C(1) 1.895(4), S(1)-C(1) 1.741(4), S(2)-C(1) 1.624(4), C(5)-N(4) 1.464(5), C(5)-C(4) 1.513(6), C(2)-N(1) 1.462(5), C(2)-C(3) 1.500(6), C(4)-N(3) 1.457(5), C(3)-N(2) 1.462(5). N(3)-P(2)-N(4) 91.43(17), N(3)-P(2)-C(1) 105.84(18), N(4)-P(2)-C(1) 99.93(18), N(2)-P(1)-N(1) 90.68(16), N(2)-P(1)-S(1) 102.11(13), N(1)-P(1)-S(1) 104.05(12), C(1)-S(1)-P(1) 99.47(15), N(4)-C(5)-C(4) 106.9(4), N(1)-C(2)-C(3) 106.5(3), N(3)-C(4)-C(5) 106.4(3), N(2)-C(3)-C(2) 105.3(3), C(4)-N(3)-P(2) 114.4(3), C(3)-N(2)-P(1) 116.0(3), C(2)-N(1)-P(1) 115.8(3), C(5)-N(4)-P(2) 114.3(3), S(2)-C(1)-S(1) 124.7(3), S(2)-C(1)-P(2) 128.4(3), S(1)-C(1)-P(2) 106.8(2).

The structure of **16** was found to contain a new phosphorus-carbon single bond, likely a product of nucleophilic attack at the δ^+ carbon atom followed by radical coupling to a terminal sulfur atom by the second phosphinyl moiety (Scheme 1.41, bottom). A second scenario is possible which features nucleophilic attack from a diphosphine lone pair to the central CS_2 carbon atom followed by a concerted type mechanism forming the final LP-C(S)-S-PL product (Scheme 1.41, top).

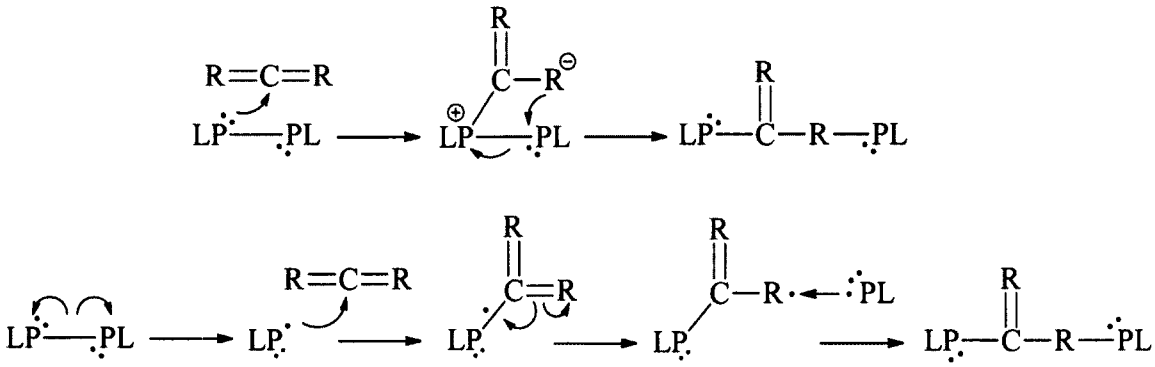

Scheme 1.41 Possible mechanisms for the reaction of the diphosphine (**2**) with CR_2 molecules *via* the lone pair (top) or radical (bottom) on phosphorus.

The P(1)-S(1) 2.2774(17) Å distance was found to be elongated compared to other P-S-C phosphorus-sulfur single bonds in the literature such as $[\{P(1\text{-}N^tBu)_2(1\text{-}S\text{-}2\text{-}HN\text{-}C_6H_4)\}]_2$ (2.176(1) and 2.188(1) Å).[97] The S(1)-C(1) 1.741(4) Å bond distance was found to be significantly longer than other carbon-sulfur double bonds in the literature such as $S_2CP(MeNCH_2CH_2)_3N$ which has a C=S distance of 1.655 Å.[98] This is unsurprising given the collection of donor atoms in this particular molecular framework. The P(2)-C(1)-S(1) bond angle was identified as 106.8(2)° while the sum of angles at C(1) was indicative of a trigonal planar geometry ($\Sigma°C(1)$ = 359.99). Two equivalent signals were observed in the ^{31}P NMR at 133.10 (d, $^3J_{P\text{-}P}$ = 8 Hz) and 92.36 (d, $^3J_{P\text{-}P}$ = 8 Hz) ppm as the only significant products of **2** with CS_2. The quaternary LP-C(S)-S-PL carbon atom was identified as a doublet of doublets in the $^{13}C\{^1H\}$ NMR at 138.36 ppm ($^1J_{P\text{-}C}$ = 134.7 Hz, $^2J_{P'\text{-}C}$ = 11.5 Hz). Rapid degradation can be observed in the ^{31}P NMR and is likely due to contamination with O_2 or H_2O. This is supported visually as the solutions transitions from bright green in colour to a pale yellow in an NMR tube when not kept under an inert atmosphere.

The success identified in the reaction of CS_2 with the diphosphine (**2**) at room temperature makes the investigation of other heteroallenes a worthwhile pursuit. The second reaction undertaken in this series was with phenyl-isocyanate. Addition of Ph-NCO to a stirring toluene solution of the diphosphine (**2**) initiated a slow transition of the characteristic orange coloured solution of **2** to pale yellow over two days. Crystallization of a concentrated toluene solution at -35 °C yielded colourless crystals of **17** (Scheme 1.42).

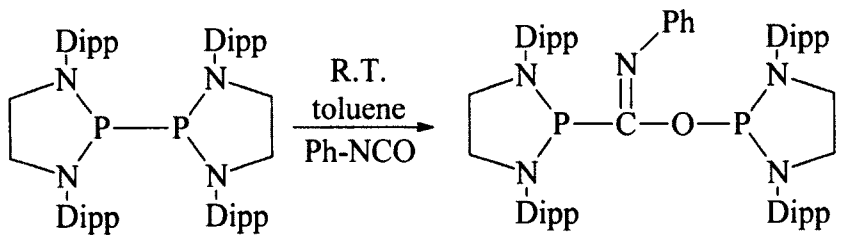

Scheme 1.42 Reaction of phenyl isocyanate with the diphosphine (**2**) forming LP-C(=NPh)-O-PL (**17**).

The structure of **17** was found to feature a new phosphorus-carbon single bond as was the case in **16**. This is once again likely a product of nucleophilic attack at the δ^+ Ph-NCO carbon atom followed by radical coupling to a terminal oxygen atom by the second phosphinyl moiety (Scheme 1.41). The P(1)-O(1) 1.751(2) Å bond distance is significantly longer than the ethereal oxidative product **9** described earlier (1.6290(18) and 1.6270(18) Å). This difference can be attributed to the change in oxidation state in **9** to P(V) whereas in this case, both phosphorus atoms remain P(III). Upon review of the literature, the P(1)-O(1) distance is similar to other phosphorus(III)-oxygen single bonds such as in $(PhN(CH_2)_2NPh)P$-O-$CH(CF_3)Ph$ (1.657(1) Å)[99] while the P(2)-C(1) distance of 1.881(3) Å is remarkably similar to that observed in the case of the CS_2 insertion product (1.895(4) Å). The imine N(1)-C(1) distance of 1.282(3) Å was consistent with

other aryl-imines in the literature such as in $\{Ph_2P\text{-}C(=NMes)\}_2$ (1.280(2) and 1.266(2) Å).[100] The P(2)-C(1)-O(1) bond angle was 121.67(19)° while the sum of angles at C(1) is indicative of trigonal planar geometry (Σ°C(1) = 359.93).

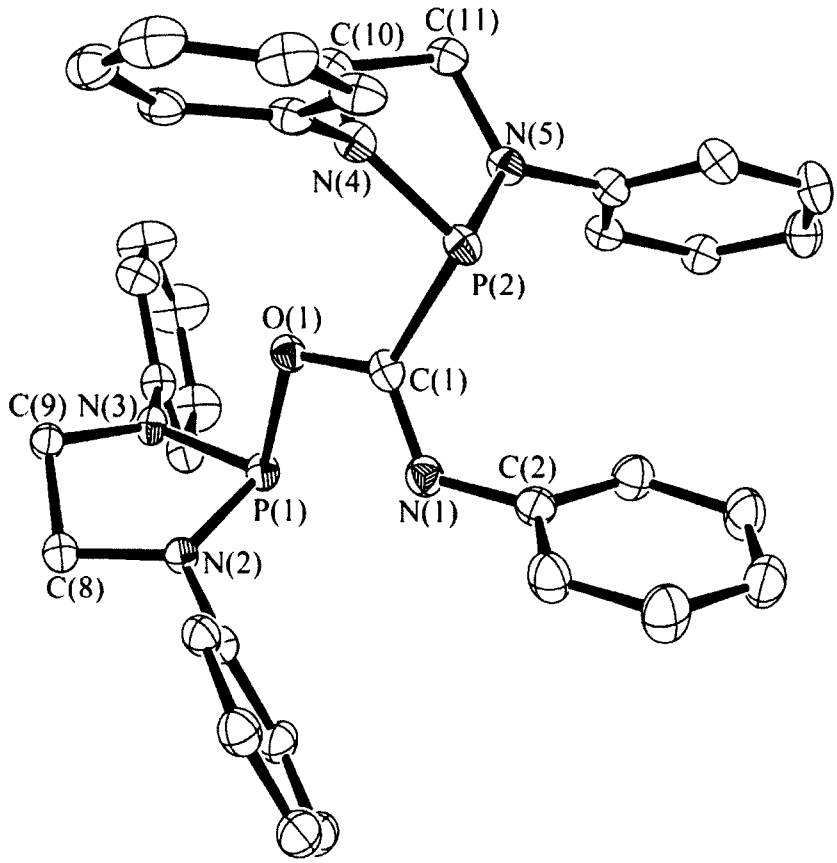

Figure 1.34 ORTEP of **17**, 50% ellipsoids are shown. Hydrogen atoms and *iso*-propyl groups are removed for clarity. Distances (Å) angles (°): P(1)-N(3) 1.676(2), P(1)-N(2) 1.697(2), P(1)-O(1) 1.7511(17), P(2)-N(4) 1.689(2), P(2)-N(5) 1.703(2), P(2)-C(1) 1.881(3), C(1)-N(1) 1.282(3), C(1)-O(1) 1.363(3), N(1)-C(2) 1.412(3), N(2)-C(8) 1.470(3), N(3)-C(9) 1.463(3), C(10)-N(4) 1.481(3), C(11)-C(10) 1.517(4), C(9)-C(8) 1.513(3), C(11)-N(5) 1.451(3). N(3)-P(1)-N(2) 90.53(10), N(3)-P(1)-O(1) 99.12(9), N(2)-P(1)-O(1) 100.90(10), N(4)-P(2)-N(5) 90.84(11), N(4)-P(2)-C(1) 105.45(11), N(5)-P(2)-C(1) 100.77(11), N(1)-C(1)-O(1) 116.3(2), N(1)-C(1)-P(2) 121.99(19), O(1)-C(1)-P(2) 121.67(19), C(1)-O(1)-P(1) 109.59(15), C(1)-N(1)-C(2) 122.2(2), C(9)-N(3)-P(1) 113.80(16), C(8)-N(2)-P(1) 114.54(17), N(5)-C(11)-C(10) 104.9(2), N(4)-C(10)-C(11) 105.0(2), N(3)-C(9)-C(8) 104.28(19), N(2)-C(8)-C(9) 104.7(2), C(11)-N(5)-P(2) 115.23(17).

The NMR spectra of **17** exhibited significant broadening at ambient temperatures. This is presumably a function of the LP-C(NPh)-O-PL core which could be dynamic in

solution. Two equivalent signals were observed in the ^{31}P NMR spectrum at 122.36 and 84.74 ppm as the only significant products formed. The C(1) carbon atom could not be identified in the $^{13}C\{^{1}H\}$ NMR spectrum at ambient temperatures due to the significant broadening of the signals however, all other analyses suggests that **17** is the only significant product in the reaction of **2** with Ph-NCO. Future work on this molecule should include collecting low temperature NMR spectra to potentially minimize the molecular motion of **17**.

The final reaction in this series was between **2** and phenyl-isothiocyanate. Addition of Ph-NCS to a toluene solution of the diphosphine (**2**) does not cause an immediately observable colour change. A ^{31}P NMR transition can be observed in which the parent diphosphine peak (143.46 ppm) splits into two equivalent signals at 132.4 and 88.1 ppm. Consecutive $^{31}P\{^{1}H\}$ NMR experiments on the same sample indicated that the reaction of **2** with Ph-NCS requires approximately one week at ambient temperatures to proceed to completion, forming **18** as the only significant product (Scheme 1.43). As the reaction nears completion, the solution transitions from the characteristic orange colour of the diphosphine (**2**) to yellow. Crystallization of a concentrated pentane solution was only possible at -35 °C with trace benzene added. Clusters of plate-like yellow crystals formed overnight (Figure 1.35).

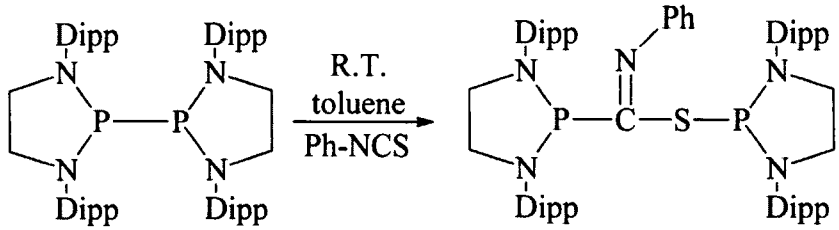

Scheme 1.43 Reaction of phenyl isothiocyanate with the diphosphine (**2**) forming LP-C(=NPh)-S-PL (**18**).

The reactions of **2** with heteroallenes yielded insertion products which could be formed by nucleophilic attack at the δ^+ carbon atom, likely followed by radical coupling to a terminal heteroatom (X = O, S) by the second phosphinyl moiety (Scheme 1.41). The reaction of **2** with Ph-NCS was not an exception, forming LP-C(=NPh)-S-PL (**18**) as the only significant product. The P(2)-S(1) 2.216(12) Å bond distance falls amongst those of the bridging sulfide product (**6-7**) described earlier (2.316(11), 2.322(10), 2.1905(15) and 2.1912(14) Å). It is significantly longer than other phosphorus(III)-sulfur single bonds in the literature such as $[(Me_3Si)_2CH]_2P\text{-}S\text{-}P[(Me_3Si)_2CH]_2$ (2.182(2) and 2.141(2) Å).[69] The P(1)-C(9) distance (1.87(3) Å) is similar to those observed in the CS_2 and Ph-NCO insertion products (**16** = 1.895(4) and **17** = 1.881(3) Å) while the N(10)-C(9) distance (1.31(3) Å) was found to be similar to LP-C(=NPh)-O-PL (1.282(3) Å). The P(1)-C(9)-S(1) bond angle was identified as 118.8(16)° while the sum of angles at C(9) was indicative of a trigonal planar geometry (Σ°C(9) = 357.22). Crystals of **18** were solved in the P1 space group with relatively large errors. An inversion center is likely present in the unit cell, a symmetry element which would define the preferred space group as P-1. Unfortunately, the quality of the crystals was not such that a workable model could be generated in P-1.

The C(1) carbon atom could not be identified in the $^{13}C\{^1H\}$ NMR at ambient temperatures due to the significant broadening of the signals as was the case for **17**. Other analyses suggest that **18** is the only significant product in the reaction of **2** with Ph-NCS. Future work on this molecule should include low temperature NMR experiments to

potentially minimize the signal broadening of **18** in solution and resolve the $^{13}C\{^1H\}$ and ^1H NMR spectra.

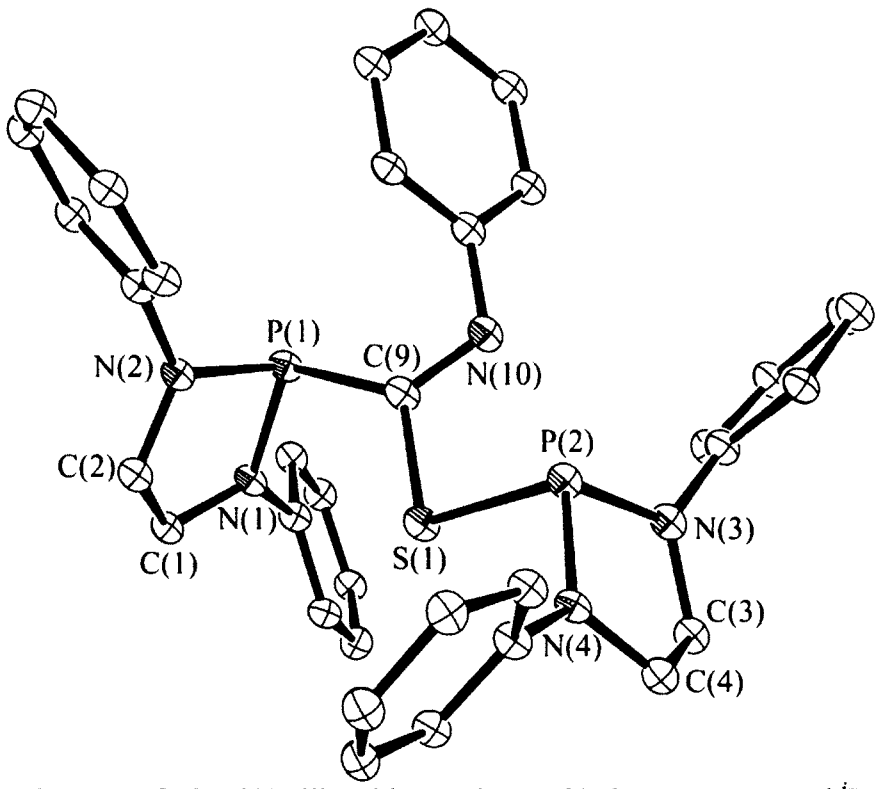

Figure 1.35 ORTEP of **18**, 50% ellipsoids are shown. Hydrogen atoms and ^{i}Pr groups are removed for clarity. One of two in asymmetric unit. Distances (Å) angles (°): S(1)-C(9) 1.74(3), S(1)-P(2) 2.216(12), P(1)-N(1) 1.70(2), P(1)-N(2) 1.76(3), N(1)-C(1) 1.37(3), C(1)-C(2) 1.51(4), P(2)-N(3) 1.73(3), P(2)-N(4) 1.73(2), N(2)-C(2) 1.37(3), N(3)-C(3) 1.45(3), C(3)-C(4) 1.65(4), N(4)-C(4) 1.41(4), C(9)-N(10) 1.31(3). C(9)-S(1)-P(2) 94.2(10), N(1)-P(1)-N(2) 88.1(13), N(1)-P(1)-C(9) 105.9(13), N(2)-P(1)-C(9) 105.1(13), C(1)-N(1)-P(1) 116(2), N(1)-C(1)-C(2) 109(2), N(3)-P(2)-N(4) 90.7(13), N(3)-P(2)-S(1) 103.1(9), N(4)-P(2)-S(1) 96.3(8), C(2)-N(2)-P(1) 114(2), N(2)-C(2)-C(1) 107(2), C(3)-N(3)-P(2) 117.0(19), N(3)-C(3)-C(4) 99(2), C(4)-N(4)-P(2) 114.0(19), N(4)-C(4)-C(3) 109(2), N(10)-C(9)-S(1) 115(2), N(10)-C(9)-P(1) 123(2), S(1)-C(9)-P(1) 118.8(16).

The diphosphine (**2**) has been shown to accept heteroallenes as insertion products between the two phosphinyl moieties. Specifically, molecules which feature a δ^+ central carbon atom were found to react with the diphosphine and/or its dissociated monomer. The reaction of **2** with CS_2 was found to be almost instantaneous while reactions with

phenyl-isocyanates were found to be relatively slow, likely due to the increased steric bulk of the aryl-cyanates. Unfortunately, less activated carbon centered main group molecules such as CO and CO_2 were found to be unreactive toward the diphosphine (**2**) even at elevated temperatures.

Section 1.6 – Conclusions

This chapter described a reliable, multi-gram synthesis toward a new sterically bulky diphosphine which persists in an equilibrated state with its dissociated monomeric radical in solution at ambient temperatures. The relative proportion of the monomer/dimer in solution can be reversibly influenced by the temperature of the sample as was observed by variable temperature EPR and NMR spectroscopies. The relaxation of the distorted diphosphine structure was studied computationally in a step-wise manner from H_2P-PH_2 to the full system $[(\{H_2C\}_2NDipp)_2P]_2$. The relaxation of the phosphinyl moieties upon dissociation represents approximately 100 kJ/mol for the full system. The favorable relaxation of **2** provides sufficient energy to homolytically cleave the central P-P bond yielding two equivalents of monomeric radical.

The diphosphine (**2**) was shown to activate readily available main group elements including phosphorus (P_4), sulfur (S_8), oxygen (O_2), selenium (Se^0) and tellurium (Te^0) forming *trans,trans*-tetraphosphabicyclobutane (LP-P_4-PL), bridging sulfide (LP-S-PL), persulfide (LP-S-S-PL), ethereal oxidative products (LP(O)-O-(O)PL, LP(Se)-Se-PL) as well as bridging selenide (LP-Se-PL) telluride (LP-Te-PL) species. A general trend was identified in the reactivity of **2** with excess chalcogen as atomic size increases from oxygen (LP(O)-O-(O)PL), to selenium (LP(Se)-Se-PL) and finally tellurium (LP-Te-PL).

The increase in atomic size appears to influence the stoichiometry of the reaction and the potential oxidation of a P(III) phosphorus atom to P(V) once initial insertion of one equivalent has taken place forming LP-X-PL (X = Se, Te).

The reactivity of the diphosphine was also investigated with Lewis acidic boranes for which formation of LPH→BR_3 (R = H or C_6F_5) adducts were observed including hydrogen atom transfer to the phosphorus atom. Unfortunately, the origin of the phosphine P-H was unable to be identified from IR, ^{31}P, $^{31}P\{^1H\}$ and ^{11}B NMR experiments. Finally, the reactivity of the diphosphine was investigated with heteroallenes (CS_2, Ph-NCO, Ph-NCS) yielding novel functional groups (LP-C(=R)-X-PL). The radical character of the dissociated phosphinyl coupled with the steric crowding about the phosphorus center generates reactivity patterns worthy of pursuit toward new molecular architectures.

Section 1.7 Future Work

Future work on this system should include a comprehensive electrochemical study on the diphosphine and it dissociated radical. A study of this nature could elucidate details on the oxidation process to the phosphorus cation, previously isolated synthetically in the Masuda group, as well as the anionic phosphide which was not able to be generated chemically from the diphosphine. Secondly, a VT solid-state EPR study should be conducted on the diphosphine. The potential for the central P-P bond to elongate in the solid state could lead to the presence of partial radical character as was observed in the calculations and solution EPR. $Dipp_2C_2H_4N_2P$-H (**14-15**) should be investigated further toward understanding the electronic configuration of the P-H bond

which X-ray and IR data suggested to be a phosphenium/hydride type interaction. Neutron diffraction would be a poignant characterization technique such that the true P-H bond length could be identified. The FLP-type reactivity observed with boranes should be exploited in reactions activating small molecules in solvents lacking available hydrogen atoms for abstraction (i.e. liquid CO_2). Significant broadening of the NMR spectra of **17** and **18** was observed for the reactions of **2** with Ph-NCO and Ph-NCS. Future work on these molecules should include recording low temperature NMR spectra to minimize signal broadening. Finally, the reactivity profile of the diphosphine (**2**) should be expanded with low oxidation state *d*- and *f*-block metals, attempting to employ its potential to act as one-, two- or three-electron donors to stabilize electron-poor metal systems.

Chapter 2 – Carbenes and S_4N_4

Section 1 – Brief Overview

- Section 2.1.1 – Introduction to Carbenes

Carbenes are compounds which contain a divalent carbon atom with a six-electron valence shell. The geometry at carbon can either be linear or bent. In the case of linear carbenes, the carbon atom has two degenerate non-bonding *p*-orbitals (p_x and p_y) in a triplet state (Figure 2.1, left). If the substituents around the divalent carbon are bent, the degeneracy of the *p*-orbitals is lost resulting in sp_2 hybridization. The p_x orbital then adopts *s*-character and the electrons spin pair yielding a carbene in the singlet state (Figure 2.1, right).[101] Singlet carbenes possess both a filled and vacant frontier orbital. Therefore, a neutral ambiphilic nature is observed for singlet carbenes. Triplet carbenes have two singly occupied frontier orbitals (p_x and p_y) which can be defined as a diradical. Thirty years after Zimmerman's attempt at isolating the first conceptual triplet carbene,[102] Tomioka generated a species that is persistent in solution for approximately one week.[103-106] Triplet carbenes are inherently reactive species making their isolation a challenging synthetic and spectroscopic undertaking.[107]

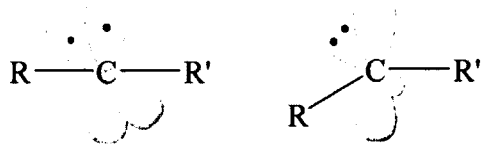

triplet carbene singlet carbene

Figure 2.1 Frontier electronic configurations of singlet and triplet carbenes.

- Section 2.1.2 Electronic Stabilization of Singlet Carbenes

Essential to the stabilization of carbenes is the nature of the substituents surrounding them. Singlet carbenes exhibit bent geometry with the frontier sp_2 hybridized orbital housing a lone pair of electrons.[101] In 1980, Linus Pauling published a summary of the *ideal* substituents required to stabilize singlet carbenes. His description involved three general bonding scenarios: (1) push, push mesomeric-pull, pull (Figure 2.2A), (2) pull, pull mesomeric-push, push (Figure 2.2B), and (3) push, pull mesomeric electronics (Figure 2.2C).[108]

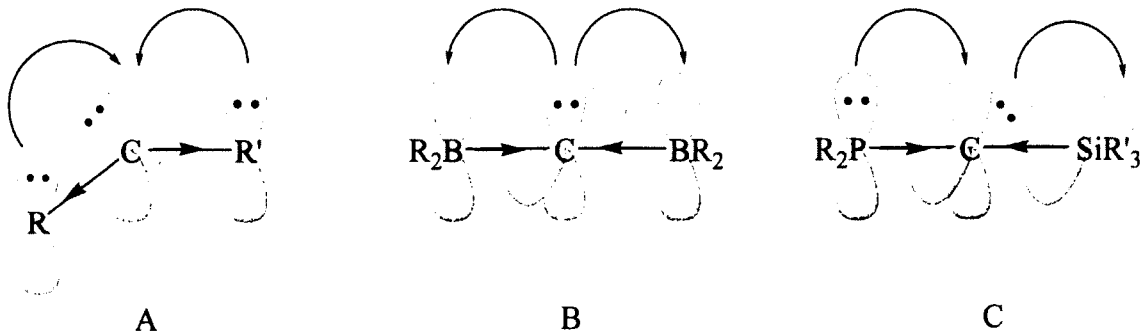

Figure 2.2 Three types of theoretical carbenes described by Pauling. [108]

In the first scenario two π-donating, σ-accepting substituents are present in a push, push mesomeric-pull, pull scenario which is the most common in the literature. The stabilization of the carbene is based on the donation of electron density into the empty *p*-orbital of the carbene-carbon while simultaneously stabilizing the lone pair *via* the inductive effect, a feature inherent with electronegative substituents. The most prevalent carbenes of this type are the N-heterocyclic diaminocarbenes such as imidazol-2-ylidenes and imidazolidin-2-ylidenes first characterized by Arduengo (Figure 2.3).[109,110]

imidizol-2-ylidenes imidizolidin-2-ylidenes

Figure 2.3 General depiction of imidazol-2-ylidene (left) and imidazolidin-2-ylidene (right) diaminocarbenes.

The second scenario described by Pauling occurs when two π-attracting, σ-donating substituents are present in a pull, pull mesomeric-push, push scenario. A theoretical example of a pull-pull system would be a diborylcarbene (Figure 2.2B). In a diborylcarbene, the lone pair on the divalent carbon center would be shared among empty *p*-orbitals on boron while simultaneously σ-accepting from the boron atoms in order to stabilize the electron deficient carbene carbon.[108]

The third example described by Pauling contains both a π-accepting and σ-donating substituent in a push, pull mesomeric electronic structure. This class of stabilization can be exemplified by phosphinosilyl-carbenes in which σ-donating substituents stabilize the electron deficient carbene center. The donation of the carbene lone pair to an empty *p*-orbital occurs as the divalent carbene accepts one such lone pair from the π-donating substituent.[108] In 2000, Bertrand *et al.* were successful in isolating a persistent, push-pull singlet carbene. Exposure of a diazo precursor to 300 nm radiation yields the transient carbene. The product was a monoheteroatom-substituted singlet carbene which was stable for weeks below 243 K.[111]

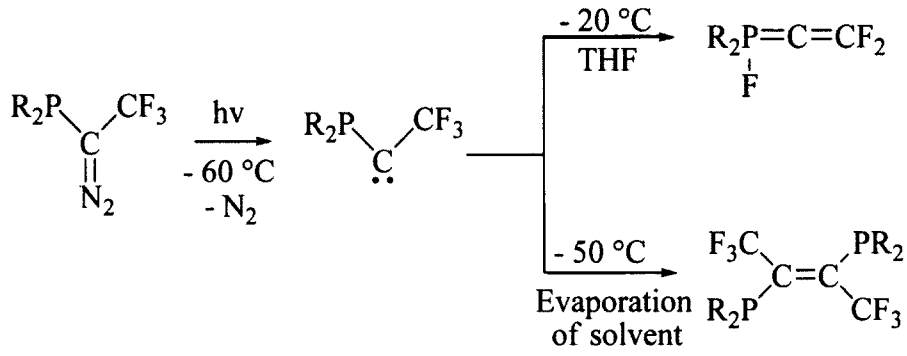

Scheme 2.1 Persistent push-pull mesomeric carbene isolated by Betrand *et al.*[111]

- Section 2.1.3 – N-Heterocyclic Carbenes

This section will concern those of the push, push mesomeric-pull, pull variety. The groundwork for diaminocarbenes was laid in the 1960's when Wanzlick proposed their synthesis, employing the thermal elimination of chloroform from a parent imidazolidin-structure (Scheme 2.2). The reaction was completed under the pretense that π-donating amino substituents could stabilize an N-heterocyclic 1,3-diphenylimidazolidin-2-ylidene structure. Dimerization of the *in situ* carbene occurred from a lack of steric bulk, yielding the olefin species which was found to be the kinetic and thermodynamically favored product.[112]

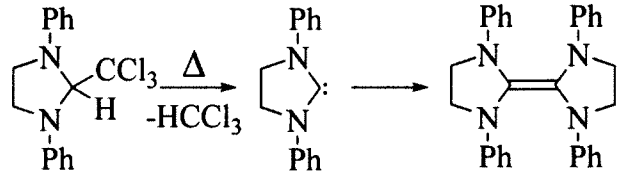

Scheme 2.2 Attempted isolation of a stable N-heterocyclic carbene through thermal elimination of chloroform.

Although Fisher-type reactivity with metal centers was facilitated by these initial trials, the first N-heterocyclic free-carbene was not published until 1991 by A. J. Arduengo III.[113] Treatment of the corresponding adamantly-imidazolium chloride with sodium hydride and a catalytic amount of *tert*-butanol in tetrahydrofuran facilitated the

deprotonation of the precursor and subsequent reduction (Scheme 2.3). Obtained and isolated in 96% yield, the resulting free-carbene was found to be stable in the absence of oxygen and moisture.

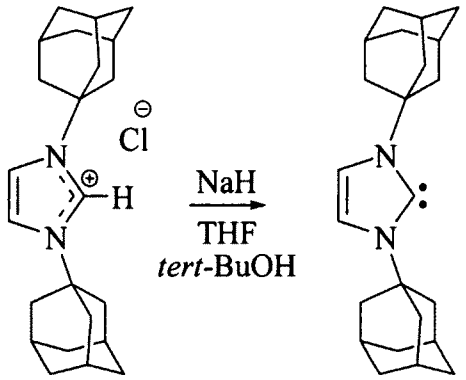

Scheme 2.3 Deprotonation of 1,3-bis(1-adamantyl)imidazolium chloride forming the first isolable free-carbene.

This discovery has served as the basis for the isolation of several free N-heterocyclic, Arduengo-type ylidenes over the last two decades.[101,114,115]

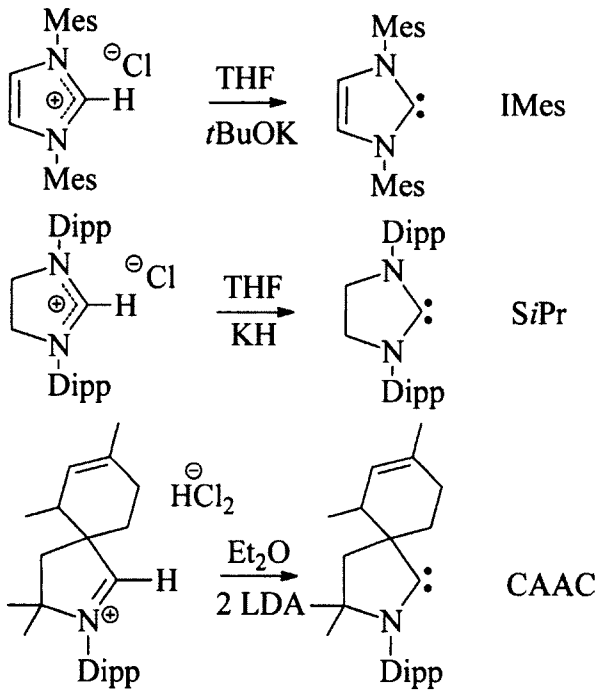

Scheme 2.4 Synthesis of IMes, SIPr and a CAAC.

Examples of extensively studied, Arduengo-type ylidenes include: the nucleophilic 1,3-bis(2,4,6-trimethylphenyl)imidazol-2-ylidene (IMes),[109] the moderately electrophilic 1,3-bis(2,6-diisopropylphenyl)imidazolidin-2-ylidene,[110] and more recently, the Cyclic-Alkyl-Amino-Carbenes (CAAC) [Scheme 2.4].[116] The isolation of free-carbenes by Bertrand,[116,117] and Arduengo,[109,110,113] has spurred an area of intense analysis in regards to the steric and electronic properties of carbenes as well as their propensity to stabilize interesting functional groups.[12,13,118] Several comprehensive reviews on the overall synthesis, reactivity, and application of singlet carbenes focused on transition metals can be found in the literature but will not be the focus herein.[101,114,115,119]

- Section 2.1.4 – Nucleophilic Ring Opening of S_4N_4

Fluck *et al.* first outlined the reaction of triphenylphosphine (PPh_3) with tetrasulfur tetranitride (S_4N_4) in 1961,[120] suggesting two possible configurations of the product, $Ph_3PS_3N_4$. The crystal structure was later reported by Holt and Holt, detailing the formation of a phosphinimine bridge to a S_3N_3 ring (Scheme 2.5),[121,122] facilitated by the elimination of a single sulfur atom which forms an equivalent of triphenylphosphine sulphide through a mechanism later proposed by Chivers *et al.*[123]

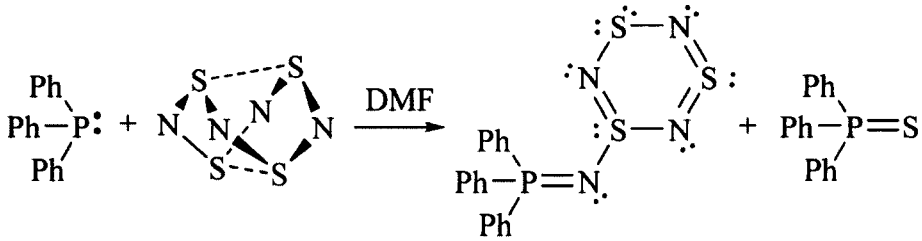

Scheme 2.5 Reaction of triphenylphosphine and tetrasulfur tetranitride forming $Ph_3P{=}NS_3N_3$ and $Ph_3P{=}S$.[120]

In a proceeding report, Chivers and Oakley studied the thermolysis product of $Ph_3P{=}NS_3N_3$ in refluxing acetonitrile yielding the open chain fragmentation product

$Ph_3P{=}NSNSS$ (Figure 2.4).[124] The authors contend that the elimination of the N_2S, substantiated by assigning a five-line EPR signal from the thermolysis mixture of $Ph_3P{=}NS_3N_3$ as the $[NSN]^{\bullet-}$ radical anion,[125] is involved in the formation of $Ph_3P{=}NSNS$ from the parent structure. Elimination of N_2S from $Ph_3P{=}NS_3N_3$ would yield $Ph_3P{=}NSNS$, which upon addition of S_8 from the disproportionation of N_2S could yield the final product, $Ph_3P{=}NSNSS$ (Scheme 2.6).[124]

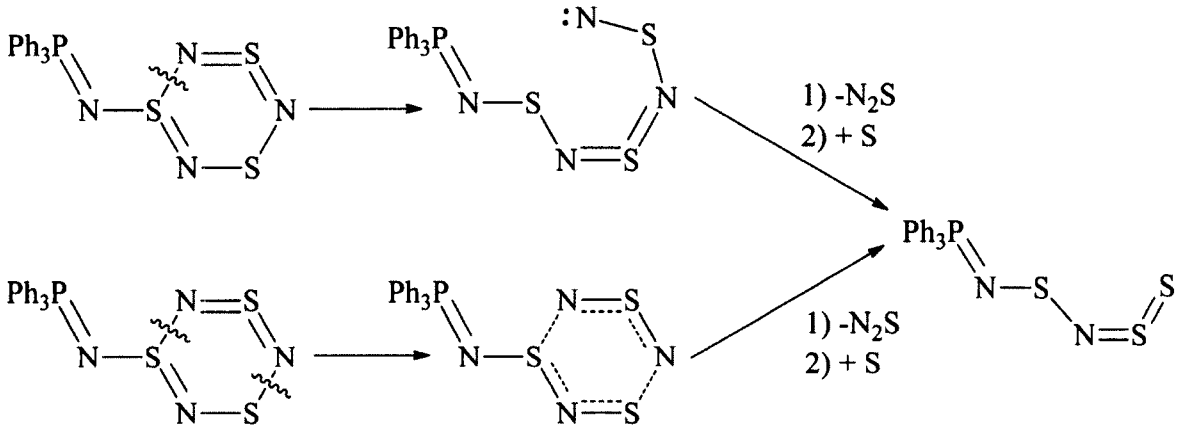

Figure 2.4 Proposed mechanism for the thermolysis of $Ph_3P{=}NS_3N_3$ to $PhP_3PNSNSS$.

From this point in the literature, a series of publications based on the nucleophilic ring-opening of S_4N_4 with tertiary-phoshines can be found, resulting in analogous ring-structures to that found in Scheme 2.5.[126-139]

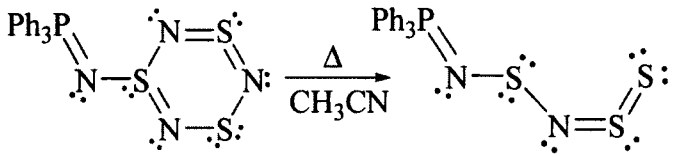

Scheme 2.6 Thermolysis product of $Ph_3P{=}NS_3N_3$ in hot acetonitrile forming $Ph_3P{=}NSNSS$.

The differences between phosphines and carbenes in various chemical situations including, but not limited to donor/nucleophilic character of the lone pair at the carbon or phosphorus atom have been examined in the literature.[140-144] Our attraction to the

reactions of carbenes with main group elements,[145,146] as well as other small molecules,[147] has led us to an investigation of the nucleophilic ring opening of S_4N_4 with carbenes.

Section 2.3 – Objectives

The purpose of this section is to investigate the nucleophilic ring-opening of S_4N_4 with three generations of amino-substituted carbenes: IMes, SIPr and a CAAC. The compounds isolated will be compared structurally to literature examples isolated in reactions of tertiary phosphines. The products will be subject to a variety of conditions in order to study potential degradation pathways. If the products are found to be structurally novel or display new reactivity, mechanistic implications will be drawn from the results in regard to literature precedent.

Section 2.4 – Discussion

- Section 2.4.1 – Reactivity of Carbenes and S_4N_4

The N-Heterocyclic Carbene (NHC), 1,3-bis(2,6-diisopropyl)imidazolidin-2-ylidene (SIPr) was first employed to identify the reactivity of S_4N_4 with carbenes due to ease of synthesis.[110] A solution of SIPr carbene was allowed to react with S_4N_4 at room temperature in toluene. The product crashes out as an insoluble red precipitate. To grow suitable crystals for X-ray diffraction, a three-tier cold diffusion of toluene layers at -35 °C was used to generate single crystals of **19** (Scheme 2.7) as the reaction occurred slowly at the solvent layer interface (see experimental). The insolubility of **19** in hydrocarbon solvents suggested an ionic framework which was supported by the single crystal structure containing an imidazolium fragment and S_3N_3 ring fused through an S-N bridge. NMR spectra could not be collected due to solubility issues in non-nucleophilic

solvents. Satisfactory elemental analysis and repeated X-ray crystallographic collections suggested that **19** is the major product of the reaction.

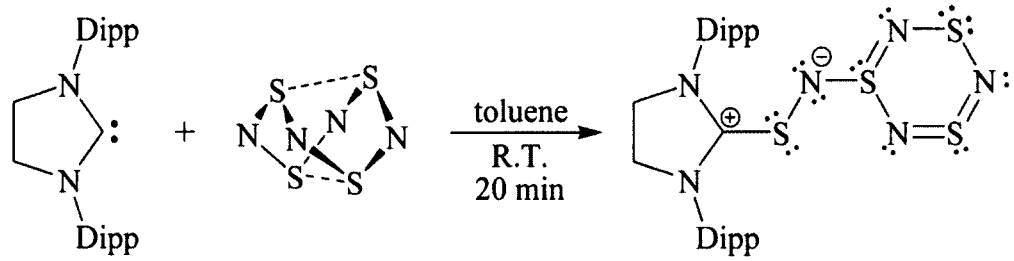

Scheme 2.7 Reaction of SIPr carbene with S_4N_4 forming SIPr-S-N-S_3N_3 (**19**).

This is supported by the extremely weak ^{1}H NMR signal which matches the spectrum of free SIPr carbene closely as the only soluble material in the reaction mixture. The other potential by-product of this reaction is SIPr=S, derived from the reaction of SIPr with elemental sulfur (S_8) impurities in S_4N_4 which cannot be removed completely for safety reasons. Pure S_4N_4 is highly unstable to physical shock. SIPr=S was not observed in the weak ^{1}H NMR spectrum or *via* crystallographic analysis. ^{13}C{^{1}H} NMR signals could not be observed even after extensive collection times.

The structure of SIPr-S-N-S_3N_3 contains a C(1)-S(1) bond length of 1.726(4) Å, supporting the zwitterionic structure in Scheme 2.7. The C(1)-S(1) is similar in length to the imidazolium sulfide [IPr-S-Ph][PF_6] (1.738 Å).[148] The S(2)-N(3) 1.594(4) Å bond distance is significantly shorter than the S(1)-N(3) distance of 1.682(4) Å, indicating that partial double bond character may contribute to the resonance stabilization of the S-N-S tether. Both bonds are significantly shorter than the S(4)-N(6) distance 1.453(6) Å. The central N(1)-C(1)-N(2) angle of 111.1(4)° coupled with the sum of angles at the two nitrogen atoms (Σ_aN(1) = 359.98°, Σ_aN(2) = 357.80°) support the conclusion that the main contributor to the molecular structure of **19** is an imidazolidinium heterocycle. Free

SIPr carbene has an N-C-N angle of 104.98(11)°,[149] representing a significant decrease in central angle from ionic SIPr precursors in the literature such as 1,3-bis(2,6-diisopropylphenyl)-imidazolidinium tetraphenylborate (114.2(2)°).[150] Admittedly, several resonances could contribute to **19** and would help to support the ranges of sulfur-nitrogen bond lengths based on their relative proportion (Figure 2.6).

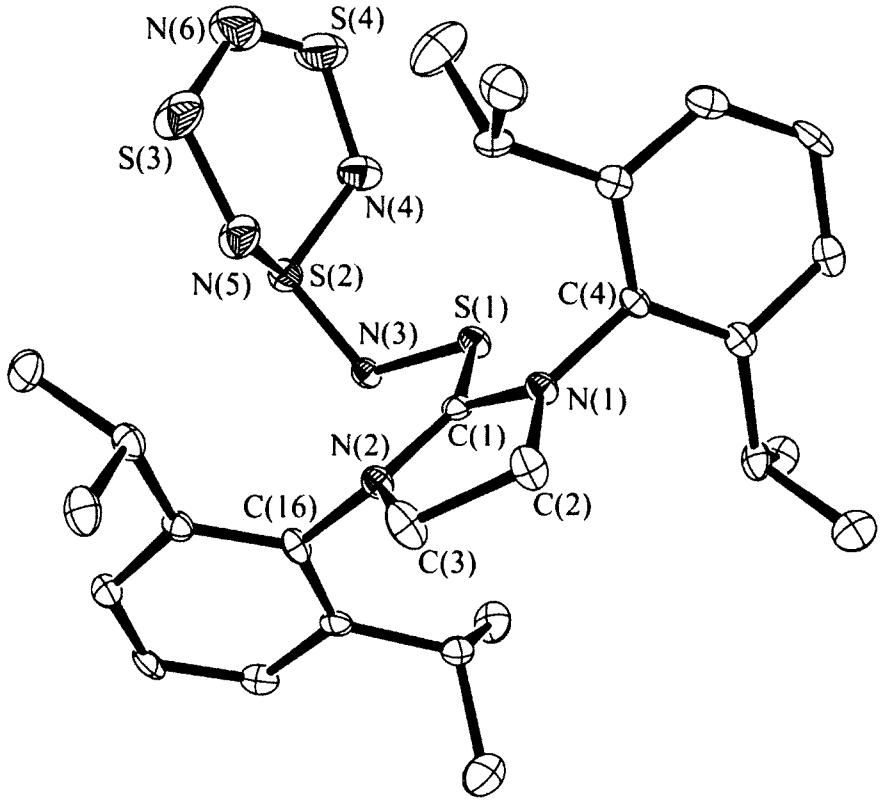

Figure 2.5 ORTEP of **19**, 50% ellipsoids are shown. Hydrogen atoms are removed for clarity. Distances (Å) angles (°): S(1)-C(1) 1.726(4), S(1)-N(3) 1.682(4), S(2)-N(3) 1.594(4), S(2)-N(5) 1.654(5), S(2)-N(4) 1.672(4), S(4)-N(6) 1.453(6), S(4)-N(4) 1.584(5), N(6)-S(3) 1.618(5), S(3)-N(5) 1.601(5), N(1)-C(1) 1.336(5), N(1)-C(4) 1.443(5), N(1)-C(2) 1.474(5), N(2)-C(1) 1.339(5), N(2)-C(16) 1.446(6), N(2)-C(3) 1.478(6), C(2)-C(3) 1.510(6). N(3)-S(1)-C(1) 107.97(19), N(3)-S(2)-N(5) 105.4(2), N(3)-S(2)-N(4) 105.8(2), N(5)-S(2)-N(4) 105.8(2), N(6)-S(4)-N(4) 115.6(3), S(4)-N(6)-S(3) 127.6(4), N(5)-S(3)-N(6) 112.5(3), C(1)-N(1)-C(4) 125.6(4), C(1)-N(1)-C(2) 111.4(3), C(4)-N(1)-C(2) 122.9(3), C(1)-N(2)-C(16) 127.7(4), C(1)-N(2)-C(3) 109.8(3), C(16)-N(2)-C(3) 120.3(3), N(1)-C(1)-N(2) 111.1(4), N(1)-C(1)-S(1) 116.4(3), N(2)-C(1)-S(1) 132.5(3), S(2)-N(3)-S(1) 113.9(2), N(1)-C(2)-C(3) 102.3(3), S(3)-N(5)-S(2) 116.4(3), S(4)-N(4)-S(2) 120.6(3), N(2)-C(3)-C(2) 104.5(3).

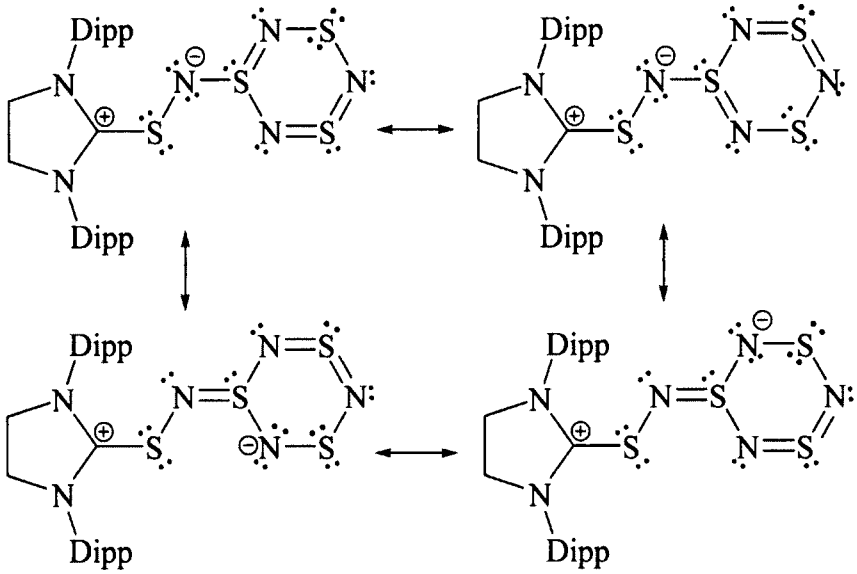

Figure 2.6 Possible contributing resonances for **19** based on bond length analysis in the single crystal structure.

A predominately nucleophilic carbene, 1,3-bis(2,4,6-trimethylphenyl)imidazol-2-ylidene (IMes),[109] was employed in order to study a range of N-heterocyclic carbenes in regards to the electronic structure at the central carbon atom. Analogous reactivity to that found in the case of triphenylphosphine was observed.[120] The formation of an IMes=NS_3N_3 imine-bridged structure was characterized as a deep-purple crystalline solid (Scheme 2.8).

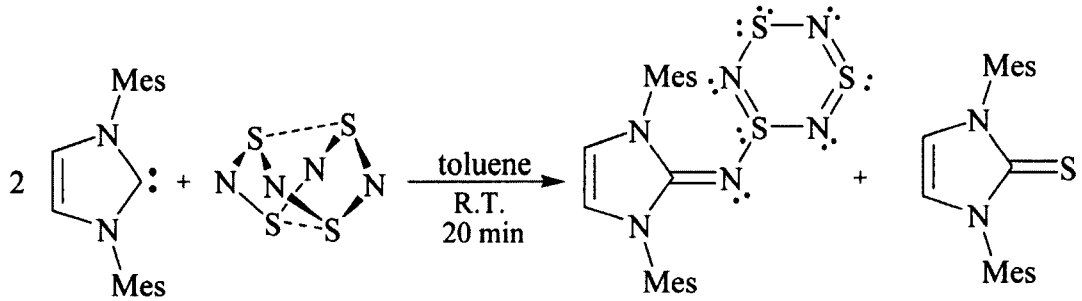

Scheme 2.8 Reaction of IMes with S_4N_4 forming IMes=NS_3N_3 (**20**) and IMes=S.

The thiourea derivative (IMes=S) was observed in the $^{13}C\{^1H\}$ NMR spectra at 165.2 ppm.[151] This structure is analogous to that in Ph_3P=N-S_3N_3. IMes is a predominantly

nucleophilic carbene which one might expect to react in a similar manner to a tertiary phosphine. The crystal structure of **20** has a C(1)=N(1) bond length of 1.331(8) Å. This is significantly longer than an analogous literature example IPr=NH (1.2888(17) Å).[152] The difference can easily be attributed to the substitution of hydrogen for the electron rich S_3N_3 ring in **20**. The bond lengths around the S_3N_3 ring suggest far less resonance contributions than was seen in **19** (Scheme 2.8). The S(3)-N(5) and S(3)-N(4) lengths of 1.539(9) and 1.595(8) Å are significantly shorter than any other S-N bond lengths in the structure which range from 1.620(6) to 1.646 (6) Å.

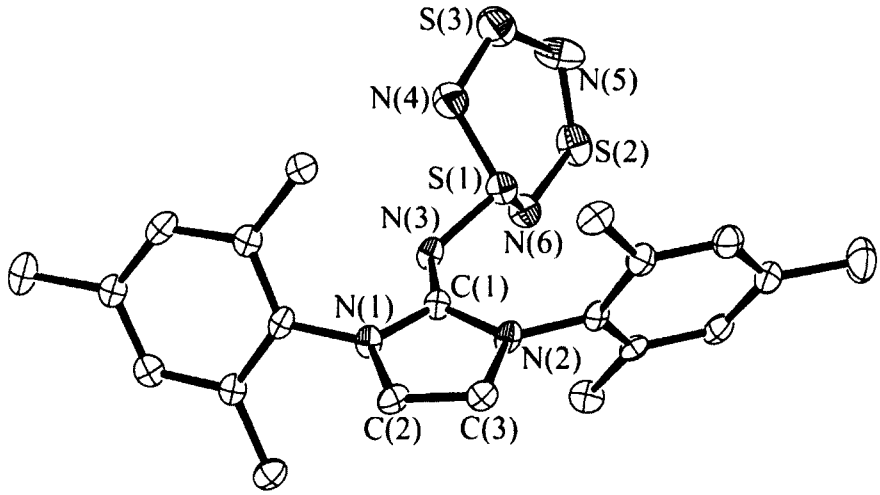

Figure 2.7 ORTEP of **20**, 50% ellipsoids are shown. Hydrogen atoms are removed for clarity. Distances (Å) angles (°): S(1)-N(3) 1.600(6), S(1)-N(4) 1.642(7), S(1)-N(6) 1.646(6), S(2)-N(6) 1.620(6), S(2)-N(5) 1.628(8), S(3)-N(5) 1.539(9), S(3)-N(4) 1.595(8), N(1)-C(1) 1.360(8), N(1)-C(2) 1.402(8), N(3)-C(1) 1.331(8), N(2)-C(1) 1.376(8), N(2)-C(3) 1.408(8), C(3)-C(2) 1.351(9). N(3)-S(1)-N(4) 102.0(3), N(3)-S(1)-N(6) 102.0(3), N(4)-S(1)-N(6) 106.8(4), N(6)-S(2)-N(5) 112.8(4), N(5)-S(3)-N(4) 115.0(4), C(1)-N(1)-C(2) 111.2(5), C(1)-N(3)-S(1) 117.9(4), C(1)-N(2)-C(3) 109.4(5), C(3)-C(2)-N(1) 106.2(6), S(2)-N(6)-S(1) 115.3(4), N(3)-C(1)-N(1) 122.6(5), N(3)-C(1)-N(2) 132.0(6), N(1)-C(1)-N(2) 105.3(5), S(3)-N(4)-S(1) 116.0(4), S(3)-N(5)-S(2) 125.5(5).

As is evident in Figure 2.7, there are few steric concerns regarding the interaction of the flanking mesityl groups with the S_3N_3 ring. The central N(1)-C(1)-N(2) angle was

found to be 105.3(5)°, which is between free IMes (101.2(5)°) and an ionic precursor 1,3-bis(2,4,6-trimethylphenyl)imidazolium chloride (108.7(4)°).[153] The two nitrogen atoms in **20** were found to be essentially planar (Σ_aN(1) = 359.87° and Σ_aN(2) = 359.94°), supporting the conclusion that a major contributor to the molecular structure of **20** is the imine derivative.[109]

The solubility of both IMes=NS_3N_3 and IMes=S made separation of the two products extremely difficult. In order to characterize IMes=N-S_3N_3, IMes=S was synthesized independently by adding an excess of elemental sulfur to IMes in toluene. The ^{1}H and ^{13}C{^{1}H} NMR spectra were recorded and manually subtracted from the spectra of the IMes=NS_3N_3 reaction mixture. The C(1) ^{13}C{^{1}H} NMR signal was found to at 147.27 ppm which is a significant shift from the parent free-carbene (219.7 ppm),[109] or the thiourea (IMes=S, 165.2 ppm).[151] The only significant shift in the ^{1}H NMR comes from the backbone protons which were found at 5.51 ppm (free IMes = 7.04 ppm).[109] The structural motif observed in the case of IMes is the same as for tertiary phosphines in the literature forming R=NS_3N_3 structures. The common by-product in these reactions is the elimination of a single sulfur atom forming an equivalent of Z=S (Z = IMes, PR_3).[151] This is not entirely surprising given the nucleophilic character of IMes when compared to SIPr.[154-156]

Finally, a cyclic-alkyl-amino carbene (CAAC) was synthesized, representing a third and most recent generation of N-heterocyclic carbenes. CAACs have been employed extensively in the past decade to stabilize remarkable structural motifs.[157] The CAACs are particularly electrophilic given the single nitrogen substituent which can

stabilize the divalent carbon through mesomeric effects.[156] The synthesis reported in the literature was able to be replicated in low yields and admittedly questionable purity.[116] Issues arising from this synthesis include the inability to separate hydrochloride salts of some starting materials from the carbene precursor. Upon reduction with lithium diisopropylamide to generate the free-carbene, inclusion of unwanted amine reagents and intermediates in the product mixture were observed. This was partially overcome by the introduction of a crystallization step at -35 °C from a highly concentrated pentane solution. The extreme solubility of the carbene reduced the isolated yields of the synthesis, although enough material was isolated to complete the reaction with S_4N_4. Sterically, the 2,4-dimethylcyclohex-3-ene substituent on this CAAC provides a physical wall on one side of the central carbon atom. The added steric protection coupled with the electrophilic nature of the carbon atom and the adjacent 2,6-diisopropylphenyl substituent may provide sufficient steric and electronic support to potentially observe a third iteration of a nucleophilic ring-opened derivative of the S_4N_4 cage.

Upon addition of a solution of CAAC to a stirring suspension of S_4N_4 in toluene, the reaction mixture transitioned to deep red in colour, similar to that in the case of SIPr. Crystallization of the reaction mixture by slow evaporation of a concentrated solution yielded the single crystal structure seen in Figure 2.9. The CAAC was found to generate a similar structure to that found in the case of SIPr, once again suggesting a zwitterionic framework (Scheme 2.9).

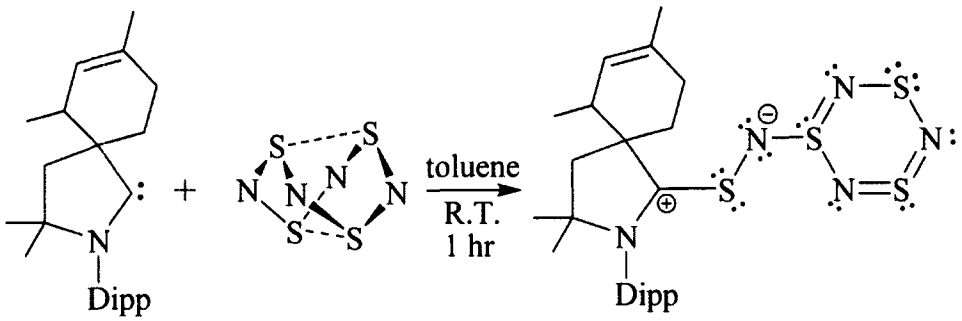

Scheme 2.9 Reaction of a CAAC with S_4N_4 to yield **21**.

CAAC-S-N-S_3N_3 was found to have a C(1)-S(1) bond length of 1.711(2) Å, similar to the case of SIPr-S-N-S_3N_3 (**19**) described earlier (1.726(4) Å), as well as the imidazolium sulfide [IPr-S-Ph][PF_6] in the literature (1.738 Å).[148] The same set of resonance structures can be drawn for CAAC-S-N-S_3N_3 as was the case for SIPr-S-N-S_3N_3 all of which can potentially contribute to the overall electronic structure of **21** (Figure 2.9). Based on the N(2)-S(2) distance of 1.590(2) Å and the longer S(2)-N(3) and S(2)-N(4) distances (1.665(2) and 1.661(2) Å respectively), the dominating contributor to the overall structure is likely one in which the positive charge is found on C(1) with the negative charge on the N(3) or N(4) positions of the S_3N_3 ring. The minor contribution would then arise from those structures in which the negative charge lies on the N(2) atom. However, it has the shortest nitrogen-sulfur bond distance in the molecule. The N(2)-S(2) distance approaches other N=S double bonds from an analogous structure in the literature, namely Ph_3P=N-S_3N_3 (1.587(4) Å).[124] The increased steric bulk surrounding the C(1) carbon atom was thought to be sufficient to form an intermediate ring opened structure, although this was not found to be the case, once again forming the S-N link to the S_3N_3 ring. The N(1)-C(1)-C(2) angle was found to be 111.4(2)° and is

adjacent to a planar nitrogen atom (Σ_aN(1) = 360°) supporting the conclusion that the structure is a zwitterionic framework.

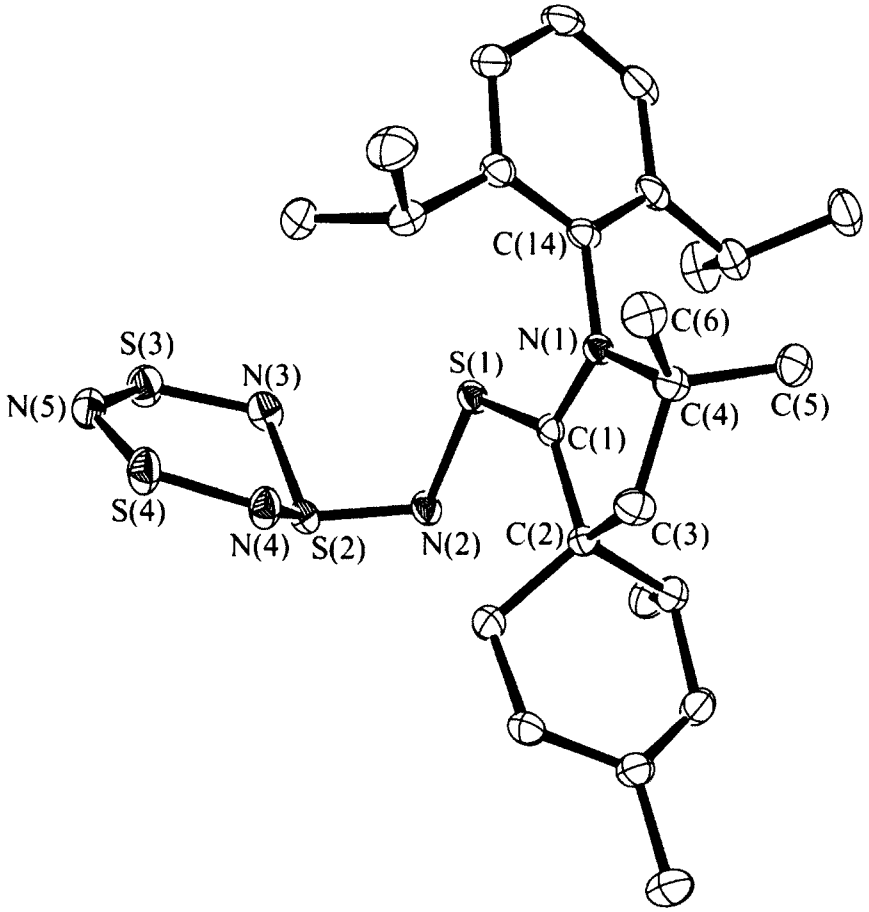

Figure 2.9 ORTEP of **22**, 50% ellipsoids are shown. Hydrogen atoms and solvent (toluene) are removed for clarity. Distances (Å) angles (°): S(1)-C(1) 1.711(2), S(1)-N(2) 1.678(2), S(2)-N(2) 1.590(2), S(2)-N(4) 1.661(2), S(2)-N(3) 1.665(2), S(4)-N(5) 1.591(2), S(4)-N(4) 1.601(2), S(3)-N(5) 1.604(2), S(3)-N(3) 1.614(2), C(1)-N(1) 1.318(3), C(1)-C(2) 1.525(3), C(2)-C(3) 1.549(3), C(5)-C(4) 1.521(4), C(3)-C(4) 1.534(3), C(4)-N(1) 1.517(3), C(4)-C(6) 1.521(4), C(14)-N(1) 1.458(3). N(2)-S(1)-C(1) 107.15(11), N(2)-S(2)-N(4) 106.48(11), N(2)-S(2)-N(3) 105.19(11), N(4)-S(2)-N(3) 106.25(11), N(5)-S(4)-N(4) 116.32(12), N(5)-S(3)-N(3) 113.49(12), N(1)-C(1)-C(2) 111.4(2), N(1)-C(1)-S(1) 116.90(18), C(2)-C(1)-S(1) 131.64(18), C(1)-C(2)-C(3) 100.34(19), C(4)-C(3)-C(2) 108.4(2), N(1)-C(4)-C(5) 110.7(2), N(1)-C(4)-C(6) 111.3(2), C(5)-C(4)-C(6) 108.4(2), N(1)-C(4)-C(3) 99.97(19), C(5)-C(4)-C(3) 115.7(2), C(6)-C(4)-C(3) 110.7(2), C(1)-N(1)-C(14) 122.7(2), C(1)-N(1)-C(4) 114.25(19), C(14)-N(1)-C(4) 123.05(19), S(3)-N(3)-S(2) 117.15(13), S(2)-N(2)-S(1) 114.04(12), S(4)-N(4)-S(2) 119.57(14), S(4)-N(5)-S(3) 123.84(14).

This molecule was found to be soluble in organic solvents including hydrocarbons. This increase in solubility is puzzling given the similarity between this and **19** (SIPr-S_4N_4) for which NMR spectra could not be collected. Unfortunately, the synthesis of pure CAAC could not be completed cleanly according to literature procedures. No other analyses were completed as the only amount of **21** isolated was a single crystal (Figure 2.9).

Nucleophilic ring opening reactions of S_4N_4 by N-heterocyclic carbenes suggest that different ring structures can be favored depending on the electronic configuration at the central carbon atom. The nucleophilic carbene IMes was shown to react as one would expect for tertiary phosphines, forming one equivalent of IMes=S and one of IMes=N-S_3N_3 as the major products. Transitioning to more electrophilic carbenes such as SIPr and the CAAC, the mechanism proposed by Chivers and Oakley for tertiary phosphines (and presumably IMes) is not necessarily favored. The elimination of the bridging sulfur atom does not occur, which upon ring closing of a linear S_4N_4 chain could form the R-S-N-S_3N_3 (R = SIPr, CAAC) structural motif.

- Section 2.4.2 – Nucleophilic Degradation of Carbene-S_xN_x Structures

In the process of attempting to acquire NMR spectra of SIPr-S-N-S_3N_3, several solvents were employed in attempts to dissolve the sample. Dissolution of **19** in THF leads to an intense red-coloured solution. Upon crystallization of the material from THF it was evident that a chemical transformation had occurred. A single-crystal from the reaction of SIPr-S-N-S_3N_3 with THF was a hook-like structure SIPr=NSNSS (Scheme 2.10). This product is analogous to that identified for the thermolysis reaction of $Ph_3P{=}NS_3N_3$ in hot acetonitrile, forming Ph_3P=NSNSS.[124] The room temperature

fragmentation of **19** was also found to occur in other nucleophilic solvents including CH_3CN, Et_2O and CH_2Cl_2. The sensitivity of SIPr-S-N-S_3N_3 to donor solvents raises questions regarding the "thermolysis" of $Ph_3P{=}NS_3N_3$ from the literature, a reaction which was completed in refluxing acetonitrile.[124,158]

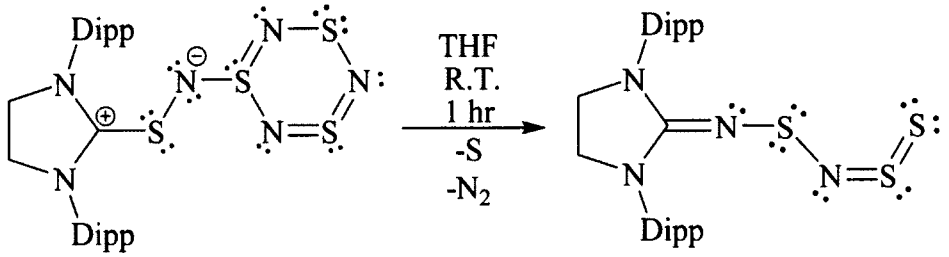

Scheme 2.10 Nucleophilic degradation of SIPr-S-N-S_3N_3 (**19**) with THF forming SIPr=NSNSS (**22**).

The fragmentation of SIPr-S-N-S_3N_3 with THF forming SIPr=NSNSS could not follow a similar decomposition pathway to that proposed by Chivers and Oakley. In **22**, the central C(1)-S(1) sulfur atom is removed in an unknown manner (Figure 2.9). The only evidence collected toward understanding the fate of this sulfur atom is the collection of several unit cells of elemental sulfur (S_8) from the reaction mixture which can be separated mechanically as striated yellow-green crystals. These crystals could simply be carried over from the synthesis of S_4N_4 which is not extensively purified for safety reasons. If N_2S is indeed lost, as was the case for $Ph_3P{=}N{-}S_3N_3$, disproportionation could be the source of the characterized sulfur crystals.

The crystal structure of **22** was found to have a C(1)=N(1) bond length of 1.320(6) Å. This is slightly shorter than a similar literature example IPr=NH (1.2888(17) Å),[152] while being similar to the IMes=N-S_3N_3 carbon-nitrogen double bond of **20** (1.331(8) Å). The S(4)-N(3) and S(4)-N(4) lengths were found to be 1.623(4) and 1.615(5) Å, significantly longer than the S(5)-N(4) bond length (1.590(5) Å). The sulfur-

nitrogen bond lengths support the structure proposed in Scheme 2.10 which depicts the structure as SIPr=N-S-N=S=S. The S(5)-S(6) bond distance of 1.963(3) Å is consistent with a terminal S=S double bond found in the literature example of a similar hook-like structure (Ph_3P=N-S-N=S=S, 1.908(2) Å).[124]

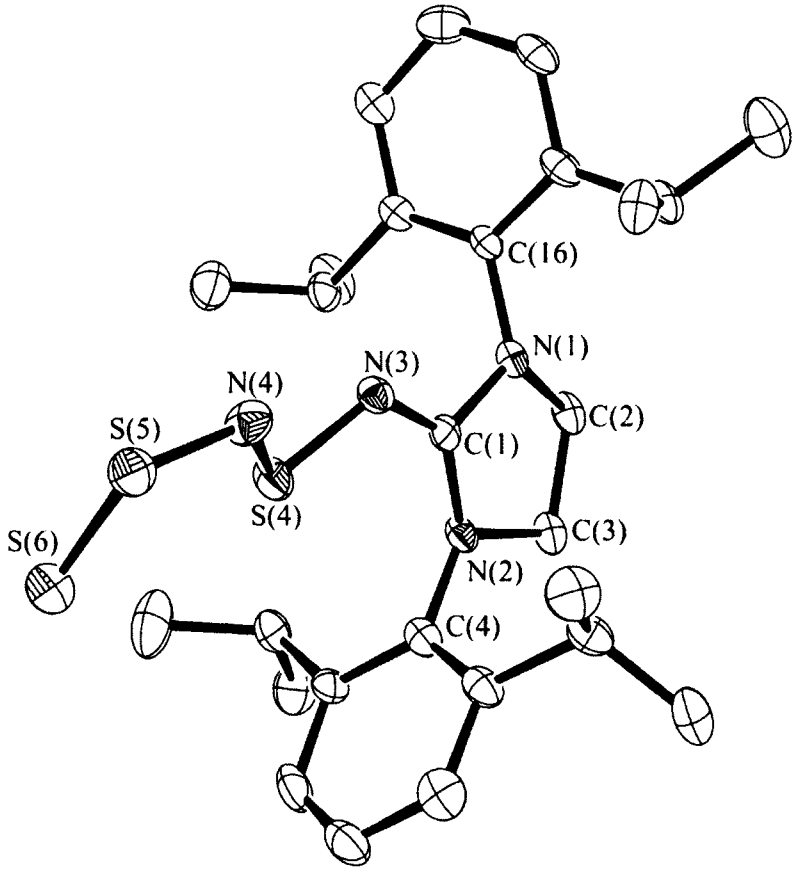

Figure 2.9 ORTEP of **22**, 50% ellipsoids are shown. One of two in the asymmetric unit. Hydrogen atoms are removed for clarity. Distances (Å) angles (°): C(1)-N(3) 1.320(6), C(1)-N(2) 1.347(6), C(1)-N(1) 1.369(6), N(1)-C(16) 1.447(6), N(1)-C(2) 1.463(6), C(2)-C(3) 1.529(7), N(2)-C(4) 1.435(6), N(2)-C(3) 1.462(6), N(3)-S(4) 1.623(4), N(4)-S(5) 1.590(5), N(4)-S(4) 1.615(5), S(5)-S(6) 1.963(3). N(3)-C(1)-N(2) 131.7(5), N(3)-C(1)-N(1) 119.0(4), N(2)-C(1)-N(1) 109.2(4), C(1)-N(1)-C(16) 121.8(4), C(1)-N(1)-C(2) 111.0(4), C(16)-N(1)-C(2) 120.1(4), N(1)-C(2)-C(3) 102.8(4), C(1)-N(2)-C(4) 124.6(4), C(1)-N(2)-C(3) 111.5(4), C(4)-N(2)-C(3) 120.9(4), N(2)-C(3)-C(2) 103.0(4), C(1)-N(3)-S(4) 119.8(4), S(5)-N(4)-S(4) 116.8(3), N(4)-S(4)-N(3) 99.7(2), N(4)-S(5)-S(6) 110.6(2).

The C(1) $^{13}C\{^1H\}$ NMR signal was found to be 148.10 ppm, a significant shift from the parent free-carbene (244.0 ppm)[110] while the central N(1)-C(1)-N(2) angle was

found to be 109.2(4)°, between free SIPr (104.98(11)°)[149] and an ionic precursor 1,3-bis(2,6-diisopropylphenyl)-imidazolidinium tetraphenylborate (114.2(2)°).[150] The sum of angles at the two nitrogen atoms (Σ_aN(1) = 352.79°, Σ_aN(2) = 356.97°) are deviated significantly from planarity, supporting the structure in Scheme 2.10 which depicts **22** as an imine carbene derivative. To understand the nature of this reaction further, an EPR study of the degradation process of SIPr-S_4N_4 should be completed in the future looking for the same five-line signal assigned to the NSN radical anion identified by Chivers and Oakley for Ph_3P=N-S_3N_3.[123]

Degradation of IMes=NS_3N_3 can also be achieved through the addition of a nucleophilic solvent (THF, CH_2Cl_2, CH_3CN) to crystals of **20**, forming IMes=N-S-N=S=S (Scheme 2.11). Because the complete separation of IMes=S from IMes=NS_3N_3 cannot be achieved, analysis of **23** contained trace IMes=S which had to be subtracted from spectra manually.

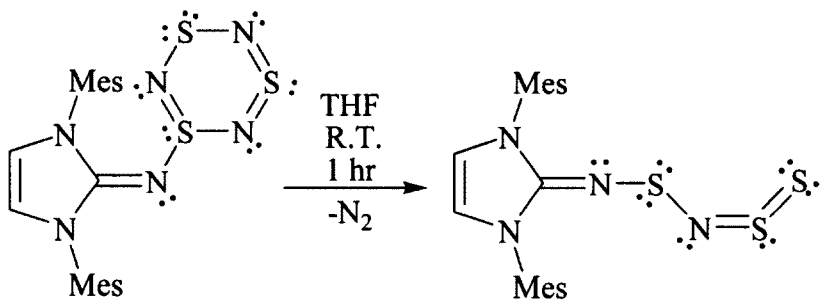

Scheme 2.11 The thermolysis of IMes=NS_3N_3 (**20**) forming IMes=NSNSS (**23**).

The crystal structure of **23** displays C(1)=N(3) bond length of 1.31(2) Å. This is similar to an analogous literature example IPr=NH 1.2888(17) Å,[152] as well as the IMes=NS_3N_3 (1.331(8) Å) and SIPr=NSNSS (1.320(6) Å) central C=N bond lengths described earlier. The S(1)-N(3) and S(1)-N(4) lengths of 1.514(13) and 1.53(2) Å respectively are significantly longer than S(2)-N(4) which was found to be 1.48(2) Å,

supporting the structure depicted in Scheme 2.11 as IMes=N-S-N=S=S. The single crystal structure of **23** is admittedly less than ideal, as is evident from the uncertainties associated with bond lengths and the size of the thermal ellipsoids. The S(3)-S(2) bond distance of 1.792(14) Å is shorter than other terminal S=S double bonds such as in Ph_3P=N-S-N=S=S (1.908(2) Å)[124] and SIPr=NSNSS described earlier (1.963(3) Å). Unfortunately, crystals of **23** are thin plates which even after several attempts and various crystallization techniques could not be improved upon.

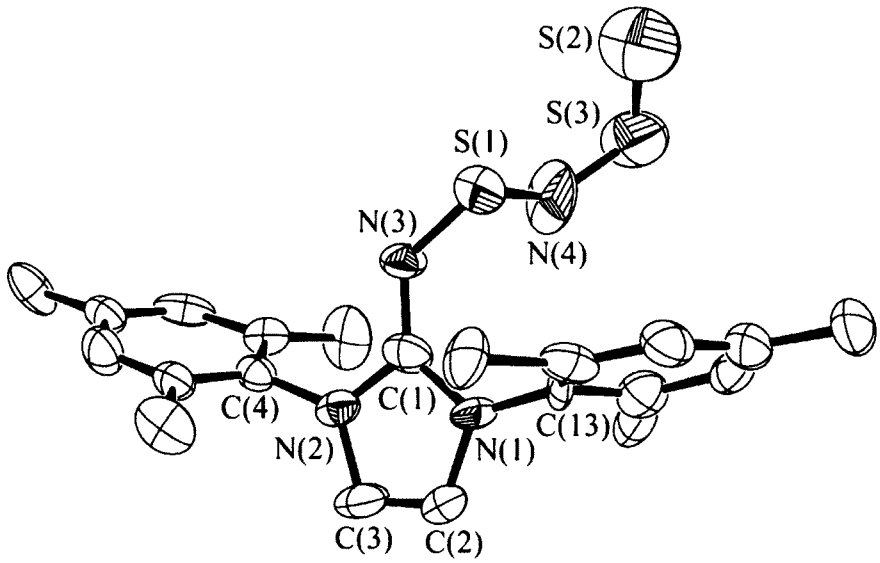

Figure 2.10 ORTEP of **23**, 50% ellipsoids are shown. Hydrogen atoms are removed for clarity. Distances (Å) angles (°): S(1)-N(3) 1.514(13), S(1)-N(4) 1.53(2), S(2)-N(4) 1.48(2), S(2)-S(3) 1.792(14), N(2)-C(3) 1.35(2), N(2)-C(1) 1.36(2), N(2)-C(4) 1.44(2), N(1)-C(2) 1.335(19), N(1)-C(1) 1.35(2), N(1)-C(13) 1.376(19), C(2)-C(3) 1.32(2), C(1)-N(3) 1.31(2). N(3)-S(1)-N(4) 106.4(12), N(4)-S(2)-S(3) 106.9(12), C(3)-N(2)-C(1) 106.8(16), C(3)-N(2)-C(4) 127.6(15), C(1)-N(2)-C(4) 125.6(13), C(2)-N(1)-C(1) 107.4(15), C(2)-N(1)-C(13) 125.0(14), C(1)-N(1)-C(13) 127.6(13), C(3)-C(2)-N(1) 109.5(16), N(3)-C(1)-N(1) 130.8(17), N(3)-C(1)-N(2) 121.3(17), N(1)-C(1)-N(2) 107.8(14), C(2)-C(3)-N(2) 108.4(17), C(1)-N(3)-S(1) 126.7(13), S(2)-N(4)-S(1) 128.0(19).

The central N(1)-C(1)-N(2) angle was found to be 107.8(14)° and is significantly relaxed compared to free IMes (101.2(5)°) while being similar to an ionic precursor in the literature 1,3-bis(2,4,6-trimethylphenyl)imidazolium chloride (108.7(4)°).[153] The two

nitrogen atoms were found to be virtually planar at $\Sigma_a N(1) = 360°$ and $\Sigma_a N(2) = 360°$. The ^1H and $^{13}C\{^1H\}$ NMR spectra were recorded and manually subtracted from the spectra of IMes=S (synthesized independently). The C(1) $^{13}C\{^1H\}$ NMR signal was found to be 147.87 ppm, significantly shifted from the parent free-carbene (219.7 ppm),[109] or even the thiourea (IMes=S, 165.2 ppm),[151] while being similar to that identified for IMes=NS_3N_3 (147.27 ppm).

The fragmentation of IMes=NS_3N_3 with a nucleophilic solvent to IMes=NSNSS could follow the decomposition pathway proposed by Chivers and Oakley,[123] although the identification of a several crystals of elemental sulfur (S_8) from the reaction mixtures by X-ray crystallography is the only evidence supporting this. The disproportionation of N_2S could in fact be the source of the characterized sulfur crystals but could also be an impurity in the starting materials. In the nucleophilic degradation of SIPr-S_4N_4, the central C(1)-S(1) sulfur atom (Figure 2.5) was eliminated. This was not required for IMes=N-S_3N_3 as the fourth sulfur atom of S_4N_4 went toward generating an equivalent of IMes=S.

- Section 2.4.3 – Mechanistic Implications

In the reaction of triphenylphosphine with S_4N_4, Bojes *et al.* proposed that the nucleophilic ring opening of S_4N_4 is initiated by attack of an N=S=N sulfur atom by the tertiary phosphine forming a zwitterionic intermediate. The proposed mechanism included rearrangement of the S_4N_4 ring to orient through a nitrogen atom in a 1,3-shift. This was followed by a ring-opening step, abstraction of a terminal sulfur atom by a

second equivalent of triphenylphosphine from the open chain and finally a ring closing step from a terminal nitrene to a sulfur atom forming the S_3N_3 ring (Figure 2.11).

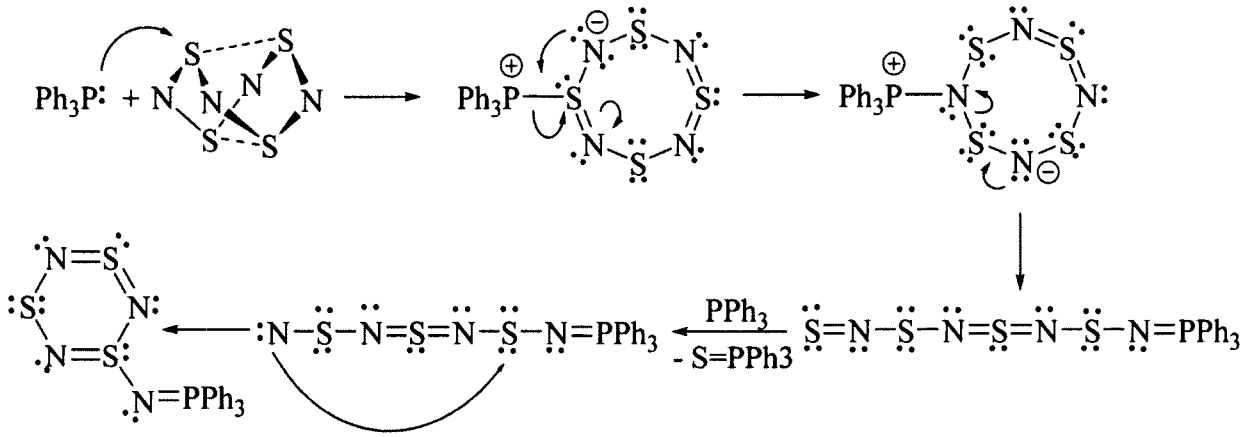

Figure 2.11 Proposed mechanism by Bojes *et al.* outlining the nucleophilic ring-opening of S_4N_4 by triphenylphosphine.[159]

In the reactions of S_4N_4 with N-heterocyclic carbenes, there are two major molecular architectures formed (Figures 2.5 and 2.7) depending on the electronic structure at the carbene carbon. The greater nucleophilic character of IMes compared to SIPr and CAAC,[154-156] could permit the rearrangement of the S_4N_4 ring to orient through a nitrogen atom after initially coordinating to a sulfur atom in the S_4N_4 cage. For more electrophilic carbenes such as SIPr and CAAC, the 1,3-nitrogen shift may not be favored simply as a function of the increase in affinity for the sulfur atom that it is initially coordinated to. The mechanism of formation for the IMes-N-S_3N_3 product could then follow a similar pathway to that described by Chivers *et al.* for triphenylphosphine, also a predominately nucleophilic molecule (Figure 2.11).[159] This type of mechanism is supported by the formation of one equivalent of the IMes=S identified in the $^{13}C\{^1H\}$ NMR spectrum. The proposed PPh_3 mechanism is not possible for SIPr-S_4N_4 and CAAC-S_4N_4, as is evident by the formation of R-S-N-S_3N_3 structures (**19** and **21**). The

electrophilic nature of these carbenes likely does not permit the rearrangement of the S_4N_4 ring once coordination has occurred and would force the reaction to proceed as a sulfur-bound imidazolium fragment (Figure 2.12). A simple ring opening and closing reaction could then take place in which the formation of the S_3N_3 ring is again favored generating an S-N linked, zwitterionic structure (Figures 2.5 and 2.9). In both SIPr-S_4N_4 and CAAC-S_4N_4, the carbon-sulfur bond distances of ~1.7 Å and are similar to an imidazolium sulfide [IPr-S-Ph][PF_6] found in the literature (1.738 Å), supporting the imine structural motif.[148]

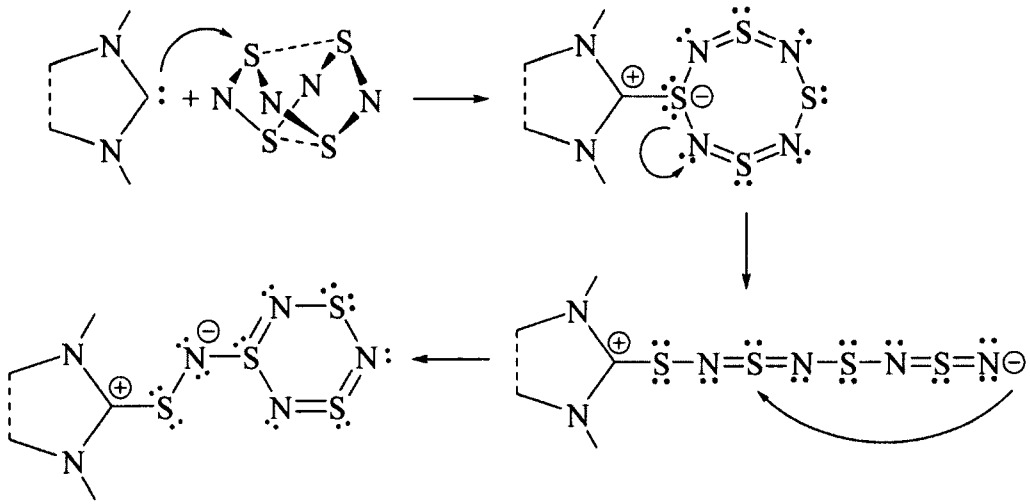

Figure 2.12 Proposed ring-opening of S_4N_4 using carbenes.

The reaction process becomes troublesome when considering the nature of the nucleophilic degradation pathway of SIPr-S_4N_4 to the hook-like structure SIPr=NSNSS. The zwitterionic structure loses N_2S_2 in some fashion, forming an analogous structure to that of IMes and triphenylphosphine. Unit cell analysis on several crystals from the SIPr-S_4N_4 reaction mixture in THF indicated that elemental sulfur (S_8) is present. This could be attributed to the disproportionation of N_2S which was reportedly observed *via* EPR in the thermolysis of Ph_3P=N-S_3N_3.[123] It is unclear how the addition of a nucleophile rather

than thermolysis drives the elimination of N_2S and does not account for the loss of an additional sulfur atom from the SIPr-S_4N_4 structure. If the nucleophile initiated rearrangement and disproportionation of N_2S does indeed generate free S_8 in solution, nucleophilic attack of S_8 by the terminal thio-imine intermediate could yield the final hook-like structure. The structures presented in this section are simply solid state representations of the major products of the reactions of carbenes with S_4N_4. Future work in this area will be to elucidate details of the nucleophilic attack and decomposition pathways computationally as well as spectroscopically.

Section 2.5 – Conclusions

The reactions of carbenes with S_4N_4 illustrate the conflicting nature of the divalent carbon center depending on the ligand scaffold. A novel reactivity pattern for the nucleophilic ring opening of S_4N_4 was identified and is presumably predicated on the electrophilic character of the divalent carbon centers. The reactions of the predominately electrophilic carbenes (SIPr and CAAC) yielded a novel molecular framework not previously identified in the literature featuring a zwitteronic C-S-N tether to an S_3N_3 ring. A more nucleophilic carbene (IMes) was found to have an analogous reaction pathway to triphenylphosphine forming an equivalent of both IMes=S and IMes=N-S_3N_3. Interestingly, the addition of a nucleophilic solvent at room temperature initiates a decomposition process in which SIPr-S-N-S_3N_3 loses N_2S_2, presumably in the form of N_2S and elemental sulfur (S_8) yielding SIPr=NSNSS. Under the same nucleophilic conditions, IMes=N-S_3N_3 was shown to eliminate N_2S and form an analogous hook-like structure IMes=NSNSS to that observed for SIPr-S-N-S_3N_3.

Section 2.6 – Future Work

A rigorous computational study should be completed regarding the nucleophilic ring-opening of S_4N_4 including the coordination of N-heterocyclic carbenes to a sulfur atom in S_4N_4 and the potential for 1,3-nitrogen shifts. Likewise, the degradation pathway of carbene-S_xN_4 (X = 3-4) structures to hook-like decomposition products (R=NSNSS, R = IMes, SIPr) could be studied spectroscopically as well computationally. Specifically, EPR and TGA-ms experiments monitoring the degradation of SIPr-S_4N_4 (**19**) and IMes=N-S_3N_3 (**20**) *in situ* should be performed, looking for the NSN radical as evidence toward the mechanism proposed by Chivers and Oakley in Figure 2.11.[123] The compounds described in this chapter represent interesting molecular architectures which may have novel thermal, absorption, fluorescent and electrochemical properties which could also be the focus of future research.

Chapter 3 – Experimental

Section 3.1 Experimental Preface

All syntheses were completed under an atmosphere of dry, O_2-free N_2 employing Schlenk line techniques or an inert atmosphere MBRAUN LABmaster SP workstation. Toluene, pentane, dichloromethane, Et_2O and THF were purchased from ACP Chemicals and purified employing a Grubbs'-type solvent purification system manufactured by Innovative Technology. Deuterated NMR solvents (C_6D_6, toluene-d_8, CD_2Cl_2, $CDCl_3$) were purchased from Cambridge Isotope Laboratory and dried over molecular sieves (4 Å) prior to use. Hyflo Super Cel® (diatomaceous earth) was purchased from Aldrich Chemical Company and dried for 24 hours in an oven prior to use. Molecular sieves (4 Å) were purchased from Aldrich Chemical Co. and dried at 140 °C under vacuum overnight. Crude white phosphorus was extracted using CS_2 and stored in a freezer (-35 °C) under inert conditions, 2-chloro-1,3-bis(2,6-diisopropylphenyl)-1,3,2-diazaphospholidine (**1**),[76] S_4N_4,[160], $B(C_6F_5)_3$,[161] SIPr,[110] IMes,[109] and CAAC,[116] were prepared according to the literature with little or no procedural modifications. H_2O_2 (40% in H_2O), CS_2, Ph-NCO, Ph-NCS, acetonitrile, lithium triethylborohydride (1.0 M in THF) and $H_3B{\bullet}S(CH_3)_2$ (2.0 M in THF) were purchased from Sigma-Aldrich. Naphthalene, Na^0, S_8, Se^0 and Te^0 obtained from chemical storage at Saint Mary's University. Ultra-pure gaseous nitrogen (N_2), liquid nitrogen and medical grade oxygen (O_2) were supplied by Praxair Technology Inc. H_2O was provided by Halifax Regional Water Commission, a subsidiary of Halifax Regional Municipality.

- Elemental Analysis

Elemental analyses were carried out at the Saint Mary's University Center for Environmental Analysis and Remediation (CEAR) on a PerkinElmer 2400 Series II CHN Analyzer. Samples of **2**, **3** and **6** were submitted to Canadian Microanalytical Service Ltd© for elemental analysis. EA for compounds **20**, **22** and **23** were found to be variable due to the inability to separate reaction by-products, some of which are unknown, and were therefore not included.

- Melting Point Analysis

Melting points were recorded on an Electrothermal MEL-Temp 3.0 using glass capillaries with samples prepared under inert conditions.

- Nuclear Magnetic Resonance Spectroscopy

Trace protonated solvent was used as internal references for all ^{1}H NMR spectra. Deuterated solvent was used as an internal reference for all $^{13}C\{^{1}H\}$ NMR spectra. $^{31}P\{^{1}H\}$ was referenced to an external 85% H_3PO_4 standard while ^{11}B and ^{19}F were both compared to an external $F_3B(OEt_2)$ sample. Coupling constants are reported as absolute values. The NMR spectra were recorded on Bruker-Avance 500 MHz, Bruker-Avance 300 MHz, AC-250 MHz and Varian EM360 60 MHz spectrometers (relative to ^{1}H). Spectra of **2** (other than ^{1}H), **12**, **17** and **18** were reported at ambient temperatures but will require low temperature analysis in the future for complete characterization. Once VT NMR is available at NMR[3] (in the coming months) the NMR analysis will be repeated at sub-ambient temperatures, reducing the dynamic nature of each system.

- Simulated $^{31}P\{^{1}H\}$ NMR (Dr. Mike Lumsden, NMR^3, Dalhousie University)

Simulated $^{31}P\{^{1}H\}$ NMR parameters were completed at the NMR^3 for compound **3** by Dr. Mike Lumsden: Solution $^{31}P\{^{1}H\}$ NMR spectra were collected at room temperature on Bruker Avance 500 and AC-250 NMR spectrometers using 5mm NMR probes for both. Chemical shifts are reported in ppm relative to 85% H_3PO_4. All reported $^{31}P\{^{1}H\}$ NMR chemical shifts and coupling constants were obtained *via* computer simulation of the experimental spectra, using the software program gNMR, version 4.0, by Cherwell Scientific.[162]

In order to simulate the complex $^{31}P\{^{1}H\}$ spectrum, experimental data was obtained at three different external magnetic field strengths (11.7 T, 5.9 T, and 1.4 T corresponding to $^{31}P\{^{1}H\}$ Larmor frequencies of 202.4, 101.2 and 24.3 MHz, respectively). Simulations were performed using the higher field data first, making use of connectivity information obtained *via* P-P COSY experiments. The uniqueness of the solution was subsequently verified using the simulated parameters obtained at 11.7 T to calculate $^{31}P\{^{1}H\}$ spectra obtained at 5.9 and 1.4 T. The quality of the fits in all cases was also verified by examining the singular value decomposition matrix provided by gNMR. The absolute signs of P-P coupling constants were assigned using the assumption that all $^{1}J_{P\text{-}P}$ coupling constants are negative.[163] Letter designations in the phosphorus spin system has been assigned by calculating the ratio of the phosphorus chemical shift differences to the magnitude of the coupling constant, using a value of 10 as the threshold between a first and second order letter designation.

- Electron Paramagnetic Resonance Spectroscopy (Dr. Tracey Roemelle)

X-band EPR spectra were recorded on a sample of $(Dipp_2C_2H_4N_2P)_2$ by Dr. Tracey Roemmele over temperatures of 253 – 312 K using a Bruker EMX 113 spectrometer at the University of Calgary. The sample was prepared inside a glove box, transferred into 4.0 mm EPR tube, and sealed prior to data collection. Hyperfine coupling constants were determined by spectral simulation using Winsim (version 0.98, 2002) software.[164]

- Single Crystal X-ray Spectroscopy

X-ray crystallographic data collection was accomplished using APEX2,[165] cell refinement using SAINT,[165] data reduction *via* SAINT, structure identification was possible by using SHELXS97,[166] structure refinement software used was SHELXL97,[166] and molecular graphics were created through ORTEP-3 for Windows.[167]

- Raman Spectroscopy

Raman spectroscopy was completed on a Thermo Scientific DXR SmartRaman equipped with a DXR 780 nm FILTER and a 180 Degree Accessory. Data processing was accomplished using OMNIC. A 780 nm, 120 mW LASER was employed with one second samples and a resolution of ± 1 cm^{-1}. LASER position: focus = 2500 mm; side-to-side = 200 mm; up/down = 92 mm.

Section 3.2 – Synthesis and Reactivity of a New Diphosphine

Preparation of $(Dipp_2C_2H_4N_2P)_2$ – (2)

1.7 g (13.3 mmol) of naphthalene was weighed directly into a 20 mL scintillation vial charged with a magnetic stir-bar and dissolved in 10 mL of THF. With rapid stirring, 0.26 g (13.3 mmol) of Na^0 was added in small, freshly divided pieces. The resultant, forest-green solution was allowed to stir for 30 minutes until sodium metal was no longer visible at which point it was added drop-wise to a stirring solution of 5.0 g (13.3 mmol) of 2-chloro-1,3-bis(2,6-diisopropylphenyl)-1,3,2-diazaphospholidine (**1**) in 10 mL of THF. The reaction mixture was allowed to stir overnight. The resulting bright-orange solution was pumped to dryness under vacuum, extracted with pentane and filtered through a pad of diatomaceous earth. Naphthalene was removed *via* sublimation *in vacuo* at 50 °C over approximately 8 hours. The resultant orange solid was crystallized from pentane at -35 °C yielding 3.40 g (73.8 % recovery), X-ray quality crystals of **2**. $^{31}P\{^1H\}$ (101.2 MHz, C_6D_6) δ: 143.46. (500 MHz, toluene-d_8, 268K) ^1H δ: 7.21-7.13 (m, 8H, Ar-*H*), 7.00-6.94 (m, 4H, Ar-*H*), 4.18 (br m, 2H, C*H*/CH_2), 4.01 (br m, 2H, C*H*/CH_2), 3.64-3.57 (br m, 4H, C*H*/CH_2), 3.44 (br m, 2H, C*H*/CH_2), 3.25 (br m, 2H, C*H*/CH_2), 2.94 (br m, 2H, C*H*/CH_2), 2.83 (br m, 2H, C*H*/CH_2), 1.47-1.42 (br m, 12H, CH_3), 1.30-1.14 (br m, 27H, CH_3), 0.93-0.87 (br m, 3H, CH_3), 0.38 (br s, 6H, CH_3). $^{13}C\{^1H\}$ (125.7 MHz, C_6D_6) δ: 149.15, 148.81, 126.40, 124.79, 124.37, 57.72, 54.55, 30.46, 29.30, 28.45, 24.67, 23.06, 14.62. PP: 219-220 °C. Anal calc for $C_{52}H_{76}N_4P_2$: C, 76.25; H, 9.35; N, 6.84. Found: C, 75.99; H, 9.72; N, 6.73.

Preparation of ($Dipp_2C_2H_4N_2P)P_4(PN_2C_2H_4Dipp_2$) – (3)

66 mg (0.081 mmol) **2** was added to a J-Young® style NMR tube. 10mg (0.0081 mmol) of P_4 and 0.6 mL toluene were added and the NMR tube was shaken vigorously. After 60 min the reaction yielded **3** quantitatively by $^{31}P\{^1H\}$ NMR. X-ray quality, yellow-gold block-like single crystals were grown from toluene at -35°C over several days (57 mg, 75 % yield). $^{31}P\{^1H\}$ δ: Modeling of the P_6 system core as AA'MM'X_2 yielded: $^{31}P\{^1H\}$ δA = 160.7 ppm, δM = -108.2 ppm, δX = -349.5 ppm, $J_{AM} = J_{A'M'} = -214.9$ Hz, $J_{MX} = J_{M'X} = -152.8$ Hz, $J_{AX} = J_{A'X} = +99.2$ Hz, $J_{MM'} = +101.1$ Hz, $J_{AM'} = J_{A'M} = -61.2$ Hz. ^1H (500 MHz, C_6D_6) δ: 6.91-7.08 (12H, Ar-*H*), 3.77 (sept, 4H, C*H*, $^3J_{H-H} = 7$ Hz), 3.60 (m, 4H, CH_2), 3.34 (sept, 4H, C*H*, $^3J_{H-H} = 7$ Hz), 2.99 (m, 4H, CH_2), 2.07 (s, 1.7H, residual solvent), 1.46 (d, 12H, CH_3, $^3J_{H-H} = 7$ Hz), 1.15 (d, 12H, CH_3, $^3J_{H-H} = 7$ Hz), 1.10 (d, 12H, CH_3, $^3J_{H-H} = 7$ Hz), 1.06 (d, 12H, CH_3, $^3J_{H-H} = 7$ Hz). $^{13}C\{^1H\}$ (125.7 MHz, C_6D_6) δ: 150.01, 148.65, 138.29, 138.19, 125.14, 125.04, 65.77, 55.95, 53.27, 30.11, 29.47, 26.51, 26.07, 25.97, 24.99, 24.80. PP: 237-240 °C. Anal calc for $C_{52}H_{76}N_4P_6 \cdot 1/2C_7H_8$: C, 67.39; H, 8.15; N, 5.66. Found: C, 67.32; H, 7.72; N, 5.49.

Preparation of ($Dipp_2C_2H_4N_2PO)O(OPN_2C_2H_4Dipp_2$) – (4)

100 mg (0.122 mmol) **2** was added to a J-Young® style NMR tube containing 0.6 mL of toluene. The sample was degassed using three freeze-pump-thaw cycles. Room temperature gaseous oxygen was introduced at approximately one atmosphere. The tube was sealed and shaken vigorously. After 30 minutes complete loss of 1,1',3,3'-tetrakis(2,6-diisopropylphenyl)-2,2'-bi(1,3,2-diazaphospholidine) in the $^{31}P\{^1H\}$ NMR which indicated virtually quantitative conversion to **4**. X-ray quality colourless block-like

crystals were grown through slow evaporation of toluene at ambient temperatures (55 mg, 52 % isolated yield). $^{31}P\{^{1}H\}$ (101.2 MHz, C_6D_6) δ: 4.34. ^{1}H (500 MHz, C_6D_6) δ: 7.30-7.16 (m, 6H, Ar-*H*), 7.14-6.97 (m, 6H, Ar-*H*), 4.04 (sept, 2H, C*H*, $^{3}J_{H-H}$ = 7 Hz), 3.87 (sept, 1H, C*H*, $^{3}J_{H-H}$ = 7 Hz), 3.81 (sept, 1H, C*H*, $^{3}J_{H-H}$ = 7 Hz), 3.69 (sept, 1H, C*H*, $^{3}J_{H-H}$ = 7 Hz), 3.59 (q, 2H, CH_2, $^{3}J_{H-H}$ = 7 Hz), 3.52-3.21 (m, 6H, C*H*/CH_2), 3.13 (sept, 1H, C*H*, $^{3}J_{H-H}$ = 7 Hz), 3.07 (s, 0.5H, residual solvent), 2.95-2.88 (m, 2H, C*H*/CH_2), 1.63 (d, 3H, CH_3, $^{3}J_{H-H}$ = 7 Hz), 1.56 (d, 3H, CH_3, $^{3}J_{H-H}$ = 7 Hz), 1.47 (d, 3H, CH_3, $^{3}J_{H-H}$ = 7 Hz), 1.40 (d, 2H, CH_3, $^{3}J_{H-H}$ = 7 Hz), 1.37-1.25 (m, 6H, CH_3), 1.23 (d, 3H, CH_3, $^{3}J_{H-H}$ = 7 Hz), 1.21-1.04 (overlapping doublets, 21H, CH_3), 1.04 (d, 3H, CH_3, $^{3}J_{H-H}$ = 7 Hz), 0.62 (d, 3H, CH_3, $^{3}J_{H-H}$ = 7 Hz). $^{13}C\{^{1}H\}$ (75.4 MHz, C_6D_6) δ: 150.66, 150.27, 136.49, 135.90, 124.53, 124.18, 51.12, 49.16, 29.58, 29.44, 29.23, 28.83, 28.65, 28.45, 27.58, 27.27, 26.77, 26.43, 26.32, 25.96, 25.82, 25.71, 25.36, 25.24, 25.02, 24.79, 24.62, 24.49. PP: 190-192 °C. Anal calc for $C_{52}H_{76}N_4P_2O_3$: C, 72.03; H, 8.83; N, 6.46. Found: C, 71.19; H, 8.86; N, 6.47.

Preparation of $Dipp_2C_2H_4N_2P(O)OH$ – (5)

100 mg (0.122 mmol) of **2** was weighed into a 20 mL scintillation vial charged with a magnetic stir-bar and dissolved in 10 mL of toluene. The vial was removed from the glovebox at which point gaseous oxygen (O_2) was bubbled through the solution until only pale yellow solution remained. Removal of toluene *in vacuo* left a pale yellow solid (**4**) which was subsequently treated with 10 mL of THF mixed with ~1 mL of H_2O. The solution was allowed to stir for ~30 min. Removal of the solvent *in vacuo* resulted in a colourless solid which upon crystallization in THF at -35°C yielded 75 mg (69 % isolated

yield) of colourless crystals. $^{31}P\{^{1}H\}$ (121.5 MHz, $CDCl_3$) δ: 6.45 ^{1}H (300 MHz, $CDCl_3$) δ: 8.64 (s, 0.5H, PO*H*•••O), 7.32-7.15 (m, 6H, Ar-*H*), 6.58 (s, 0.5H, PO*H*), 3.77-3.56 (m, 6H, *CH*/CH_2), 3.37 (sept, 2H, C*H*, $^{3}J_{H-H}$ = 7 Hz), 1.36 (d, 6H, CH_3, $^{3}J_{H-H}$ = 7 Hz), 1.32 (d, 6H, CH_3, $^{3}J_{H-H}$ = 7 Hz), 1.30 (d, 12H, CH_3, $^{3}J_{H-H}$ = 7 Hz). $^{13}C\{^{1}H\}$ (75.4 MHz, $CDCl_3$) δ: 150.11, 148.63, 133.16, 128.44, 124.74, 123.94, 49.99, 49.93, 28.83, 28.68, 25.25, 24.93, 24.44, 24.33. PP: 168-170 °C. Anal calc for $C_{26}H_{39}N_2PO_2$: C, 70.56; H, 8.88; N, 6.33. Found: C, 70.62; H, 8.87; N, 6.19. *This product (**5**) can also be made from the diphosphine (**2**) using: H_2O_2 (40% in H_2O) in THF, or by simply adding H_2O in THF.

Preparation of $(Dipp_2C_2H_4N_2P)(S)_{1\text{-}2}(PN_2C_2H_4Dipp_2)$ – (6-7)

100 mg (0.122 mmol) of **2** was weighed into a 20 mL scintillation vial charged with a magnetic stir-bar and dissolved in 10 mL of toluene. With rapid stirring, 31.2 mg (0.122 mmol) of S_8 was added as a partially dissolved suspension in 2 mL of toluene. The resultant pale-yellow solution was allowed to stir for 30 min at which point it transitions to colourless. The solution was filtered through a pad of diatomaceous earth and crystallized *via* slow evaporation of the solvent at ambient temperatures yielding 85 mg of X-ray quality, colourless crystals. $^{31}P\{^{1}H\}$ (101.2 MHz, C_6D_6) δ: 154.36 (P-S-S-P), 136.03 (P-S-P). ^{1}H (250 MHz, C_6D_6) δ: 7.23-7.17 (m, 4H, Ar-*H*), 7.14-7.01 (m, 8H, Ar-*H*), 3.40 (sept, 2H, C*H*, $^{3}J_{H-H}$ = 7 Hz), 3.87-3.68 (m, 4H, CH_2/C*H*), 3.64 (q, 1H, CH_2, $^{3}J_{H-H}$ = 7 Hz), 3.31-3.52 (m, 4H, C*H*, $^{3}J_{H-H}$ = 7 Hz), 3.25 (sept, 1H, C*H*, $^{3}J_{H-H}$ = 7 Hz), 3.04-3.09 (m, 4H, CH_2), 1.56 (d, 3H, CH_3, $^{3}J_{H-H}$ = 7 Hz), 1.45 (d, 3H, CH_3, $^{3}J_{H-H}$ = 7 Hz), 1.35 (br m, 3H, CH_3), 1.24-1.30 (m, 6H, CH_3), 1.21 (d, 3H, CH_3, $^{3}J_{H-H}$ = 7 Hz), 1.20 (d, 3H, CH_3, $^{3}J_{H-H}$ = 7 Hz), 1.17 (d, 6H, CH_3, $^{3}J_{H-H}$ = 7 Hz), 1.15 (d, 6H, CH_3, $^{3}J_{H-H}$ = 7 Hz), 1.11-1.07 (m,

9H, CH_3), 0.96-0.84 (m, 6H, CH_3). $^{13}C\{^1H\}$ (75.4 MHz, C_6D_6) δ: 150.36, 149.49, 124.81, 124.29, 123.78, 123.53, 54.53, 50.01, 29.83, 28.69, 25.63, 25.43, 24.97, 24.58, 24.30, 24.03, 23.56. PP: 175-177 °C. Anal calc for 90% $C_{52}H_{76}N_4P_2S$·10% $C_{52}H_{76}N_4P_2S_2$·1/2C_7H_8: C, 73.20; H, 8.96; N, 6.52. Found: C, 73.03; H, 9.46; N, 5.98.

Preparation of ($Dipp_2C_2H_4N_2P)_2Se$ – (8)

100 mg (0.122 mmol) of **2** was weighed into a 20 mL scintillation vial charged with a magnetic stir-bar and dissolved in 5 mL of THF. With rapid stirring, 9.6 mg (0.122 mmol) of Se^0 was added as a suspension in 5 mL of THF. The orange solution with grey precipitate was allowed to stir overnight at which point the solution transitions to pale yellow. The solvent was removed *in vacuo*, dissolved in toluene, filtered through a pad of diatomaceous earth to remove excess selenium metal and crystallized *via* slow evaporation of the solvent at ambient temperatures yielding 83 mg of X-ray quality, yellow crystals (75.7 % yield). $^{31}P\{^1H\}$ (121.5 MHz, C_6D_6) δ: 160.01 (sat t, P-Se, $^1J_{P\text{-}Se}$ = 141 Hz). ^1H (300 MHz, C_6D_6) δ: 7.18 (2H, Ar-*H*), 7.13 (m, 2H, Ar-*H*), 7.06-7.03 (m, 8H, Ar-*H*), 3.79-3.64 (m, 8H, C*H*/CH_2), 3.57 (m, residual THF), 3.41 (sept, 4H, CH, $^3J_{H\text{-}H}$ = 7 Hz), 3.11-3.06 (m, 4H, CH_2), 1.40 (m, residual THF), 1.19-1.16 (overlapping doublets, 24H, CH_3), 1.07-1.03 (overlapping doublets, 24H, CH_3). $^{13}C\{^1H\}$ (75.4 MHz, C_6D_6) δ: 149.60, 147.93, 138.08, 127.34, 124.89, 124.05, 55.24, 28.86, 28.80, 28.73, 25.96, 25.79, 25.57, 24.54, 24.22. PP: 182-185 °C. Anal calc for $C_{52}H_{76}N_4P_2Se$: C, 69.54; H, 8.53; N, 6.24. Found: C, 69.59; H, 8.65; N, 6.15.

Preparation of $(Dipp_2C_2H_4N_2P)_2Te$ – (10)

100 mg (0.122 mmol) of **2** was weighed into a 20 mL scintillation vial charged with a magnetic stir-bar and dissolved in 5 mL of THF. With rapid stirring, 78 mg (0.61 mmol, 5 equivalents) of Te^0 was added as a suspension in 5 mL of THF. The orange solution with grey/black precipitate was allowed to stir overnight at which point the solution transitions to yellow in colour. THF was removed *in vacuo*. The solid was dissolved in toluene, filtered through a pad of diatomaceous earth to remove excess tellurium metal and crystallized *via* slow evaporation of the solvent at ambient temperatures yielding 95 mg of X-ray quality, yellow crystals of **10** (82.3 % yield). $^{31}P\{^1H\}$ (121.5 MHz, C_6D_6) δ: 177.07 (sat t, P-Te, $^1J_{P\text{-}Te}$ = 278 Hz) ^1H (300 MHz, C_6D_6) δ: 7.18-7.04 (m, 12H, Ar-*H*), 7.01 (m, 5H, Ar-*H* residual toluene), 3.66 (q, 4H, C*H*$_2$, $^3J_{H\text{-}H}$ = 7 Hz), 3.59 (sept, 4H, C*H*, $^3J_{H\text{-}H}$ = 7 Hz), 3.43 (sept, 4H, C*H*, $^3J_{H\text{-}H}$ = 7 Hz), 3.12 (q, 4H, C*H*$_2$, $^3J_{H\text{-}H}$ = 7 Hz), 2.11 (s, 3H, C*H*$_3$, residual toluene), 1.89 (d, 12H, C*H*$_3$, $^3J_{H\text{-}H}$ = 7 Hz), 1.14 (d, 12H, C*H*$_3$, $^3J_{H\text{-}H}$ = 7 Hz), 1.08 (d, 12H, C*H*$_3$, $^3J_{H\text{-}H}$ = 7 Hz), 1.00 (d, 12H, C*H*$_3$, $^3J_{H\text{-}H}$ = 7 Hz). $^{13}C\{^1H\}$ (75.4 MHz, C_6D_6) δ: 149.53, 148.07, 129.29, 127.43, 125.17, 124.02, 55.07, 29.00, 28.66, 25.91, 25.47, 25.40, 24.38. PP: 196-199 °C. Anal calc for $C_{52}H_{76}N_4P_2Te{\cdot}C_7H_8$: C, 68.21; H, 8.15; N, 5.39. Found: C, 68.52; H, 8.22; N, 5.69.

Preparation of $Dipp_2C_2H_4N_2PH \rightarrow BH_3$ – (11)

100 mg (0.122 mmol) of **2** was weighed into a 20 mL scintillation vial charged with a magnetic stir-bar and dissolved in 5 mL of toluene. With rapid stirring, 0.122 mL (0.244 mmol) of $H_3B{\bullet}S(CH_3)_2$ (2.0M in THF) was added. The orange solution was allowed to stir for 30 min at which point it transitioned to yellow. The solution was filtered through

a pad of diatomaceous earth and crystallized *via* slow evaporation of the solvent at ambient temperatures yielded X-ray quality, colourless crystals. Complete removal of the solvent yielded 90 mg of an off-white solid. ^{31}P (121.5 MHz, C_6D_6) δ: 82.0 (dd, $^1J_{P-H}$ = 357 Hz, $^1J_{P-B}$ = 73 Hz). $^{31}P\{^1H\}$ (121.5 MHz, C_6D_6) δ: 82.0 (d, $^1J_{P-B}$ = 73 Hz). ^1H (300 MHz, C_6D_6) δ: 7.47 (br d, 1H, P-*H*, $^1J_{P-H}$ = 357 Hz), 7.20-7.12 (m, 4H, Ar-*H*), 7.03-7.00 (m, 2H, Ar-*H*) 3.74 (sept, 2H, CH, $^3J_{H-H}$ = 7 Hz), 3.36-3.18 (m, 6H, C*H*/CH_2), 1.47 (d, 6H, CH_3, $^3J_{H-H}$ = 7 Hz), 1.37-1.29 (m, 2H, BH_3), 1.24 (d, 6H, CH_3, $^3J_{H-H}$ = 7 Hz), 1.22 (d, 6H, CH_3, $^3J_{H-H}$ = 7 Hz), 1.17 (d, 6H, CH_3, $^3J_{H-H}$ = 7 Hz). $^{13}C\{^1H\}$ (75.4 MHz, C_6D_6) δ: 149.95, 149.38, 135.20, 135.11, 128.81, 124.98, 124.29, 52.24, 29.45, 28.73, 25.85, 25.14, 24.51, 24.22. ^{11}B (96.2 MHz, C_6D_6) δ: -40.42 (t, $^1J_{P-B}$ = 73 Hz). PP: 156-159 °C. Anal calc for $C_{26}H_{42}N_2PB{\bullet}C_4H_8O$: C, 72.57; H, 10.15; N, 5.64. Found: C, 72.18; H, 10.17; N, 6.24.

Preparation of $Dipp_2C_2H_4N_2PH \rightarrow B(C_6F_5)_3$ – (12)

30 mg (0.122 mmol) of **2** was weighed into a 20 mL scintillation vial charged with a magnetic stir-bar and dissolved in 5 mL of toluene. With rapid stirring, 37.5 mg (0.244 mmol) of $B(C_6F_5)_3$ in 5 mL of toluene was added drop-wise over 5 min. The orange solution with was allowed to stir for 30 min at which point it transitions to colourless. The solution was filtered through a pad of diatomaceous earth and crystallized *via* slow evaporation of the solvent at ambient temperatures yielding X-ray quality, colourless crystals. Complete removal of solvent afforded 55 mg of a colorless solid. $^{31}P\{^1H\}$ (121.5 MHz, C_6D_6) δ: 66.8 (br s). ^{31}P (121.5 MHz, C_6D_6) δ: 66.8 (br d, $^1J_{P-H}$ = 404 Hz). ^1H (300 MHz, C_6D_6) δ: 8.35 (br s, 0.5H, P*H*) 7.13-6.80 (br m, 6H, Ar-*H*), 3.54-2.86 (br m, 8H,

C*H*/C*H*$_2$), 1.16-0.84 (br m, 24H, C*H*$_3$). $^{13}C\{^1H\}$ (75.4 MHz, C_6D_6) δ: 150.30, 149.24, 147.34, 146.48, 139.02, 135.82, 129.06, 124.88, 54.68, 52.36, 29.63, 28.54, 28.38, 26.50, 24.17, 22.32. ^{11}B (96.2 MHz, C_6D_6) δ: 74.3 (br s), 61.3 (br s, excess tris(pentafluorophenyl)borane). ^{19}F (282.4 MHz, C_6D_6) δ: Prohibitively broad at ambient temperatures. PP: 145-148 °C. Anal calc for $C_{44}H_{39}N_2PBF_{15}$: C, 57.28; H, 4.26; N, 3.04. Found: C, 57.13; H, 4.53; N, 2.99.

Preparation of $Dipp_2C_2H_4N_2PH$ – (14-15)

3.0 g (6.7 mmol) of $Dipp_2C_2H_4N_2PCl$ (**1**) was weighed into a 100 mL Schlenk flask charged with a magnetic stir-bar and dissolved in 25 mL of THF. With rapid stirring, 6.75 mL (6.7 mmol) of lithium triethylborohydride (1.0 M in THF) was added drop-wise over 10 min. The reaction was allowed to stir for 30 min, remaining colourless throughout. THF was removed *in vacuo* and the resulting white solid dissolved in c. 50 mL of pentane. The suspension was filtered through a pad of diatomaceous earth and the resulting colourless solution pumped to dryness, yielding 2.20 g of **11** (79.8 % yield) as a white powder. Colourless crystals could be grown from slow evaporation of a concentrated toluene solution at ambient temperatures. ^{31}P (121.5 MHz, C_6D_6) δ: 72.0 (d, $^1J_{P-H}$ = 141 Hz). ^1H (300 MHz, C_6D_6) δ: 7.04 (d, $^1J_{P-H}$ = 141 Hz), 7.19-7.04 (m, Ar-*H*, 6H), 3.70 (sept, 2H, C*H*, $^3J_{H-H}$ = 7 Hz), 3.46-3.29 (m, overlapping septet/quartets, 6H, C*H*/C*H*$_2$), 1.31 (d, 6H, C*H*$_3$, $^3J_{H-H}$ = 7 Hz), 1.28 (d, 6H, C*H*$_3$, $^3J_{H-H}$ = 7 Hz), 1.21 (d, 6H, C*H*$_3$, $^3J_{H-H}$ = 7 Hz), 1.17 (d, 6H, C*H*$_3$, $^3J_{H-H}$ = 7 Hz). $^{13}C\{^1H\}$ (75.4 MHz, C_6D_6) δ: 150.9, 149.1, 139.5, 139.3, 124.5, 124.3, 56.2, 56.1, 29.2, 28.7, 25.8, 25.0, 24.9, 24.3. IR (KBr, cm^{-1}) υ: 2958(s), 2924(m), 2967(m), 2025(m) P-H, 1464(m), 1441(m), 1381(m),

1360(m), 1321(m), 1265(m), 1205(m), 1107(w), 1063(m), 1040(m). IR (solution in heptane, cm^{-1}) υ: 2047 P-H. PP: 139-140 °C. Anal calc for $C_{26}H_{39}N_2P$: C, 76.06; H, 9.57; N, 6.82. Found: C, 76.10; H, 9.57; N, 6.75.

Preparation of $Dipp_2C_2H_4N_2P$-S-C(=S)-$PN_2H_4C_2Dipp_2$ – (16)

200 mg (0.244 mmol) of **2** was weighed into a 20 mL scintillation vial charged with a magnetic stir-bar and dissolved in 5 mL of toluene. With rapid stirring, 15.0 μL (0.244 mmol) of CS_2 was added using a micro-pipette. The orange solution transitions to bright green in several seconds. After stirring for 30 min, the solution was filtered through a pad of diatomaceous earth and crystallized *via* slow evaporation of the solvent at ambient temperatures yielded X-ray quality, green crystals. Removal of the solvent afforded 205 mg of a bright green solid (94 % yield). $^{31}P\{^1H\}$ (121.5 MHz, C_6D_6) δ: 133.10 (d, $^3J_{P\text{-}P}$ = 8 Hz) , 92.36 (d, $^3J_{P\text{-}P}$ = 8 Hz). ^1H (300 MHz, C_6D_6) δ: 7.20-7.16 (m, 6H, Ar-*H*), 7.14-7.03 (m, 6H, Ar-*H*), 4.19-4.04 (m, 4H, overlapping sept(*CH*)/m{CH_2}) 3.82 (sept, 2H, C*H*, $^3J_{H\text{-}H}$ = 7 Hz), 3.71 (m, 2H, CH_2, $^3J_{H\text{-}H}$ = 7 Hz), 3.60 (sept, 4H, C*H*, $^3J_{H\text{-}H}$ = 7 Hz), 3.23 (sept, 4H, C*H*, $^3J_{H\text{-}H}$ = 7 Hz), 1.45-1.41 (overlapping doublets, 12H, CH_3), 1.30-1.26 (overlapping doublets, 27H, CH_3), 1.15 (d, 6H, CH_3, $^3J_{H\text{-}H}$ = 7 Hz) 0.94-0.89 (m, 3H, CH_3). $^{13}C\{^1H\}$ (75.4 MHz, C_6D_6) δ: 149.55, 149.36, 147.59, 147.50, 138.36 (dd, LP-*C*(S)-S-PL, $^1J_{P\text{-}C}$ = 134.7 Hz, $^2J_{P'\text{-}C}$ = 11.5 Hz), 127.00, 124.54, 124.17, 55.51, 55.40, 34.41, 29.45, 29.31, 29.23, 28.99, 28.80, 26.10, 26.00, 25.91, 25.57, 25.37, 25.31, 24.41, 24.25, 22.69, 14.24. PP: 169-172 °C. Anal calc for $C_{53}H_{76}N_4PS_2$•1/2C_7H_8: C, 72.09; H, 8.57; N, 5.95. Found: C, 71.70; H, 7.98; N, 6.20.

Preparation of $Dipp_2C_2H_4N_2P$-O-C(=N-Ph)-$PN_2H_4C_2Dipp_2$ – (17)

100mg (0.122 mmol) of **2** was weighed into a 20 mL scintillation vial charged with a magnetic stir-bar and dissolved in 5 mL of toluene. With rapid stirring, 13.3 μL (0.244 mmol) of phenyl isocyanate (Ph-NCO) was added using a micro-pipette. The orange solution transitions to pale yellow overnight. Removal of solvent yielded a white powder which was dissolved in c. 5 mL of pentanes and filtered through a pad of diatomaceous earth. Colourless X-ray quality crystals of **17** were grown from a pentane solution at -35 °C. Complete removal of solvent yielded 92 mg of a pale yellow solid (80 % yield). $^{31}P\{^1H\}$ (121.5 MHz, C_6D_6) δ: 122.36, 84.74. ^1H (300 MHz, C_6D_6) δ: 7.23-6.99 (br m, 16H, Ar-*H*), 6.61 (br s, 2H, Ar-*H*), 5.56 (br s, 2H, Ar-*H*), 4.37-3.95 (br m, 4H, C*H*/CH_2), 3.87-3.64 (br m, 2H, C*H*/CH_2), 3.49 (br m, 4H, C*H*/CH_2), 3.33 (br m, 2H, C*H*/CH_2), 3.13 (br m, 4H, C*H*/CH_2), 2.10 (s, 2H, residual toluene CH_3), 1.72-0.57 (br m, 48H, CH_3). $^{13}C\{^1H\}$ (75.4 MHz, C_6D_6) δ: 149.91, 148.86, 147.41, 139.66, 129.29, 126.74, 124.66, 123.05, 121.91, 55.55, 55.32, 28.88, 28.14, 25.92, 24.85, 24.66, 23.76. PP: 112-114 °C. Anal calc for $C_{59}H_{81}N_5PO \cdot 1/2C_7H_8$: C, 76.26; H, 8.70; N, 7.11. Found: C, 76.30; H, 8.57; N, 6.86.

Preparation of $Dipp_2C_2H_4N_2P$-S-C(=N-Ph)-$PN_2H_4C_2Dipp_2$ – (18)

100mg (0.122 mmol) of **2** was weighed into a 20 mL scintillation vial charged with a magnetic stir-bar and dissolved in 5 mL of toluene. With rapid stirring, 14.5 μL (0.244 mmol) of phenyl isothiocyanate (Ph-NCS) was added using a micro-pipette. The orange solution transitions to a pale yellow over 5 days. Removal of solvent afforded a yellow powder which was subsequently dissolved in c. 5 mL of pentanes and filtered through a

pad of diatomaceous earth. X-ray quality crystals of **18** were grown from a pentane solution at -35 °C containing a trace amount of benzene. Complete removal of solvent afforded 98 mg of a yellow solid (84 % yield). $^{31}P\{^{1}H\}$ (121.5 MHz, C_6D_6) δ: 128.07 (br s), 83.81 (br s). ^{1}H (300 MHz, C_6D_6) δ: 7.26-7.06 (br m, 12H, Ar-H), 6.74-6.69 (br m, 2H, Ar-*H*), 6.62-6.56 (br m, 3H, Ar-*H*), 5.54 (br s, 2H), 4.58 (br s, 1H), 4.30 (br s, 2H), 3.91-3.47 (br m, 11H, C*H*/CH_2), 3.14 (br m, 5H, C*H*/CH_2), 1.76-0.60 (br m, 48H, CH_3). $^{13}C\{^{1}H\}$ (75.4 MHz, C_6D_6) δ: 149.87, 149.08, 148.58, 147.18, 139.21, 139.03, 129.42, 126.97, 125.70, 124.93, 124.64, 124.18, 123.45, 121.05, 55.25, 54.78, 29.07, 28.77, 25.95, 25.03, 24.13, 22.69, 14.45. PP: 193 °C. Anal calc for $C_{59}H_{81}N_5PS$: C, 74.26; H, 8.56; N, 7.34. Found: C, 73.82; H, 8.89; N, 7.2

Section 3.3 – Reactivity of Carbenes and S_4N_4

Preparation of SIPr-S_4N_4 – (19)

100 mg (0.256 mmol) of 1,3-bis(2,6-diisopropylphenyl)-imidazolidin-2-ylidene (SIPr) was dissolved in 5 mL of toluene and added to a stirring suspension of 47.2 mg (0.256 mmol) of tetrasulfur tetranitride (S_4N_4) in 5 mL of toluene. As the orange solution transitions to red, the product precipitates out as a fine red powder which was allowed to stir for 20 min. The solid was rinsed with pentane to remove excess 1,3-bis(2,6-diisopropylphenyl)-imidazolidin-2-ylidene yielding 138 mg of **19** (94 % yield). To generate suitable single crystals for X-ray analysis the following procedure was employed: A suspension of 47.2 mg (0.256 mmol) of S_4N_4 in 5mL of toluene was first cooled to -35 °C in a 100 mL Schlenk tube. 5 mL of toluene was added as a second layer and subsequently cooled to -35 °C. Finally, 100 mg (0.256 mmol) of SIPr was dissolved

in 5 mL of toluene and added as a third layer to the Schlenk tube. The reaction vessel was cooled to -35 °C allowing the layers to diffuse together slowly overnight. Decanting the toluene yielded plate-like single crystals of **1**. IR (KBr, cm^{-1}) υ: 2961.92(s), 2926.12(m), 2866.95(m), 2366.81(w, S-N), 2341.03(m, C-S), 1507.00(s), 1463.14(s), 1422.16(s). PP: 145 °C (decomposition). Anal calc for $C_{27}H_{38}N_6S_4$: C, 56.41; H, 6.66; N, 14.62. Found: C, 56.13; H, 6.62; N, 14.27. NMR spectra could not be obtained for this sample due to solubility issues in non-nucleophilic solvents.

Preparation of IMes-S_3N_4 – (20)

100 mg (0.328 mmol) of 1,3-bis(2,4,6-trimethylphenyl)-imidazol-2-ylidene (IMes) was dissolved in 5 mL of toluene and subsequently added to a stirring suspension of 60.5 mg (0.328 mmol) of tetrasulfur tetranitride (S_4N_4) in 5 mL of toluene. Upon addition of the carbene, the solution transitions to dark purple in colour. After stirring for 20 minutes, the toluene was reduced *in vacuo* and placed in a -35 °C freezer yielding purple crystals of **20**. Yellow-green single crystals of elemental sulfur (S_8) could be separated mechanically using a light microscope and identified as S_8 by single crystal X-ray analysis. ^{1}H NMR (250 MHz, C_6D_6) δ: 6.68 (m, 4H, Ar-*H*), 5.51 (d, 2H, NC*H*), 2.08 (m, 18H, Ar-CH_3) ppm. $^{13}C\{^1H\}$ NMR (75.4 MHz, C_6D_6) δ: 147.27 (*C*=N), 139.70, 136.28, 136.21, 134.67, 132.52, 132.38, 129.57, 129.43, 125.65, 115.78, 115.19, 21.01, 17.97 ppm. IR (KBr, cm^{-1}) υ: 2919.03(s), 2854.04(m), 2361.51 (w, S-N), 1522.81(s). PP: 144-146 °C.

Preparation of CAAC-S_4N_4 – (21)

150 mg (0.43 mmol) 2-(2,6-diisopropylphenyl)-3,3-6-8-tetramethyl-2-azospiro[4.5]-dec-7-enyl-1-ylidene of was dissolved in 5 mL of toluene and subsequently added to a stirring

suspension of 78 mg (0.43 mmol) of tetrasulfur tetranitride (S_4N_4) in 5 mL of toluene. Upon addition of the CAAC solution drop-wise, the orange colour of S_4N_4 transitions to a dark red. After stirring overnight (c. 15 hrs) the toluene was evaporated slowly at room temperature yielding red, X-ray quality single crystals of **21**. A single crystal structure of **21** was obtained however all other analyses indicated a highly impure reaction mixture.

Preparation of SIPr-S_3N_2 – (22)

100 mg (0.256 mmol) of 1,3-bis(2,6-diisopropylphenyl)-imidazolidin-2-ylidene (SIPr) was dissolved in 5 mL of toluene and subsequently added to a stirring suspension of 47.2 mg (0.256 mmol) of tetrasulfur tetranitride (S_4N_4) in 5 mL of toluene. After stirring overnight (c. 15 hrs) the solution transitions to deep red with red precipitate. Toluene was removed *in vacuo* yielding **19** as a fine red powder. Upon addition of 10 mL of THF, the precipitate becomes soluble. The dark red solution was stirred for approximately 1 hr. THF was removed *in vacuo* and the resulting solid was dissolved in warm pentane and filtered through a diatomaceous earth plug. X-ray quality, dark red block-like crystals of **22** were grown by slow evaporation of solvent. Fragmentation of the parent ring-structure was also observed upon addition of dichloromethane and acetonitrile. ^{1}H NMR (250 MHz, CD_2Cl_2) δ: 7.40-7.15 (m, 6H, Ar-*H*), 4.05-3.80 (m, 4H, NC*H*$_2$), 3.19 (sept, 2H, C*H*CH$_3$), 3.07 (sept, 2H, C*H*CH$_3$), 1.40-1.10 (m, 24H, C*H*$_3$). ^{13}C{^{1}H} NMR (75.4 MHz, CD_2Cl_2) δ: 148.10, 130.15, 124.82, 124.33, 49.62, 29.22, 24.55, 24.24. IR (KBr, cm^{-1}) υ: 2962.20(s), 2926.13(m), 2867.87(m), 2370.13(w), 2342.17(w), 1544.14(s), 1485.21(s), 1459.45(s). PP: 226-229 °C.

Preparation of IMes-S_3N_2 – (23)

100 mg (0.328 mmol) of 1,3-bis(2,4,6-trimethylphenyl)-imidazol-2-ylidene (IMes) was dissolved in 5 mL of toluene and subsequently added to a stirring suspension of 60.5 mg (0.328 mmol) of tetrasulfur tetranitride (S_4N_4) in 5 mL of toluene. After being allowed to stir for 1 hr, the toluene was removed *in vacuo* yielding **20** as a purple solid. Addition of THF yields **23** as a purple solid. Fragmentation of the parent ring-structure was again observed upon addition of other nucleophilic solvents such as dichloromethane and acetonitrile. X-ray quality single crystals of **23** were grown from a solution of hot heptane which was filtered through a diatomaceous earth pad, forming purple needle-like crystals upon cooling to ambient temperatures. ^{1}H (300 MHz, C_6D_6) δ: 6.70 (s, 1H, Ar-*H*), 6.68 (s, 2H, Ar-*H*), 6.64 (s, 1H, Ar-*H*), 5.70 (s, 0.5H, unknown), 5.58 (s, 1H, C*H*), 5.56 (s, 1H, C*H*), 3.56 (m, res THF), 2.13 (s, 6H, CH_3), 2.05 (s, 6H, CH_3), 2.02 (s, 3H, CH_3), 1.97 (s, 3H, CH_3), 1.41 (m, res THF). ^{13}C{^{1}H} (75.4 MHz, C_6D_6) δ: 147.87, 136.61, 129.85, 115.86, 115.26, 114.63, 67.78, 25.78, 17.73. IR (KBr, cm^{-1}) υ: 2919.33(m), 2859.66(m), 2731.64(m), 2368.77(w), 2341.27(w), 1524.26(s), 1484.69(s), 1459.34(m), 1442.98(m), 1405.22(m). PP: 170-171 °C.

Section 3.4 – Selected X-ray Crystallographic Data

All data collected with M_o Kα radiation (λ = 0.71073 Å)
$R = \Sigma||Fo|-|Fc|| / \Sigma|Fo|$, $Rw = [\Sigma[\omega Fo^2-Fc^2)^2] / \Sigma[\omega Fo^2)^2]]^{0.5}$

Table 3.1 Selected crystallographic data for compounds **1-5**.

Compound:	**1**	**2**	**3**	**4**	**5**
Formula	$C_{26}H_{38}N_2PCl$	$C_{52}H_{76}N_4P_2$	$C_{52}H_{76}N_4P_6$	$C_{52}H_{76}N_4P_2O_3$	$C_{26}H_{39}N_2O_2P$
Formula Weight	444.25	818.55	942.45	883.13	442.56
a(Å)	12.017(5)	12.3916(15)	12.954(3)	16.186(4)	13.147(4)
b(Å)	16.597(7)	17.744(2)	12.954(3)	17.938(4)	14.643(4)
c(Å)	12.765(5)	24.391(3)	35.031(12)	17.738(4)	14.707(4)
α(°)	90	90	90	90	90
β(°)	97.632(5)	90	90	101.922(3)	113.624(4)
γ(°)	90	90	90	90	90
Crystal System	Monoclinic	Orthorhombic	Tetragonal	Monoclinic	Monoclinic
Space Group	P2(1)/c	Pccn	P4(1)2(1)2	P2(1)/c	P2(1)/n
$V(Å)^3$	2523.3(17)	5362.8(11)	5878.4(28)	5039(2)	2594.1(12)
Density (Mg/m^3)	1.171	1.015	1.065	1.143	1.133
Z	4	4	4	4	4
Abs Coeff, μ, mm^{-1}	0.23	0.115	0.217	0.13	0.129
Data Collected	26400	40991	71003	48892	15111
Data $F_o^2 > 3\sigma(F_o^2)$	4957	6578	7296	8872	4524
Restraints	0	7	2064	290	0
Variables	279	298	336	618	292
R	0.042	0.052	0.063	0.05	0.1035
R_w	0.072	0.123	0.169	0.13	0.1198
GOF	1.608	1.031	1.07	1.005	0.96
T (K)	130(2)	296(2)	130(2)	135(2)	100(2)

Table 3.2 Selected crystallographic data for compounds **6-10**.

Compound:	**6**	**7**	**8**	**9**	**10**
Formula	$C_{52}H_{76}N_4P_2S_{1.87}$	$C_{52}H_{76}N_4P_2S_{1.13}$	$C_{52}H_{76}N_4P_2Se$	$C_{52}H_{76}N_4P_2Se_2$	$C_{125}H_{176}N_8P_4Te_2$
Formula Weight	879.06	855.26	898.07	977.03	2169.82
a(Å)	12.108(6)	21.123(10)	20.648(5)	12.5119(17)	12.5708(10)
b(Å)	21.507(11)	10.822(5)	23.568(6)	14.5818(19)	13.2461(10)
c(Å)	21.647(11)	24.174(12)	24.274(6)	28.011(4)	20.3636(16)
α(°)	65.859(7)	90	67.160(3)	90	83.0370(10)
β(°)	89.905(7)	113.480(5)	84.262(3)	92.268(2)	77.0790(10)
γ(°)	86.889(7)	90	83.823(3)	90	70.3580(10)
Crystal System	Triclinic	Monoclinic	Triclinic	Monoclinic	Triclinic
Space Group	P1	P21/n	P1	P2(1)/c	P1
$V(Å)^3$	5135(4)	5068(4)	10801(5)	5106.5(12)	3108.7(4)
Density (Mg/m^3)	1.137	1.121	1.105	1.271	1.159
Z	4	4	8	4	1
Abs Coeff, μ, mm^{-1}	0.198	0.169	0.789	1.548	0.586
Data Collected	34578	32342	70274	32064	20865
Data $F_o^2 > 3\sigma(F_o^2)$	17760	8926	37157	8980	17209
Restraints	38	2	2112	0	1222
Variables	1164	551	2189	554	1222
R	0.067	0.0584	0.0993	0.0691	0.0507
R_w	0.1867	0.1779	0.2451	0.0957	0.1205
GOF	0.973	1.078	0.963	1.196	0.963
T (K)	150(2)	160(2)	130(2)	150(2)	150(2)

Table 3.3 Selected crystallographic data for compounds **11-15**.

Compound:	**11**	**12**	**13**	**14**	**15**
Formula	$C_{26}H_{42}BN_2P$	$C_{44}H_{39}BF_{15}N_2P$	$C_{44}H_{39}BF_{15}N_2PO$	$C_{26}H_{39}N_2P$	$C_{26}H_{39}N_2P$
Formula Weight	424.4	922.55	938.55	410.56	410.56
a(Å)	12.066(5)	11.410(3)	11.667(3)	19.691(4)	19.760(3)
b(Å)	20.851(8)	17.962(5)	17.939(5)	6.4265(15)	6.4410(9)
c(Å)	10.627(4)	20.961(6)	20.490(6)	20.389(5)	20.443(3)
α(°)	90	90	90	90	90
β(°)	90	99.656(4)	95.621(4)	107.550(3)	107.588(2)
γ(°)	90	90	90	90	90
Crystal System	Orthorhombic	Monoclinic	Monoclinic	Monoclinic	Monoclinic
Space Group	Pnma	P2(1)/c	P2(1)/c	P2(1)/c	P2(1)/c
$V(Å)^3$	2673.6(18)	4235(2)	4268(2)	2459.9(10)	2480.3(6)
Density (Mg/m^3)	1.054	1.447	1.461	1.109	1.099
Z	4	4	4	4	4
Abs Coeff, μ, mm^{-1}	0.117	0.166	0.168	0.126	0.125
Data Collected	25592	41000	40575	15886	14418
Data $F_o^2 > 3\sigma(F_o^2)$	2570	7462	7492	4343	4376
Restraints	0	906	0	0	0
Variables	153	706	589	285	274
R	0.0376	0.0435	0.0443	0.0587	0.0426
R_w	0.1019	0.1126	0.1076	0.1514	0.1105
GOF	1.05	0.933	1.027	1.049	1.017
T (K)	130(2)	150(2)	130(2)	100(2)	150(2)

Table 3.4 Selected crystallographic data for compounds **16-20**.

Compound:	**16**	**17**	**18**	**19**	**20**
Formula	$C_{53}H_{76}N_4P_2S_2$	$C_{59}H_{81}N_5OP_2$	$C_{59}H_{81}N_5P_2S$	$C_{27}H_{38}N_6S_4$	$C_{21}H_{26}N_6S_3$
Formula Weight	895.24	938.23	954.29	574.87	458.66
a(Å)	16.506(3)	29.594(7)	12.688(10)	10.606(2)	12.554(4)
b(Å)	14.607(2)	19.280(5)	13.073(10)	18.225(4)	12.424(4)
c(Å)	21.516(3)	22.869(6)	17.814(14)	15.805(4)	15.396(5)
α(°)	90	90	86.743(10)	90	90
β(°)	93.218(2)	112.239(3)	85.709(10)	106.899(3)	114.06
γ(°)	90	90	65.142(9)	90	90
Crystal System	Monoclinic	Monoclinic	Triclinic	Monoclinic	Monoclinic
Space Group	P2(1)/c	C2/c	P1	P2(1)/c	P2(1)/c
$V(Å)^3$	5179.4(14)	12078(5)	2673(4)	2923.2(11)	2192.6(12)
Density (Mg/m^3)	1.148	1.032	1.186	1.306	1.389
Z	4	8	2	4	4
Abs Coeff, μ, mm^{-1}	0.202	0.111	0.163	0.353	0.36
Data Collected	33947	39227	20362	19300	23464
Data $F_o^2 > 3\sigma(F_o^2)$	9115	10619	3089	5109	3508
Restraints	1	0	12772	42	0
Variables	566	620	1209	330	277
R	0.0668	0.0561	0.1354	0.0665	0.094
R_w	0.1774	0.1413	0.4413	0.1761	0.2884
GOF	0.998	0.905	0.882	0.959	1.056
T (K)	150(2)	130(2)	150(2)	100(2)	100(2)

Table 3.4 Selected crystallographic data for compounds **2** (high and low temp) and **21-23**.

Compound:	**21**	**22**	**23**	**2 - Low Temp**	**2 - High Temp**
Formula	$C_{32}H_{45}N_5S_4$	$C_{27}H_{38}N_4S_3$	$C_{21}H_{24}N_4S_3$	$C_{52}H_{76}N_4P_2$	$C_{52}H_{76}N_4P_2$
Formula Weight	627.97	514.79	428.62	819.11	819.11
a(Å)	10.3867(7)	12.718(3)	8.15(2)	19.6540(19)	19.995(15)
b(Å)	32.343(2)	10.904(3)	21.70(6)	13.1587(13)	13.304(10)
c(Å)	10.5585(7)	20.882(5)	12.06(3)	20.828(2)	20.966(15)
α(°)	90	90	90	90	90
β(°)	112.6490(10)	92.146(3)	95.81(3)	98.104(2)	98.334(12)
γ(°)	90	90	90	90	90
Crystal System	Monoclinic	Monoclinic	Monoclinic	Monoclinic	Monoclinic
Space Group	P2(1)/c	Pc	P2(1)/c	P2(1)/n	P2(1)/n
$V(Å)^3$	3273.5(4)	2893.9(12)	2121(10)	5332.9(9)	5518(7)
Density (Mg/m^3)	1.274	1.182	1.342	1.02	0.986
Z	4	4	4	4	4
Abs Coeff, μ, mm^{-1}	0.32	0.278	0.364	0.116	0.112
Data Collected	21673	18797	12352	30644	36270
Data $F_o^2 > 3\sigma(F_o^2)$	5770	8930	3687	9295	9622
Restraints	0	11	6	0	0
Variables	379	640	259	539	539
R	0.0455	0.061	0.2189	0.053	0.0543
R_w	0.1233	0.1547	0.5534	0.1158	0.1475
GOF	1.072	1.035	1.104	0.801	0.942
T (K)	150(2)	100(2)	100(2)	103(2)	323(2)

Chapter 4 – Appendices

Appendix A – Computational Results

The data found in this section (Tables A1-A9) was calculated and compiled by Dr. Cory Pye at Saint Mary's University using the ACEnet cluster.

Table A1. Energy of $(PH_2)_2$ forms (kJ/mol) relative to C_2 structure. For the C_2 structure, the energy is relative to 2 PH_2 units (i.e. the bond dissociation energy D_e).

	HF				B3LYP	
	STO-3G	3-21G	6-31G*	6-31+G*	6-31G*	6-31+G*
$(PH_2)_2 - D_{2h}$	513.3	326.6	368.0	363.8	347.2	342.2
$(PH_2)_2 - D_{2d}$	404.3	222.0	229.0	228.3	207.8	206.4
$(PH_2)_2 - C_{2v}$	15.3	13.7	19.5	19.4	17.5	17.4
$(PH_2)_2 - C_{2h}$	-3.7	1.3	4.4	4.3	0.4	0.5
$(PH_2)_2 - C_s$	207.3	117.6	125.1	124.2	116.4	115.1
$(PH_2)_2 - C_2$	-213.3	-98.4	-138.6	-137.6	-227.5	-225.0

Table A2. Energy of $P(NH_2)_2$ forms (kJ/mol) relative to C_2 #1 structure.

	HF				B3LP	
	STO-3G	3-21G	6-31G*	6-31+G*	6-31G*	6-31+G*
$P(NH_2)_2 - C_{2v}$ *#1*	26.3	21.7	23.0	27.5	32.5	36.6
$P(NH_2)_2 - C_{2v}$ *#2*	36.8	12.5	27.8	23.6	30.6	24.9
$P(NH_2)_2 - C_s$ *#1*	9.9	9.5	13.4	13.9	12.7	13.8
$P(NH_2)_2 - C_2$ *#1*	0.0	0.0	0.0	0.0	0.0	0.0
$P(NH_2)_2 - C_2$ *#2*			14.0			
$P(NH_2)_2 - C_s$ *#2*			21.1	23.7	24.6	
$P(NH_2)_2 - C_1$ *#1*	9.3		7.1		5.2	
$P(NH_2)_2 - C_1$ *#2*					5.1	

Table A3. Energy of bis-$P(NH_2)_2$ forms (kJ/mol) relative to C_2 #1 structure. The C_2 #1 form is relative to 2 $P(NH_2)_2$ C_2 *#1* units (i.e. the bond dissociation energy D_e).

	HF				B3LYP	
	STO-3G	3-21G	6-31G*	6-31+G*	6-31G*	6-31+G*
bis-$PAm_2 - C_2$ *#1*	-156.9	-95.4	-133.5	-120.7	-190.3	-175.8
bis-$PAm_2 - C_{2h}$	15.4	16.5	12.0	-3.4	15.0	12.0
bis-$PAm_2 - C_2$ *#2*		13.7			7.9	8.0

Table A4. Energy of $PEtAm_2$ forms (kJ/mol) relative to C_2 structure.

	HF				B3LYP	
	STO-3G	3-21G	6-31G*	6-31+G*	6-31G*	6-31+G*
$PEtAm_2 - C_{2v}$	29.6	10.4	20.2	18.0	23.3	20.2
$PEtAm_2 - C_2$	0.0	0.0	0.0	0.0	0.0	0.0
$PEtAm_2 - C_s$	11.6		15.1	13.8	16.3	14.4
$PEtAm_2 - C_1$	7.0		7.5	6.8	7.2	6.4

Table A5. Energy of bis-$PEtAm_2$ forms (kJ/mol) relative to C_2 #4 structure. The C_2 #4 form is relative to 2 $PEtAm_2$ C_2 units (i.e. the bond dissociation energy D_e).

	HF				B3LYP	
	STO-3G	3-21G	6-31G*	6-31+G*	6-31G*	6-31+G*
bis-$PEtAm_2 - C_2$ *#1*	15.3	9.3	34.5	41.3	9.5	18.7
bis-$PEtAm_2 - C_2$ *#2*	90.7			112.3	86.4	95.1
bis-$PEtAm_2 - C_2$ *#3*	9.1	5.5	30.5	15.2	11.5	15.2
bis-$PEtAm_2 - C_{2h}$ *#1*	6.8	13.9	12.8	11.4	13.9	12.5
bis-$PEtAm_2 - C_{2h}$ *#2*	74.7		50.3	50.5	49.6	47.5
bis-$PEtAm_2 - C_2$ *#4*	-144.1	-32.0	-91.6	-88.3	-147.0	-141.1
bis-$PEtAm_2 - C_2$ *#5*	74.3		17.0	18.3	15.6	16.4
bis-$PEtAm_2 - C_i$ *#1*	0.4	2.3	0.9	0.8	1.2	1.0
bis-$PEtAm_2 - C_i$ *#2*			10.9	11.8	10.2	10.0

Table A6. Energy of $PEtAm_2Ph_2$ forms (kJ/mol) relative to C_2 structure.

	HF				B3LYP	
	STO-3G	3-21G	6-31G*	6-31+G*	6-31G*	6-31+G*
$PEtAm_2Ph_2 - C_{2v}$ *#1*	3.3	8.1	12.1	10.3	7.7	6.5
$PEtAm_2Ph_2 - C_{2v}$ *#2*	56.4	34.1	26.7	24.5	52.6	49.2
$PEtAm_2Ph_2 - C_2$	0.0	0.0	0.0	0.0	0.0	0.0

Table A7. Energy of bis-$PEtAm_2Ph_2$ forms (kJ/mol) relative to C_2 #2structure. The C_2 #2 form is relative to 2 $PEtAm_2$ Ph_2 C_2 units (i.e. the bond dissociation energy D_e).

	HF				B3LYP	
	STO-3G	3-21G	6-31G*	6-31+G*	6-31G*	6-31+G*
$PEtAm_2Ph_2 - C_2$ *#1*		8.7	3.6	4.6	6.1	7.5
$PEtAm_2Ph_2 - C_2$ *#2*		-25.3	-56.4	-49.1	-108.2	-100.7
$PEtAm_2Ph_2 - C_i$ *#2*		5.8	5.6	4.3	2.8	2.7

Table A8. Energy of bis-$PEtAm_2Ph_2{}^iPr_4$ forms (kJ/mol) relative to C_2 #2 structure. The C_2 form is relative to 2 $PEtAm_2$ $Ph_2{}^iPr_4$ C_2 units (i.e. the bond dissociation energy D_e).

	HF				B3LYP	
	STO-3G	3-21G	6-31G*	6-31+G*	6-31G*	6-31+G*
$PEtAm_2Ph\,{}^iPr_4 - C_2$ *#1*	52.7	92.1	113.7	124.4	-8.7	11.6

Table A9. Total energies of all structures. Underlined energies correspond to a local minimum energy structure.

	HF				B3LYP	
	STO-3G	3-21G	6-31G*	6-31+G*	6-31G*	6-31+G*
$PH_2 - C_{2v}$	-338.0294285	-340.1196080	-341.8495995	-341.8503298	-342.5042136	-342.5058778
$(PH_2)_2 - D_{2h}$	-675.9446114	-680.1522911	-683.6118274	-683.6145151	-684.9628292	-684.9671145
$(PH_2)_2 - D_{2d}$	-675.9861203	-680.1921549	-683.6647454	-683.6661287	-685.0159167	-685.0188266
$(PH_2)_2 - C_{2v}$	-676.1342974	-680.2714902	-683.7445505	-683.7456779	-685.0884070	-685.0907992
$(PH_2)_2 - C_{2h}$	-676.1415039	-680.2761862	-683.7502996	-683.7514425	-685.0949277	-685.0972296
$(PH_2)_2 - C_s$	-676.0611479	-680.2319079	-683.7043351	-683.7057579	-685.0507411	-685.0535876
$(PH_2)_2 - C_2$	-676.1401064	-680.2766956	-683.7519802	-683.7530714	-685.0950774	-685.0974382
$P(NH_2)_2 - C_{2v}$ *#1*	-446.6849800	-449.5969669	-451.9221443	-451.9306828	-453.2238494	-453.2374351
$P(NH_2)_2 - C_{2v}$ *#2*	-446.6809803	-449.6004665	-451.9203190	-451.9321899	-453.2245557	-453.2418893
$P(NH_2)_2 - C_s$ *#1*	-446.6912554	-449.6015928	-451.9258199	-451.9358643	-453.2314022	-453.2461365
$P(NH_2)_2 - C_2$ *#1*	-446.6950087	-449.6052238	-451.9309096	-451.9411671	-453.2362225	-453.2513836
$P(NH_2)_2 - C_2$ *#2*		C_2 *#1*	-451.9255948	C_2 *#1*	C_2 *#1*	C_2 *#1*
$P(NH_2)_2 - C_s$ *#2*		C_s *#1*	-451.9228740	-451.9321385	-453.2268466	C_s *#1*
$P(NH_2)_2 - C_1$ *#1*	-446.6914841	C_2 *#1*	-451.9281940	C_2 *#1*	-453.2342284	C_2 *#1*
$P(NH_2)_2 - C_1$ *#2*			C_2 *#1*	C_2 *#1*	-453.2342882	
$P(NH_2)_2 - C_1$ *#3*			C_1 *#1*			
bis-$PAm_2 - C_2$ *#1*	-893.4497901	-899.2467768	-903.9126561	-903.9283103	-906.5449298	-906.5697239
bis-$PAm_2 - C_{2h}$	-893.4439254	-899.2404929	-903.9081035	-903.9295941	-906.5392044	-906.5651412
bis-$PAm_2 - C_2$ *#2*		-899.2415444			-906.5419038	-906.5666875
$PEtAm_2 - C_{2v}$	-522.6977333	-526.0682293	-528.8185071	-528.8280369	-530.6387960	-530.6531460
$PEtAm_2 - C_2$	-522.7090089	-526.0721934	-528.8262153	-528.8348846	-530.6476826	-530.6608256
$PEtAm_2 - C_s$	-522.7045837		-528.8204525	-528.8296367	-530.6414728	-530.6553236
$PEtAm_2 - C_1$	-522.7063587		-528.8233453	-528.8323058	-530.6449270	-530.6583731
bis-$PEtAm_2 - C_2$ *#1*	-1045.4670977	-1052.1530549	-1057.6741822	-1057.6876745	-1061.3477100	-1061.3682564
bis-$PEtAm_2 - C_2$ *#2*	-1045.4383649	C_2 *#1*	C_{2h} *#1.*	-1057.6606405	-1061.3184177	-1061.3391727
bis-$PEtAm_2 - C_2$ *#3*	-1045.4694523	-1052.1544987	-1057.6756886	-1057.6976194	-1061.3469517	-1061.3696050
bis-$PEtAm_2 - C_{2h}$ *#1*	-1045.4703336	-1052.1512852	-1057.6824507	-1057.6990530	-1061.3460455	-1061.3706505
bis-$PEtAm_2 - C_{2h}$ *#2*	-1045.4444528	C_{2h} *#1*	-1057.6681500	-1057.6841745	-1061.3324319	-1061.3573145
bis-$PEtAm_2 - C_2$ *#4*	-1045.4729110	-1052.1565919	-1057.6873116	-1057.7034037	-1061.3513391	-1061.3753972
bis-$PEtAm_2 - C_2$ *#5*	-1045.4446137		-1057.6808513	-1057.6964440	-1061.3453839	-1061.3691469
bis-$PEtAm_2 - C_i$ *#1*	-1045.4727730	-1052.1557260	-1057.6869718	-1057.7031064	-1061.3508650	-1061.3750170

Table A9 (continued). Total energies of all structures. Underlined energies correspond to a local minimum energy structure.

bis-PEtAm$_2$ – C_i #2			-1057.6831533	-1057.6989039	-1061.3474686	-1061.3715877
PEtAm$_2$Ph$_2$ – C_{2v} #1	-976.2256015	-982.6116208	-987.9122983	-987.9317055	-992.7553644	-992.7804462
PEtAm$_2$Ph$_2$ – C_{2v} #2	-976.2053678	-982.6017114	-987.9067447	-987.9263106	-992.7382693	-992.7641552
PEtAm$_2$Ph$_2$ – C_2	-976.2268468	-982.6147142	-987.9169239	-987.9356385	-992.7583147	-992.7829063
bis-PEtAm$_2$Ph$_2$ – C_2 #1	-1952.4880227	-1965.2357345	-1975.8539680	-1975.8882385	-1985.5554976	-1985.6013094
bis-PEtAm$_2$Ph$_2$ – C_2 #2		-1965.2390662	-1975.8553473	-1975.8899934	-1985.5578329	-1985.6041685
bis-PEtAm$_2$Ph$_2$ – C_i #1	-1952.4888348	C_i #2	C_i #2	C_i #2	C_i #2	C_i #2
bis-PEtAm$_2$Ph$_2$ – C_i #2	-1952.4889625	-1965.2368627	-1975.8532030	-1975.8883376	-1985.5567657	-1985.6031517
PEtAm$_2$Ph$_2$ ^{i}Pr$_4$ – C_2	-1439.1730220	-1448.4406517	-1456.3157325	-1456.3347368	-1464.5112187	-1464.5437579
bis-PEtAm$_2$Ph$_2$ ^{i}Pr$_4$ – C_2	-2878.3259575	-2896.8462375	-2912.5881698	-2912.6220953	-2929.0257612	-2929.0830831

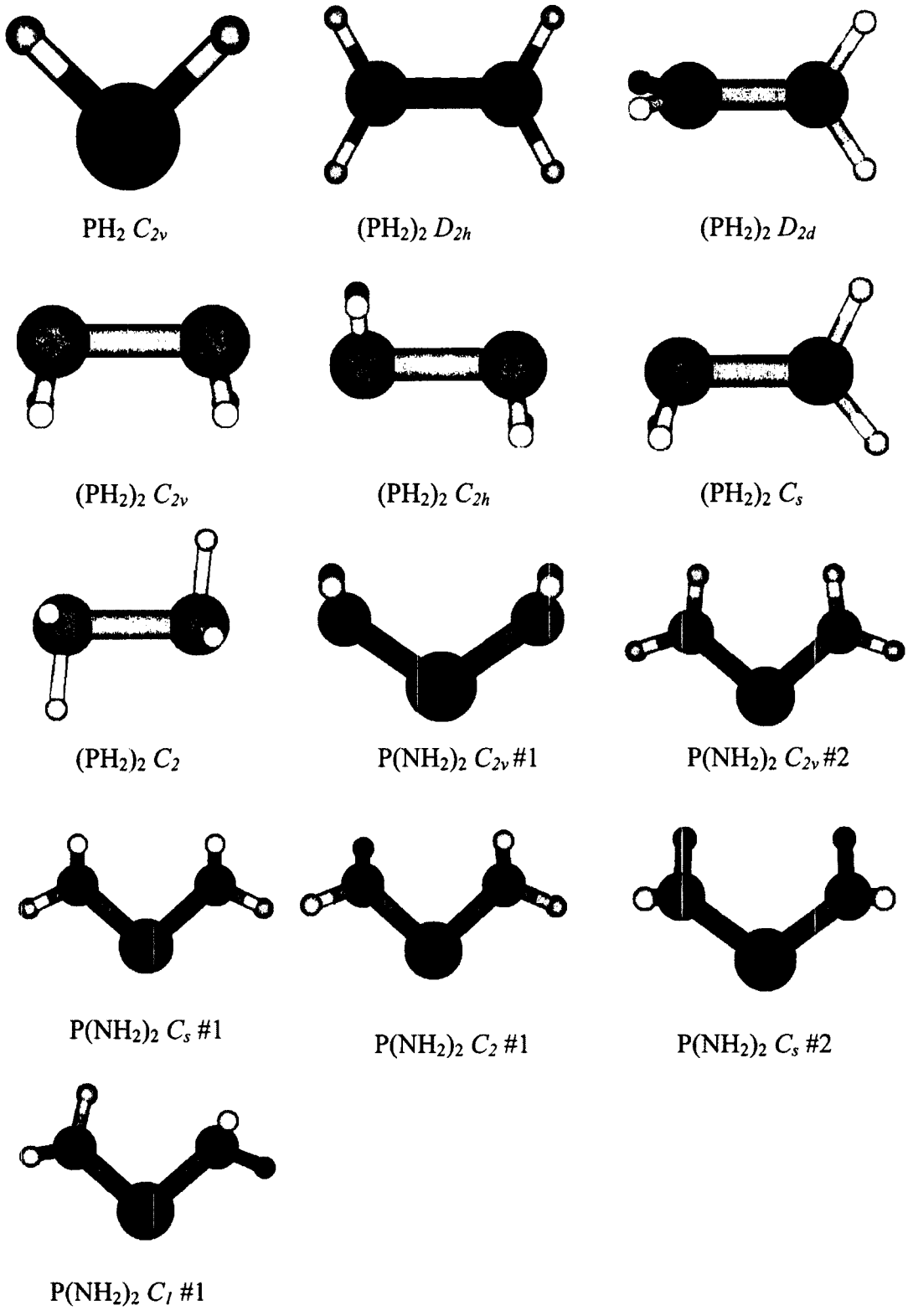

Figure A1. Selected symmetries for calculated monomers (PR_2) and dimers $(PR_2)_2$.

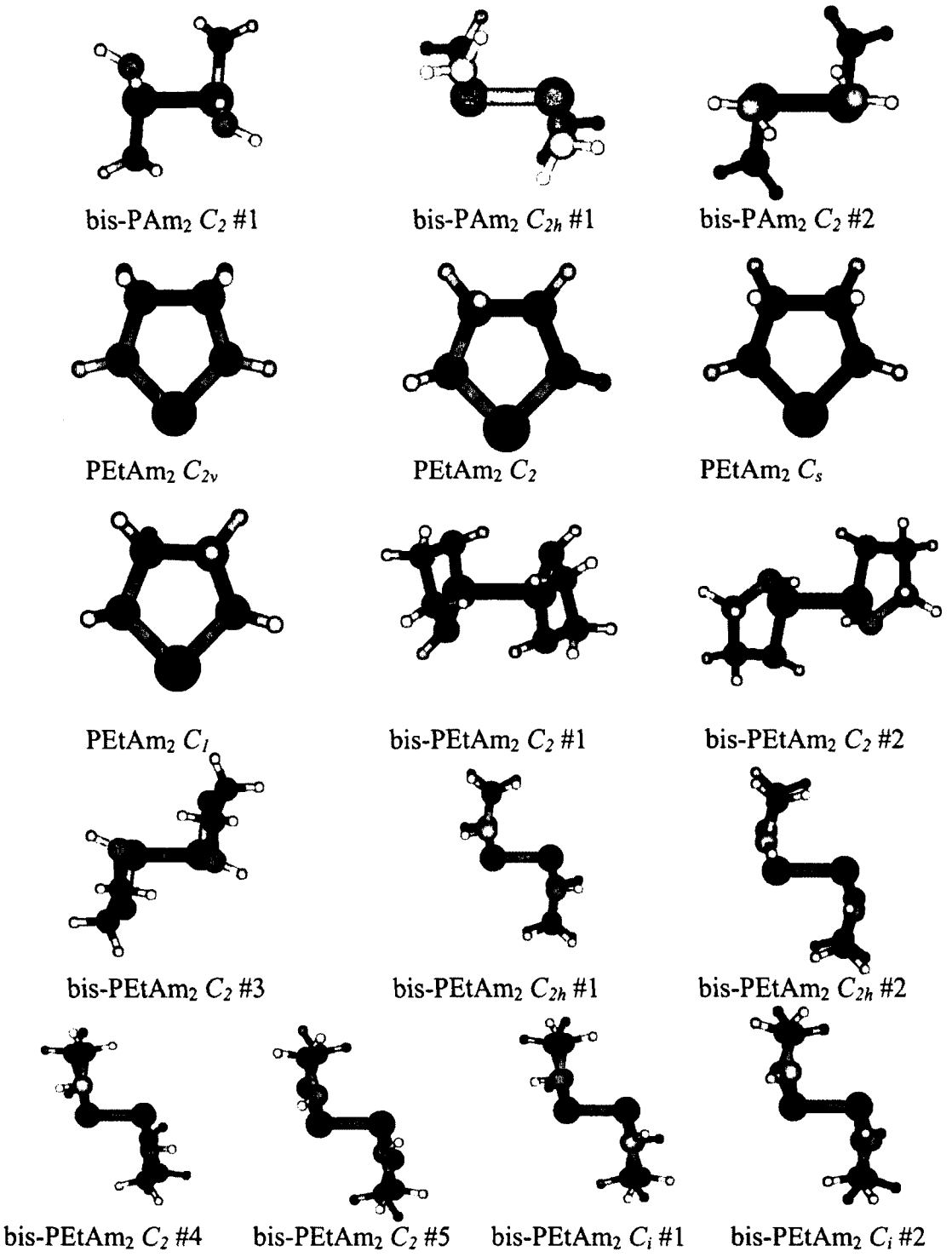

Figure A2. Selected symmetries for calculated monomers (PR_2) and dimers $(PR_2)_2$.

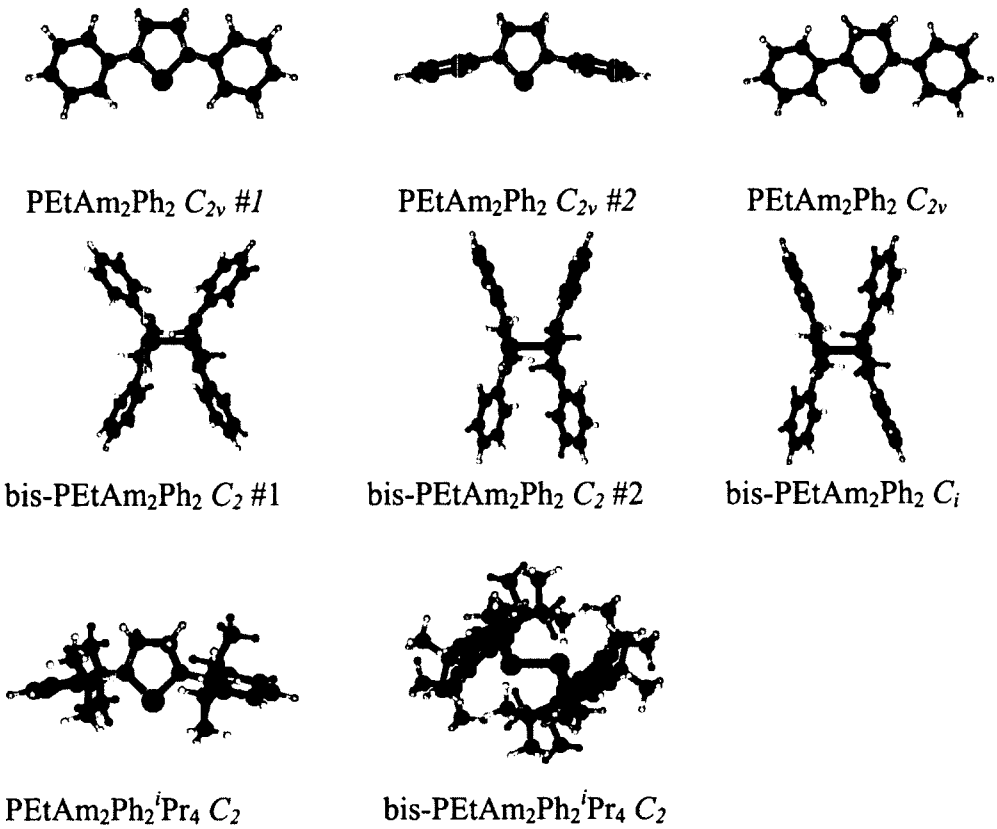

Figure A3. Selected symmetries for calculated monomers (PR_2) and dimers $(PR_2)_2$.

Appendix B – Unsuccessful Reactivity

In the process of this project, there were several reactions attempted with the diphosphine and other reagents which were found to be unsuccessful. There were cases in which complex mixtures of products were identified by $^{31}P\{^{1}H\}$ NMR as well as those where no reaction could be observed. Based on the time restrictions of this project, reactions which were not able to be characterized as either single products or simple mixtures were viewed as work which could be undertaken in the future.

Firstly, reactions were completed of the diphosphine (**2**) with several main group-centered molecules (Figure B1). Environmentally relevant gases including CO, CO_2, NO and SO_2 were allowed to react with the diphosphine→phosphinyl system. In the case of NO, a single product could be observed in the $^{31}P\{^{1}H\}$ NMR at 118.58 ppm. This represents a significant shift from the parent diphosphine (146.34 ppm) however, after several attempts in isolating a crystalline sample of this highly oxygen, moisture and temperature sensitive material, none were found to be a product directly related to the reaction. From the nature of the reaction and the $^{31}P\{^{1}H\}$ chemical shift in the P(III) region it could be postulated that the product is a radical coupled P-N-O system. This would be an exceedingly interesting molecule as a novel, terminal-triatomic functional group however structural analysis could not be completed with the infrastructure at Saint Mary's.

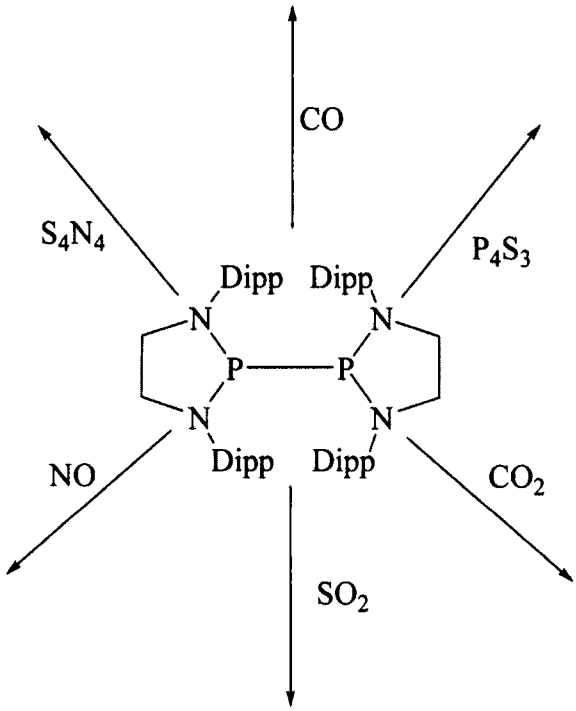

Figure B1. Failed reactions of the diphosphine (**2**) with main group centered small molecules.

In the case of CO, CO_2 and SO_2 no reaction was observed visually or in the $^{31}P\{^1H\}$ NMR after introduction of the gas to a J-Young style NMR tube. Heating the samples to reflux in the NMR tube (in toluene) did not push the reactions forward and no products were ever observed or isolated. Based on the success of the diphosphine (**2**) to activate both elemental phosphorus (P_4) and sulfur (S_8), other sulphur- and phosphorus-based molecules were investigated for their reactivity profile. Tetrasulphur tetranitride (S_4N_4) and phosphorus sesquasulphide (P_4S_3) were both reacted with **2** however, in these cases intractable mixtures of products were observed in the $^{31}P\{^1H\}$ NMR, likely due to the nucleophilic degradation and fragmentation of the cage structures.

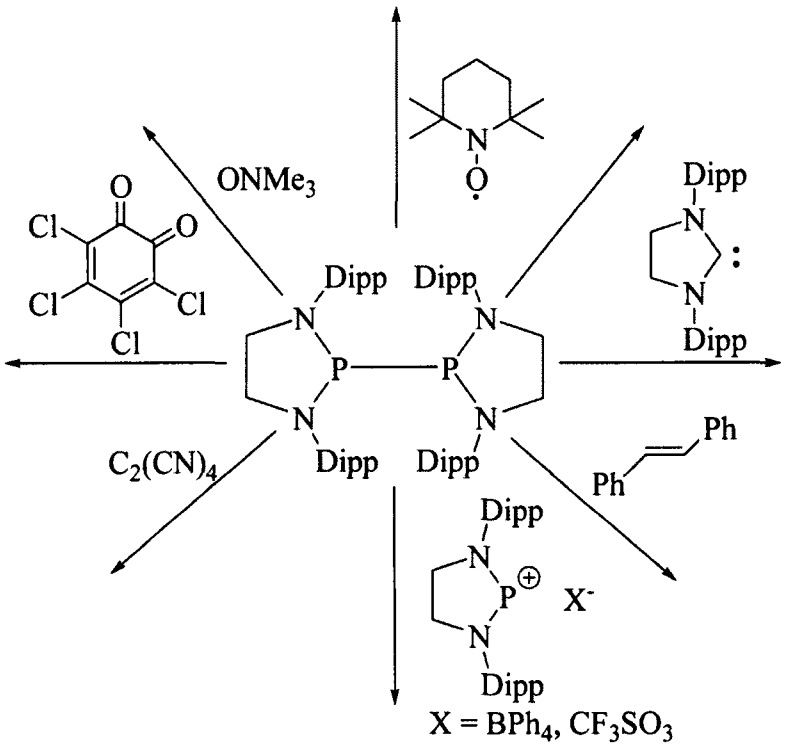

Figure B2. Failed reactions of the diphosphine (**2**) with radicals, potential radical acceptors and electrophiles.

As can be seen in Figure B2, several other molecules of interest were investigated in conjunction with the diphosphine (**2**). Particularly, molecules which could be loosely defined as radical acceptors including a quinone, ethylenes (tetracyanoethylene, *trans*-stilbene), a radical (TEMPO), as well as electrophiles (NHC, NHP) were employed. TEMPO and tetracyanoethylene were found to form intractable mixtures of products while in the cases of the NHC, NHP, stilbene, quinone and trimethylamine-N-oxide no reaction was observed by $^{31}P\{^{1}H\}$ NMR; only the diphosphine peak was present in the spectra in each case. Reactions which were unsuccessful at room temperature were generally heated to reflux in the NMR tube and checked again for reactivity.

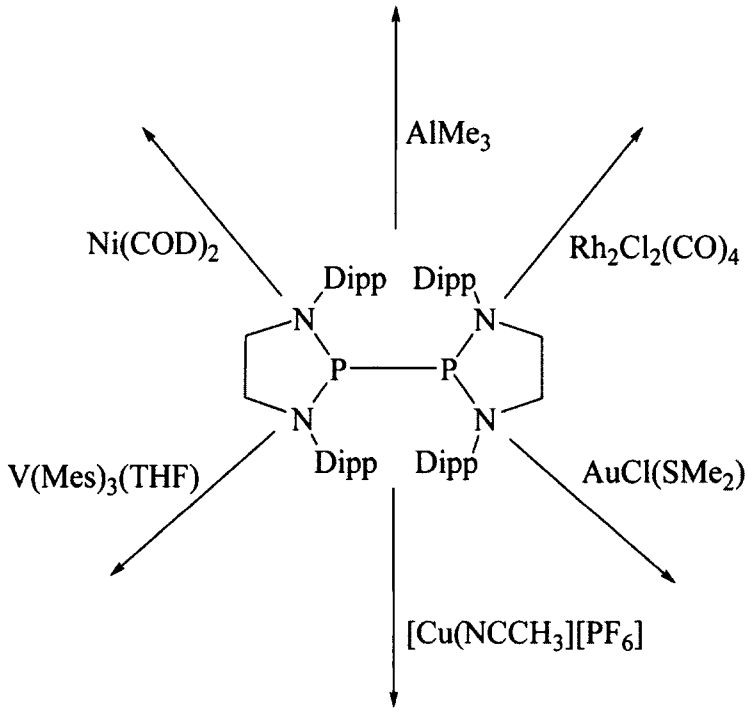

Figure B3. Failed reactions of the diphosphine (**2**) with metal-centered compounds.

Upon review of the literature it was evident that phosphorus centered radicals could play an interesting role in reactions with low-oxidation state metals. In the course of this project several metal complexes were attempted to react with the diphosphine (**2**) however, isolable products were never able to be characterized. In the cases of the rhodium chloride dimer [$Rh_2Cl_2(CO)_4$], gold chloride [$AuCl(SMe_2)$], a copper hexafluorophosphate [$Cu(NCCH_3)][PF_6$] and *bis*-cyclooctadiene nickel [$Ni(COD)_2$] the only observable products consisted of what appeared to be the deposition of metal on the walls of the scintillation vial. In the cases of $AlMe_3$ and $V(Mes)_3(THF)$, no reactivity could be seen visually or in the $^{31}P\{^1H\}$ NMR. From the experiments completed in this work regarding the reactivity profile of the diphosphine (**2**) with metal species there is no clear trend regarding the nature of the reactions and which criteria, if any, could be employed toward the potential stabilization of metal species containing the phosphinyl (**2**·) acting as a one-, two- or three-electron donor to a metal center.

References

(1) Gomberg, M. *J. Am. Chem. Soc.* **1900**, *22*, 757-771.

(2) Walling, C.; Pearson, M. S. *Top. Phosphorus Chem.* **1966**, *3*, 1-56.

(3) Schmidt, U.; Kabitzke, K.; Markau, K.; Mueller, A. *Chem. Ber.* **1966**, *99*, 1497-1501.

(4) Kochi, J. K.; Krusic, P. J. *J. Amer. Chem. Soc.* **1969**, *91*, 3944-3946.

(5) Cetinkaya, B.; Hudson, A.; Lappert, M. F.; Goldwhite, H. *J. Chem. Soc. Chem. Commun.* **1982**, 609-610.

(6) Gynane, M. J. S.; Hudson, A.; Lappert, M. F.; Power, P. P.; Goldwhite, H. *J. Chem. Soc. Dalton Trans.* **1980**, 2428-2433.

(7) Gynane, M. J. S.; Hudson, A.; Lappert, M. F.; Power, P. P.; Goldwhite, H. *J. Chem. Soc. Chem. Commun.* **1976**, 623-624.

(8) Agarwal, P.; Piro, N. A.; Meyer, K.; Mueller, P.; Cummins, C. C. *Angew. Chem. Int. Ed.* **2007**, *46*, 3111-3114.

(9) Ndiaye, B.; Bhat, S.; Jouaiti, A.; Berclaz, T.; Bernardinelli, G.; Geoffroy, M. *J. Phys. Chem. A* **2006**, *110*, 9736-9742.

(10) Ito, S.; Kikuchi, M.; Sugiyama, H.; Yoshifuji, M. *J. Organomet. Chem.* **2007**, *692*, 2761-2767.

(11) Ito, S.; Kikuchi, M.; Yoshifuji, M.; Arduengo, A. J.,III; Konovalova, T. A.; Kispert, L. D. *Angew. Chem. Int. Ed.* **2006**, *45*, 4341-4345.

(12) Back, O.; Donnadieu, B.; Parameswaran, P.; Frenking, G.; Bertrand, G. *Nat. Chem.* **2010**, *2*, 369-373.

(13) Back, O.; Celik, M. A.; Frenking, G.; Melaimi, M.; Donnadieu, B.; Bertrand, G. *J. Am. Chem. Soc.* **2010**, *132*, 10262-10263.

(14) Back, O.; Donnadieu, B.; von Hopffgarten, M.; Klein, S.; Tonner, R.; Frenking, G.; Bertrand, G. *Chem. Sci.* **2011**, *2*, 858-861.

(15) Carroll, L. In *Through the Looking-Glass, and What Alice Found There;* Macmillan: United Kingdom, 1871.

(16) Griller, D.; Ingold, K. U. *Acc. Chem. Res.* **1976**, *9*, 13-19.

(17) Hinchley, S. L.; Morrison, C. A.; Rankin, D. W.; Macdonald, C. L.; Wiacek, R. J.; Voigt, A.; Cowley, A. H.; Lappert, M. F.; Gundersen, G.; Clyburne, J. A.; Power, P. P. *J. Am. Chem. Soc.* **2001**, *123*, 9045-9053.

(18) Sheberla, D.; Tumanskii, B.; Tomasik, A. C.; Mitra, A.; Hill, N. J.; West, R.; Apeloig, Y. *Chem. Sci.* **2010**, *1*, 234-241.

(19) Barks, J. M.; Gilbert, B. C.; Parsons, A. F.; Upeandran, B. *Tetrahedron Lett.* **2001**, *42*, 3137-3140.

(20) Roberts, B. P. *Adv. Free-Radical Chem.* **1980**, *6*, 225-289.

(21) Bentrude, W. G. *Acc. Chem. Res.* **1982**, *15*, 117-125.

(22) Bentrude, W. G. *React. Intermed.* **1983**, *3*, 199-298.

(23) Bentrude, W. G. In *In Phosphorus radicals.* Section Title: Physical Organic Chemistry; 1973; Vol. 2, pp 595-663.

(24) Berchadsky, Y.; Bernard-Henriet, C.; Finet, J.; Lauricella, R.; Marque, S. R. A.; Tordo, P. *Chem. Eur. J.* **2006**, *12*, 7084-7094.

(25) Power, P. P. *Chem. Rev.* **2003**, *103*, 789-809.

(26) Marque, S.; Tordo, P. *Top. Curr. Chem.* **2005**, *250*, 43-76.

(27) Konu, J.; Chivers, T. In *Stable Radicals of the Heavy p-Block Elements;* Hicks, R. G., Ed.; Stable Radicals: Fundamentals and Applied Aspects of Odd-Electron Compounds. John Wiley & Sons, Ltd: 2010; pp 381.

(28) Chivers, T.; Armstrong, A.; Boere, R. T. In *In Stable phosphorus-containing radicals.* 2004; pp 798.

(29) Armstrong, A.; Chivers, T.; Boere, R. T. *ACS Symp. Ser.* **2006**, *917*, 66-80.

(30) Rowlands, G. J. *Tetrahedron* **2009**, *65*, 8603-8655.

(31) Bell, I. S.; Qian, H.; Hamilton, P. A.; Davies, P. B. *J. Chem. Phys.* **1997**, *107*, 8311-8316.

(32) Andrews, L.; Withnall, R. *J. Am. Chem. Soc.* **1988**, *110*, 5605-5611.

(33) Emsley, J. In *The 13th Element: The Sordid Tale of Murder, Fire, and Phosphorus;* Wiley & Sons, Inc.: New York, 2002; pp 352.

(34) Cadogan, J. I. G. *Advan. Free-Radical Chem.* **1967**, *2*, 203-250.

(35) Cowley, A. H.; Ebsworth, E. A. V.; Kemp, R. A.; Rankin, D. W. H.; Stewart, C. A. *Organometallics* **1982**, *1*, 1720-1721.

(36) Corvaja, C. In *Introduction to Electron Paramagnetic Resonance;* Electron Paramagnetic Resonance; John Wiley & Sons, Inc: 2008; pp 1-36.

(37) Weil, J. A.; Bolton, J. R. In *Basic Principles of Paramagnetic Resonance;* Electron Paramagnetic Resonance; John Wiley & Sons, Inc: 2006; pp 1-35.

(38) Cowley, A. H.; Kemp, R. A.; Wilburn, J. C. *J. Am. Chem. Soc.* **1982**, *104*, 331-332.

(39) Cowley, A. H.; Kemp, R. A. *Synth. React. Inorg. Met. Org. Chem.* **1981**, *11*, 591-595.

(40) Ozbolat-Schon, A.; Bode, M.; Schnakenburg, G.; Anoop, A.; van Gastel, M.; Neese, F.; Streubel, R. *Angew. Chem. Int. Ed.* **2010**, *49*, 6894-6898.

(41) Scheer, M.; Kuntz, C.; Stubenhofer, M.; Linseis, M.; Winter, R. F.; Sierka, M. *Angew. Chem. Int. Ed.* **2009**, *48*, 2600-2604.

(42) Cataldo, L.; Dutan, C.; Misra, S. K.; Loss, S.; Gruetzmacher, H.; Geoffroy, M. *Chem. Eur. J.* **2005**, *11*, 3463-3468.

(43) Kadirov, M. K.; Budnikova, Y. G.; Kholin, K. V.; Valitov, M. I.; Krasnov, S. A.; Gryaznova, T. V.; Sinyashin, O. G. *Russ. Chem. Bull.* **2010**, *59*, 466-468.

(44) Sebastian, M.; Nieger, M.; Szieberth, D.; Nyulaszi, L.; Niecke, E. *Angew. Chem. Int. Ed.* **2004**, *43*, 637-641.

(45) Kato, T.; Gornitzka, H.; Schoeller, W. W.; Baceiredo, A.; Bertrand, G. *Angew. Chem. Int. Ed.* **2005**, *44*, 5497-5500.

(46) Dutan, C.; Shah, S.; Smith, R. C.; Choua, S.; Berclaz, T.; Geoffroy, M.; Protasiewicz, J. D. *Inorg. Chem.* **2003**, *42*, 6241-6251.

(47) Loss, S.; Magistrato, A.; Cataldo, L.; Hoffmann, S.; Geoffroy, M.; Rothlisberger, U.; Grutzmacher, H. *Angew. Chem. Int. Ed.* **2001**, *40*, 723-726.

(48) Geier, J.; Harmer, J.; Grutzmacher, H. *Angew. Chem. Int. Ed.* **2004**, *43*, 4093-4097.

(49) Sasamori, T.; Mieda, E.; Nagahora, N.; Sato, K.; Shiomi, D.; Takui, T.; Hosoi, Y.; Furukawa, Y.; Takagi, N.; Nagase, S.; Tokitoh, N. *J. Am. Chem. Soc.* **2006**, *128*, 12582-12588.

(50) Egorochkin, A. N.; Voronkov, M. G.; Zderenova, O. V.; Mushtina, T. G. *Russ. J. Gen. Chem.* **2003**, *73*, 880-887.

(51) Egorochkin, A. N.; Kuznetsova, O. V.; Khamaletdinova, N. M.; Domratcheva-Lvova, L. G. *Magn. Reson. Chem.* **2011**, *49*, 175-183.

(52) Rosa, P.; Gouverd, C.; Bernardinelli, G.; Berclaz, T.; Geoffroy, M. *J. Phys. Chem. A* **2003**, *107*, 4883-4892.

(53) Ionkin, A. S.; Marshall, W. J.; Fish, B. M.; Marchione, A. A.; Howe, L. A.; Davidson, F.; McEwen, C. N. *Eur. J. Inorg. Chem.* **2008**, 2386-2390.

(54) Biaso, F.; Cantat, T.; Mezailles, N.; Ricard, L.; Le Floch, P.; Geoffroy, M. *Angew. Chem. Int. Ed.* **2006**, *45*, 7036-7039.

(55) Armstrong, A.; Chivers, T.; Parvez, M.; Boere, R. T. *Angew. Chem. Int. Ed.* **2004**, *43*, 502-505.

(56) Armstrong, A.; Chivers, T.; Parvez, M.; Schatte, G.; Boere, R. T. *Inorg. Chem.* **2004**, *43*, 3453-3460.

(57) Armstrong, A.; Chivers, T.; Krahn, M.; Parvez, M.; Schatte, G. *Chem. Commun.* **2002**, 2332-2333.

(58) Salomon, C.; Dal Molin, S.; Fortin, D.; Mugnier, Y.; Boere, R. T.; Juge, S.; Harvey, P. D. *Dalton Trans.* **2010**, *39*, 10068-10075.

(59) Ewels, C. P.; El Cheikh, H.; Suarez-Martinez, I.; Van Lier, G. *Phys. Chem. Chem. Phys.* **2008**, *10*, 2145-2148.

(60) Sasaki, S.; Murakami, F.; Yoshifuji, M. *Angew. Chem. Int. Ed.* **1999**, *38*, 340-343.

(61) Sasaki, S.; Sutoh, K.; Murakami, F.; Yoshifuji, M. *J. Am. Chem. Soc.* **2002**, *124*, 14830-14831.

(62) Sutoh, K.; Sasaki, S.; Yoshifuji, M. *Inorg. Chem.* **2006**, *45*, 992-998.

(63) Yasui, S.; Tojo, S.; Majima, T. *Org. Biomol. Chem.* **2006**, *4*, 2969-2973.

(64) Boere, R. T.; Bond, A. M.; Cronin, S.; Duffy, N. W.; Hazendonk, P.; Masuda, J. D.; Pollard, K.; Roemmele, T. L.; Tran, P.; Zhang, Y. *New J. Chem.* **2008**, *32*, 214-231.

(65) Kinjo, R.; Donnadieu, B.; Bertrand, G. *Angew. Chem. Int. Ed.* **2010**, *49*, 5930-5933.

(66) Weber, L. *Angew. Chem. Int. Ed.* **2010**, *49*, 5829-5830.

(67) Hinchley, S. L.; Morrison, C. A.; Rankin, D. W. H.; Macdonald, C. L. B.; Wiacek, R. J.; Cowley, A. H.; Lappert, M. F.; Gundersen, G.; Clyburne, J. A. C.; Power, P. P. *Chem. Commun.* **2000**, 2045-2046.

(68) Burck, S.; Gotz, K.; Kaupp, M.; Nieger, M.; Weber, J.; Schmedt auf, d. G.; Gudat, D. *J. Am. Chem. Soc.* **2009**, *131*, 10763-10774.

(69) Hill, N. J.; Reeske, G.; Cowley, A. H. *Main Group Chemistry* **2010**, *9*, 5-10.

(70) Bezombes, J.; Borisenko, K. B.; Hitchcock, P. B.; Lappert, M. F.; Nycz, J. E.; Rankin, D. W. H.; Robertson, H. E. *Dalton Trans.* **2004**, 1980-1988.

(71) Bezombes, J.; Hitchcock, P. B.; Lappert, M. F.; Nycz, J. E. *Dalton Trans.* **2004**, 499-501.

(72) Giffin, N. A.; Masuda, J. D. *Coord. Chem. Rev.* **2011**, *255*, 1342-1359.

(73) Dumitrescu, A.; Rudzevich, V. L.; Romanenko, V. D.; Mari, A.; Schoeller, W. W.; Bourissou, D.; Bertrand, G. *Inorg. Chem.* **2004**, *43*, 6546-6548.

(74) Edge, R.; Less, R. J.; McInnes, E. J. L.; Muether, K.; Naseri, V.; Rawson, J. M.; Wright, D. S. *Chem. Commun.* **2009**, 1691-1693.

(75) Ishida, S.; Hirakawa, F.; Iwamoto, T. *J. Am. Chem. Soc.* **2011**, *133*, 12968-12971.

(76) Caputo, C. A.; Price, J. T.; Jennings, M. C.; McDonald, R.; Jones, N. D. *Dalton Trans.* **2008**, 3461-3469.

(77) Burck, S.; Gudat, D.; Naettinen, K.; Nieger, M.; Niemeyer, M.; Schmid, D. *Eur. J. Inorg. Chem.* **2007**, 5112-5119.

(78) Baxter, S. G.; Cowley, A. H.; Davis, R. E.; Riley, P. E. *J. Am. Chem. Soc.* **1981**, *103*, 1699-1702.

(79) Schoeller, W. W.; Staemmler, V.; Rademacher, P.; Niecke, E. *Inorg. Chem.* **1986**, *25*, 4382-4385.

(80) Schoeller, W. W.; Lerch, C. *Inorg. Chem.* **1983**, *22*, 2992-2998.

(81) Kovacs, I.; Baum, G.; Fritz, G.; Fenske, D.; Wiberg, N.; Schuster, H.; Karaghiosoff *Z. Anorg. Allg. Chem.* **1993**, *619*, 453-460.

(82) Weisbarth, R.; Jansen, M. *Z. Kristallogr. New Cryst. Struct.* **2002**, *217*, 94.

(83) Guillen, F.; Rivard, M.; Toffano, M.; Legros, J.; Daran, J.; Fiaud, J. *Tetrahedron* **2002**, *58*, 5895-5904.

(84) Gallacher, A. C.; Pinkerton, A. A., **1993**, *49*, 1793-1796.

(85) Sekar, P.; Ibers, J. A. *Inorg. Chem.* **2003**, *42*, 6294-6299.

(86) Peuser, I.; Neu, R. C.; Zhao, X.; Ulrich, M.; Schirmer, B.; Tannert, J. A.; Kehr, G.; Froehlich, R.; Grimme, S.; Erker, G.; Stephan, D. W. *Chem. Eur. J.* **2011**, *17*, 9640-9650.

(87) Stephan, D. W.; Greenberg, S.; Graham, T. W.; Chase, P.; Hastie, J. J.; Geier, S. J.; Farrell, J. M.; Brown, C. C.; Heiden, Z. M.; Welch, G. C.; Ullrich, M. *Inorg. Chem.* **2011**, *50*, 12338-12348.

(88) Menard, G.; Stephan, D. W. *Angew. Chem. Int. Ed.* **2011**, *50*, 8396-8399.

(89) Williams, D. B. G.; Kotze, P. D. R.; Ferreira, A. C.; Holzapfel, C. W. *J. Iran. Chem. Soc.* **2011**, *8*, 240-246.

(90) Lane, E. M.; Chapp, T. W.; Hughes, R. P.; Glueck, D. S.; Feland, B. C.; Bernard, G. M.; Wasylishen, R. E.; Rheingold, A. L. *Inorg. Chem.* **2010**, *49*, 3950-3957.

(91) Yue, N. L. S.; Stephan, D. W. *Organometallics* **2001**, *20*, 2303-2308.

(92) King, R. B.; Sundaram, P. M. *J. Org. Chem.* **1984**, *49*, 1784-1789.

(93) Hudson, H. R. In *Acid-base and hydrogen-bonding properties of phosphines;* Organophosphorus Compounds (1990); John Wiley & Sons, Inc: 2010; pp 473-487.

(94) Xu, W.; Lough, A. J.; Morris, R. H. *Inorg. Chem.* **1996**, *35*, 1549-1555.

(95) Burck, S.; Gudat, D.; Nieger, M.; Du Mont, W. *J. Am. Chem. Soc.* **2006**, *128*, 3946-3955.

(96) Gudat, D.; Haghverdi, A.; Nieger, M. *Angew. Chem. Int. Ed.* **2000**, *39*, 3084-3086.

(97) Garcia, F.; Goodman, J. M.; Kowenicki, R. A.; McPartlin, M.; Riera, L.; Silva, M. A.; Wirsing, A.; Wright, D. S. *Dalton Trans.* **2005**, 1764-1773.

(98) Xi, S. K.; Schmidt, H.; Lensink, C.; Kim, S.; Wintergrass, D.; Daniels, L. M.; Jacobson, R. A.; Verkade, J. G. *Inorg. Chem.* **1990**, *29*, 2214-2220.

(99) Artyushin, O.; Odinets, I.; Goryunov, E.; Fedyanin, I.; Lyssenko, K.; Mastryukova, T.; Raschenthaler, G.; Kagl, T.; Keglevich, G.; Kollor, L. *Journal of Organometallic Chemistry* **2006**, *691*, 5547-5559.

(100) Walther, D.; Liesicke, S.; Fischer, R.; Gorls, H.; Weston, J.; Batista, A. *Eur. J. Inorg. Chem.* **2003**, *2003*, 4321-4331.

(101) de Fremont, P.; Marion, N.; Nolan, S. P. *Coord. Chem. Rev.* **2009**, *253*, 862-892.

(102) Zimmerman, H. E.; Paskovich, D. H. *J. Am. Chem. Soc.* **1964**, *86*, 2149-2160.

(103) Tomioka, H. *Acc. Chem. Res.* **1997**, *30*, 315-321.

(104) Tomioka, H.; Iwamoto, E.; Itakura, H.; Hirai, K. *Nature* **2001**, *412*, 626-628.

(105) Iiba, E.; Hirai, K.; Tomioka, H.; Yoshioka, Y. *J. Am. Chem. Soc.* **2002**, *124*, 14308-14309.

(106) Iwamoto, E.; Hirai, K.; Tomioka, H. *J. Am. Chem. Soc.* **2003**, *125*, 14664-14665.

(107) Schrock, R. R. *Chem. Rev.* **2002**, *102*, 145-179.

(108) Pauling, L. *J. Chem. Soc. Chem. Commun.* **1980**, 688-689.

(109) Arduengo, A. J.,III; Dias, H. V. R.; Harlow, R. L.; Kline, M. *J. Am. Chem. Soc.* **1992**, *114*, 5530-5534.

(110) Arduengo, A. J.,III; Krafczyk, R.; Schmutzler, R.; Craig, H. A.; Goerlich, J. R.; Marshall, W. J.; Unverzagt, M. *Tetrahedron* **1999**, *55*, 14523-14534.

(111) Buron, C.; Gornitzka, H.; Romanenko, V.; Bertrand, G. *Science* **2000**, *288*, 834-836.

(112) Wanzlick, H. W.; Kleiner, H. J. *Chem. Ber.* **1963**, *96*, 3024-3027.

(113) Arduengo, A. J.,III; Harlow, R. L.; Kline, M. *J. Am. Chem. Soc.* **1991**, *113*, 361-363.

(114) Diez-Gonzalez, S.; Marion, N.; Nolan, S. P. *Chem. Rev.* **2009**, *109*, 3612-3676.

(115) Bourissou, D.; Guerret, O.; Gabbaie, F. P.; Bertrand, G. *Chem. Rev.* **2000**, *100*, 39-91.

(116) Zeng, X.; Frey, G. D.; Kinjo, R.; Donnadieu, B.; Bertrand, G. *J. Am. Chem. Soc.* **2009**, *131*, 8690-8696.

(117) Igau, A.; Grutzmacher, H.; Baceiredo, A.; Bertrand, G. *J. Am. Chem. Soc.* **1988**, *110*, 6463-6466.

(118) Back, O.; Kuchenbeiser, G.; Donnadieu, B.; Bertrand, G. *Angew. Chem. Int. Ed.* **2009**, *48*, 5530-5533.

(119) Arnold, P. L.; Pearson, S. *Coord. Chem. Rev.* **2007**, *251*, 596-609.

(120) Fluck, E.; Becke-Goehring, M.; Dehoust, G. *Z. anorg. allg. Chem.* **1961**, *312*, 60-69.

(121) Holt, E. M.; Holt, S. L. *J. Chem. Soc. D* **1970**, 1704.

(122) Holt, E. M.; Holt, S. L. *J. Chem. Soc. Dalton Trans.* **1974**, 1990-1992.

(123) Chivers, T.; Cordes, A. W.; Oakley, R. T.; Swepston, P. N. *Inorg. Chem.* **1981**, *20*, 2376-2380.

(124) Chivers, T.; Oakley, R. T.; Cordes, A. W.; Swepston, P. *J. Chem. Soc. Chem. Commun.* **1980**, 35-36.

(125) Ruppert, I.; Bastian, V.; Appel, R. *Chem. Ber.* **1974**, *107*, 3426-3443.

(126) Mohan, T.; Rao, M. N. S. *Heteroat. Chem.* **1997**, *8*, 225-232.

(127) Thomas, C. J.; Rao, M. N. S. *J. Chem. Soc. Dalton Trans.* **1988**, 1445-1447.

(128) Swarnalatha, U.; Sivaramakrishna, A.; Venkatachalam, C. S.; Rao, M. N. S.; Inoue, T.; Ueda, T.; Hojo, M. *Can. J. Chem.* **2002**, *80*, 1428-1434.

(129) Swarnalatha, U.; Rao, M. N. S.; Udupa, M. R. *Thermochim. Acta* **1997**, *297*, 139-142.

(130) Srinivas, J.; Murthy, G. S.; Swarnalatha, U.; Rao, M. N. S. *J. Chem. Crystallogr.* **2001**, *31*, 267-270.

(131) Janaswamy, S.; Sreenivasa Murthy, G.; Mohan, T.; Rao, M. N. S. *Crystallogr. Rep.* **2003**, *48*, 68-72.

(132) Janaswamy, S.; Murthy, G. S.; Mohan, T.; Rao, M. N. S. *Acta Crystallogr. Sect. C: Cryst. Struct. Commun.* **1996**, *C52*, 1250-1252.

(133) Janaswamy, S.; Murthy, G. S.; Mohan, T.; Rao, M. N. S. *J. Chem. Crystallogr.* **2005**, *35*, 27-34.

(134) Gopalakrishnan, J.; Varghese, B.; Doddi, A.; Rao, M. N. S. *Appl. Organomet. Chem.* **2006**, *20*, 880-885.

(135) Gopalakrishnan, J.; Srinivas, J.; Murthy, G. S.; Rao, M. N. S. *Proc. Indian Acad. Sci. , Chem. Sci.* **1998**, *110*, 89-95.

(136) Gopalakrishnan, J.; Rao, M. N. S.; Srinivas, J.; Srinivasamurthy, G. *Polyhedron* **1997**, *16*, 1089-1094.

(137) Gopalakrishnan, J. *Appl. Organomet. Chem.* **2009**, *23*, 291-318.

(138) Elias, A. J.; Rao, M. N. S.; Varghese, B. *Polyhedron* **1990**, *9*, 1433-1440.

(139) Elias, A. J.; Rao, M. N. S. *Inorg. Chim. Acta* **1989**, *164*, 45-48.

(140) Antonova, N. S.; Carboì , J. J.; Poblet, J. M. *Organometallics* **2009**, *28*, 4283-4287.

(141) Frisch, A. C.; Zapf, A.; Briel, O.; Kayser, B.; Shaikh, N.; Beller, M. *Journal of Molecular Catalysis A: Chemical* **2004**, *214*, 231-239.

(142) Lee, M.; Hu, C. *Organometallics* **2004**, *23*, 976-983.

(143) Lee, M.; Lee, H. M.; Hu, C. *Organometallics* **2007**, *26*, 1317-1324.

(144) Liu, M.; Yang, I.; Buckley, B.; Lee, J. K. *Org. Lett.* **2010**, *12*, 4764-4767.

(145) Masuda, J. D.; Schoeller, W. W.; Donnadieu, B.; Bertrand, G. *Angew. Chem. Int. Ed.* **2007**, *46*, 7052-7055.

(146) Masuda, J. D.; Schoeller, W. W.; Donnadieu, B.; Bertrand, G. *J. Am. Chem. Soc.* **2007**, *129*, 14180-14181.

(147) Giffin, N. A.; Makramalla, M.; Hendsbee, A. D.; Robertson, K. N.; Sherren, C.; Pye, C. C.; Masuda, J. D.; Clyburne, J. A. C. *Org. Biomol. Chem.* **2011**, *9*, 3672-3680.

(148) Inos, B.; Holle, S.; Goddard, R.; Alcarazo, M. *Angew. Chem. Int. Ed.* **2010**, *49*, 8389-8391.

(149) Giffin, N. A.; Hendsbee, A. D.; Masuda, J. D. *Acta Crystallogr. Sect. E: Struct. Rep. Online* **2010**, *E66*, o2194.

(150) Giffin, N. A.; Hendsbee, A. D.; Masuda, J. D. *Acta Crystallogr. Sect. E: Struct. Rep. Online* **2010**, *E66*, o2090-o2091.

(151) Arduengo, A. J.; Calabrese, J. C.; Cowley, A. H.; Dias, H. V. R.; Goerlich, J. R.; Marshall, W. J.; Riegel, B. *Inorg. Chem.* **1997**, *36*, 2151-2158.

(152) Panda, T. K.; Trambitas, A. G.; Bannenberg, T.; Hrib, C. G.; Randoll, S.; Jones, P. G.; Tamm, M. *Inorg. Chem.* **2009**, *48*, 5462-5472.

(153) Arduengo, A. J. I.,II; Gamper, S. F.; Tamm, M.; Calabrese, J. C.; Davidson, F.; Craig, H. A. *J. Am. Chem. Soc.* **1995**, *117*, 572-573.

(154) Boehme, C.; Frenking, G. *J. Am. Chem. Soc.* **1996**, *118*, 2039-2046.

(155) Dorta, R.; Stevens, E. D.; Hoff, C. D.; Nolan, S. P. *J. Am. Chem. Soc.* **2003**, *125*, 10490-10491.

(156) Mieusset, J.; Brinker, U. H. *J. Org. Chem.* **2008**, *73*, 1553-1558.

(157) Melaimi, M.; Soleilhavoup, M.; Bertrand, G. *Angew. Chem. Int. Ed.* **2010**, *49*, 8810-8849.

(158) Chivers, T.; Oakley, R. T.; Scherer, O. J.; Wolmershaeuser, G. *Inorg. Chem.* **1981**, *20*, 914-917.

(159) Bojes, J.; Chivers, T.; Cordes, A. W.; MacLean, G.; Oakley, R. T. *Inorg. Chem.* **1981**, *20*, 16-21.

(160) Becke-Goehring, M.; Jolly, W. L.; Camp, U. D. L.; Macomber, J. D.; Woeller, H. F. In *Sulfur Nitrides;* Inorganic Syntheses; John Wiley & Sons, Inc: 2007; pp 123-128.

(161) Koppe, K.; Bilir, V.; Frohn, H.; Mercier, H. P. A.; Schrobilgen, G. J. *Inorg. Chem.* **2007**, *46*, 9425-9437.

(162) gNMR v4.0. Cherwell Scientific Publishing, Oxford, UK.

(163) Forgeron, M. A. M.; Gee, M.; Wasylishen, R. E. *J. Phys. Chem. A* **2004**, *108*, 4895-4908.

(164) Duling, D. R. *J. Magn. Reson. Ser. B* **1994**, *104*, 105-110.

(165) Bruker, B. A. I. **2008**.

(166) Sheldrick, G. M. *Acta Crystallogr. Sect. A: Found. Crystallogr.* **2008**, *A64*, 112-122.

(167) Farrugia, L. J. *J. Appl. Crystallogr.* **1997**, *30*, 565.